Higher Order Corrections to Jet Observables

Dissertation

zur
Erlangung der naturwissenschaftlichen Doktorwürde
(Dr. sc. nat.)
vorgelegt der
Mathematisch-Naturwissenschaftliche Fakultät
der
Universität Zürich
von

Gionata Luisoni

aus
Stabio, TI

Promotionskomitee

Prof. Dr. Thomas Gehrmann
Prof. Dr. Aude Gehrmann-De Ridder
Prof. Dr. Daniel Wyler
Prof. Dr. Günther Dissertori

Zürich, 2010

Zusammenfassung

Jet-Observablen sind sehr wichtig für das Verständnis der Physik der starken Wechselwirkung, da die partonische Dynamik nur anhand von Jets experimentell beobachtet werden kann. Aufgrund der vielfältigen präzisen Messungen dieser Observablen (und damit eng verwandter Ereignisformvariablen), die bei LEP, HERA und am Tevatron durchgeführt wurden, und in Hinblick auf die zu erwartende Qualität der Messdaten am LHC, werden Jet Observablen heutzutage für Präzisionsstudien benutzt. Hierfür ist eine hohe Genauigkeit der theoretischen Vorhersagen erforderlich, welche Berechnungen in der zweitführenden Ordnung (NNLO) in der Störungstheorie benötigt.

In den letzten Jahren wurden mit Hilfe des Antenna Subtraktionsformalismus NNLO QCD Korrekturen zu 3-Jet Produktion in Elektron-Positron Annihilation berechnet. Im ersten Teil dieser Arbeit wird dieses Subtraktionsschemata auf Prozesse mit einem hadronischen Anfangszustand erweitert. Dies erlaubt nun die Implementierung eines Monte Carlo Generators auf Parton-Niveau zur Berechnung von NNLO Korrekturen zu Jet-Observablen in tief inelastischer Elektron-Proton Streuung. Ausserdem ist diese Erweiterung ein fundamentaler Baustein für die Konstruktion eines derartigen Programms für rein hadronische Teilchenkollisionen.

Im zweiten Teil der Dissertation betrachten wir die Kombination von NNLO Rechnungen mit Resummationsrechnungen, welche dominante Terme in allen Ordnungen der Störungstheorie aufsummieren. Verschiedene Schemen werden hierfür hergeleitet. Das Matching wird auf NLLA+NNLO Genauigkeit für sechs Ereignisformvariablen angewendet, die sehr genau am LEP Beschleuniger gemessen worden sind. Die resultierenden Vorhersagen wurden für eine neue Bestimmung der starken Kopplungskonstante α_s benutzt:

$$\alpha_s^{\mathrm{NLLA+NNLO}}(M_Z) = 0.1224 \pm 0.0009\,(\mathrm{stat}) \pm 0.0009\,(\mathrm{exp}) \pm 0.0012\,(\mathrm{had}) \pm 0.0035\,(\mathrm{theo})\ .$$

Im letzten Teil werden höhere Momente von Ereignisformvariablen auf NNLO betrachtet und dazu anhand eines dispersiven Models analytische nicht-perturbative Potenzkorrekturen (NPPC) berechnet. Ein kombinierter Fit von α_s und der nicht-perturbativen effektiven Kopplung α_0 wurde durchgeführt:

$$\begin{aligned} \alpha_s^{\mathrm{NNLO+NPPC}}(M_Z) &= 0.1153 \pm 0.0017\,(\mathrm{exp}) \pm 0.0023\,(\mathrm{theo}), \\ \alpha_0^{\mathrm{NNLO}} &= 0.5132 \pm 0.0115\,(\mathrm{exp}) \pm 0.0381\,(\mathrm{theo})\,. \end{aligned}$$

Die zwei α_s Bestimmungen erlauben desweiteren Hadronisierungskorrekturen mit verschiedenen Monte Carlo Event-Generatoren zu studieren, und die mit den Vorhersagen von analytischen Modellen zu vergleichen.

Abstract

Jet observables are of fundamental importance in the physics of strong interactions since the parton dynamic can be studied experimentally only observing jets. Thanks to the many very accurate measurements carried out at LEP, at HERA and at Tevatron, and in view of the high quality data expected at LHC, jets are nowadays objects of precision studies, for which next-to-next-to-leading (NNLO) order QCD calculations are mandatory.

Recently NNLO QCD corrections to 3-jet production in electron-positron annihilation were computed using the antenna subtraction formalism. In the first part of this work we extend this subtraction scheme to incorporate processes with one hadronic initial state at NNLO. This allows the implementation of a parton-level Monte Carlo event generator programme for the calculation of NNLO corrections to jet production observables in deeply inelastic electron-proton scattering. Furthermore it is an important ingredient for the construction of a similar parton-level programme for hadron colliders.

In the second part of the thesis we consider the matching of the fixed NNLO calculations mentioned above with resummation calculations. Several matching schemes are derived at different orders in perturbation theory. In a second step we apply the matching at NLLA+NNLO to a set of six event-shape variables measured very precisely at LEP. These new matched results were used to perform a new fit of the strong coupling constant α_s resulting in

$$\alpha_s^{\mathrm{NLLA+NNLO}}(M_Z) = 0.1224 \pm 0.0009\,(\mathrm{stat}) \pm 0.0009\,(\mathrm{exp}) \pm 0.0012\,(\mathrm{had}) \pm 0.0035\,(\mathrm{theo})\ .$$

In the final part of the thesis we consider moments of event-shape variables at NNLO and compute analytic non-perturbative power corrections (NPPC) to them, using the dispersive model. A combined fit of α_s and a non-perturbative effective coupling α_0 is performed finding

$$\begin{aligned} \alpha_s^{\mathrm{NNLO+NPPC}}(M_Z) &= 0.1153 \pm 0.0017\,(\mathrm{exp}) \pm 0.0023\,(\mathrm{theo}), \\ \alpha_0^{\mathrm{NNLO}} &= 0.5132 \pm 0.0115\,(\mathrm{exp}) \pm 0.0381\,(\mathrm{theo})\,. \end{aligned}$$

The two determinations of α_s permitted also to investigate the role of hadronization corrections using different generations of Monte Carlo event generator predictions and analytic models.

To Anika and my Family

Acknowledgements

First of all I wish to thank my supervisor Prof. Thomas Gehrmann for his most valuable help, for his patience and for the many opportunities he gave me during the three years I spent in his group. His support on technical questions about physics, but also his suggestions in many issues regarding the daily activities in research were of fundamental importance. I also would like to thank Hasko Stenzel for his help on questions about statistical analysis, and Aude Gehrmann-De Ridder for having shared with me her computational expertise in computing phase space master integrals. Furthermore I am very thankful to Pier Francesco Monni and Beat Tödli for the many hours spent together learning some particular aspects of QCD. I am very grateful also to Radja Boughezal, Alejandro Daleo, Nicolas Greiner, Gudrun Heinrich, Mario Lubini, Tobias Motz, Pedro Schwaller, Cedric Studerus and Nurhana Tajuddin for the numerous fruitful suggestions and conversations. I wish to thank all the people of the Theoretical Institute of the University of Zürich for their company and for the time spent together. I wish to thank also Michele D'Anna, my physics teacher from high school, for getting me enthusiastic about physics several years ago. I'm also very grateful to Thomas Gehrmann and Cedric Studerus for reading through the manuscript. Their hints and comments have been decisive in bringing this thesis to its final form. Last but not least, a big thank you to my family for the support they gave me in these years and to Anika for her love and her patience in supporting me and waiting for me in the busy times of my PhD.

Contents

List of Figures

List of Tables

Glossary

$\overline{\text{MS}}$	Modified minimal subtraction scheme.
CERN	Conceille Europeénne pour la Recherche Nucléaire.
CM	Center-of-Mass.
DESY	Deutsches Elektronen-Synchrotron: the biggest German particle physics research center.
DIS	Deep Inelastic Scattering.
GR	General Relativity.
HERA	Hadron-Elektron-Ringanlage: hadron-electron particle accelerator which built at DESY in Hamburg.
IR	Infra-Red.
LEP	Large Electron-Positron Collider.
LHC	Large Hadron Collider.
LO	Leading Order.
NLLA	Next-to-Leading-Logarithmic Approximation.
NLO	Next-to-Leading Order.
NNLO	Next-to-Next-to-Leading Order.
NPPC	Non-Perturbative-Power-Corrections.
OPE	Operator Product Expansion.
PETRA	Positron-Elektron Tandem Ring Anlage: electron-positron particle accelerator built at DESY in Hamburg.
QCD	Quantum Chromodynamics.
QED	Quantum Electrodynamics.
QFT	Quantum Field Theory.
SCET	Soft-Collinear-Effective-Theory.
SLAC	Stanford Linear Accelerator Center: a United States Department of Energy National Laboratory.
SM	The Standard Model of elementary particles and their interactions.
UV	Ultra-Violet.

1

Introduction

For some strange coincidence, this thesis has begun to be written in concomitance with the first couple of days of running of the world most powerful particle accelerator ever build: the Large Hadron Collider (LHC) at CERN in Geneva. The LHC will allow to explore energies and distances never reached before. The entire particle physics community, and together with it the whole humanity, is looking forward to see some signs of new physics phenomena and of course of the only piece missing in the theory which today describes all of the known interactions between elementary particles: the Higgs boson. Although this theory, called the Standard Model of elementary particle physics (SM), is by now established, an important part responsible for explaining the origin of the mass of all elementary particles is still missing. This chapter is a brief overview of a history which started many centuries ago, when people started to believe that matter should consist of some fundamental building blocks, and culminated with the formulation and the discovery of the SM: one of the most elegant and fascinating theories that human mind could ever conceive. In this chapter we will describe some basic concepts of particle physics and of the SM and slowly focus on the part describing the strong interaction, which will concern us in the next chapters: the so-called Quantum Chomodynamics (QCD).

1.1 The idea of matter building blocks

The idea that our universe can be understood as an assembly of some basic building blocks is very old. Although the idea was motivated for many centuries only by philosophical reasons, the concept of atom dates back to the 6th century BC. The earliest references were found in ancient India. About one century later Leucippus, followed by his pupil Demokritos, developed the atomism: a natural philosophy whose basic idea was that the natural world consists of two opposite and indivisible constituents:

atoms and void. The word atom derives from the Greek *átomos*, which means "uncuttable". For the atomists atoms were the building blocks of all knowable matter. They were invisible and, as the etymology of the word says, they were indivisible and thus also unchangeable and eternal. Void was seen as the opposite of matter or, in other words, the space in which matter can move. Atomism as a natural philosophy became very controversial already at the time of Plato and it was almost forgotten in later times since it was considered as unacceptable form of materialism and atheism and thus heretical.

Only after the renaissance, in the late 16th and during the 17th century atomism reappeared, though in new forms. Important contributions to the new spread and the development of the atomistic ideas came from Francis Bacon, Galileo Galilei, René Descartes and Robert Boyle. In the 18th century the scientific method initiated by Galileo Galilei started to influence the philosophical concepts about the structure of matter, since some of the ideas and hypotheses could be verified by repeatable demonstrations. In the 19th century the developments in chemistry lead to important discoveries which could be explained very naturally by assuming the existence of atoms. In the late 19th century and the first years of the 20th century many experiments confirmed the existence of atoms. In 1905 A. Einstein published a work on the Brownian motion [5] which is considered as one of the contributions which gave a definitive confirmation of the existence of molecules, and therefore of what we today call atoms.

1.2 The long way to the Standard Model of particle physics

The confirmation of the existence of atoms was actually only the beginning. That this was not the ultimate answer to the question about the building blocks of matter became somehow clear already some years before, in 1897, when J. J. Thomson discovered the first subatomic particle: the electron. As around 1911 E. Rutherford carried out his famous scattering experiment in which he bombarded a gold foil with α particles, it became clear that atoms have an inner structure with a central part responsible for nearly the whole mass, the so-called nucleus, and a cloud of electrons orbiting around it. In 1919 Rutherford observed that hydrogen nuclei were present also in other nuclei. This claim can be paraphrased by saying that the proton is also part of the nuclei of other atoms. For this reason, this observation is usually indicated as the discovery of the proton. However, only after J. Chadwick discovered the neutron, in 1932, it became clear that the nuclei are actually build up by protons and neutrons tightly bound together. In the same year also the positron, the antiparticle of the electron, was discovered by C. D. Anderson by studying cosmic rays.

In the first half of the last century the new discoveries in the microscopic world in terms of elementary particles came along with a huge evolution (sometimes even seen

as a "revolution") in the paradigm and the way of thinking about them. The theory of special relativity and quantum mechanics, followed by the unification of the two in a framework which is known today as Quantum Field Theory (QFT), pointed out that our intuitive way of thinking about the world faces severe problems in describing the nature and the behaviour of elementary particles. In fact all elementary particles are quantum mechanical objects, in the sense that they obey the rules of quantum mechanics. According to them, the behaviour of, say, an electron is sometimes well described by thinking of it as a point-like particle, whereas some other times it is more appropriate to see it as a wave or a wave packet.

After the second world war, when the first particle colliders were built, many other particles were found. At that time scientists also realized that they needed to join their efforts in order to realize the bigger and bigger experiments and research laboratories needed. Many new research centers were build in those years. We mention just a few like CERN (1954), DESY (1959) or SLAC (1962). In the sixties, seventies and eighties many important experimental discoveries and theoretical developments lead to the quantum field theory now called "The Standard Model". Among them there is also the discovery that protons and neutrons are not elementary particles, but are rather constituted by some more fundamental particles called quarks and gluons. The first one were first discovered in deep-inelastic scattering experiments at SLAC [6, 7], whereas evidence for latter was observed first at the electron-positron collider PETRA at DESY [8]. For a detailed historical review of the development of particle physics we refer to e.g [9].

1.3 The Standard Model of particle physics

The Standard Model of particle physics (SM) is a QFT-based model which describes the interactions among elementary particles due to three of the four known forces existing in nature. Gravitation, although being the most evident force for people in everyday's life, is the weakest of the four forces and its proper quantum description is still an open issue. Classically it is very well described by General Relativity (GR). The SM consists of two basic theories: the electroweak theory, which describes the electroweak interactions and Quantum Chromodynamics (QCD), which deals with strongly interacting particles. It is formulated mathematically in terms of a Lagrange density which is invariant under local $\mathrm{SU}(3)_C \otimes \mathrm{SU}(2)_L \otimes \mathrm{U}(1)_Y$ gauge transformations. In the framework of quantum field theories, interactions among elementary spin-1/2 particles are always mediated by some other spin-1 particles, called gauge bosons. Figure 1.1 shows the complete particle content of the Standard Model.

Quantum-Electrodynamics (QED) is the theory of electromagnetic interactions at quantum level. All electrically charged elementary particles feel the electromagnetic

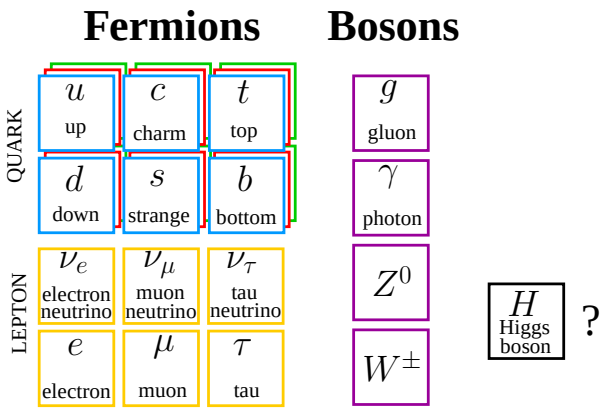

Figure 1.1: Particles and forces described by the Standard Model. Fermions are present in three different quark and lepton families. Furthermore, the six quark flavours can have three different colours.

interaction, which is mediated by electromagnetic waves. In the quantum descriptions these waves are seen as particles and are called photons. In the Standard Model QED is unified with the weak interaction to form the so-called broken part of the SM Lagrangian. In fact the original $\mathrm{SU}(2)_L \otimes \mathrm{U}(1)_Y$ symmetry is spontaneously broken to a $\mathrm{U}(1)_{\mathrm{em}}$ symmetry by the Higgs-Kibble [10–14] mechanism, by which all the particles of the SM acquire a mass[1]. The strong force described by QCD is the part of the SM having the non-Abelian $\mathrm{SU}(3)_C$ symmetry. The label C stands for "colour". The strong force is responsible for the interaction among quarks and is mediated by gluons. For historical reasons quarks and gluons are collectively called partons [18]. For reasons which will become clear in the next chapter, partons cannot be isolated at low energy, but are always combined into bound states called hadrons.

Although the Higgs boson, which is connected to the breaking of the electroweak symmetry, was not found yet and there are currently two colliders[2] hunting for it, the SM is very successful in describing electroweak and strong interactions. Its major achievements were the prediction of the $\mathrm{W}^\pm$ and Z^0 bosons discovered in 1983 at CERN SPS collider, the prediction of the top quark discovered at Tevatron in 1995 and the many precise descriptions of electroweak and strong observables measured at LEP, at HERA and at the Tevatron. The very precise measurements of jet observables need to be compared with correspondingly accurate theoretical predictions.

[1] For a review of the Standard Model and of the Higgs mechanism we refer to a text book on the SM like e.g. [15–17].

[2] One of the many aims of the LHC, which is starting up in these weeks, is to reveal the mechanism of electroweak symmetry breaking, either by finding the SM Higgs boson or some other particle. Also at Tevatron physicists are looking for the Higgs boson and in the last years they were able to exclude it in a mass range around 160 GeV [19].

The aim of this thesis is to improve higher order corrections for some of the QCD observables measured at LEP and to extend computational tools in order to improve the theoretical predictions for observables measured at HERA, at the Tevatron and in future also at LHC.

At LEP a class of observables which describes the topology of hadronic final states was measured very precisely. Up to recently, the theoretical predictions for these so-called event-shape observables were based on a computation at next-to-leading order (NLO) in perturbation theory, matched with a resummed prediction at next-to-leading-logarithmic accuracy (NLLA). The development of the antenna subtraction formalism [20, 21], which is described in detail in Chapter 3, permitted to extend the order of the computation to next-to-next-to-leading order (NNLO). In this thesis we match the NNLO calculations onto the resummed NLLA and give some insight on how to extend the matching procedure to higher orders. The matched results were used to make new fits of the strong coupling constant α_s [22]. Furthermore the means and higher moments of event-shape distributions were combined with non-perturbative corrections using a dispersive model for α_s [23]. In a second step the antenna subtraction formalism was extended in order to be applicable to deep-inelastic scattering (DIS) and hadron-hadron scattering processes, where there is at least one parton in the initial state [24].

In Chapter 2 we give a brief theoretical overview of QCD, focusing on some basic properties which will be used in the following chapters. In Chapter 3 we present the antenna subtraction formalism used to compute event-shape variables at NNLO, and we extend it to the case in which there is a parton in the initial state. Chapter 4 is dedicated to event-shape observables in e^+e^--annihilation. We explain how the matching procedure works and how it was implemented in the C++ programm `Lormeso`. Chapter 5 is dedicated to an analysis of non-perturbative corrections to the moments of event-shape variables. Finally Chapter 6 is dedicated to the conclusions and an outlook.

2

Quantum Chromodynamics

In this chapter we introduce all the important concepts which are needed to understand the following chapters and the new results presented in the thesis. It is not meant to substitute any of the many very good textbooks on QCD, to which we refer for further details [25–27]. It is rather a collection of the key ideas and it explains and develops the language and the framework used in the next chapters.

2.1 Cross section calculations in QFT

Before starting with the description of the basis of QCD, we very briefly review the basic concepts used in particle physics and how the structure of a theoretical calculation looks like.

Apart from experiments which deal with cosmic rays, almost all other experiments in high energy and particle physics are colliding experiments, where either two beams of particles are accelerated and collided or a single beam is accelerated and smashed against a fixed target. The resulting particles in the final state are analysed with the goal of reconstructing the collision and understanding its dynamic. For this purpose the most important quantities to be measured are *cross sections*, which are intrinsic to the colliding particles and thus allow for comparisons among experiments with different characteristics. Considering two bunches of particles of type $\mathcal{A}$ and $\mathcal{B}$, with a length $l_{\mathcal{A}}$, $l_{\mathcal{B}}$ and a density per volume $\rho_{\mathcal{A}}$, $\rho_{\mathcal{B}}$, we can define the cross section to be

$$\sigma = \frac{\sharp \text{ Scattering events}}{\rho_{\mathcal{A}}\, l_{\mathcal{A}}\ \rho_{\mathcal{B}}\, l_{\mathcal{B}}\ A}\,, \tag{2.1}$$

where A is the cross-sectional area common to the two bunches (Figure 2.1). It is customary to measure the momenta $k_1, \ldots, k_m$ of the outgoing particles. By specifying the exact momenta which we want to select in the reaction, the quantity σ will be infinitesimal. For this reason physicists are in general not only interested in the total cross section σ, but also in the so-called *differential cross section* $d\sigma/(d^3k_1 \ldots d^3k_m)$,

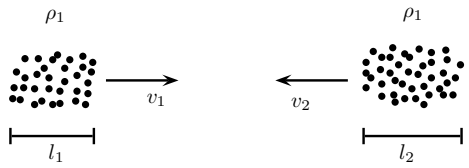

Figure 2.1: Two bunches of particles cross each other and some of them scatter together.

which is the infinitesimal quantity in the momenta of the outgoing particles[1]. Integrating the differential cross section over the full range of momenta of all final state particles, one obtains again the total cross section. Usually, instead of considering the differential cross section in the momenta of the final state particles, physicists compute the differential cross section in some other kinematical quantity $\mathcal{O}_m(k_1, \ldots, k_m)$, for example transverse momentum rapidity, which is a function of the final state momenta itself. The theoretical predictions for the differential cross section in an observable $\mathcal{O}_n$ are computed according to the following master formula:

$$\frac{\mathrm{d}\sigma}{\mathrm{d}\mathcal{O}_m} = \frac{1}{\text{Flux}} \sum_m \frac{1}{S_m} \int \mathrm{d}\Phi_m \left|\mathcal{M}\left(p_\mathcal{A}, p_\mathcal{B} \to \{k_f\}\right)\right|^2 J_m^{(m)}(k_1, \ldots, k_m) \,. \tag{2.2}$$

The first factor on the right hand side is the flux factor. It takes care of the correct normalization with respect to the total incoming particles according to eq. (2.1). The sum runs over all possible configurations with m particles in the final state and S_m is a symmetry factor, which ensures that contributions from indistinguishable final states are not double counted. The integral goes over $\mathrm{d}\Phi_m$ which is the m-particle phase space, whereas $\mathcal{M}\left(p_\mathcal{A}, p_\mathcal{B} \to \{k_f\}\right)$ is the matrix element for the reaction, whose absolute value squared gives the probability for the transition. Finally $J_m^{(m)}(k_1, \ldots, k_m)$ is a weight called *jet function*, which defines the measurement and depends on the observable $\mathcal{O}_m$. The matrix element contains all the information about the dynamic of the interaction and is computed in QFT by making perturbation theory in the coupling constant. In practice this means that all observables in QCD are computed by making a series expansion in the strong coupling constant α_s. We consider now a $2 \to m$ scattering. For the moment we do not specify whether the initial state particles are partons or leptons. The leading-order (LO) contribution will then be given by

$$\mathcal{M}\left(p_\mathcal{A}, p_\mathcal{B} \to \{k_f\}\right) = \left|M_m^0\right\rangle$$

where $\left|M_m^0\right\rangle$ denotes the amplitude of the process. Inserting this into (2.2) we obtain a theoretical prediction for the cross section. This is however only the leading contribution and therefore just a first approximation. To this prediction one can compute

[1] In the differential cross section we count the events where the outgoing particles have momenta in an interval $\left[k_i^j, k_i^j + \mathrm{d}k_i^j\right]$. The index i labels the particle whereas the index j labels the spatial component.

quantum corrections, which might turn out to be important. The first approximation of the quantum corrections is called next-to-leading order (NLO) and is one order higher in the coupling constant. NLO corrections can be of two types: either virtual (this means that they take into account a quantum fluctuation which is represented by a loop in the Feynman diagram) or real. In $\left|M_m^0\right\rangle$ the label "0" denotes the number of loops in the amplitude, whereas "m" is the number of final state particles. In the real corrections an additional particle is present in the final state ($m \to m+1$) and it is allowed to be arbitrarily collinear to the parton from which it was emitted and also its energy can be arbitrarily small. One can go even higher in the perturbative expansion by computing second order quantum corrections generally called next-to-next-to-leading order (NNLO) corrections. In fact experimental data on several observables often attain an accuracy of a few per cent or better, such that meaningful precision studies must rely on theoretical predictions that require corrections at NNLO accuracy. A cross section at NNLO is based on different amplitudes belonging to different Hilbert spaces: the amplitude for the production of m particles at two loops

$$|M_m\rangle = \left|M_m^0\right\rangle + \left(\frac{\alpha_s}{2\pi}\right)\left|M_m^1\right\rangle + \left(\frac{\alpha_s}{2\pi}\right)^2\left|M_m^2\right\rangle + \mathcal{O}\left(\alpha_s^3\right) , \tag{2.3}$$

the amplitude for $(m+1)$-particle production at one loop:

$$|M_{m+1}\rangle = \left|M_{m+1}^0\right\rangle + \left(\frac{\alpha_s}{2\pi}\right)\left|M_{m+1}^1\right\rangle + \mathcal{O}\left(\alpha_s^2\right) , \tag{2.4}$$

and the amplitude for the production of $(m+2)$ particles at tree-level

$$|M_{m+2}\rangle = \left|M_{m+2}^0\right\rangle + \mathcal{O}\left(\alpha_s^1\right) . \tag{2.5}$$

The probability is found by summing the absolute value squared of the different amplitudes:

$$\begin{aligned}\left|\mathcal{M}^{\mathrm{NNLO}}\right|^2 = \\ &\left\langle M_m^0|M_m^0\right\rangle + \left(\frac{\alpha_s}{2\pi}\right)\left(2\Re\left\langle M_m^0|M_m^1\right\rangle + 8\pi^2\left\langle M_{m+1}^0|M_{m+1}^0\right\rangle\right) \\ &+ \left(\frac{\alpha_s}{2\pi}\right)^2\left(2\Re\left\langle M_m^0|M_m^2\right\rangle + 2\left\langle M_m^1|M_m^1\right\rangle + 16\pi\Re\left\langle M_{m+1}^0|M_{m+1}^1\right\rangle + \left\langle M_{m+2}^0|M_{m+2}^0\right\rangle\right) ,\end{aligned} \tag{2.6}$$

where $\Re$ denotes the real part. All the QCD amplitudes are computed starting from the QCD Lagrangian density $\mathcal{L}_{\mathrm{QCD}}$. Before writing down the QCD Lagrangian we recall briefly the historical development which lead to it.

2.2 The origin of QCD

After the second world war the interest in nuclear and high energy physics was very high. This permitted to build a sequence of increasingly more powerful accelerators which, by probing matter at ever smaller distances, lead to the discovery of many new particles[1]. In the 60s there were so many different particles, that it was common to speak about a *particles zoo*. All these hadrons could successfully be classified on a group-theoretical basis in higher representations of SU(3) by M. Gell-Mann, Y. Dothan and Y. Ne'eman [28]. It was even possible to predict the existence of a further particle resonance which was discovered some time later and called Ω^-. The particles in the fundamental representation of $SU(3)_F$, building up all other particles, were called *quarks* and came in three *flavours* (therefore the label 'F'): up (u), down (d) and strange (s). In parallel the results of many deep-inelastic lepton-nucleon scattering (DIS) experiments were consistent with the *parton model*, which assumes that the nucleon is build up by pointlike constituents and the electron scatters incoherently against them in DIS experiments. However the description of some hadrons gave rise to problems. In particular some resonances were discovered, which have a fully symmetric spin- and flavour-wavefunction nevertheless they have a half-integer spin and therefore obey Fermi statistics. The canonical example is the resonance Δ^{++} which is a composite state of three valence up quarks and has spin $J_z = +3/2$:

$$\left|\Delta^{++}; +3/2\right\rangle \;=\; |u\uparrow\rangle\,|u\uparrow\rangle\,|u\uparrow\rangle\;. \tag{2.7}$$

This situation would imply a violation of Pauli's spin-statistic theorem. The Pauli-principle can be restored by introducing a new degree of freedom called *colour* [29] and assuming that the resonance is completely antisymmetric in this new quantum number:

$$\left|\Delta^{++}; +3/2\right\rangle \;=\; \frac{1}{\sqrt{6}} \sum_{i,j,k=1}^{3} \varepsilon_{ijk}\,|u_i\uparrow\rangle\,|u_j\uparrow\rangle\,|u_k\uparrow\rangle\;, \tag{2.8}$$

where ε_{ijk} is the completely antisymmetric Levi-Civita tensor. The idea behind the $SU(3)_C$ colour symmetry is that all hadrons are "white" or colour-less, this means that they must either be made by a totally antisymmetric composition of the three colours or by a colour-anticolour pair. The success of the colour-symmetry lead to the definitive development of Quantum Chromodynamics (chromo derives from the Greek *khrôma* and means colour) where the $SU(3)_C$ symmetry is promoted to a gauge symmetry. The corresponding gauge bosons, called gluons, transform by construction under the eight-dimensional adjoint representation. In the 70s, 80s and 90s three other heavier quark flavours were discovered. They can be ordered in three families as shown in Figure 1.1.

[1] For a broader historical overview, we refer to other books on QCD like [25], and QCD history as [9].

2.3 The QCD Lagrangian

QCD is an example of a non-Abelian Yang-Mills theory [30], whose Lagrangian density is composed by three important pieces:

$$\mathcal{L}_{QCD} = \mathcal{L}_{\text{inv.}} + \mathcal{L}_{\text{gauge-fixing}} + \mathcal{L}_{\text{ghost}} \,. \tag{2.9}$$

The first term $\mathcal{L}_{\text{inv.}}$ is invariant under local $\text{SU}(3)_C$ gauge transformations. It can be constructed starting from the Dirac Lagrangian by demanding local $\text{SU}(3)_C$ gauge invariance and it contains the kinetic terms of quark and gluon fields and all the quark-gluon and gluon-gluon interaction terms. Adopting Einstein's summation convention we can write it as

$$\mathcal{L}_{\text{inv.}} = \sum_f \bar{q}_{f_i} \left(i \not{D} - m_q \right)_{ij} q_{f_j} - \frac{1}{4} F^{\mu\nu,\,a} F^a_{\mu\nu} \,, \tag{2.10}$$

where the sum runs over all quark flavours f. The field strength tensor $F^a_{\mu\nu}$ and the covariant derivative $\not{D}$ can be written in terms of the gluon field A^a_μ as

$$F^a_{\mu\nu} = \partial_\mu A^a_\nu - \partial_\nu A^a_\mu - g_s \, f^{abc} \, A^b_\mu \, A^c_\nu \,, \tag{2.11}$$

$$\not{D}_{ij} = (\gamma^\mu D_\mu)_{ij} = \gamma^\mu \left(\delta_{ij} \partial_\mu + i \, g_s \, T^a_{ij} \, A^a_\mu \right) \,, \tag{2.12}$$

$$(m_q)_{ij} = m_q \delta_{ij} \,. \tag{2.13}$$

In the above equations g_s is the bare gauge coupling, T^a_{ij} the generators of the SU(3) gauge group in the fundamental representation and f^{abc} are its structure constants.

In a covariant gauge the large degeneracy between sets of gluon field configurations, which are equivalent under gauge transformations, requires the addition of two more terms to the QCD Lagrangian. A gauge-fixing term $\mathcal{L}_{\text{gauge-fixing}}$ and a term for the ghost fields $\mathcal{L}_{\text{ghost}}$, which are auxiliary fields η^a. Their interactions compensate for unphysical polarizations in 3-boson vertices and external gauge boson states. The popular choice of covariant gauge leads to the gauge fixing term

$$\mathcal{L}_{\text{gauge-fixing}} = \frac{1}{2\xi} \left(\partial^\mu A^a_\mu \right)^2 \,, \tag{2.14}$$

where ξ is a parameter contributing only to the overall normalization. The Lagrangian of the ghost fields is given by

$$\mathcal{L}_{\text{ghost}} = \partial_\mu \bar{\eta}^a \left(\partial^\mu \delta^{ab} + g_S \, f_{abc} \, A^{c,\mu} \right) \eta^b \,. \tag{2.15}$$

The two terms $\mathcal{L}_{\text{gauge-fixing}}$ and $\mathcal{L}_{\text{ghost}}$ break gauge symmetry by imposing a particular gauge choice. However a more general symmetry is still intact and was first derived by C. Becchi, A. Rouet and R. Stora [31]. From $\mathcal{L}_{QCD}$ it is possible to derive the

Feynman rules and compute scattering processes by making a perturbative expansion in the strong coupling constant α_s which is equal to

$$\alpha_s = \frac{g_s^2}{4\pi}\,. \tag{2.16}$$

A set of QCD Feynman rules in covariant gauge is given in Figure 2.2. In this thesis we

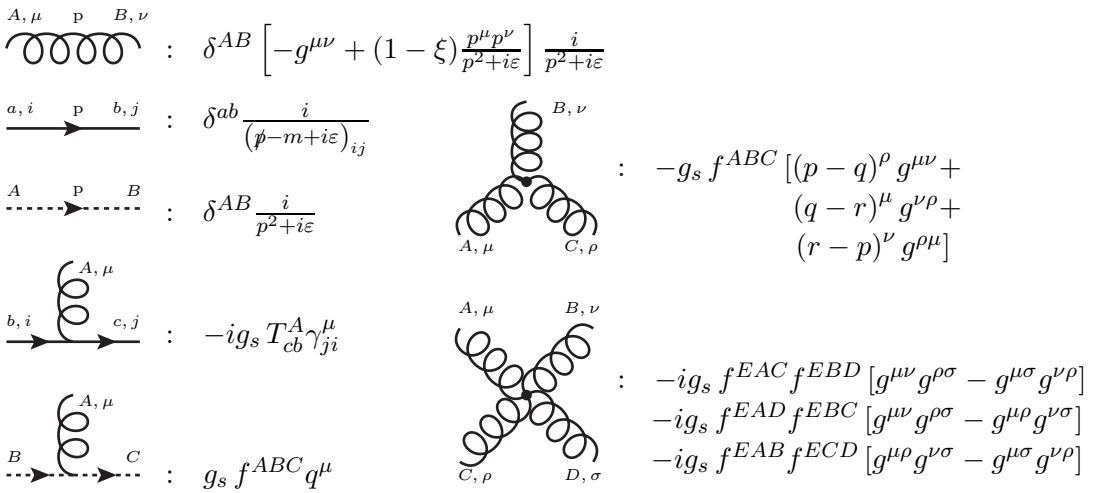

Figure 2.2: QCD Feynman rules in covariant gauge.

will consider scattering amplitudes for processes where the centre-of-mass (CM) energy Q is much larger than the quark mass m_q. The only exception is the top quark, which will be neglected since its mass is to high to be produced in the experiments we will consider. From a renormalization group analysis of quark masses [25, 26] it turns out that all masses can safely be set to zero in this regime. We will therefore work in a completely massless theory with only five active flavours ($N_F = 5$), unless something different is stated.

2.3.1 Renormalization and running coupling constant

In computing loop corrections to scattering processes one encounters divergencies due to very large momenta which can circulate in the loop. These divergencies are called ultraviolet (UV) divergencies. They are typically of the following form:

$$\int \mathrm{d}^4k \frac{1}{(k+p)^2\,k^2} \sim \lim_{\Lambda\to\infty}\int \mathrm{d}\Omega_3 \int_0^\Lambda \mathrm{d}k\,k^3 \frac{1}{(k^2)^2} \sim \lim_{\Lambda\to\infty}\int_0^\Lambda \frac{\mathrm{d}k}{k} \sim \lim_{\Lambda\to\infty}\ln\Lambda\,. \tag{2.17}$$

In a renormalizable theory UV divergencies can be absorbed in a redefinition of the parameters and the fields of the Lagrangian. Since we are neglecting all the quark

masses, the only a priori free parameter in the Lagrangian is the bare coupling parameter g_s. In massless QCD renormalization amounts in practice to replacing the fields by their renormalized counterparts and to redefining g_s. However, before absorbing the divergencies into the renormalized quantities, we need to find a way to isolate them. The mathematically most elegant method to do this is probably dimensional regularization [32], since it preserves gauge and Lorentz invariance[1]. Unlike in Quantum Electrodynamics (QED), where the point at which the subtraction to remove the UV divergences is naturally given by the on-shell conditions, in QCD one can choose at which scale μ the theory should be renormalized, since there is no a priori preferable scale. The renormalization procedure introduces therefore a new mass scale μ. In the modified minimal subtraction scheme ($\overline{\text{MS}}$) the bare coupling constant α_s^0 is related to the renormalized coupling $\alpha_s \equiv \alpha_s\left(\mu^2\right)$ evaluated at the renormalization scale μ^2 by

$$\alpha_s^0 \mu_0^{2\epsilon} S_\epsilon = \alpha_s \mu^{2\epsilon} \left[1 - \frac{2\beta_0}{\epsilon}\frac{\alpha_s}{2\pi} + \left(\frac{4\beta_0^2}{\epsilon^2} - \frac{2\beta_1}{\epsilon}\right)\left(\frac{\alpha_s}{2\pi}\right)^2 + \mathcal{O}\left(\alpha_s^3\right)\right], \tag{2.18}$$

where

$$S_\epsilon = (4\pi)^\epsilon e^{-\epsilon\gamma_E} \qquad \text{with the Euler constant} \quad \gamma_E = 0.5772\ldots$$

and μ_0^2 is the mass parameter introduced in dimensional regularization to maintain the coupling parameter of the Lagrangian dimensionless. The coefficient S_ϵ is an artefact of dimensional regularization. The coefficients β_0 and β_1 are the first two coefficients of the QCD β-function derived below and given in (2.23).

A physical dimensionless observable R should now be calculated as a perturbation series in the strong coupling α_s. We assume that R depends only on an energy scale Q. Since we are neglecting all quark masses, the observable R can depend only on the ratio Q^2/μ^2 and on the renormalized coupling α_s. In general, higher order corrections to the observable R are proportional to $\alpha_s^m \ln^n\left(Q^2/\mu^2\right)$ $(m \leq n+1)$. Although in principle we can choose the value of μ freely, those terms become large if μ is very different from Q. This leads to some restrictions on the choice of μ due to the requirement that the perturbative series in α_s converges well. Since μ is an arbitrary parameter, physical quantities like R cannot depend on the choice of it. Mathematically this can be written as

$$\mu^2 \frac{d}{d\mu^2} R\left(\frac{Q^2}{\mu^2}, \alpha_s\right) = \left(\mu^2 \frac{\partial}{\partial \mu^2} + \mu^2 \frac{\partial \alpha_s}{\partial \mu}\frac{\partial}{\partial \alpha_s}\right) R \stackrel{!}{=} 0\,. \tag{2.19}$$

We can rewrite this more compactly by introducing the variables

$$t = \ln\left(\frac{Q^2}{\mu^2}\right) \qquad , \qquad \beta\left(\alpha_s\right) = \mu^2 \frac{\partial \alpha_s}{\partial \mu^2}. \tag{2.20}$$

[1] An introduction to dimensional regularization can be found in many textbooks, we refer for example to [33] or [34].

The β function gives the evolution of the renormalized coupling α_s with respect to the arbitrary scale μ. It can be derived from the relation between the bare and the renormalized coupling given in (2.18). We rewrite it more generally as

$$\alpha_s^0 \;=\; Z_{\alpha_s}\left(\mu\right)\alpha_s\left(\mu\right), \tag{2.21}$$

where Z_{α_s} is the coupling renormalization factor. Since the bare coupling constant α_s^0 cannot depend on the arbitrary scale introduced for the renormalization

$$\mu^2\frac{\mathrm{d}}{\mathrm{d}\mu^2}\alpha_s^0 = 0\,.$$

From this equation we can derive the β-function, which in QCD is given by

$$\beta\left(\alpha_s\right) \;=\; \mu^2\frac{\partial\alpha_s}{\partial\mu^2} \;=\; -2\beta_0\left(\frac{\alpha_s}{2\pi}\right)^2 \;-\; 4\beta_1\left(\frac{\alpha_s}{2\pi}\right)^3 \;-\; 8\beta_2\left(\frac{\alpha_s}{2\pi}\right)^4 \;-\; \mathcal{O}\left(\bar{\alpha}_s^5\right)\,, \tag{2.22}$$

where

$$\begin{aligned}
\beta_0 &= \frac{1}{12}\left(11C_A - 2N_F\right) \;=\; \frac{1}{12}\left(33 - 2N_F\right),\\
\beta_1 &= \frac{1}{24}\left(17C_A^2 - 5C_AN_F - 3C_FN_F\right) \;=\; \frac{1}{24}\left(153 - 19N_F\right),\\
\beta_2 &= \frac{1}{3456}\left(2857C_A^3 + 54C_F^2N_F - 615C_FC_AN_F - 1415C_A^2N_F + 66C_FN_F^2 + 79C_AN_F^2\right)\\
&= \frac{1}{64}\left(\frac{2857}{2} - \frac{5033}{18}N_F + \frac{325}{54}N_F^2\right).
\end{aligned} \tag{2.23}$$

and $C_F = \frac{4}{3}$, $C_A = 3$ are the Casimir operator of SU(3) in the fundamental and adjoint representation. In terms of the number of colours N they can be expressed as

$$C_F = \frac{N^2-1}{2N} \qquad ; \qquad C_A = N\,. \tag{2.24}$$

With (2.20) equation (2.19) can be rewritten as

$$\left(-\frac{\partial}{\partial t} \;+\; \beta\left(\alpha_s\right)\frac{\partial}{\partial\alpha_s}\right) R\left(e^t,\,\alpha_s\right) \;=\; 0\,. \tag{2.25}$$

This partial differential equation can be solved defining a new function $\alpha_s\left(Q^2\right)$ called the *running coupling constant*. The running coupling constant is defined by

$$t \;=\; \int_{\alpha_s}^{\alpha_s(Q^2)} \frac{dx}{\beta\left(x\right)}, \tag{2.26}$$

where $\alpha_s \equiv \alpha_s\left(\mu^2\right)$ is the value of the renormalized coupling constant complying with our choice of the renormalization scale μ: it plays the role of initial condition for the running coupling constant. Differentiating (2.26) we obtain

$$\frac{\partial\,\alpha_s\left(Q^2\right)}{\partial\,t} \;=\; \beta\left(\alpha_s\left(Q^2\right)\right) \qquad , \qquad \frac{\partial\,\alpha_s\left(Q^2\right)}{\partial\,\alpha_s} \;=\; \frac{\beta\left(\alpha_s\left(Q^2\right)\right)}{\beta\left(\alpha_s\right)}, \tag{2.27}$$

and therefore $R\left(1, \alpha_s\left(Q^2\right)\right)$ is a solution of equation (2.25). This means that all of the scale dependence in R enters through the running of the coupling constant. Solving (2.26) and knowing $R\left(1, \alpha_s\right)$ allows to predict the dependence of R on Q.

If both, $\alpha_s\left(\mu^2\right)$ and $\alpha_s\left(Q^2\right)$, are in the perturbative region, we can truncate the β-function at a given order and solve equation (2.26). Considering the β-function only at leading order we find

$$\frac{1}{\bar{\alpha}_s\left(Q^2\right)} = \frac{1}{\bar{\alpha}_s\left(\mu^2\right)} + 2\beta_0 \ln\left(\frac{Q^2}{\mu^2}\right), \tag{2.28}$$

where $\bar{\alpha}_s(\mu^2) \equiv \alpha_s(\mu^2)/(2\pi)$, and thus

$$\bar{\alpha}_s\left(Q^2\right) = \frac{\bar{\alpha}_s\left(\mu^2\right)}{1 + 2\bar{\alpha}_s\left(\mu^2\right)\beta_0 \ln\left(\frac{Q^2}{\mu^2}\right)}. \tag{2.29}$$

Inserting this in $R\left(1, \alpha_s\left(Q^2\right)\right)$ and expanding $\bar{\alpha}_s\left(Q\right)$ in powers of $\bar{\alpha}_s\left(\mu^2\right)$ we obtain again an expansion in powers of $\bar{\alpha}_s^{n+1} \ln^n\left(Q^2/\mu^2\right)$. This means that the running coupling constant resums all these logarithmic coefficients. Considering higher order terms in the β-function leads to a resummation of more subleading logarithmic terms of the form $\alpha_s^m \ln^n\left(Q^2/\mu^2\right)$ with $(m < n+1)$. From (2.29) it is also clear that the running coupling constant $\bar{\alpha}_s\left(Q^2\right)$ goes to zero, as t becomes very large. This is the so-called *asymptotic freedom* of QCD. Since large momentum means short distances, the behaviour of the running coupling constant for large Q^2 tells us that the interaction between quarks and gluons is relatively weak at short distances. On the other hand it is very strong at long distances and it leads to the so-called *confinement*. The fact that QCD is a non-Abelian theory and therefore gluons are charged under the same interaction, can be seen as an intuitive explanation of this latter phenomenon. The sign of β_0 plays a crucial role[1] in determining whether the coupling increases or decreases.

It is usual in QCD to define a parameter Λ_{QCD} where the coupling diverges. Starting from (2.28) we define

$$\frac{1}{\bar{\alpha}_s\left(Q^2 = \Lambda^2_{\mathrm{QCD}}\right)} = 0. \tag{2.30}$$

Setting the thereby obtained Λ_{QCD} as the new reference parameter we find

$$\bar{\alpha}_s\left(Q^2\right) = \frac{1}{2\beta_0 \ln\left(\frac{Q^2}{\Lambda^2_{\mathrm{QCD}}}\right)}. \tag{2.31}$$

The exact numerical value of Λ_{QCD} depends on the definition of the β_i coefficients and on the considered order in $\bar{\alpha}_s$; generally it is around $\Lambda_{\mathrm{QCD}} = 200$ MeV. It means

[1] In fact, it is easy to see that if the number of flavours were big enough, the negative sign of β_0 becomes positive and the coupling would have a different behaviour.

that the coupling constant becomes large and the perturbation theory has no predictive power any more for scales comparable with the masses of the light hadrons ($Q \approx 1$ GeV).

In our calculations we will use the following renormalization scale dependence for the coupling constant in the $\overline{\text{MS}}$ scheme [35] (we now slightly change the notation using μ instead of Q for the momentum scale at which we compute the running coupling constant):

$$\alpha_s(\mu) = \frac{\pi}{\beta_0 \ln\left(\frac{\mu^2}{\Lambda^2_{\text{QCD}}}\right)}\left[1 - \frac{\beta_1}{\beta_0^2}\frac{\ln\left(\ln\left(\frac{\mu^2}{\Lambda^2_{\text{QCD}}}\right)\right)}{\ln\left(\frac{\mu^2}{\Lambda^2_{\text{QCD}}}\right)} + \frac{1}{\beta_0^2 \ln\left(\frac{\mu^2}{\Lambda^2_{\text{QCD}}}\right)^2}\left(\frac{\beta_1^2}{\beta_0^2}\left(\ln\left(\ln\left(\frac{\mu^2}{\Lambda^2_{\text{QCD}}}\right)\right)^2 - \ln\left(\ln\left(\frac{\mu^2}{\Lambda^2_{\text{QCD}}}\right)\right) - 1\right) + \frac{\beta_2}{\beta_0}\right)\right] \tag{2.32}$$

The world average of $\alpha_s(M_{Z^0}) = 0.1184$ [36], where M_{Z^0} is the mass of the Z^0 boson, yields $\Lambda_{\text{QCD}} = 213$ MeV.

2.4 Infrared divergencies

In calculating QCD cross sections one does not only encounter UV divergencies, but also infrared (IR) divergencies. However, unlike UV divergencies, which can be absorbed in a redefinition of the parameters in the Lagrangian, IR divergencies[1] can not be "renormalized away"[2].

We can see more explicitly how IR singularities arise, by considering a generic $2 \to 2$ process with an outgoing quark-antiquark pair and by assuming that the outgoing quark emits a further gluon:

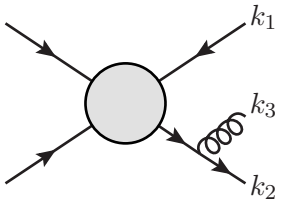

We shall assume that all the three momenta k_1, k_2, k_3 are outgoing. The internal fermion propagator of the quark goes on-shell, if the energy of the gluon or the angle

[1] By IR singularities we mean both soft and collinear singularities.

[2] In an effective theory approach like Soft-collinear-effective-theory (SCET) IR divergences can be treated like UV divergences and absorbed into renormalization constants. Following this approach several important studies on the IR structure of QCD could recently be made [37–40].

between the quark and the gluon goes to zero

$$\frac{1}{(k_2 + k_3)^2} = \frac{1}{2E_1E_3(1 - \cos\theta_{13})} \longrightarrow \infty \quad \text{if} \quad E_3 \to 0 \quad \text{or} \quad \theta_{13} \to 0.$$

In the collinear case ($\theta_{13} \to 0$) the propagator becomes strictly singular only in the limit of massless quarks. Taking into account also the spinors of the outgoing quark (antiquark) it is easy to see that the limit $E_1 \to 0$ leads to an integrable singularity. The internal fermion propagator is off-shell by an amount $p_{g_\perp}^2 = 2p_q \cdot p_g$, where $p_{g_\perp}$ is the transverse momentum of the gluon relative to the quark-antiquark system. The virtual quark (antiquark) survives for a time $1/p_{g_\perp}$ before the gluon is radiated and can therefore travel an indefinite distance if the radiated gluon is soft, collinear or both. We therefore see that the origin of IR singularities are processes happening at large distances. We already know from the previous section that perturbative QCD is not applicable for long distances, however the real reason for the IR singularities goes even beyond this. In fact, divergencies due to soft bremsstrahlung are already known from QED, where the emission of a soft photon by a scattered electron is enhanced by a factor of $\ln\left(\frac{q^2}{m^2}\right)$ for collinear radiation[1]. The parameter m here is the mass of the electron and q is the 4-momentum transferred to the electron in the scattering process. The same holds for quarks emitting soft and collinear gluons. The real theoretical problem is the assumption made in constructing the quantum field theory, that the asymptotic states are free of any interaction, which is not true if a particle can propagate indefinitely before radiating soft bremsstrahlung. The real asymptotic states can be perturbatively approximated by constructing coherent states [41]. On the other side, both in QCD and in QED there is an experimental limit in the sensitivity to soft and collinear radiation. In both cases it is experimentally impossible to measure indefinitely soft radiation[2]. In these cases quantum mechanics tells us that we have to sum over all possible and undistinguishable reactions that lead to the same final state configuration. This idea was formalized in a theorem by F. Bloch and A. Nordsieck [42] and by T. Kinoshita [43], T. Lee and M. Nauenberg [44] (the so-called KLN theorem), which states that observable transition probabilities are free of IR singularities. In fact, in summing over all possible configurations we have to take into account also virtual

[1] A detailed discussion of IR-divergencies in QED can be found for example in [33].

[2] There is nevertheless a big difference between QED and QCD in how collinear and soft emission is measured experimentally. In QED there is no confinement and the final state, including soft bremsstrahlung, can in principle be measured. The bremsstrahlung detected in an experiment only depends on the sensitivity and the energy resolution of the detector. A soft photon is only measurable if the finite resolution of the detector allows it. In QCD however, there are also physical restrictions in addition to the technical ones. Whether a soft or collinear gluon is radiated or not, the quarks will undergo some soft interaction in the hadronization process, until all coloured particles are collected into colour-singlet hadrons. In a final state the particles produced in the hadronization and the result of the hadronization of a soft gluon are not distinguishable if the gluon has a transverse momentum smaller than the typical scale of soft gluon interactions: roughly 1 GeV.

corrections, which also contain IR divergencies when the momentum in the loop tends to zero leading to long-lived virtual fluctuations. Because of the KLN theorem the IR divergencies appearing in the virtual contributions exactly cancel against the real ones. The big difference between the real and the virtual case is that in the latter one, divergencies occur already in the loop integral and, being part of the matrix element, they can be extracted explicitly before integrating over the phase space, whereas in the former case they become explicit only once phase space integration is performed. How to cancel these singularities against each other when computing differential cross sections is the subject of Chapter 3. Later in this chapter we will compute an example where the cancellation of real and virtual IR singularities can be seen explicitly. We will also see a case where the KLN theorem in principle applies, but is not used in practice. In this case we need to resort to other strategies to cancel the divergencies.

Real experiments cannot measure quarks and gluons, but rather hadrons. For this reason, before looking at some typical QCD reactions, we need to define more precisely what we meant at the very beginning of this chapter in speaking about jets.

2.5 Jet observables

As already seen, QCD is characterized by the phenomena of confinement and asymptotic freedom. Confinement describes the fact that quarks and gluons do not exist as free particles but only in bound states. On the other hand, asymptotic freedom tells us that the dynamics of QCD reactions at high energies are determined by quarks and gluons. These two peculiarities of QCD allow us to investigate the nature of partons at high energy colliders, but do not permit us to look at them directly. What we can measure are just final states, which consist of several hadrons and leptons, whose energy and momentum are measured in detectors. Between the hard process (i.e. what happens at parton level) and the measured final state, the process of hadronization takes place. This is not a perturbative process and therefore cannot be computed in the framework of perturbative QCD. In Chapter 5 we will look at the issue of hadronization more carefully. In order to understand what happens at the parton level, we need some observables which are independent of the final state particles' nature. If the final state particles produced in the hadronization are originated with a small transverse momentum, the final state will consist of some well-defined clusters of hadrons and leptons. It is reasonable to think, though far from trivial, that each cluster results from the hadronization of a parton produced in the hard process. For this reason, collimated sprays of particles in the final state are often grouped together in so-called *jets*. It is not obvious at all, that hadronization corrections to QCD parton level predictions are small. Fortunately hadronization studies have shown that at least at high energies, these corrections are indeed small and theoretical predictions can be reliably compared

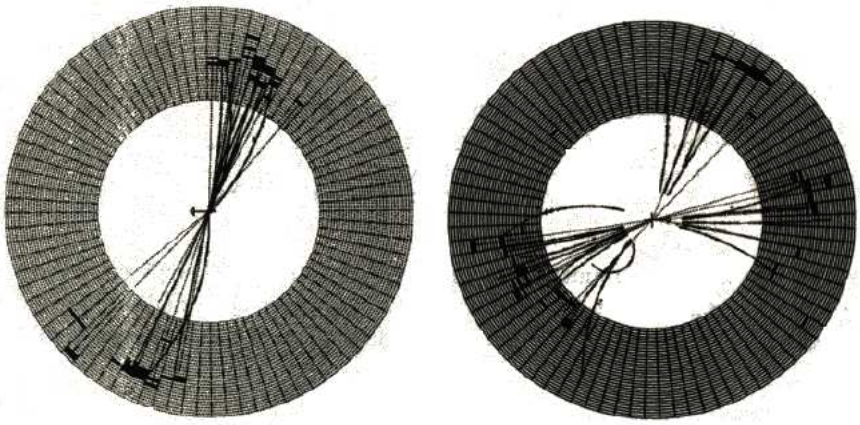

Figure 2.3: A two-jet (left) and a three-jet (right) event measured by the Jade detector at the e^+e^- collider PETRA (DESY).

to experimental data. The study of jets permits to understand and to measure many aspects of QCD. This is the reason why jets have become an important bridge between theoretical calculations at parton level and experimentally measured hadronic final states. In practice, jets are studied using so-called *jet observables*. These observables have to satisfy the criterion of infrared safety, which consists of two requirements.

1. If, in a final state consisting of m particles, two particles have collinear momenta, the observable should allow to consider the two collinear particles as one particle with a momentum equal to the sum of the two original ones. This criterion is called *collinear safety*.

2. A jet observable should also be *infrared safe*. This means that if in a final state consisting of m particles one of them has an almost vanishing energy, the observable should allow to neglect it.

We can write these two criteria more formally:

$$\begin{aligned} \mathcal{O}_m\left(p_1, p_2, \ldots, p_m\right) &\overset{p_1 \| p_2}{\longrightarrow} \mathcal{O}_{m-1}\left(p_1 + p_2, p_3, \ldots, p_m\right) , \\ \mathcal{O}_m\left(p_1, p_2, \ldots, p_m\right) &\overset{E_1 \to 0}{\longrightarrow} \mathcal{O}_{m-1}\left(p_2, p_3, \ldots, p_m\right) . \end{aligned} \tag{2.33}$$

There are several infrared and collinear safe jet observables. More generally jets are defined by means of jet algorithms, which are algorithms applied both at parton level and at hadron level, to define which particle forms or belongs to which jet. In e^+e^- colliders a very popular class of jet observables are event-shape observables. We will

define them more exactly later and study them in great detail in Chapter 4. At the beginning of this chapter we introduced the jet function $J_m^{(n)}$ as an observable dependent weight in the phase space integral. More precisely it defines the procedure for building m jets out of n partons. It is a function of the final state momenta $k_1, \ldots, k_n$ and satisfies the criteria (2.33) for IR safety. In general $J_m^{(n)}$ contains θ- and δ-distributions. In considering event-shape observables $J_m^{(n)}$ can also represent the definition of the n-parton contribution to an event-shape observable related to m-jet final states.

2.5.1 Jet algorithms

As already anticipated, in a scattering process the bridge between a measured final state and the hard process are the clusters of final state particles called jets. Often it is experimentally not obvious at all, how final state particles have to be grouped into jets. The difficulty consists in distinguishing, for example, a soft emitted gluon from the result of a hadronization process. The definition of *jet algorithms* permits a suitable procedure for the classification of a final state consisting of hadrons (experimentally) or quarks and gluons (theoretically) according to the number of jets. In practice a jet algorithm consists of two important parts. The algorithm itself is a set of rules for grouping the particles into jets and usually involves a set of parameters that specify how close two particles must be to belong to the same jet. Furthermore, there is the so-called *recombination scheme*, which indicates what momentum must be assigned to the combination of two particles. The Snowmass accord of 1990 [45] collects all the main features a jet algorithm should have in order to be successfully used both in theory and in experiments. There are two broad categories of jet algorithms: the cone algorithms and the sequential recombination algorithms. Today the first ones are mainly used in hadron colliders and are based on the idea that a jet consists of a spray of particles contained in a cone around the particle with larger transverse momentum. Recently, in view of the large jet activity which will be seen in collisions at the LHC, a lot of progress was made in the development of fast and theoretically well defined cone algorithms. The *SISCone* algorithm presented in [46] is a seedless[1] and IR safe algorithm but, instead of taking a time of order $\mathcal{O}(N2^N)$ to find jets among N particles as older seedless algorithms do [47], it runs in polynomial $(N^2 \ln N)$ time.

Sequential recombination algorithms found their roots in electron-positron collider experiments. The idea behind them is to reconstruct jets by repeatedly combining the closest pair of particles according to some predefined distance measure. They are usually simpler to state than cone algorithms and they are somehow believed to go beyond just finding the jets since they assign a sequence to the clustering procedure

[1] The directions of dominant energy flow are usually found by taking some (or all) of the event particles as trials: so-called *seeds*. However this procedure often leads to infrared unsafe algorithms since the addition of a new soft gluon may give a new stable cone.

which is somewhat connected to the branching at the parton level. Since in this thesis we will concentrate mainly on observables in e^+e^- collisions, we look a bit closer at recombination algorithms[1]. Historically the JADE algorithm [49] is one of the most important algorithms of this kind and for this reason we will briefly describe it. We consider the production of m particles with momenta $k_1, \ldots, k_m$, in an electron-positron annihilation process. This can be thought both at the parton level in a theoretical computation or at hadron level in a real experimental final state (Figure 2.3). The number of jets in such a final state can be determined by fixing a minimum invariant mass y_{cut} and then compute the quantity

$$y_{ij}^{\text{JADE}} = \frac{2E_iE_j\,(1 - \cos\theta_{ij})}{s}\,, \tag{2.34}$$

where s is CM energy, for each pair of particles i, j. Among all the y_{ij} we pick out the minimum

$$y_{\text{min}} = \min_{i,j}\left(y_{ij}^{\text{JADE}}\right)$$

and check if it is greater than the fixed y_{cut}. If $y_{\text{min}} < y_{\text{cut}}$, the two particles i and j used to compute y_{min} are recombined in a new pseudoparticle with a momentum defined by the recombination scheme. Three main schemes exist in literature:

- the E-scheme: the two 4-momenta are summed together: $k_{ij} = k_i + k_j$,
- the E_0-scheme: the two energies are summed together:

$$E_{ij} = E_i + E_j \quad \text{and} \quad \vec{k}_{ij} = \frac{E_{ij}}{\left|\vec{k}_i + \vec{k}_j\right|}\left(\vec{k}_i + \vec{k}_j\right)\,,$$

  such that $m_{ij} = 0$,
- the P-scheme: the two 3-momenta are summed together:

$$E_{ij} = \left|\vec{k}_i + \vec{k}_j\right| \quad \text{and} \quad \vec{k}_{ij} = \vec{k}_i + \vec{k}_j\,,$$

  such that $m_{ij} = 0$.

This procedure can be applied several times, until $y_{ij}^{\text{JADE}} > y_{\text{cut}}$ for all remaining pairs of particles. At this point the number of pairs y_{ij}^{JADE} corresponds to the number of jets. This algorithm is illustrated in Figure 2.4.

From the theoretical point of view, the JADE algorithm has the advantage that it satisfies the criteria (2.33), however it also suffers from some limitations. It has the tendency to reconstruct spurious jets. The presence of the term E_iE_j in (2.34) favours to recombine two soft particles even if they are moving in opposite directions. An example is given in Figure 2.5. Although the two gluons are collinear to the two

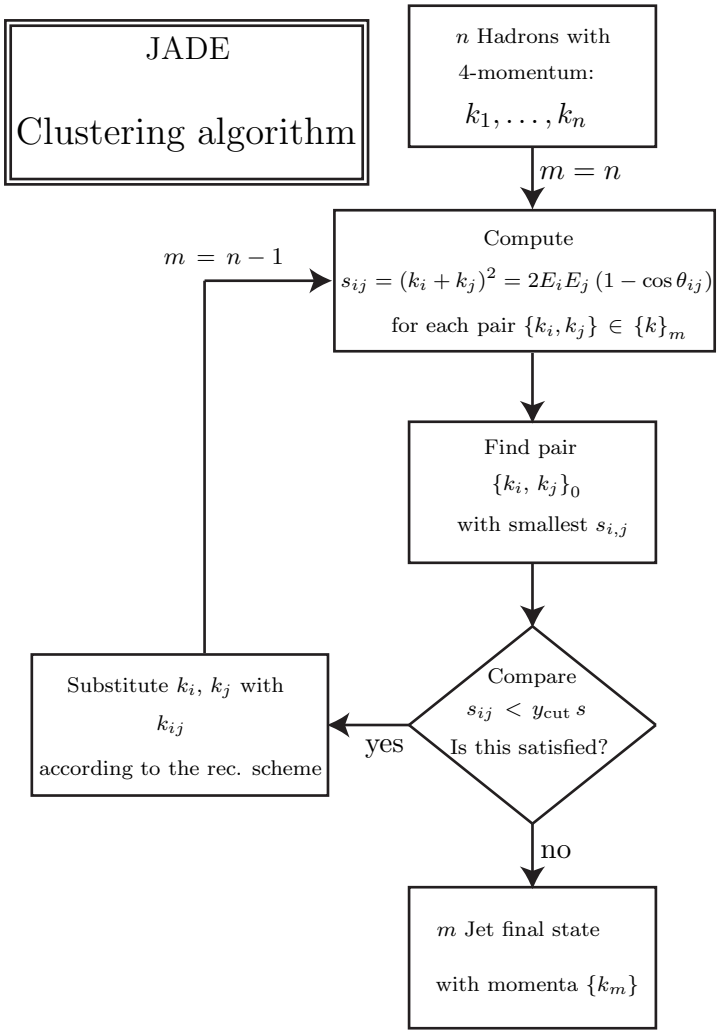

Figure 2.4: Diagram for a typical clustering algorithm.

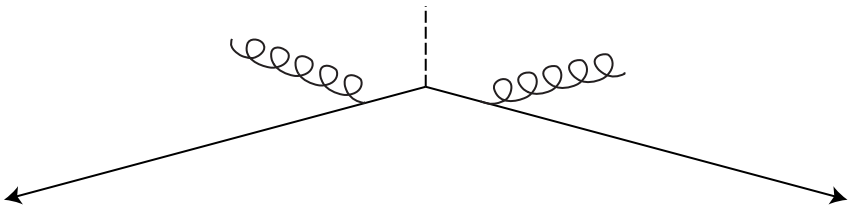

Figure 2.5: A typical event classified by the JADE algorithm as three-jet event.

quarks, if their energy is small enough, they are clustered to form a third jet which does not coincide with any of the original partons of the event. This problem of non-local soft correlation can be overcome by defining a slightly modified variant of the JADE algorithm, which is called the $k_\perp$-algorithm or Durham algorithm [50]. Instead of the minimum of the invariant mass squared, the $k_\perp$-algorithm minimizes a quantity, which for small angles between the partons corresponds to the relative transverse momenta. In the CM frame the Durham algorithm clusters hadrons or partons using the condition

$$y_{ij}^D = \frac{2 \min\left(E_i^2, E_j^2\right)(1 - \cos\theta_{ij})}{s}. \tag{2.35}$$

With this new criterion, the configuration in Figure 2.5 is classified in a more natural way as a two-jet event. The Durham jet algorithm can be also used to define an event-shape variable. We will come back to this in the next section.

2.5.2 Event-shape variables

Event-shape variables are mainly used to define a quantity, generically called y here, which characterizes the topology of an event. The idea is to parameterize in a smooth way the topology of hadronic final states by studying its energy-momentum flow. Event-shape observables were developed in the context of electron-positron annihilation processes but, although this still remains the main field of application, some attempt to use them also in lepton-hadron or hadron-hadron colliders has been proposed and studied recently [51–53]. Despite of this, in this thesis we will consider them only in high precision calculation for e^+e^- collision. Event-shape variables are normalized in order to be dimensionless and independent of the production cross section. The range of values such a variable can take is usually delimited by the minimal configuration of two jets in the final state $y \to 0$, and an upper kinematic limit y_{max}, which in some cases corresponds to either completely spherical or at least a symmetric event configuration. In the following we briefly give the definitions of the variables which we will study in Chapter 4:

Thrust: T [54, 55] The thrust is defined with a unit vector $\vec{n}_T$ called the thrust axis, which maximizes the following quantity:

$$T = \max_{\vec{n}_T}\left(\frac{\sum_i |\vec{p}_i \cdot \vec{n}_T|}{\sum_i |\vec{p}_i|}\right), \tag{2.36}$$

where the sum extends over all final state particles i of the event. In order to be consistent with the limit $y \to 0$ being the two jet limit, we consider $\tau = 1 - T$.

[1] For a more general analysis of the recent developments in this field we refer to [48].

Heavy jet mass: ρ [56] Considering a plane perpendicular to the thrust axis $\vec{n}_T$, one can divide the event in two hemispheres H_1 and H_2. For each hemisphere the invariant mass squared is given by

$$M_{H_i}^2 = \left(\sum_{n \in H_i} p_n \right)^2 . \tag{2.37}$$

The heavy jet mass ρ is defined as the larger of the two hemisphere masses normalized over the total visible energy $E_{\text{tot-vis.}}$

$$\rho \equiv \frac{\max\left(M_{H_1}^2, M_{H_2}^2\right)}{E_{\text{tot-vis.}}^2} . \tag{2.38}$$

Wide jet broadening: B_W [57] A measure of the broadening of particles in transverse momentum with respect to the thrust axis can be calculated for each hemisphere H_i using

$$B_i = \frac{\sum_{k \in H_i} |\vec{p}_k \times \vec{n}_T|}{2 \sum_j |\vec{p}_j|} , \quad i = 1, 2 , \tag{2.39}$$

where j runs over all of the particles in the event. The wide jet broadening is the larger of the two hemisphere broadenings:

$$B_W = \max\left(B_1, B_2\right) . \tag{2.40}$$

In analogy one can also define the narrow jet broadening as $B_N = \min\left(B_1, B_2\right)$.

Total jet broadening: B_T The total jet broadening is the sum of wide jet broadening and narrow jet broadening:

$$B_T = B_W + B_N . \tag{2.41}$$

C-parameter: C [58, 59] The linearized momentum tensor $\Theta^{\alpha\beta}$ is defined as

$$\Theta^{\alpha\beta} = \frac{1}{\sum_i |\vec{p}_i|} \sum_i \frac{p_i^\alpha p_i^\beta}{|\vec{p}_i|} , \tag{2.42}$$

where the index i runs over all the final state momenta $\vec{p}_i$. This tensor has three eigenvalues λ_j, $j = 1, 2, 3$ satisfying

$$0 \leq \lambda_j \leq 1 \qquad , \qquad \sum_j \lambda_j = 1 .$$

The C-parameter is defined as

$$C = 3 \left(\lambda_1\lambda_2 + \lambda_2\lambda_3 + \lambda_3\lambda_1\right) . \tag{2.43}$$

Durham jet resolution parameter: Y_3 [50, 60–63] As anticipated, the Durham jet algorithm (2.35) can also define an event-shape variable. The Y_3 value for an event is the threshold value of the resolution parameter y_{cut}, below which the event is classified as a two-jet event and not as a three-jet event any more. It is usual to consider $\ln(Y_3)$ instead of only Y_3. A detailed description of this event-shape variable is given in [64].

2.6 Born level QCD cross sections

In this section we introduce the main features of two processes which will come up again in the following chapters. We will first compute the leading order cross section for electron-positron annihilation into 3 jets. In Chapter 4 we will use NNLO results and match them to resummation calculations. In Chapter 5 we will add power corrections arising from analytical models of non-perturbative contributions. In Chapter 3 we will review how the NNLO results for e^+e^- annihilation could be computed and we will extend this method to compute processes in deep-inelastic scattering. The formalism developed in the following section on DIS will also be useful to understand the comparisons made to cross-check our calculations with results already available in the literature.

2.6.1 e^+e^--annihilation into 3-jets

Electron-positron annihilation to hadrons plays historically a very prominent role for QCD phenomenology, and it provides also the simplest colliding beam process that can be described using perturbative QCD. The simplicity is twofold: on one side the initial state particles have well-defined energies, allowing to determine the centre-of-mass energy of the hard collision with high accuracy, on the other side the initial state leptons annihilate into a colourless photon or Z^0-boson via electroweak interaction providing a very "clean" final state environment. All the partonic and jet activity belongs clearly to the final state. This is not the case in proton-proton collisions, where the remnants of the initial state proton also appear as jets in the final state, though usually at high rapidities.

The leading order process is given by the annihilation of e^+e^- into a quark-antiquark pair, which will then emit further soft gluons and finally hadronize into 2 jets. A typical 2-jet final state is shown left in Figure 2.3. The Feynman diagram contributing to the process is shown in Figure 2.6, which also specifies the definition of the momenta. The squared amplitude, summed over final state spins, colours and quark flavour and averaged over initial state spins can be factorized into a tensor describing the leptonic

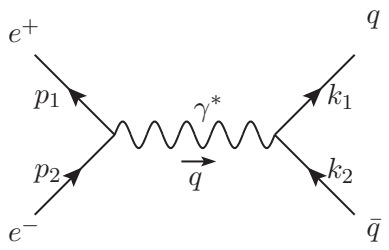

Figure 2.6: Leading order Feynman diagram for $e^+e^- \to 2$ jets.

part $L^{\mu\nu}$ and a tensor describing the hadronic part $H_{\mu\nu}$

$$\frac{1}{4}\sum_{\text{Spin}} \left|\mathcal{M}\left(e^+e^- \to 2 \text{ jets}\right)\right| = L^{\mu\nu}\frac{1}{s^2}H_{\mu\nu}\,, \tag{2.44}$$

where

$$s = q^2 = (p_1+p_2)^2 = 2p_1p_2 = (k_1+k_2)^2\ .$$

The leptonic tensor corresponds to the square of the leptonic part, which can be seen as a cut[1] photon self-energy at 1-loop

$$L_{\mu\nu} = \tfrac{1}{4}$$ 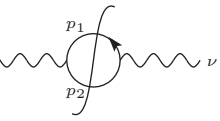 $$= e^2\,(p_1^\mu p_2^\nu + p_2^\mu p_1^\nu - p_1\cdot p_2\, g^{\mu\nu}).$$

The factor 1/4 is due to the average over the initial leptons spin and e is the electromagnetic coupling constant usually also written in terms of the fine structure constant

$$\alpha = \frac{e^2}{4\pi}\,.$$

The expression for $H_{\mu\nu}$ is similar to the one of $L^{\mu\nu}$ with k_1, k_2 instead of p_1, p_2 and a prefactor taking into account the different quark electric charges Q_f and the number of colours N. Both tensors satisfies

$$q_\mu L^{\mu\nu} = q^\mu H_{\mu\nu} = 0\,, \tag{2.45}$$

which is a consequence of QED gauge invariance. Expressing the matrix element in terms of the kinematically invariant Mandelstam variables

$$s = (p_1+p_2)^2 \quad ; \quad t = (p_1-k_1)^2 \quad ; \quad u = (p_1-k_2)^2$$

[1] For an introduction to cut-techniques we refer e.g. to [65].

we find

$$\frac{1}{4}\sum_{\text{Spin}}\left|\mathcal{M}\left(e^+e^-\to\ q\bar{q}\right)\right|^2 = 2e^2N\sum_f Q_f^2\,\frac{t^2+u^2-\epsilon s^2}{s^2}\,. \tag{2.46}$$

If we are not interested in the angular correlation between the leptons and the partons we can use the orientation-averaged lepton tensor, which in d dimensions is given by

$$\langle L^{\mu\nu}\rangle \;=\; \frac{e^2}{2}\frac{d-2}{d-1}\left(-g^{\mu\nu}+\frac{q^\mu q^\nu}{q^2}\right)s\,. \tag{2.47}$$

Because of (2.45) only the first term in the parenthesis gives a non-zero contribution and we find

$$\begin{aligned}\frac{1}{4}\sum_{\text{Spin}}\left|\mathcal{M}\left(e^+e^-\to\ 2\text{ jets}\right)\right|^2 &= s\,e^2\frac{1-\epsilon}{3-2\epsilon}\left(-g^{\mu\nu}\right)\frac{1}{s^2}H_{\mu\nu}\\ &= 4\,e^4\frac{(1-\epsilon)^2}{3-2\epsilon}N\sum_f Q_f^2\,.\end{aligned} \tag{2.48}$$

The total cross section can be found by integrating over the two particle phase space. Because of momentum conservation the integration turns out to be trivial[1] and the total cross section is thus

$$\sigma_0 = \alpha^2 N\sum_f Q_f^2\frac{(1-\epsilon)^2}{3-2\epsilon}2^{2+2\epsilon}\pi^{1+\epsilon}\frac{\Gamma(1-\epsilon)}{\Gamma(2-2\epsilon)}s^{-1-\epsilon}\overset{\epsilon\to 0}{=}\frac{4\pi\alpha^2}{3s}N\sum_f Q_f^2\,. \tag{2.49}$$

In order to obtain a three jet final state, the $q\bar{q}$-pair must emit at least a further hard gluon. The probability for the emission of a gluon from a quark (antiquark) is proportional to the strong coupling constant α_s. For this reason the precise determination of $e^+e^-\to\ 3$ jet observables plays a very important role in the determination of the strong coupling constant. Figure 2.7 shows the relevant Feynman diagrams without the leptonic part, which remains unchanged. Instead of considering the reaction $e^+e^-\to\ q\bar{q}g$ we can therefore just consider the decay $\gamma^*\to\ q\bar{q}g$ knowing from eq. (2.48) that

$$\frac{1}{4}\sum_{\text{Spin}}\left|\mathcal{M}\left(e^+e^-\to\ q\bar{q}g\right)\right|^2 = \frac{e^2}{s}\frac{(1-\epsilon)}{(3-2\epsilon)}\sum_{\text{Spin}}\left|\mathcal{M}\left(\gamma^*\to\ q\bar{q}g\right)\right|^2\,. \tag{2.50}$$

The computation of the spin averaged matrix element in $d=4-2\epsilon$ dimensions gives

$$\begin{aligned}\sum_{\text{Spin}}\left|\mathcal{M}\left(\gamma^*\to\ q\bar{q}g\right)\right|^2 =& 4\pi\alpha_s\mu^{2\epsilon}N\,C_F\,e^2\sum_f Q_f^2\\ &\times\ 8\,(1-\epsilon)\left[\frac{s_{23}}{s_{13}}+\frac{s_{13}}{s_{23}}+2\frac{s\,s_{12}}{s_{13}s_{13}}-\epsilon\left(\frac{s_{23}}{s_{13}}+\frac{s_{13}}{s_{23}}+2\right)\right],\end{aligned} \tag{2.51}$$

[1] The explicit computation is reported in Appendix B and the result is given in eq. B.3.

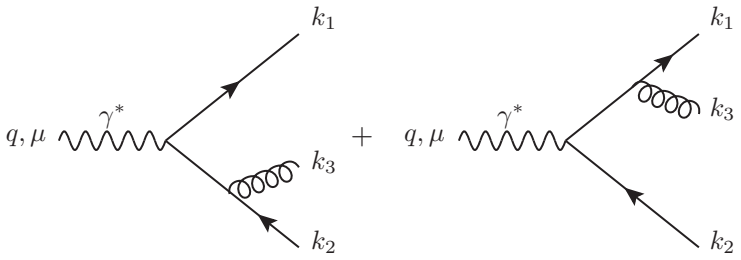

Figure 2.7: Next-to-leading real correction to $e^+e^- \to$ 2 jets. Only the hadronic part is shown.

where the invariants s_{ij} are defined as $s_{ij} = (k_i + k_j)^2$. In $d = 4$ dimensions ($\epsilon = 0$) this can be written in a very compact form

$$\frac{1}{4}\sum_{\text{Spin}} \left|\mathcal{M}\left(\gamma^* \to q\bar{q}g\right)\right|^2 = 32\pi\alpha_s e^2 N C_F \sum_f Q_f^2 \frac{x_1^2 + x_2^2}{(1-x_1)(1-x_2)} \tag{2.52}$$

where $x_i = \frac{2qk_i}{s}$. In the centre-of-mass frame $x_i = 2E_i/\sqrt{s}$, and the sum of them gives

$$\sum_i x_i = \frac{2}{\sqrt{s}}\left(E_q + E_{\bar{q}} + E_g\right) = 2\,.$$

Furthermore it is easy to show that the x_i satisfy the following constraints:

$$0 \le x_i \le 1 \quad ; \quad x_i + x_j \ge 1 \quad \text{with} \quad i \ne j\,;\, i,j = q,\,\bar{q},\,g. \tag{2.53}$$

Using eqs. (2.52) and (2.50) we find

$$\left|\mathcal{M}\left(e^+e^- \to q\bar{q}g\right)\right|^2 = \hat{K}\left(\frac{x_q^2 + x_{\bar{q}}^2}{(1-x_q)(1-x_{\bar{q}})}\right) \tag{2.54}$$

where

$$\hat{K} = \frac{512}{3}\pi^3\alpha^2\alpha_s C_F C_A \sum_f Q_f^2 \frac{1}{s}\,.$$

In the next section we will use this result to compute the leading order contribution to the differential cross section for thrust.

If we consider the contributions of Figure 2.7 as NLO corrections to $e^+e^- \to$ 2 jets, take into account also the virtual contribution at order α_s (Figure 2.8) by interfering it with the tree-level contribution and integrate both over their own total phase space, we obtain

$$\sigma_{\text{NLO}}^R = \bar{\alpha}_s C_F \left(\frac{4\pi\mu^2}{q^2}\right)^\epsilon \frac{\sigma_0}{\Gamma(1-\epsilon)}\left[\frac{2}{\epsilon^2} + \frac{3}{\epsilon} + \frac{19}{2} - \pi^2 + \mathcal{O}(\epsilon)\right], \tag{2.55}$$

$$\sigma_{\text{NLO}}^V = \bar{\alpha}_s C_F \left(\frac{4\pi\mu^2}{q^2}\right)^\epsilon \frac{\sigma_0}{\Gamma(1-\epsilon)}\left[-\frac{2}{\epsilon^2} - \frac{3}{\epsilon} - 8 + \pi^2 + \mathcal{O}(\epsilon)\right], \tag{2.56}$$

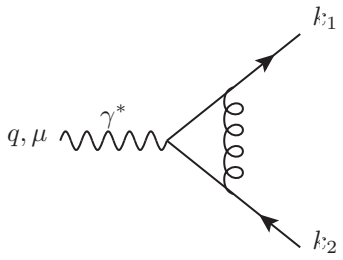

Figure 2.8: Next-to-leading virtual correction to $e^+e^- \to 2$ jets. Only the hadronic part is shown.

where σ^R_{NLO} is the contribution coming from the real correction and σ^V_{NLO} the one coming from the virtual correction. The are both IR divergent and have soft-collinear $1/\epsilon^2$- and collinear $1/\epsilon$-poles. However the total hadronic cross section at NLO, given by the sum of the two contributions is equal to

$$\begin{aligned} \sigma^{NLO}_{\text{had}} = \sigma_0 + \sigma^R_{\text{NLO}} + \sigma^V_{\text{NLO}} \quad &= \quad \sigma_0 \left[1 + \bar{\alpha}_s C_F \left(\frac{4\pi\mu^2}{q^2} \right)^{\epsilon} \frac{1}{\Gamma(1-\epsilon)} \frac{3}{2} + \mathcal{O}(\epsilon) \right] \\ &\overset{\epsilon \to 0}{=} \quad \sigma_0 \left[1 + \frac{3}{2} \bar{\alpha}_s C_F \right] . \end{aligned} \tag{2.57}$$

This is an example in which we see the cancelations between real and virtual contributions predicted by the KLN theorem.

2.6.2 Thrust at leading order

Thrust is the most prominent example of event-shape variables. We study it here at leading order as a benchmark. In Chapter 4 we will see results at NNLO for all the six observables defined in Section 2.5.2.

Thrust is an infrared and collinear safe variable: the contributions from soft particles with $\vec{p}_i \to 0$ drop out and collinear splitting does not change its values:

$$|(1 - \lambda)\, \vec{p}_i \cdot \vec{n}| + |\lambda\, \vec{p}_i \cdot \vec{n}| = |\vec{p}_i \cdot \vec{n}| . \tag{2.58}$$

From the definition (2.36) it follows directly that for a two-jet event, a so-called pencil-like event, the value of thrust is $T = 0$. Instead, for a spherical event we have to average over the sphere and we obtain

$$T = \lim_{n\to\infty} \frac{\sum_{i=1}^{n} \cos(\theta_i)}{n} = \frac{1}{4\pi} \int_0^{2\pi} \int_0^{\pi} |\cos\theta| \sin\theta \, \mathrm{d}\theta \, \mathrm{d}\phi = \frac{1}{2} . \tag{2.59}$$

With the constraints (2.53) on the x_i variables we can project the allowed phase space on the $(x_q, x_{\bar{q}})$ plane. We obtain a Daliz plot (Figure 2.9), which shows the

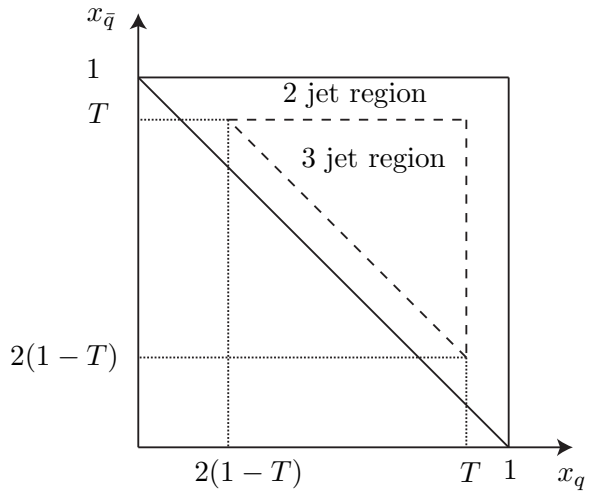

Figure 2.9: Daliz plot showing the allowed region for the event $\gamma^* \to q\bar{q}g$. The singular 2-jet regions are along the sides of the upper-right triangle.

kinematically allowed regions for x_q and $x_{\bar{q}}$ represented by the upper right-triangle. Lines of constant x_g run parallel to the diagonal. The regions outside the dashed triangle are the two-jet regions. Indeed, if the angle θ_{qg} or $\theta_{\bar{q}g}$ between a quark and the gluon tends to zero, then

$$2\, p_q \cdot\, p_g \;=\; (1 - x_q)\, q^2 \;\to\; 0$$

meaning that $x_q\,,\; x_{\bar{q}} \to 1$. This is a collinear singularity: the matrix element squared diverges if the gluon is emitted parallel to one of the quarks, as can be seen from equation (2.54). If this happens we cannot physically distinguish the two collinear partons and only two jets are observed. Similarly, if the gluon becomes soft ($E_g \to 0$), then both $x_q, x_{\bar{q}} \to 1$.

To compute explicitly the cross section for thrust, we need to know the jet function $J_T = J_T\,(x_1, \ldots, x_n)$. It can be found with the following consideration. We assume that we have 3 partons in the final state and an energy ordered configuration $x_1 > x_2 > x_3$. We do not know which of the x_i ($i = q,\, \bar{q},\, g$) corresponds to x_1, x_2 or x_3. Nevertheless, for a given three-jet configuration and assuming massless particles ($|\vec{p}_i| \;=\; E_i$), the thrust is given by

$$\begin{aligned} T = \max_{\vec{n}_T} \left(\frac{\sum_{j=1}^{3} |\vec{p}_j \cdot \vec{n}_T|}{\sum_{j=1}^{3} |\vec{p}_j|} \right) \;&=\; \frac{|\vec{p}_1|^2 + |\vec{p}_1|\,|\vec{p}_2| \cos\theta_{12} + |\vec{p}_1|\,|\vec{p}_3| \cos\theta_{13}}{|\vec{p}_1|^2 + |\vec{p}_1|\,|\vec{p}_2| + |\vec{p}_1|\,|\vec{p}_3|} \\ = \frac{\vec{p}_1^{\,2} - \vec{p}_1 \cdot \vec{p}_2 - \vec{p}_1 \cdot \vec{p}_3}{|\vec{p}_1|^2 + |\vec{p}_1|\,|\vec{p}_2| + |\vec{p}_1|\,|\vec{p}_3|} &= \frac{2\,|\vec{p}_1|}{|\vec{p}_1| + |\vec{p}_2| + |\vec{p}_3|} \;=\; \frac{2\,E_1}{\sqrt{s}} \;=\; x_1\,. \end{aligned} \tag{2.60}$$

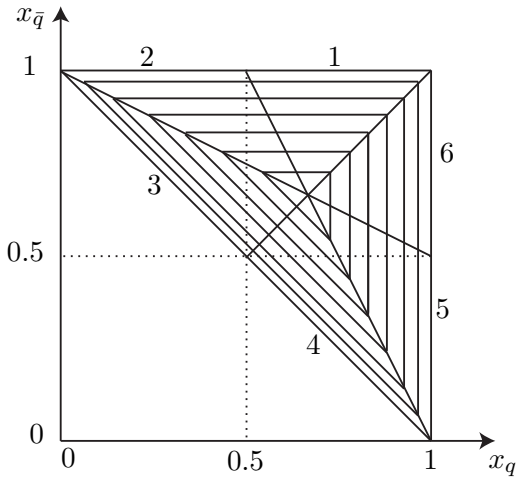

Figure 2.10: Line of equal cross section for Thrust. The plot shows also the six region of different ordering of the x_i, $i = q, \bar{q}, g$.

Therefore, the value of T is given by the maximum value of the three x_i, and the jet function is

$$J_T(x_1, \ldots, x_n) = \max\{(x_1, \ldots, x_n)\}. \tag{2.61}$$

It is now easy to draw the lines of constant cross section into the Daliz plot as shown in Figure 2.10. The figure also shows the six different regions in the $(x_q, x_{\bar{q}})$-plane with different ordering of the energy fractions x_q, $x_{\bar{q}}$ and x_g. In region 1 for example we have:

$$x_{\bar{q}} > x_q > x_g,$$

whilst in region 2 the ordering of x_q and x_g is reversed and we have

$$x_{\bar{q}} > x_g > x_q.$$

Knowing the measurement function it is now possible to compute the leading order (LO) cross section given by

$$\frac{1}{\sigma_0}\frac{\mathrm{d}\sigma_{LO}(T)}{\mathrm{d}T} = \int \mathrm{d}PS_3\, \hat{K}\left(\frac{x_q^2 + x_{\bar{q}}^2}{(1-x_q)(1-x_{\bar{q}})}\right) \delta\left(T - \max(x_q, x_{\bar{q}}, x_g)\right). \tag{2.62}$$

where σ_0 is the Born term in $d = 4$ dimensions given in (2.49) and $\mathrm{d}PS_3$ is the 3-particle phase space.

Before performing the integral, it is possible to use the symmetry of the matrix element to simplify the integration. Because of the invariance of $|\mathcal{M}(\gamma^* \to q\bar{q}g)|^2$ under the exchange $x_q \leftrightarrow x_{\bar{q}}$, we can integrate twice only over the regions 1, 2 and 3 in

Figure 2.10. We therefore obtain

$$\begin{aligned}\frac{1}{\sigma_0}\frac{\mathrm{d}\sigma_{LO}(T)}{dT} &= 2C_F\frac{\alpha_s}{2\pi}\int\int \mathrm{d}x_q\,\mathrm{d}x_{\bar{q}}\left(\frac{x_q^2+x_{\bar{q}}^2}{(1-x_q)(1-x_{\bar{q}})}\right)\delta(T-x_g)\\ &\quad + C_F\frac{\alpha_s}{2\pi}\int\int \mathrm{d}x_q\,\mathrm{d}x_{\bar{q}}\left(\frac{x_q^2+x_{\bar{q}}^2}{(1-x_q)(1-x_{\bar{q}})}\right)\delta(T-x_{\bar{q}})\\ &= C_F\frac{\alpha_s}{2\pi}\frac{1}{1-T}\left[\left(9T^2-24T+12\right)+\frac{6T^2-6T+4}{T}\ln\left(\frac{2T-1}{1-T}\right)\right]\\ &= \frac{\alpha_s}{2\pi}a_0'(T)\,, \end{aligned} \tag{2.63}$$

with the leading order coefficient $a_0'(T)$ given by

$$a_0'(T) = \frac{C_F}{1-T}\left[\left(9T^2-24T+12\right)+\frac{6T^2-6T+4}{T}\ln\left(\frac{2T-1}{1-T}\right)\right]. \tag{2.64}$$

It is important to remark that $a_0'(T)$ vanishes for $T=\frac{2}{3}$. This has a clear physical meaning: since the minimal value for the thrust in a three-jet configuration (reached in the case, where the three jets have the same energy and their momenta form an angle of 120 degrees between each other) is exactly $T=\frac{2}{3}$, it is obvious that the cross section for a configuration with more spherical symmetry, realizable only with more jets, has to vanish. The value of $a_0'(T)$ for $T<\frac{2}{3}$ does not have any physical sense. Another important remark is that $a_0'(T)$ still contains the collinear and infrared enhancements. In fact the logarithm in $a'(T)$ becomes large in the two-jet limit where $T\to 1$ and the convergence of the perturbation series is spoiled. The divergence in the limit $T\to 1$ is clearly visible in Figure 2.11, where the leading order prediction for $\tau = 1-T$ is plotted against the experimental measurements. The perturbative prediction clearly fails to describe the data in the 2-jet region, where the measured cross section has a peak and then tends to vanish, whereas the theoretical LO prediction diverges. The tendency for the experimental data to vanish in the limit $\tau\to 0$ can be understood thinking that the probability of measuring a perfectly pencil-like event with no spread in both jets is almost zero.

As already anticipated it is convenient to write the cross section in terms of τ instead of T. From now on, speaking about thrust we will always refer to τ. In this case the leading order cross section is given by

$$\frac{1}{\sigma_0}\frac{d\sigma_{LO}(\tau)}{d\tau} = \frac{\alpha_s}{2\pi}a_0(\tau)\,, \tag{2.65}$$

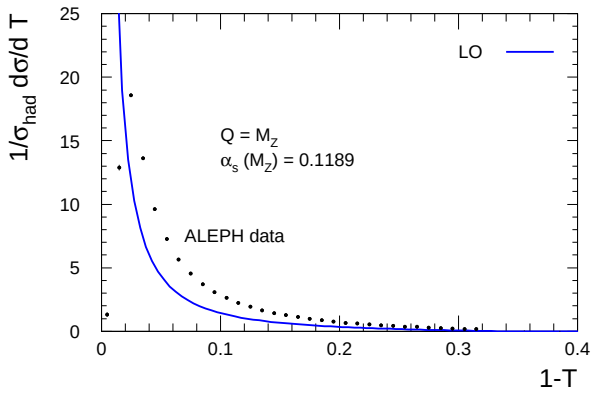

Figure 2.11: Leading order parton level prediction for thrust compared to the data measured by the ALEPH collaboration at LEP.

with

$$\begin{aligned} a_0(\tau) &= \frac{C_F}{\tau}\left[\left(9(1-\tau)^2 - 24(1-\tau) + 12\right) + \frac{6(1-\tau)^2 - 6(1-\tau) + 4}{1-\tau}\ln\left(\frac{1-2\tau}{\tau}\right)\right] \\ &= -\frac{3C_F}{\tau} + 4C_F\frac{1}{\tau}\ln\left(\frac{1}{\tau}\right) + \frac{4C_F}{\tau}\ln(1-2\tau) + 6C_F + 9C_F\tau \\ &\qquad - 6C_F\ln\left(\frac{1-2\tau}{\tau}\right) + \frac{4C_F}{1-\tau}\ln\left(\frac{1-2\tau}{\tau}\right). \end{aligned} \tag{2.66}$$

In the second line we made the logarithmic structure explicit. We will study it for general event-shape observables in Chapter 4.

The NLO contribution $b_0(\tau)$, which contains configurations of up to four jets is known only numerically. In four-jet final states the thrust is minimal when the four jets have the same momentum and lie on two planes, rotated by 90 degrees and forming a tetrahedron with an angle of $\arccos\left(\frac{1}{\sqrt{3}}\right)$ between each other. In this case the thrust can takes values of

$$0 < \tau < 1 - \frac{1}{\sqrt{3}}.$$

In order to obtain reliable theoretical predictions also in the soft and collinear region, the fixed order computations have to be matched we resummed calculations. All the details of the matching procedure are given in Chapter 4.

2.6.3 Deep-inelastic lepton-nucleon scattering

Another very important process, which historically led to the development of the parton model [7] is deep-inelastic lepton-nucleon scattering. It allows to probe the content of hadrons like protons and neutrons and led to the discovery of their substructure. The

typical kinematical setup is shown in Figure 2.12: an electron (e^-) and a nucleon (N) scatter inelastically exchanging a photon, a Z^0 or a $W^\pm$ boson. In case of a neutral current exchange, in the final state the scattered electron is again present together with hadrons coming from the scattered nucleon and labeled by X. In case of a charged current exchange a neutrino is produced, whose presence can eventually be inferred from missing transverse momentum or missing energy. Referring to the momenta defined in

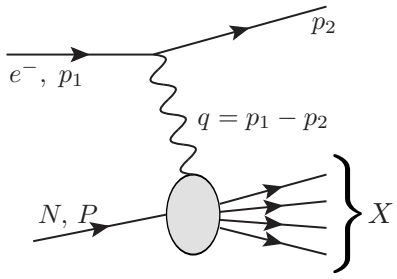

Figure 2.12: Kinematical setup of a deep-inelastic scattering process.

Figure 2.12 we can define the following standard deep-inelastic kinematical variables:

$$\begin{aligned} Q^2 &= -q^2 && \text{(squared transferred momentum)}, \\ x &= \frac{Q^2}{2P\cdot q} && \text{(Bjorken } x\text{-variable)}, \\ y &= \frac{q\cdot P}{p_1\cdot P} && \text{(energy transferred to the nucleon in its restframe)}. \end{aligned} \tag{2.67}$$

In the following we will consider only deep-inelastic electron-proton scattering with the exchange of a virtual photon. In this case the inclusive differential cross section is given by

$$\mathrm{d}\sigma = \frac{1}{4\sqrt{(P\cdot p_1)^2 - M_p m_e}} \frac{1}{4} \sum_X |\mathcal{M}_{\mathrm{fi}}|^2\, \delta^{(4)}\left(P + p_1 - p_2 - P_X\right) \frac{\mathrm{d}^3 p_2}{(2\pi)^3\, 2E_2}\,, \tag{2.68}$$

where the first factor on the right hand side is the flux factor, which depends on the momenta and the masses of the incoming particles, the factor 1/4 takes care of the spin average and the last factor is the phase space of the outgoing lepton. The matrix element $\mathcal{M}_{\mathrm{fi}}$ is

$$\mathcal{M}_{\mathrm{fi}} = -e^2 \bar{u}(p_2)\gamma^\mu u(p_1) \frac{1}{q^2} \left\langle X, P_X \right| j_\mu(0) \left| N, P \right\rangle\,, \tag{2.69}$$

where $j_\mu(0)$ is the electromagnetic current operator and $|N, P\rangle$ the unpolarized nucleon state with momentum P. Neglecting the mass of both the electron and the proton and

factorizing the cross section into a leptonic and a hadronic tensor we can write

$$\mathrm{d}\sigma = \frac{xy}{2Q^2}\frac{\mathrm{d}^3 p_2}{2E_2} L^{\mu\nu}\frac{1}{Q^4} W_{\mu\nu}\,, \tag{2.70}$$

with

$$L^{\mu\nu} = 2\alpha^2\left(p_1^\mu p_2^\nu + p_1^\nu p_2^\mu - g^{\mu\nu} p_1\cdot p_2\right)\,, \tag{2.71}$$

$$W_{\mu\nu} = \frac{1}{2}\frac{1}{4\pi}\sum_{X,\mathrm{Spin}} (2\pi)^4\,\delta^{(4)}\left(P+q-P_X\right)\langle N,P|\, j_\nu^\dagger(0)\,|X,P_X\rangle\,\langle X,P_X|\, j_\mu(0)\,|N,P\rangle\,. \tag{2.72}$$

Very generally, the tensorial structure of $W_{\mu\nu}$ must be given by the vectors q_μ and P_μ and the metric tensor $g_{\mu\nu}$. The two requirements of parity invariance ($W_{\mu\nu} = W_{\nu\mu}$) and electromagnetic current conservation ($q^\mu W_{\mu\nu} = 0$) lead us to the following form

$$W_{\mu\nu}(P,q) = \left(-g_{\mu\nu} + \frac{q^\mu q^\nu}{q^2}\right) F_1\left(x,Q^2\right) + \left(P_\mu + \frac{q_\mu}{2x}\right)\left(P_\nu + \frac{q_\nu}{2x}\right)\frac{F_2\left(x,Q^2\right)}{P\cdot q} \tag{2.73}$$

$$= \frac{1}{2x}\left(-g_{\mu\nu} + \frac{q^\mu q^\nu}{q^2}\right) F_L\left(x,Q^2\right) + \left(P_\mu P_\nu - \frac{P\cdot q}{q^2}\left(P_\mu q_\nu + P_\nu q_\mu\right) + g_{\mu\nu}\frac{(P\cdot q)^2}{q^2}\right)\frac{F_2\left(x,Q^2\right)}{P\cdot q}\,. \tag{2.74}$$

The functions $F_i(x,Q^2)$ $(i=1,2)$ are called structure functions and parameterize the substructure of the proton. The function

$$F_L(x,Q^2) = F_2(x,Q^2) - 2xF_1(x,Q^2)$$

is the longitudinal structure function. Inserting the general form (2.74) contracted with the lepton tensor $L^{\mu\nu}$ into the cross section (2.70) we find

$$\frac{\mathrm{d}^2\sigma}{\mathrm{d}x\,\mathrm{d}Q^2} = \frac{4\pi\alpha^2}{Q^4}\left[\left(1+(1-y)^2\right)F_1(x,Q^2) + \frac{(1-y)}{x}\left(F_2(x,Q^2) - 2xF_1(x,Q^2)\right)\right]$$
$$= \frac{2\pi\alpha^2}{xQ^4}\left[\left(1+(1-y)^2\right)F_2(x,Q^2) - y^2 F_L(x,Q^2)\right]\,. \tag{2.75}$$

The two terms in the squared bracket of eq. (2.75) correspond to the absorption of a transversely (F_1) and longitudinally (F_L) polarized virtual photon.

In order to find the cross section we need to find an expression for the structure functions $F_2(x,Q^2)$ and $F_L(x,Q^2)$. We can compute them by multiplying the hadronic tensor $W_{\mu\nu}$ with appropriate projectors, which in d dimensions are

$$\frac{F_L(x,Q^2)}{x} = \frac{2Q^2}{(P\cdot q)^2} P_\mu^T P_\nu^T W^{\mu\nu}\,, \tag{2.76}$$

$$F_2(x,Q^2) = -\frac{1}{d-2}\left(W_\mu^\mu - (d-1)\frac{Q^2}{(P\cdot q)^2} P_\mu^T P_\nu^T W^{\mu\nu}\right)\,, \tag{2.77}$$

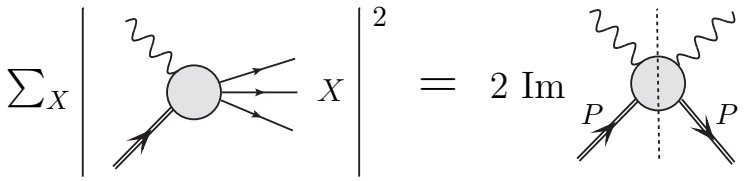

Figure 2.13: Application of the optical theorem to DIS: the hadronic tensor is related to the imaginary part of the forward Compton amplitude.

where

$$P_\mu^T = P_\mu + q_\mu \frac{P\cdot q}{Q^2}\,.$$

Using the Fourier representation of the δ-distribution

$$(2\pi)^4\,\delta^{(4)}\left(P - P_X + q\right) = \int \mathrm{d}^4 z\, e^{iqz} e^{i(P-P_X z)}\,,$$

translation invariance

$$\langle P|\, j_\mu^\dagger(z)\,|P_X\rangle = e^{iz(P-P_X)}\,\langle P|\, j_\mu^\dagger(0)\,|P_X\rangle$$

and the completeness of the state $|X, P_X\rangle$, we can rewrite the hadronic tensor as[1]

$$W_{\mu\nu} = \int \frac{\mathrm{d}^4 z}{4\pi} e^{iqz}\,\langle N,P|\,[j_\mu^\dagger(z), j_\nu(0)]\,|N,P\rangle\ . \tag{2.78}$$

The second term of in the commutator can be added because it vanishes. Equation (2.78) is the starting point for an operator product expansion (OPE). In the so-called Bjorken limit, $Q^2 \to \infty$, x fixed, the integral (2.78) is dominated by the integration region near the lightcone $z^2 \sim 0$. Thus, using the optical theorem which relates the hadronic tensor to the forward Compton amplitude (Figure 2.13) together with the OPE it is possible to perform a formal expansion of the current product in (2.78) around the lightcone into a series of local composite operators of leading twist[2]. The details of the OPE go beyond the scope of this introduction and for a nice review on this we refer to [17].

An important result of this field theoretical treatment is the connection between the hadronic and the partonic structure functions. If we consider the elastic scattering of an electron and a quark with a fraction ξ of the proton momentum P (Figure 2.14a), equation (2.70) still holds but the hadronic tensor $W_{\mu\nu}$ is replaced by a parton level hadronic tensor

$$\begin{aligned}\hat{W}_{\mu\nu}(P,q) =& \frac{1}{2x}\left(-g_{\mu\nu} + \frac{q^\mu q^\nu}{q^2}\right)\hat{F}_L\left(x,Q^2\right)\\ &+\left(P_\mu P_\nu - \frac{P\cdot q}{q^2}\left(P_\mu q_\nu + P_\nu q_\mu\right) + g_{\mu\nu}\frac{(P\cdot q)^2}{q^2}\right)\frac{\hat{F}_2\left(x,Q^2\right)}{P\cdot q}\,.\end{aligned} \tag{2.79}$$

[1] We leave implicit the average over the proton spin.

[2] The difference between the dimension and the angular momentum of an operator is called *twist*.

with parton level structure functions $\hat{F}_2$, $\hat{F}_L$ which can now be computed explicitly from perturbative QCD. Crossing the result (2.46) obtained in e^+e^- annihilation we obtain[1]

$$\frac{\mathrm{d}^2\sigma}{\mathrm{d}Q^2\mathrm{d}x} = \frac{4\pi\alpha^2}{Q^4}\left[1+(1-y)^2\right]\frac{1}{2}Q_f^2\delta(x-\xi)\,, \tag{2.80}$$

from which it follows that at leading order

$$\hat{F}_2\left(x,Q^2\right) = x\,Q_f^2\delta(x-\xi) \qquad ; \qquad \hat{F}_L\left(x,Q^2\right) = 0\,. \tag{2.81}$$

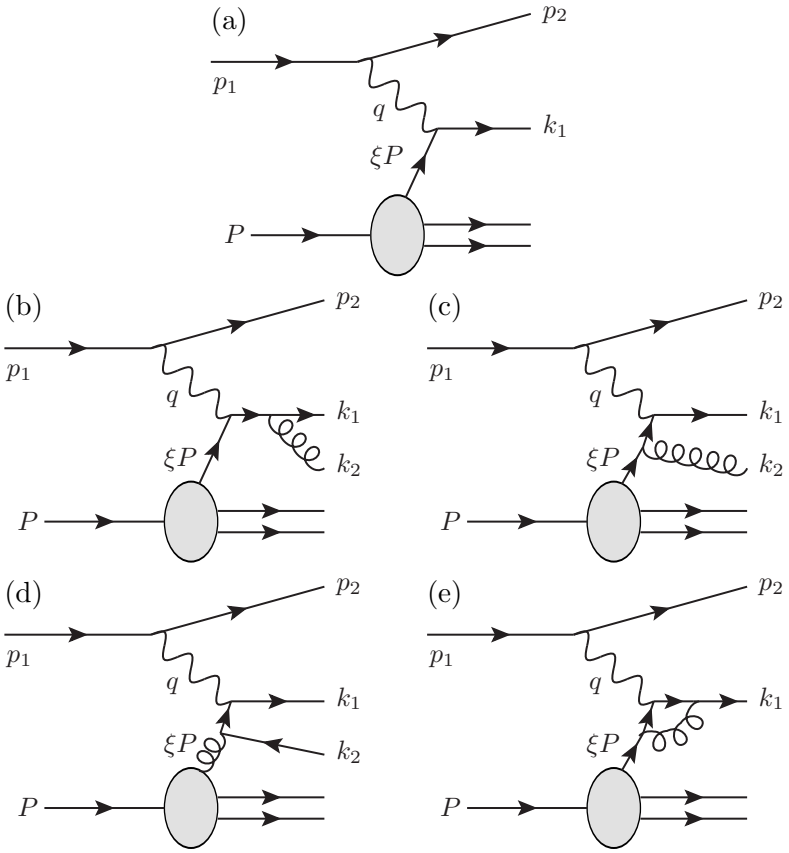

Figure 2.14: Leading order (a) and order $\mathcal{O}(\alpha_s)$ QCD corrections (b)-(e) to deep-inelastic electron-proton scattering.

The relation between the hadronic differential cross section and the differential cross section at parton level is given by the following universal factorization formula

$$\mathrm{d}\sigma\left(P,Q^2\right) = \sum_{i=q,\bar{q},g}\int_0^1 \frac{\mathrm{d}\xi}{\xi}\, f_i^h\left(\xi,\mu_F\right)\mathrm{d}\hat{\sigma}^{li}\left(\xi P,Q^2,\mu_F\right)\,. \tag{2.82}$$

[1]From momentum conservation it follows that $x=\xi$.

This formula is of fundamental importance in cross section computations of reactions with hadronic initial states. The factor $1/\xi$ can be traced back to the scaling $P \to \xi P$ used to obtain the lepton-parton flux factor. The function $f_i^h(\xi, \mu_F)$ is the *parton distribution function* (PDF) and gives the probability of finding a quark (antiquark or gluon) of flavour i and momentum fraction z inside hadron h:

$$f_i^h(\xi, \mu_F)\, \mathrm{d}\xi = \mathcal{P}\left(\xi' \in [\xi, \xi + \mathrm{d}\xi]\right) \qquad \text{with} \qquad i = q, \bar{q}, g\,.$$

A similar relation holds also between the hadron level and the parton level structure functions [66]:

$$F_i\left(x, Q^2\right) = \sum_{j=q,\bar{q},g} \int_x^1 \frac{\mathrm{d}z}{z}\, f_j^h\left(\frac{x}{z}, \mu_F, \mu_R\right) \hat{F}_i^j\left(Q^2, z, \mu_F, \mu_R\right)\,, \tag{2.83}$$

where $i = 2, L$. The last two equations need some further explanations. First of all, the new variable z is equal to the ratio $z = x/\xi$, which is the Bjorken x-variable of the parton level process where only a fraction ξ of the proton momentum P is involved. In passing from (2.82) to (2.83) a change of variable was made. The partonic structure function has a label j for the flavour, in order to distinguish the structure functions of quark, antiquark and gluon. Both the PDF and the partonic structure functions depend on the renormalization scale[1] μ_R and on the factorization scale μ_F, which appears also in (2.82). The scale μ_F is a non-physical scale which is introduced to separate the computable perturbative dynamics described in the partonic cross section and structure functions from the low energy non-perturbative physics contained in the PDFs. In fact, in computing higher order corrections to the partonic process $q\gamma^* \to q$ (Figure 2.14 (b)-(e)), the cross section becomes sensitive to initial state collinear singularities, which are not canceled against virtual contributions like final state collinear divergences. In the case of final state collinear splitting, the momentum flow is the same as in the case where there is no splitting, since we are not able to distinguish the two different collinear particles. In the case of an initial state collinear splitting however, the momentum carried away from the collinear particle does not enter in the electromagnetic vertex and therefore the collinear singularities from the real correction do not cancel against the virtual one. To say it in other words, the photon is able to distinguish between an initial state quark q and a collinear quark-gluon pair qg. This is a case in which the KLN theorem is not applicable[2]. Nevertheless, we do not want to be sensitive to low-energy and long-distance physics, which is not computable in perturbative QCD. Using a procedure called mass factorization, which is similar the

[1] We put a label R in order to distinguish the renormalization scale from the factorization scale.

[2] This does not mean that the KLN theorem does not hold. The problem is that hadrons are given as they are, and we do not know the relative weight of parton Fock states in a hadron.

renormalization, we can absorb these divergencies introducing an arbitrary factorization scale μ_F and redefining the bare parton distribution functions which describe the universal low energy hadron-specific physics, such that we are left with a finite result. Parton density functions are not computable in perturbation theory and have to be found by fits to experimental data. However they acquire a dependence on μ_F which is computable in perturbative QCD and is described by a set of integro-differential equations called[1] DGLAP equations.

Formally the equations (2.82) and (2.83) are exact only in the Bjorken limit $Q^2 \to \infty$ since they are only the leading contribution in the OPE we mentioned before. At finite values of Q^2 there are higher twist corrections which are suppressed as

$$\frac{\ln^{m<n}\left(Q^2/Q_0^2\right)}{Q^n},$$

where $n = 4$ in DIS.

The partonic structure functions $F_2\left(x, Q^2\right)$ and $F_L\left(x, Q^2\right)$ were computed at 2-loop accuracy by E. B. Zijlstra and W. L. van Neerven [3] and later by S. Moch and J. A. M. Vermaseren [70]. We report the expansion of the structure functions in terms of splitting functions and coefficient functions at NLO in the Section 3.7. Nowadays structure functions are known at three loops [71].

2.7 Factorization and parton branching

We now investigate the behaviour of a matrix element $\mathcal{M}_m$ with m final state particles if we add one further particle and let it become soft or collinear. We will see that the matrix element for $m + 1$ particles factorizes into the original m-particle matrix element times an expression which is universal. In Figure 2.15 we define the setup and the momenta.

The index i of the colour matrix T_i^a represents the parton from which the gluon was emitted, i.e. it can be in the fundamental or adjoint representation. The m-parton matrix element has a tilde since it is a vector in Dirac space.

2.7.1 Factorization in the soft limit

The soft limit is defined by setting $k_j^\mu = \lambda q^\mu$ with $\lambda > 0$ and by sending $\lambda \to 0$ keeping q^μ fixed. In this limit the emission of the soft gluon from internal propagators is IR

[1] DGLAP stands for Dokshitzer [67], Gribov and Lipatov [68], Altarelli and Parisi [69]. For more details about the universal factorization theorem and the DGLAP evolution of PDFs we refer to some standard QCD textbook like [25–27].

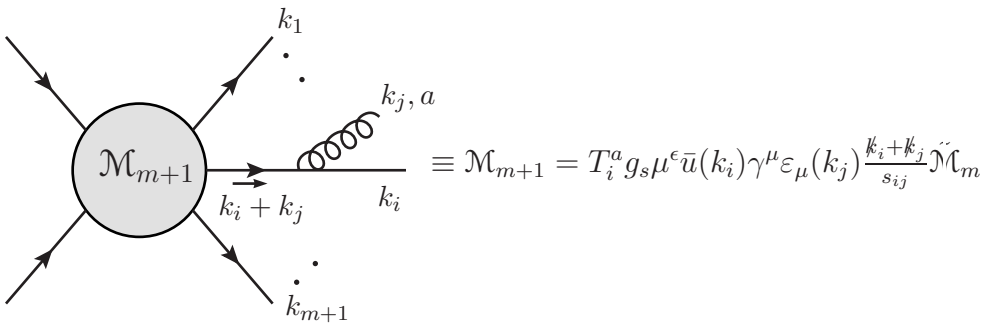

Figure 2.15: Soft or collinear emission from one external leg.

finite. If we consider the emission of a soft gluon off an external quark (Figure 2.15), the amplitude $\mathcal{M}_{m+1}$ reduces to

$$\begin{aligned} \mathcal{M}_{m+1} &= T_i^a \, g_s \mu^\epsilon \bar{u}(k_i)\gamma^\mu \varepsilon_\mu(k_j) \frac{\not{k}_i + \not{k}_j}{s_{ij}} \tilde{\mathcal{M}}_m \\ &\overset{k_j \to 0}{=} T_i^a \, g_s \mu^\epsilon \frac{1}{s_{ij}} \bar{u}(k_i)\gamma^\mu \varepsilon_\mu(k_j) \not{k}_i \tilde{\mathcal{M}}_m \\ &= T_i^a \, g_s \mu^\epsilon \frac{k_i^\mu}{k_i \cdot k_j} \varepsilon_\mu(k_j) \mathcal{M}_m \, . \end{aligned} \tag{2.84}$$

In the last line we used the anticommutation relation between γ-matrices and the Dirac equation. The Dirac spinor was absorbed in the m-parton matrix element $\mathcal{M}_m$ and therefore we can drop the tilde on it. A similar result can be obtained also in case a gluon emits another gluon, while the emission of soft quarks leads to a integrable singularity because the fermion propagator is less singular then that of the gluon. Since in general we do not know from which leg the soft gluon is emitted, we have to sum over all external partons. We find that in the soft limit the $m+1$ matrix element reduces to

$$\left| M_{m+1}^0 \right\rangle \overset{k_j \to 0}{\to} g_s \mu^\epsilon \varepsilon_\mu(k_j) J^\mu(k_j) \left| M_m^0 \right\rangle \, , \tag{2.85}$$

where

$$J^\mu(k_j) = \sum_{n=1}^{m} T_n^a \frac{k_n^\mu}{k_n \cdot k_j} \, . \tag{2.86}$$

For the matrix element squared we find

$$\begin{aligned} \left\langle M_{m+1}^0 | M_{m+1}^0 \right\rangle &\overset{k_j \to 0}{\to} 4\pi\alpha_s \mu^{2\epsilon} \sum_{n,o=1}^{m} \varepsilon_\mu(k_j) \varepsilon_\nu^*(k_j) \frac{k_n^\mu k_o^\nu}{k_n \cdot k_j \, k_o \cdot k_j} \left\langle M_m^0 \right| T_n \cdot T_o \left| M_m^0 \right\rangle \\ &= -4\pi\alpha_s \mu^{2\epsilon} \sum_{n,o=1}^{m} \frac{2 s_{no}}{s_{nj} s_{oj}} \left\langle M_m^0 \right| T_n \cdot T_o \left| M_m^0 \right\rangle \, . \end{aligned} \tag{2.87}$$

The factor $2s_{no}/(s_{nj}s_{oj})$ is called *eikonal* factor. We observe that there is a factorization of the $(m+1)$-parton matrix element into a m-parton matrix element (which is clearly process dependent) and a universal eikonal factor. This feature will be of crucial importance in the next chapter. Something very similar happens in the collinear case too.

2.7.2 Factorization in the collinear limit

To study the collinear limit of a $(m+1)$-parton matrix element we work in a physical gauge and consider directly a squared matrix element. There are different possible splittings summarized in Table 2.1. We look here again at the case already considered before, of a quark splitting into a collinear gluon and a quark. Focusing only on the splitting part of the squared amplitude we have

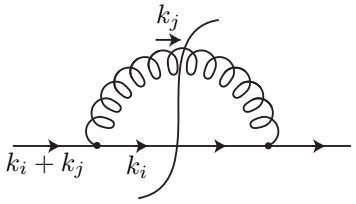

$$\equiv \mathcal{A} = C_F g_s^2 \mu^{2\epsilon} \frac{\not{k}_i + \not{k}_j}{s_{ij}} \gamma^\mu \not{k}_i \gamma^\nu d_{\mu\nu}(k_j, n) \frac{\not{k}_i + \not{k}_j}{s_{ij}},$$

where $d_{\mu\nu}(k_j, n)$ is the propagator in the physical gauge

$$d_{\mu\nu}(p, n) = -g_{\mu\nu} + \frac{p_\mu n_\nu + n_\mu p_\nu}{p \cdot n},$$

and n^μ is an arbitrary light-like vector. Inserting this in $\mathcal{A}$ we find

$$\mathcal{A} = C_F \, 4\pi\alpha_s \mu^{2\epsilon} \frac{\not{k}_i + \not{k}_j}{s_{ij}} \left(-\gamma^\mu \not{k}_i \gamma_\mu + \frac{\not{k}_j \not{k}_i \not{n} + \not{n} \not{k}_i \not{k}_j}{k_j \cdot n} \right) \frac{\not{k}_i + \not{k}_j}{s_{ij}}, \tag{2.88}$$

and after some Dirac algebra this becomes

$$\mathcal{A} = C_F \, 4\pi\alpha_s \mu^{2\epsilon} \frac{1}{s_{ij}} \left[(d-2)\not{k}_j + \frac{1}{k_j \cdot n} \left(4k_i \cdot n \not{k}_i + 2k_i \cdot n \not{k}_j + 2k_j \cdot n \not{k}_i - s_{ij} \not{n} \right) \right]. \tag{2.89}$$

The collinear limit of momenta k_i and k_j is defined by the Sudakov parametrization:

$$\begin{aligned} k_i^\mu &= z k^\mu + k_{i\perp}^\mu - \frac{k_{i\perp}^2}{z} \frac{n^\mu}{2\, k \cdot n}, \\ k_j^\mu &= (1-z) k^\mu + k_{j\perp}^\mu - \frac{k_{j\perp}^2}{(1-z)} \frac{n^\mu}{2\, k \cdot n}, \end{aligned}$$

where $k_{i\perp}^\mu + k_{j\perp}^\mu = 0$. The vector k^μ gives the collinear direction and

$$k^2 = 0 \quad , \quad n^2 = 0 \quad , \quad k_{i\perp} \cdot k = k_{j\perp} \cdot k = k_{i\perp} \cdot n = k_{j\perp} \cdot n = 0 .$$

In the collinear limit $k_{i\perp}^{\mu}$, $k_{j\perp}^{\mu} \to 0$ and $s_{ij} \to -\frac{k_{j\perp}^2}{z(1-z)}$.

Inserting the Sudakov parametrization in (2.89) and keeping only the most divergent term in the limit $k_{i\perp} = -k_{j\perp} \to 0$ we obtain

$$\begin{aligned} \mathcal{A} &\overset{k_{i\perp}\to 0}{\to} 4\pi\alpha_s\mu^{2\epsilon}\frac{2C_F}{s_{ij}}\left[\frac{1+z^2}{1-z} - \epsilon\,(1-z)\right]\not{k} + \mathcal{O}\left(k_{i\perp}^{\mu}\right) \\ &= 4\pi\alpha_s\mu^{2\epsilon}\frac{1}{s_{ij}}\tilde{P}^0_{q\to qg}\,(z)\not{k} + \mathcal{O}\left(k_{i\perp}^{\mu}\right)\,, \end{aligned} \tag{2.90}$$

where

$$\tilde{P}^0_{q\to qg}\,(z) = 2C_F\left[\frac{1+z^2}{1-z} - \epsilon\,(1-z)\right]\,.$$

Therefore the collinear limit for the whole matrix element squared is given by

$$\left\langle M^0_{m+1}|M^0_{m+1}\right\rangle \overset{k_j\|k_i}{\to} 4\pi\alpha_s\mu^{2\epsilon}\frac{\tilde{P}^0_{q\to qg}}{s_{ij}}\left\langle M^0_m|M^0_m\right\rangle + \mathcal{O}\left(k_{i\perp}^{\mu}\right)\,. \tag{2.91}$$

The function $\tilde{P}^0_{q\to qg}(z)$ is one of the so-called Altarelli-Parisi [69] splitting functions and is associated with the branching $q \to qg$. There are four different splitting functions associated with the different possible splittings and they can be expanded in powers of α_s. Furthermore there are two families of splitting functions associated with timelike or spacelike splitting. At leading order they are the equal, but they differ at higher orders.

The result we derived for $\tilde{P}^0_{q\to qg}(z)$ is divergent for $z \to 1$. This behaviour encapsulates the soft singularity, since for $z \to 0$ the gluon becomes not only collinear but also soft. In order to remove this singularity we have to add the contribution from the virtual pieces

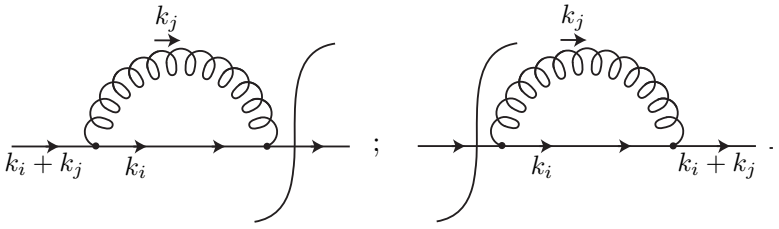

However, instead of computing these contribution explicitly we can make use of fermion number conservation, from which it follows directly that[1]

$$\int_0^1 \mathrm{d}z\, P^0_{q\to qg}(z) = 0\,. \tag{2.92}$$

[1]The spacelike $P^0_{q\to qg}(z)$ splitting function appears in the $\mathcal{O}(\alpha_s)$ corrections to the quark PDF, where z is the Bjorken variable of the quark. From $\int \mathrm{d}z\, q(z, Q^2) = 0$ it follows that the integral over z of the splitting function must vanish.

Since the virtual contributions can only have influence on terms proportional to $\delta(1-z)$, we make the ansatz

$$P^0_{q\to qg}(z) = 2C_F\left[\frac{1+z^2}{1-z} + C\,\delta(1-z)\right] + \mathcal{O}(\epsilon)\,.$$

From condition (2.92) it follows

$$C = -\delta(1-z)\int_0^1 \mathrm{d}z\, P^0_{q\to qg}(z)\,,$$

however, if we perform the integral naïvely, it diverges at the upper boundary. The problem is that $P^0_{q\to qg}(z)$ is not a proper function but rather a distribution[1]. By splitting up the singular part we obtain

$$\begin{aligned}
P^0_{q\to qg}(z) =& 2C_F\left[\frac{2}{1-z} - (1+z) - \delta(1-z)\int_0^1 \mathrm{d}z'\left(-(1+z') + \frac{2}{1-z'}\right)\right]\\
=& 2C_F\left[\frac{2}{1-z} - (1+z) + \frac{3}{2}\delta(1-z) - \delta(1-z)\int_0^1 \mathrm{d}z'\frac{2}{1-z'}\right]\\
=& 2C_F\left[\frac{2}{(1-z)_+} - (1+z) + \frac{3}{2}\delta(1-z)\right]\\
=& 2C_F\left[\frac{1+z^2}{(1-z)_+} + \frac{3}{2}\delta(1-z)\right]\,,
\end{aligned} \tag{2.93}$$

with the (+)-distribution defined as

$$\begin{aligned}
\int_0^1 \mathrm{d}z\,[f(z)]_+\,g(z) &= \int_0^1 \mathrm{d}z f(z)\,[g(z)-g(1)]\\
&= \int_0^1 \mathrm{d}z\left[f(z)g(z) - \delta(1-z)g(z)\int_0^1 \mathrm{d}z' f(z)\right]\,,
\end{aligned} \tag{2.94}$$

where $g(z)$ is a smooth and divergence-free function in the interval $z\in[0,1]$.

The other splitting functions can be derived in a similar way. The leading order results, labeled by a 0, are summarized in Table 2.1, where we shortened a bit the notation by labeling a splitting of the type $a\to bX$ as $P^0_{ba}(z)$. This is the customary notation for splitting functions used in many textbooks. Nowadays splitting functions are known at NNLO [72, 73].

Knowing how the matrix elements behave in soft and collinear regions, we can compute higher order corrections to QCD processes taking care of all the cancelations occurring in IR regions. The method we use is called antenna subtraction and is presented in the next chapter.

[1] Some important properties and some computational feature of distributions are summarized in Appendix A.

Splitting process	Altarelli-Parisi splitting function
$q \to qg$	$P^0_{qq} = 4C_F \left[\frac{1+z^2}{(1-z)_+} + \frac{3}{2}\delta(1-z)\right]$
$q \to gq$	$P^0_{gq} = 4C_F \left[\frac{1+(1-z)^2}{z}\right]$
$g \to q\bar{q}$	$P^0_{qg} = 4\left[z^2 + (1-z^2)\right]$
$g \to gg$	$P^0_{gg} = 8C_A \left[\frac{z}{(1-z)_+} + \frac{(1-z)}{z} + z(1-z)\right] + 2\delta(1-z)\frac{(11C_A - 2N_F)}{3}$

Table 2.1: Leading order splitting functions normalized according to [3, 4].

This concludes this short introduction to QCD and collider physics. Nothing contained in this chapter is new or was developed during my thesis, however it is part of the basic knowledge needed to develop and understand the computations and the results presented in the next chapters.

3

Antenna Subtraction

In this chapter we present the antenna subtraction formalism developed to compute cross sections at NNLO. The first part is an introduction to the formalism and relies mainly on [21] and on a series of lectures given at the University of Zürich by T. Gehrmann and A. Gehrmann-DeRidder. In the second part we present the extension to include processes with one hadronic initial state at NLO [74] and the computations which now allows to construct subtraction terms for hadronic initial states also NNLO [24].

3.1 The need for a subtraction scheme

In order to understand better the need for a subtraction formalism, we specify the notation introduced in (2.2) by considering electron-positron annihilation and in particular the cross-section for $e^+e^- \to m$ jets. At leading order in perturbation theory the differential cross section for an m-jet observable is obtained by computing the integral over the m-particle phase space of the Born cross section

$$\mathrm{d}\sigma_{\mathrm{LO}} = \int_{\mathrm{d}\Phi_m} \mathrm{d}\sigma^{\mathrm{B}}\,, \tag{3.1}$$

where $\mathrm{d}\sigma^{\mathrm{B}}$ is given by

$$\mathrm{d}\sigma^{\mathrm{B}} = \mathcal{N} \sum_m \mathrm{d}\Phi_m\left(k_1,\ldots,k_m;q\right) \frac{1}{S_m} |\mathcal{M}_m\left(k_1,\ldots,k_m;q\right)|^2 J_m^{(m)}(k_1,\ldots,k_m)\,. \tag{3.2}$$

The normalization factor $\mathcal{N}$ includes all QCD-independent factors as well as the dependence on the renormalized strong coupling constant α_s, $\sum_m$ denotes the sum over all configurations with m partons, finally $\mathrm{d}\Phi_m$ is the m-parton phase space (B.1). As displayed in (2.6), at NLO the following two contributions have to be computed:

$$\mathrm{d}\sigma_{\mathrm{NLO}} = \int_{\mathrm{d}\Phi_{m+1}} \mathrm{d}\sigma^{\mathrm{R}}_{\mathrm{NLO}} + \int_{\mathrm{d}\Phi_m} \mathrm{d}\sigma^{V,1}_{\mathrm{NLO}}\,. \tag{3.3}$$

In the previous chapter we have seen that at NLO the real and the virtual corrections are both infrared divergent, but, according to the KLN theorem, the two divergencies are equal and of opposite sign and therefore cancel once the two contributions are summed together. However the real and the virtual corrections must be integrated over different phase spaces. Furthermore the virtual corrections develop IR singularities by integrating over the loop momentum whereas in the real contribution the IR singularities become explicit only after integrating the matrix element over the appropriate phase space. Since the phase space integration in most of the cases is not feasible analytically because of the jet function $J_m^{(m)}$, which is often defined recursively, one has to find a way to isolate the IR singularities of the real corrections such that they can be canceled against the ones coming from the virtual loop integration. In practice this can be done by introducing a subtraction term $\mathrm{d}\sigma^{\mathrm{S}}$ at the integrand level, which must satisfy the following two requirements:

(A) it should approximate the real radiation matrix element in all singular limits, and

(B) it should be sufficiently simple to be integrated analytically over a section of the phase space that encompasses all regions corresponding to singular configurations.

At NLO this subtraction term can then be added and subtracted in (3.3) as follows:

$$\mathrm{d}\sigma_{\mathrm{NLO}} = \left[\int_{\mathrm{d}\Phi_{m+1}} \left(\mathrm{d}\sigma^{\mathrm{R}}_{\mathrm{NLO}} - \mathrm{d}\sigma^{\mathrm{S}}_{\mathrm{NLO}}\right)\right] + \left[\int_{\mathrm{d}\Phi_{m+1}} \mathrm{d}\sigma^{\mathrm{S}}_{\mathrm{NLO}} + \int_{\mathrm{d}\Phi_m} \mathrm{d}\sigma^{V,1}_{\mathrm{NLO}}\right] . \tag{3.4}$$

Both pieces in the squared brackets are now finite and a numerical integration can safely be performed. The numerical problem and its solution has been formulated by means of a nice and simple example by Z. Kunszt and D.E. Soper [75].

The same idea apply also at NNLO. However, from (2.6) we see that several more ingredients are needed in this case: the two-loop corrected m-parton matrix elements, the one-loop corrected $(m+1)$-parton matrix elements, and the tree-level $(m+2)$-parton matrix elements. For most massless jet observables of phenomenological interest, the two-loop matrix elements have been computed some time ago [76–91], while the other two types of matrix elements are usually known from calculations of NLO corrections to $(m+1)$-jet production [92–101]. The one-loop $(m+1)$-parton matrix elements contribute to m-jet observables at NNLO if one of the partons involved becomes unresolved (soft or collinear) [102–106]. In these cases, the infrared singular parts of the matrix elements need to be extracted and integrated over the phase space appropriate to the unresolved configuration to make the infrared pole structure explicit. Methods for the extraction of soft and collinear limits of one-loop matrix elements are worked out in detail in the literature [102–112]. Likewise, the $(m+2)$-parton matrix elements contain double real radiation singularities corresponding to two partons becoming simultaneously soft and/or collinear [113–119]. To determine the contribution to NNLO

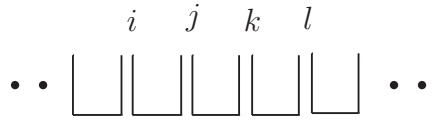

Figure 3.1: Schematic representation of colour connection in a matrix element.

jet observables from these configurations, one has to find two-parton subtraction terms which coincide with the full matrix element and are still sufficiently simple to be integrated analytically, in order to cancel their infrared pole structure with the two-loop virtual and the one-loop single-unresolved contributions. The full NNLO contribution is then given by

$$\begin{aligned} \mathrm{d}\sigma_{\mathrm{NNLO}} \;=\; & \left[\int_{\mathrm{d}\Phi_{m+2}} \left(\mathrm{d}\sigma^{\mathrm{R}}_{\mathrm{NNLO}} - \mathrm{d}\sigma^{\mathrm{S}}_{\mathrm{NNLO}}\right)\right] + \left[\int_{\mathrm{d}\Phi_{m+1}} \left(\mathrm{d}\sigma^{\mathrm{V,1}}_{\mathrm{NNLO}} - \mathrm{d}\sigma^{\mathrm{VS,1}}_{\mathrm{NNLO}}\right)\right] \\ & \left[\int_{\mathrm{d}\Phi_{m+2}} \mathrm{d}\sigma^{\mathrm{S}}_{\mathrm{NNLO}} + \int_{\mathrm{d}\Phi_{m+1}} \mathrm{d}\sigma^{\mathrm{VS,1}}_{\mathrm{NNLO}} + \int_{\mathrm{d}\Phi_{m}} \mathrm{d}\sigma^{\mathrm{V,2}}_{\mathrm{NNLO}}\right] . \end{aligned} \tag{3.5}$$

Again all the terms in squared brackets are separately finite. Often starting from systematic methods for subtraction at NLO [20, 75, 120–123], several NNLO subtraction methods have been proposed in the literature [124–135], and are worked out to a varying level of sophistication. One of these methods is the so-called antenna subtraction scheme. It was derived at NNLO in [21] for partons only in the final state. In this thesis we compute the extension of the NNLO antenna subtraction formalism to include configurations, where one of the hard radiator partons is in the initial state. Before presenting the details of the calculations we briefly review the antenna subtraction method in general.

The characteristics and the differences between the several subtractions methods lie mainly in the construction of the subtraction terms. In general they all rely on the factorization of matrix elements, which was sketched in Chapter 2, and of the phase space, shown later. In the antenna subtraction formalism colour ordered squared matrix elements are considered. This means that $|\mathcal{M}_{m+1}(k_1,\ldots,k_{m+1};q)|^2$ in (3.3) denotes a squared, colour ordered matrix element where the particles are colour connected to their next neighbour particles. An illustration of colour ordering is given in Figure 3.4.

There are some advantages in considering colour ordered amplitudes. One of them is that a particle becoming unresolved can become collinear or soft only to its colour connected neighbours. In this case the soft factorization (2.87) is simplified since instead of summing over all external partons, we have to consider only the partons colour connected to the one becoming unresolved. Therefore, if parton j, colour connected

to the partons i and k becomes soft, the colour ordered matrix element undergoes QED-like factorization

$$|\mathcal{M}_{m+1}(k_1,\dots,k_i,k_j,k_k,\dots,k_{m+1};q)|^2 \to \frac{2s_{ik}}{s_{ij}s_{jk}}|\mathcal{M}_m(k_1,\dots,k_i,k_k,\dots,k_{m+1};q)|^2\,. \tag{3.6}$$

Antenna functions are constructed such that in the limit of parton j becoming soft they exactly reproduce the eikonal factor $2s_{ik}/(s_{ij}s_{jk})$ of (3.6). The same happens also in the collinear case, where the antennae reproduce the correct factorization with the splitting function as shown in (2.91).

3.2 Final-final antenna subtraction

We start looking at antenna subtraction by considering infrared singularities appearing only due to final state radiation. We call these configurations final-final configurations. In the following we will consider only massless partons. Antenna subtraction with massive partons was derived at NLO in [136].

Since we are considering m-jet production in electron-positron annihilation, and the initial state is colour less, infrared singularities can appear only due to final state radiation. At NLO the real radiation matrix element of eq. (3.4) depends on $(m+1)$ momenta $k_1,\dots,k_{m+1}$. Its general form corresponds to the Born cross section $\mathrm{d}\sigma^B$ with $m \to m+1$. In the antenna formalism the antenna subtraction terms are obtained as a sum of antennae

$$\begin{aligned}\mathrm{d}\sigma^S_{NLO} = \mathcal{N}\sum_{m+1}\mathrm{d}\Phi_m\left(k_1,\dots,k_{m+1};q\right)\frac{1}{S_{m+1}}\\ \times\sum_j X^0_{ijk}|\mathcal{M}_m(k_1,\dots,K_I,K_K,\dots,k_{m+1};q)|^2 J^{(m)}_m(k_1,\dots,K_I,K_K,\dots,k_{m+1})\,.\end{aligned} \tag{3.7}$$

such that

$$\begin{aligned}\mathrm{d}\sigma^R_{NLO} - \mathrm{d}\sigma^S_{NLO} = \mathcal{N}\sum_{m+1}\mathrm{d}\Phi_m\left(k_1,\dots,k_{m+1};q\right)\frac{1}{S_{m+1}}\\ \times\Big[|\mathcal{M}_{m+1}(k_1,\dots,k_{m+1};q)|^2 J^{(m+1)}_m(k_1,\dots,k_{m+1})\\ -\sum_j X^0_{ijk}|\mathcal{M}_m(k_1,\dots,K_I,K_K,\dots,k_{m+1};q)|^2 J^{(m)}_m(k_1,\dots,K_I,K_K,\dots,k_{m+1})\Big]\,.\end{aligned} \tag{3.8}$$

In the limit where parton j becomes unresolved the $(m+1)$-parton matrix element tends to a reduced m-parton matrix with redefined momenta K_I, K_K which are a

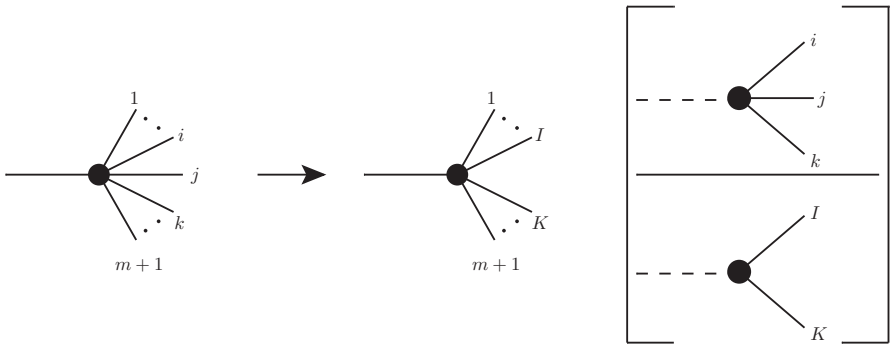

Figure 3.2: Illustration of NLO antenna factorization for final-final configurations representing both the factorization of the squared matrix element and of the phase space. The antenna function X^0_{ijk}, respectively the antennae phase space $\mathrm{d}\Phi_{X_{ijk}}$, are represented by the term in squared brackets.

linear combinations[1] of the original momenta k_i, k_j, k_k, times the tree antenna function X^0_{ijk} which depends only on the momenta k_i, k_j, k_k. This is shown schematically in Figure 3.2 which also shows that the antenna X^0_{ijk} is build up by a physical 3-parton matrix element depending on k_i, k_j, k_k normalized to a 2-parton matrix element which depends on the renormalized momenta K_I, K_K. The antenna X^0_{ijk} describes all of the soft and collinear configurations (for a given colour ordered amplitude) in which a parton j is emitted between two hard colour-connected partons i and k. The difference

$$\mathrm{d}\sigma^R_{NLO} - \mathrm{d}\sigma^S_{NLO}$$

is therefore finite in all soft and collinear limits of the phase space and can be safely integrated numerically. The requirement (A) defined in the previous section is thus satisfied.

In order to be useful, the antenna subtraction formalism has to satisfy also the requirement (B). A key observation in this regard is that the jet function in (3.7) does not depend on the individual momenta k_i, k_j, k_k, but only on K_I, K_K. Therefore, exploiting the factorization of the phase space[2],

$$\mathrm{d}\Phi_{m+1}(k_1, \ldots, k_{m+1}) = \mathrm{d}\Phi_m(k_1, \ldots, K_I, K_K, \ldots, k_{m+1}) \cdot \mathrm{d}\Phi_{X_{ijk}}(k_i, k_j, k_k; K_I + K_K)\,, \tag{3.9}$$

[1] The definition of the momenta K_I, K_K in terms of k_i, k_j, k_k is called momentum mapping. We will look more carefully at this issue later.

[2] The factorization of the phase space is intimately connected to the choice of the momentum mapping. This is particularly true in the initial-final case.

we can rewrite the integral over the subtraction term appearing in (3.4) as

$$\begin{aligned}\int_{\mathrm{d}\Phi_{m+1}} \mathrm{d}\sigma^S_{NLO} =& \mathcal{N}\int_{\mathrm{d}\Phi_{m+1}} \sum_{m+1} \mathrm{d}\Phi_{m+1} \frac{1}{S_{m+1}} \sum_j X^0_{ijk} |\mathcal{M}_m|^2 J^{(m)}_m \\ =& \mathcal{N}\int_{\mathrm{d}\Phi_m} \sum_{m+1} \mathrm{d}\Phi_m \frac{1}{S_{m+1}} |\mathcal{M}_m|^2 J^{(m)}_m \times \sum_j \int_{\mathrm{d}\Phi_{X_{ijk}}} X^0_{ijk} \mathrm{d}\Phi_{X_{ijk}} \,.\end{aligned} \tag{3.10}$$

The NLO antenna phase space $\mathrm{d}\Phi_{X_{ijk}}$ corresponds to the inclusive 3-particle phase space normalized to the 2-particle phase space P_2 (B.3), which is a constant[1]. This is also represented pictorially in Figure 3.2 and can be seen by setting $m = 2$ in (3.9) such that

$$\mathrm{d}\Phi_3 = P_2 \, \mathrm{d}\Phi_{X_{ijk}} \,. \tag{3.11}$$

The integration of the tree antenna X^0_{ijk} over its phase space in (3.10) can be done analytically and its result, properly normalized, defines the integrated antenna function

$$\mathcal{X}^0_{ijk}(s_{ijk}) = \frac{1}{C(\epsilon)} \int_{\mathrm{d}\Phi_{X_{ijk}}} X^0_{ijk} \,, \tag{3.12}$$

where

$$C(\epsilon) = (4\pi) \frac{e^{\epsilon\gamma_E}}{8\pi^2} \qquad \text{with Euler constant} \quad \gamma_E = 0.5772\ldots \,.$$

The normalization factor $C(\epsilon)$ is related to the renormalized coupling constant, and its relation to the bare coupling constant α^0_s, given in (2.18).

Up to now we denoted the antenna functions very generally as X. However every antenna is determined by both the external state and the pair of hard partons it collapses to. At NLO the following possibilities exists:

- antennae that collapse onto a hard quark-antiquark pair:

$$q g \bar{q} \to q \bar{q} \qquad : \quad X = A \,,$$

- antennae that collapse onto a hard quark-gluon pair:

$$q g g \to q g \qquad : \quad X = D \,,$$

$$q q' \bar{q}' \to q g \qquad : \quad X = E \,,$$

- antennae that collapse onto a hard gluon-gluon pair:

$$g g g \to g g \qquad : \quad X = F \,,$$

$$g q \bar{q} \to g g \qquad : \quad X = G \,.$$

[1] The 2- and 3-particle phase spaces are computed in Appendix B.

As already anticipated, all antenna functions are derived in a systematic manner from physical matrix elements known to possess the correct limits: the quark-antiquark antenna functions from $\gamma^* \to q\bar{q} + (\text{partons})$ [137], the quark-gluon antenna functions from $\tilde{\chi} \to \tilde{g} + (\text{partons})$ [138] and the gluon-gluon antenna functions from $H \to (\text{partons})$ [139]. Similarly to the antenna phase space, also the antenna functions are obtained by normalizing the colour ordered 3-parton squared matrix elements to the squared matrix element for the underlying 2-parton process

$$X^0_{ijk} = S_{ijk,IK} \frac{\left|\mathcal{M}^0_{ijk}\right|^2}{\left|\mathcal{M}^0_{IK}\right|^2}, \tag{3.13}$$

where $S_{ijk,IK}$ denotes the symmetry factor associated to the specific antenna. All the possible final-final NLO antennae, together with their limits are summarized in Table 3.1.

Quark-Quark	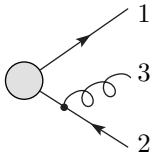	$A^0_{qg\bar{q}}$	Singular limits: Soft: $3_g \to 0$ Collinear: $3_g \| 1_q \quad 3_g \| 2_{\bar{q}}$
Quark-Gluon	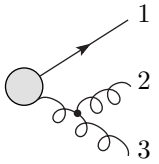	D^0_{qgg}	Singular limits: Soft: $2_g \to 0 \quad 3_g \to 0$ Collinear: $1_q \| 2_g \quad 1_q \| 3_g \quad 2_g \| 3_g$
	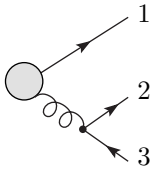	$E^0_{qq'\bar{q}'}$	Singular limits: Collinear: $2_q \| 3_{\bar{q}}$
Gluon-Gluon	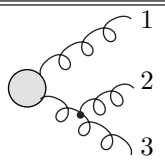	F^0_{ggg}	Singular limits: Soft: $1_g \to 0 \quad 2_g \to 0 \quad 3_g \to 0$ Collinear: $1_g \| 2_g \quad 1_g \| 3_g \quad 2_g \| 3_g$
	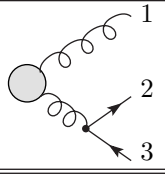	$G^0_{gq\bar{q}}$	Singular limits: Collinear: $2_q \| 3_{\bar{q}}$

Table 3.1: Final-final antennae at NLO.

We now focus on the issue of the momentum remapping and the corresponding phase space factorization. We consider again a colour ordered configuration of momenta k_i, k_j, k_k in which momentum k_j becomes unresolved. In this case the three momenta have to be remapped into a pair of momenta K_I, K_K:

$$k_i, k_j, k_k \overset{k_j \text{ unresolved}}{\to} K_I, K_K \,.$$

This remapping must fulfill the following conditions

- momentum conservation must be guaranteed: $k_i + k_j + k_k = K_I + K_K$,
- the new momenta K_I, K_K must be on the mass shell: $K_I^2 = K_K^2 = 0$,
- the new momenta should reduce to the old ones in the exact singular limits.

The first two conditions are also the reason why we consider always three momenta in the mapping instead of just two. If particle j becomes collinear to particle i, the parton k is not involved directly. However it is not possible to fulfill momentum conservation and on-shellness contemporarily with only two momenta.

The remapped momenta K_I and K_K must be a linear combination of the old ones and we can very generally choose

$$K_I = ak_i + bk_j + ck_k \quad ; \quad K_K = (1-a)k_i + (1-b)k_j + (1-c)k_k \quad \text{with } a, b, c \in \mathbb{R}\,,$$

in order to ensure momentum conservation. From the on-shellness condition it follows

$$ab\, s_{ij} + ac\, s_{ik} + bc\, s_{jk} = 0 \qquad ; \qquad a(s_{ij} + s_{ik}) + b(s_{ij} + s_{jk}) + c(s_{ik} + s_{jk}) = s_{ijk}\,,$$

where $s_{ijk} = (k_i + k_j + k_k)^2$. Finally, the third condition is fulfilled if

$$\begin{array}{lllll} \text{for } k_j \to 0\text{:} & K_I = k_i & ; & K_K = k_k, \\ \text{for } k_i || k_j\text{:} & K_I = k_i + k_j & ; & K_K = k_k, \\ \text{for } k_j || k_k\text{:} & K_I = k_i & ; & K_K = k_j + k_k. \end{array}$$

The way to satisfy these three conditions is not unique. As shown in [20], there is a 1-parameter family of possible choices. One possible choice is the one used also in the dipole subtraction formalism [121], a more symmetric choice [20] is

$$b = \frac{s_{jk}}{s_{ij} + s_{jk}} \quad ; \quad a = \frac{(1-\rho)s_{ijk} - 2bs_{jk}}{2(s_{ij} + s_{ik})} \quad ; \quad c = \frac{(1+\rho)s_{ijk} - 2bs_{ij}}{2(s_{jk} + s_{ik})}\,, \tag{3.14}$$

with

$$\rho^2 = 1 + \frac{4(1-b)bs_{ij}s_{jk}}{s_{ijk}s_{ij}}\,.$$

Correspondingly the m-parton phase space $\mathrm{d}\Phi_m$ in d dimensions can be factorized by inserting

$$1 = \frac{\int \mathrm{d}\Phi_2}{P_2} = \frac{1}{P_2}\int \frac{\mathrm{d}^d K_I}{(2\pi)^{d-1}}\delta^+(K_I^2)\frac{\mathrm{d}^d K_K}{(2\pi)^{d-1}}\delta^+(K_K^2)(2\pi)^d\delta(K_I+K_K-q)\,,$$

in the following way:

$$\begin{aligned}
\int \mathrm{d}\Phi_{m+1}(k_1,\ldots,k_{m+1};q) = \\
&= \frac{\mathrm{d}^d k_1}{(2\pi)^{d-1}}\delta^+(k_1^2)\cdots\frac{\mathrm{d}^d K_I}{(2\pi)^{d-1}}\delta^+(K_I^2)\frac{\mathrm{d}^d K_K}{(2\pi)^{d-1}}\delta^+(K_K^2)\cdots\frac{\mathrm{d}^d k_{m+1}}{(2\pi)^{d-1}}\delta^+(k_{m+1}^2) \\
&\quad\times(2\pi)^d\delta^d(q-k_1-\ldots-K_I-K_K-\ldots-k_{m+1}) \\
&\quad\times\frac{1}{P_2}\frac{\mathrm{d}^d k_i}{(2\pi)^{d-1}}\delta^+(k_i^2)\frac{\mathrm{d}^d k_j}{(2\pi)^{d-1}}\delta^+(k_j^2)\frac{\mathrm{d}^d k_k}{(2\pi)^{d-1}}\delta^+(k_k^2)\delta(q-k_i-k_j-k_k) \\
&= \int \mathrm{d}\Phi_m(k_1+\cdots+K_I+K_K+\cdots+k_{m+1};q)\cdot\mathrm{d}\Phi_{X_{ijk}}(k_i,k_j,k_k;K_I+K_K)\,.
\end{aligned}$$

We now have all the ingredients to construct NLO subtraction terms for singular final-final configurations. The next possible step is to extend this formalism to one order higher in perturbation theory. As shown in (3.5), at NNLO there are two different subtraction terms which must be computed: one for the double real emission contribution and one for the mixed real-virtual correction. All the details about the construction of subtraction terms at NNLO for final-final configurations can be found in [21], whereas the construction of subtraction terms and the real implementation of the antenna subtraction to compute $e^+e^-\to 3$ jet at NNLO is explained in [140]. The new results obtained with this computation concern event-shape variables and jet rates [141–144]. The matching of this results with resummation and an analysis of non-perturbative corrections to them are presented in Chapter 4 and 5. In the next section we present the antenna subtraction at NNLO for reactions where there is one parton in the initial state, the so-called initial-final configurations.

3.3 Initial-final antenna subtraction

In a reaction with two hadronic initial states h_1, h_2, the cross section is found by convoluting the partonic cross section with parton distribution functions

$$\mathrm{d}\sigma^{h_1h_2} = \sum_{a,b=q,\bar{q},g}\int\frac{\mathrm{d}\xi_1}{\xi_1}\frac{\mathrm{d}\xi_2}{\xi_2}f_a^{h_1}(\xi_1)f_b^{h_2}(\xi_2)\mathrm{d}\hat{\sigma}^{ab}(\xi_1P_1,\xi_2P_2)\,, \tag{3.15}$$

where ξ_1 and ξ_2 are the momentum fractions of the partons of species a and b. In the case of DIS, where there is only one incoming parton, we can replace one of the

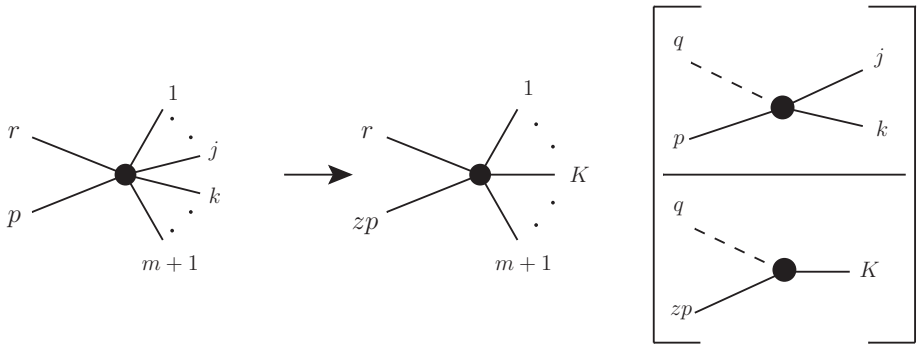

Figure 3.3: Illustration of NLO antenna factorization for initial-final configurations representing the factorization of the squared matrix element. The antenna function $X^0_{i,jk}$ is represented by the term in squared brackets.

PDF by a δ-distribution ($f(\xi) \to \delta(1-\xi)$) and we recover the universal factorization formula (2.82). It should be noted that the parton level cross section $\mathrm{d}\hat{\sigma}^{ab}$ is normalized to the hadron-hadron flux factor, which is transformed into the parton-parton flux factor by dividing out ξ_1 and ξ_2.

Subtraction terms in the case of one hard parton in the initial state are built in the same fashion as for the final-final case given in (3.7). All the antennae needed at NLO are derived in detail in [74]. The factorization of an $(m+1)$-parton matrix element into a reduced matrix element and an initial-final antenna is depicted schematically in Figure 3.3. We have the following subtraction term associated to a hard radiator parton i with momentum p in the initial state:

$$\mathrm{d}\hat{\sigma}^{S,(if)}(p,r) = \mathcal{N} \sum_{m+1} \mathrm{d}\Phi_{m+1}(k_1,\ldots,k_{m+1};p,r)\,\frac{1}{S_{m+1}}$$
$$\times \sum_j X^0_{i,jk}\,|\mathcal{M}_m(k_1,\ldots,K_K,\ldots,k_{m+1};zp,r)|^2\; J^{(m)}_m(k_1,\ldots,K_K,\ldots,k_{m+1})\,. \quad (3.16)$$

The additional momentum r stands for the momentum of the second incoming particle, for example, a virtual boson in DIS, or a second incoming parton in a hadronic collision process. This contribution has to be appropriately convoluted with the parton distribution function f^h_i. The tree antenna $X^0_{i,jk}$, depending only on the original momenta p, k_j and k_k, contains all the configurations in which parton j becomes unresolved. The m-parton amplitude depends only on redefined on-shell momenta $k_1,\ldots,K_K,\ldots$, and on the momentum fraction z[1].

The jet function, $J^{(m)}_m$, in (3.16) depends on the momenta k_j and k_k only through K_K. Thus, provided a suitable factorization of the phase space, one can perform the

[1] In the limit of parton j becoming unresolved this momentum fraction z correspond the partonic Bjorken-variable z defined in (2.83).

integration of the antennae analytically. Due to the hard particle in the initial state, the factorization of phase space is not as straightforward as for final-final antennae. The starting point is again the $(m+1)$-particle phase space $\mathrm{d}\Phi_{m+1}$. We can again insert twice the unity as

$$1 = \int \mathrm{d}^d q \delta(q + p - k_j - k_j)\,, \tag{3.17}$$

and

$$1 = \frac{Q^2}{2\pi} \int \frac{\mathrm{d}z}{z} \int \mathrm{d}^d K_K (2\pi)^{d-1} \delta^+(K_K^2)(2\pi)^d \delta(q + zp - K_K)\,, \tag{3.18}$$

with $Q^2 = -q^2$. Integrating over q, the phase space can be factorized in an m-parton phase space convoluted with a two particle phase space:

$$\begin{aligned} \mathrm{d}\Phi_{m+1}(k_1, \ldots, k_{m+1}; p, r) =& \mathrm{d}\Phi_m(k_1, \ldots, K_K, \ldots, k_{m+1}; zp, r) \\ & \times \frac{Q^2}{2\pi} \mathrm{d}\Phi_2(k_j, k_k; p, q) \frac{\mathrm{d}z}{z}\,, \end{aligned} \tag{3.19}$$

where $Q^2 = -q^2 = -(k_j + k_k - p)^2$. Replacing the factorized phase space in (3.16), we can explicitly carry out the integration of the antenna factors over the two particle phase space. When combining the integrated subtraction terms with virtual contributions and mass factorization terms, it turns out to be convenient to normalize the integrated antennae as follows

$$\mathcal{X}^0_{i,jk} = \frac{1}{C(\epsilon)} \int \mathrm{d}\Phi_2 \frac{Q^2}{2\pi} X^0_{i,jk}\,, \tag{3.20}$$

where as before

$$C(\epsilon) = (4\pi)^\epsilon \, \frac{e^{-\epsilon\gamma_E}}{8\pi^2}\,. \tag{3.21}$$

The integrated form of the subtraction term is then

$$\begin{aligned} \mathrm{d}\hat{\sigma}^{S,(if)}(p, r) = & \sum_{m+1} \sum_j \frac{\mathcal{N}}{S_{m+1}} \int \frac{\mathrm{d}z}{z}\, \mathcal{X}^0_{i,jk}(z, Q^2)\, \mathrm{d}\Phi_m(k_1, \ldots, K_K, \ldots, k_{m+1}; z\, p, r) \\ & \times |\mathcal{M}_m(k_1, \ldots, K_K, \ldots, k_{m+1}; z\, p, r)|^2\, J^{(m)}_m(k_1, \ldots, K_K, \ldots, k_{m+1})\,. \end{aligned}$$

Finally, the subtraction term has to be convoluted with the parton distribution functions to give the corresponding contribution to the hadronic cross section. The explicit poles in the integrated form cancel the corresponding ones in the virtual and mass factorization contributions. To carry out the explicit cancellation of poles, it is convenient to recast, by a shift of variables, the integrated subtraction term, once convoluted with the PDFs, in the following form

$$\begin{aligned} d\sigma^{S,(if)}(p, r) = & \sum_{m+1} \sum_j \frac{S_m}{S_{m+1}} \int \frac{\mathrm{d}\xi_1}{\xi_1} \int \frac{\mathrm{d}\xi_2}{\xi_2} \int_{\xi_1}^1 \frac{\mathrm{d}z}{z} f_{i/1}\left(\frac{\xi_1}{z}\right) f_{b/2}\left(\xi_2\right) \\ & \times C(\epsilon)\, \mathcal{X}^0_{i,jk}(z)\, \mathrm{d}\hat{\sigma}^B(\xi_1 H_1, \xi_2 H_2)\,. \end{aligned} \tag{3.22}$$

This convolution has already the appropriate structure and mass factorization can be carried out explicitly leaving a finite contribution. The remaining phase space integration, implicit in the Born cross section, $\mathrm{d}\hat{\sigma}^B$, and the convolutions can be safely done numerically. Again, when considering reactions with only one incoming hadron, the second PDF has to be replaced by a Dirac delta. Reactions with two hadrons will require additional subtractions containing initial-final antennae involving the second parton in the initial state and initial-initial antennae as well. This case is discussed to NLO in [74]. All the initial-final antennae at NLO with their unresolved limits are summarized in Table 3.2 and Table 3.3.

Quark-Quark	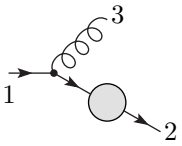	$A^0_{q,gq}$	Singular limits: Soft: $3_g \to 0$ Collinear: $3_g \| \| 1_q \quad 3_g \| \| 2_q$
Quark-Gluon	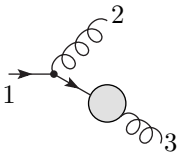	$D^0_{q,gg}$	Singular limits: Soft: $2_g \to 0 \quad 3_g \to 0$ Collinear: $1_q \| \| 2_g \quad 1_q \| \| 3_g \quad 2_g \| \| 3_g$
	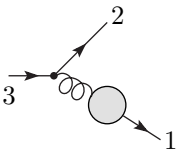	$E^0_{q',q'q}$	Singular limits: Collinear: $2_q \| \| 3_q$
	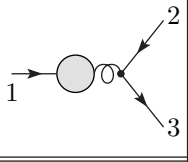	$E^0_{q,q'\bar{q}'}$	Singular limits: Collinear: $2_q \| \| 3_{\bar{q}}$
Gluon-Gluon	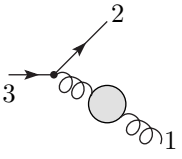	$G^0_{q,gq}$	Singular limits: Collinear: $2_q \| \| 3_q$

Table 3.2: Initial-final quark-initiated antennae at NLO.

As shown in (3.5), at NNLO two types of contributions to m-jet observables require subtraction: the tree-level $m+2$ parton matrix elements (where one or two partons can become unresolved), and the one-loop $m+1$ parton matrix elements (where one parton can become unresolved). The corresponding subtraction terms are denoted by

Quark-Quark	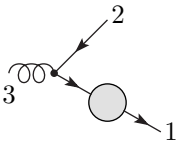	$A^0_{g,q\bar{q}}$	Singular limits: Collinear: $1_q \| 3_g \quad 2_q \| 3_g$
Quark-Gluon	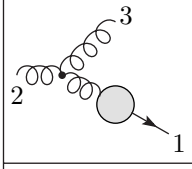	$D^0_{g,gq}$	Singular limits: Soft: $3_g \to 0$ Collinear: $1_q \| 3_g \quad 2_g \| 3_g$
	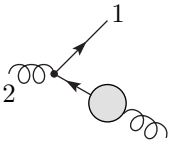	$D^0_{g,qg}$	Singular limits: Collinear: $1_q \| 3_g$
	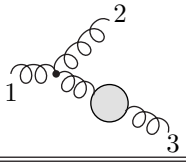	$F^0_{g,gg}$	Singular limits: Soft: $2_g \to 0 \quad 3_g \to 0$ Collinear: $1_g \| 2_g \quad 1_g \| 3_g \quad 2_g \| 3_g$
Gluon-Gluon	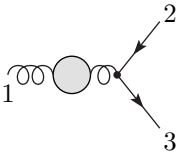	$G^0_{g,q\bar{q}}$	Singular limits: Collinear: $2_q \| 3_{\bar{q}}$

Table 3.3: Initial-final gluon-initiated antennae at NLO. The D-type quark-gluon antenna is split into two subantennae according to [74].

$\mathrm{d}\sigma^S_{\mathrm{NNLO}}$ and $\mathrm{d}\sigma^{VS,1}_{\mathrm{NNLO}}$ in (3.5).

In $\mathrm{d}\sigma^S_{\mathrm{NNLO}}$, we have to distinguish four different types of unresolved configurations (Figure 3.4):

(a) One unresolved parton but the experimental observable selects only m jets;

(b) Two colour-connected unresolved partons (colour-connected);

(c) Two unresolved partons that are not colour connected but share a common radiator (almost colour-unconnected);

(d) Two unresolved partons that are well separated from each other in the colour chain (colour-unconnected).

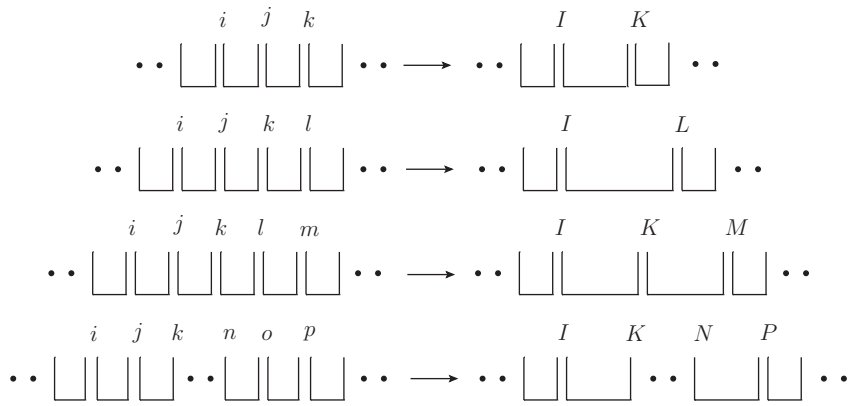

Figure 3.4: The four different possible unresolved configurations at NNLO.

Among those, configuration (a) is properly accounted for by a single tree-level three-parton antenna function like used already at NLO. Configuration (b) requires a tree-level four-parton antenna function (two unresolved partons emitted between a pair of hard partons), while (c) and (d) are accounted for by products of two tree-level three-parton antenna functions. With radiator parton i in the initial state, the subtraction terms for these configurations read:

$$\begin{aligned}
\mathrm{d}\sigma^{S,a}_{\mathrm{NNLO}} =& \mathcal{N} \sum_{m+2} \mathrm{d}\Phi_{m+2}(k_1,\ldots,k_{m+2};p,r)\frac{1}{S_{m+2}} \\
&\times \Bigg[\sum_j X^0_{i,jk} \, |\mathcal{M}_{m+1}(k_1,\ldots,K_K,\ldots,k_{m+2};zp,r)|^2 \\
&\qquad\qquad \times J^{(m+1)}_m(k_1,\ldots,K_K,\ldots,k_{m+2}) \Bigg] , \qquad (3.23) \\
\mathrm{d}\sigma^{S,b}_{\mathrm{NNLO}} =& \mathcal{N} \sum_{m+2} \mathrm{d}\Phi_{m+2}(k_1,\ldots,k_{m+2};p,r)\frac{1}{S_{m+2}} \\
&\times \Bigg[\sum_{jk} \left(X^0_{i,jkl} - X^0_{i,jk} X^0_{I,Kl} - X^0_{jkl} X^0_{i,JL} \right) \\
&\times |\mathcal{M}_m(k_1,\ldots,K_L,\ldots,k_{m+2};zp,r)|^2 \, J^{(m)}_m(k_1,\ldots,K_L,\ldots,k_{m+2}) \Bigg] , \qquad (3.24) \\
\mathrm{d}\sigma^{S,c1}_{\mathrm{NNLO}} =& -\mathcal{N} \sum_{m+2} \mathrm{d}\Phi_{m+2}(k_1,\ldots,k_{m+2};p,r)\frac{1}{S_{m+2}} \\
&\times \Bigg[\sum_{j,l} X^0_{i,jk} \, x^0_{mlK} \, |\mathcal{M}_m(k_1,\ldots,K_K,K_M,\ldots,k_{m+2};zp,r)|^2
\end{aligned}$$

$$\times J_m^{(m)}(k_1,\ldots,K_K,K_M,\ldots,k_{m+2})$$
$$+\sum_{j,l} X^0_{klm}\, x^0_{i,jK}\, |\mathcal{M}_m(k_1,\ldots,K_K,K_M,\ldots,k_{m+2});zp,r|^2$$
$$\times J_m^{(m)}(k_1,\ldots,K_K,K_M,\ldots,k_{m+2})\Bigg], \tag{3.25}$$

$$\mathrm{d}\sigma^{S,c2}_{\mathrm{NNLO}} = -\mathcal{N}\sum_{m+2}\mathrm{d}\Phi_{m+2}(k_1,\ldots,k_{m+2};p,r)\frac{1}{S_{m+2}}$$
$$\times\Bigg[\sum_{j,l} X^0_{i,jk}\, x^0_{I,lm}\, |\mathcal{M}_m(k_1,\ldots,K_K,K_M,\ldots,k_{m+2};zp,r)|^2$$
$$\times J_m^{(m)}(k_1,\ldots,K_K,K_M,\ldots,k_{m+2})$$
$$+\sum_{j,l} X^0_{i,lm}\, x^0_{I,jk}\, |\mathcal{M}_m(k_1,\ldots,K_K,K_M,\ldots,k_{m+2});zp,r|^2$$
$$\times J_m^{(m)}(k_1,\ldots,K_K,K_M,\ldots,k_{m+2})\Bigg], \tag{3.26}$$

$$\mathrm{d}\sigma^{S,d}_{\mathrm{NNLO}} = -\mathcal{N}\sum_{m+2}\mathrm{d}\Phi_{m+2}(k_1,\ldots,k_{m+2};p,r)\frac{1}{S_{m+2}}$$
$$\times\Bigg[\sum_{j,o} X^0_{i,jk}\, X^0_{nop}\, |\mathcal{M}_m(k_1,\ldots,K_K,\ldots,K_N,K_P,\ldots,k_{m+2};zp,r)|^2$$
$$\times J_m^{(m)}(k_1,\ldots,K_K,\ldots,K_N,K_P,\ldots,k_{m+2})\Bigg]. \tag{3.27}$$

As before, the original momenta of the $(m+2)$-parton phase space are denoted by $j,k,\ldots$, while the combined momenta obtained from a phase space mapping are labeled by $J,K,\ldots$. Only the combined momenta appear in the jet function. x^0_{abc} is a 3-parton sub-antenna function containing only limits where parton b is unresolved with respect to parton a, but not limits where parton b is unresolved with respect to parton c. $\mathrm{d}\sigma^{S,c1}_{\mathrm{NNLO}}$ applies if the common radiator is in the final state, while $\mathrm{d}\sigma^{S,c2}_{\mathrm{NNLO}}$ applies if the common radiator is in the initial state. The only genuinely new ingredient here is the four-parton initial-final antenna function $X^0_{i,jkl}$, which can be obtained by crossing the corresponding final-final antenna functions, and has to be integrated analytically over the appropriate antenna phase space. The factorization of the matrix element in case of two colour-connected unresolved partons into a reduced matrix element and an NNLO initial-final antenna is shown in Figure 3.5. The resulting integrated antenna

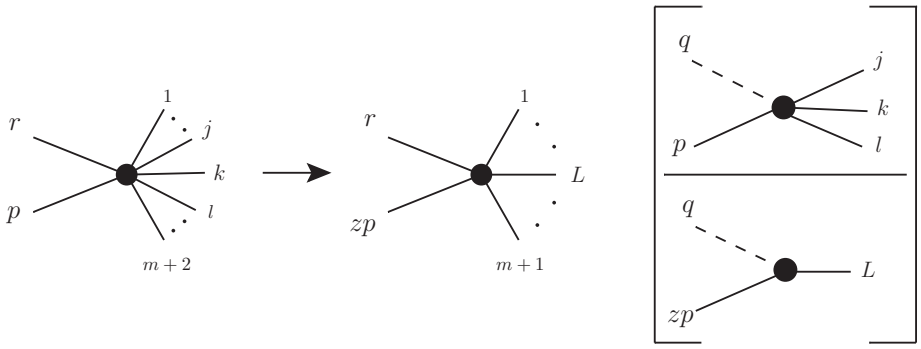

Figure 3.5: Illustration of NNLO double-real antenna factorization for initial-final configurations representing the factorization of the squared matrix element. The antenna function $X^0_{i,jkl}$ is represented by the term in squared brackets.

function exploits the phase space factorization (analogous to the NLO case),

$$\begin{aligned} \mathrm{d}\Phi_{m+2}(k_1,\ldots,k_{m+2};p,r) &= \mathrm{d}\Phi_m(k_1,\ldots,K_L,\ldots,k_{m+2};zp,r) \\ &\times \frac{Q^2}{2\pi}\mathrm{d}\Phi_3(k_j,k_k,k_l;p,q)\frac{\mathrm{d}z}{z}\,, \end{aligned} \tag{3.28}$$

yielding the integrated antenna

$$\mathcal{X}^0_{i,jkl} = \frac{1}{[C(\epsilon)]^2}\int \mathrm{d}\Phi_3 \frac{Q^2}{2\pi} X^0_{i,jkl}\,. \tag{3.29}$$

In all products of two three-parton antenna functions, the analytic integration has to be performed only over the outmost antenna function, yielding the integrated NLO antenna functions in the appropriate (final-final or initial-final) kinematics.

The one-loop single unresolved subtraction term $\mathrm{d}\sigma^{VS,1}_{\mathrm{NNLO}}$ must account for three types of singular contributions:

(a) Explicit infrared poles of the virtual one-loop $(m+1)$ parton matrix element.

(b) Single unresolved limits of the virtual one-loop $(m+1)$ parton matrix element.

(c) Terms common to both above contributions, which are oversubtracted.

With radiator parton i in the initial state, the subtraction terms for these configurations read:

$$\begin{aligned} \mathrm{d}\sigma^{VS,1,a}_{\mathrm{NNLO}} =& \mathcal{N}\sum_{m+1}\mathrm{d}\Phi_{m+1}(k_1,\ldots,k_{m+1};p,r)\frac{1}{S_{m+1}} \\ &\times\left[\sum_{ik} - \int\frac{\mathrm{d}z}{z}\,\mathcal{X}^0_{i,jk}(z,-t_{ik})\,|\mathcal{M}_{m+1}(k_1,\ldots,k_k,\ldots,k_{m+1};zp,r)|^2\right. \end{aligned}$$

$$\times J_m^{(m+1)}(k_1,\ldots,k_k,\ldots,k_{m+1})\Bigg], \tag{3.30}$$

$$\begin{aligned}\mathrm{d}\sigma^{VS,1,b}_{\mathrm{NNLO}} =&\mathcal{N}\sum_{m+1}\mathrm{d}\Phi_{m+1}(k_1,\ldots,k_{m+1};p,r)\frac{1}{S_{m+1}}\\ &\times\sum_j\Bigg[X^0_{i,jk}\,|\mathcal{M}^1_m(k_1,\ldots,K_K,\ldots,k_{m+1};zp,r)|^2\,J_m^{(m)}(k_1,\ldots,K_K,\ldots,k_{m+1})\\ &+\;X^1_{i,jk}\,|\mathcal{M}_m(k_1,\ldots,K_K,\ldots,k_{m+1};zp,r)|^2\,J_m^{(m)}(k_1,\ldots,K_K,\ldots,k_{m+1})\Bigg],\end{aligned} \tag{3.31}$$

$$\begin{aligned}\mathrm{d}\sigma^{VS,1,c1}_{\mathrm{NNLO}} =&\mathcal{N}\sum_{m+1}\mathrm{d}\Phi_{m+1}(k_1,\ldots,k_{m+1};p,r)\frac{1}{S_{m+1}}\\ &\times\Bigg[\sum_{ik}\int\frac{\mathrm{d}z}{z}\,\mathcal{X}^0_{i,jk}(z,-t_{ik})\sum_o X^0_{nop}\\ &\qquad\times|\mathcal{M}_m(k_1,\ldots,k_k,\ldots,K_N,K_P,\ldots,k_{m+1};zp,r)|^2\\ &\qquad\times J_m^{(m)}(k_1,\ldots,k_k,\ldots,K_N,K_P,\ldots,k_{m+1})\Bigg],\end{aligned} \tag{3.32}$$

$$\begin{aligned}\mathrm{d}\sigma^{VS,1,c2}_{\mathrm{NNLO}} =&\mathcal{N}\sum_{m+1}\mathrm{d}\Phi_{m+1}(k_1,\ldots,k_{m+1};p,r)\frac{1}{S_{m+1}}\\ &\times\Bigg[\sum_{np}\mathcal{X}^0_{nop}(s_{np})\sum_j X^0_{i,jk}\,|\mathcal{M}_m(k_1,\ldots,K_K,\ldots,k_n,k_p,\ldots,k_{m+1};zp,r)|^2\\ &\qquad\times J_m^{(m)}(k_1,\ldots,K_K,\ldots,k_n,k_k,\ldots,k_{m+1})\Bigg],\end{aligned} \tag{3.33}$$

In here, $X^1_{i,jk}$ denotes a one-loop three-parton initial-final antenna function, which is the only new ingredient. Figure 3.6 show the factorization of a real-virtual matrix element into the corresponding reduced real and virtual matrix elements and the real and virtual antennae. These one-loop antenna functions can be obtained by crossing from their final-final counterparts, listed in [21], and have to be integrated over the appropriate phase space:

$$\mathcal{X}^1_{i,jk}=\frac{1}{C(\epsilon)}\int\mathrm{d}\Phi_2\frac{Q^2}{2\pi}X^1_{i,jk}\,. \tag{3.34}$$

Also in this case the subtraction terms $\mathrm{d}\sigma^S_{\mathrm{NLO}}$, $\mathrm{d}\sigma^S_{\mathrm{NNLO}}$ and $\mathrm{d}\sigma^{VS,1}_{\mathrm{NNLO}}$ require three different types of antenna functions corresponding to the different pairs of hard partons forming the antenna: quark-antiquark, quark-gluon and gluon-gluon antenna functions.

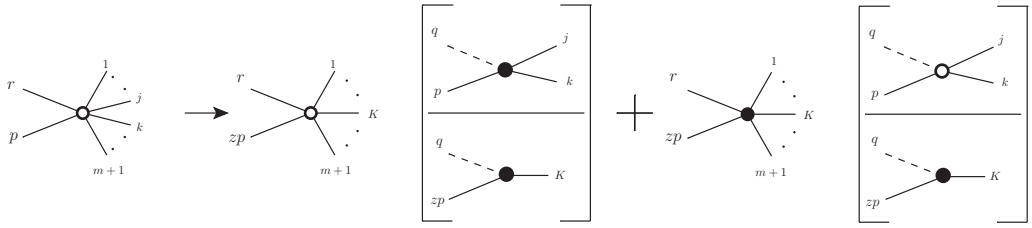

Figure 3.6: Illustration of NNLO real-virtual antenna factorization for initial-final configurations representing the factorization of the squared matrix element. The antenna function $X^1_{i,jk}$ is represented by the second term in squared brackets.

For the initial-final kinematics, we consider the antenna derived in [21] for the final-final case and we cross one parton into the initial state. Special care has to be taken in these crossings, if we start from those final-final antenna functions which contain more than one quark/antiquark or more than one gluon in the final state. In the case of more than one quark/antiquark pair of different flavour (final-final antenna functions B^0_4, E^0_3, E^1_3-type, E^0_4-type), we have to distinguish the crossing of the primary quark q (which is coupled to the external current) and the secondary quark q' (which is not coupled to the external current). The identical flavour antenna function $C^0_4(1_q, 3_q, 4_{\bar{q}}, 2_{\bar{q}})$ is constructed from the interference of the four-quark amplitudes with the antiquark-momenta interchanged, and it contains only the $(3_q, 4_{\bar{q}}, 2_{\bar{q}})$ triple collinear limit. Consequently, it is symmetric in the two antiquark momenta, but not in the two quark momenta, and has thus three different crossings: $C^0_{q,q\bar{q}q}$ (either antiquark crossed), $C^0_{\bar{q},\bar{q}q\bar{q}}$ (quark (1_q) crossed) and $C^0_{\bar{q},q\bar{q}\bar{q}}$ (quark (3_q) crossed). Crossing one of several gluons into the initial state is unambiguous for most antenna functions owing to their symmetry properties. The only exception is the quark-gluon antenna function $D^0_4(1_q, 3_g, 4_g, 5_g)$, where gluons (3_g) and (5_g) are colour-connected to the quark, while gluon (4_g) is not. We thus distinguish two crossings, $D^0_{g,ggq}$ (gluon (3_g) or (5_g) crossed) and $D^0_{g',ggq}$ (gluon (4_g) crossed). We list all NLO and NNLO initial-final antenna functions with an initial state quark in Table 3.4 and with an initial state gluon in Table 3.5.

It was shown in [145, 146] that these antenna subtraction terms result in an oversubtraction of large-angle soft gluon radiation. To correct for this oversubtraction, one introduces the soft antenna function

$$S_{ajc} = 2\frac{s_{ac}}{s_{aj}s_{cj}}\,, \tag{3.35}$$

where a and c label arbitrary hard partons. Those soft factors are associated with an antenna phase space mapping $(i, j, k) \to (I, K)$ (final-final) or $(p, j, k) \to (zp, K)$ (initial-final). In contrast to all previous subtraction terms, the hard momenta a, c do

Quark initiated	tree level	one loop
quark-quark		
$q \to gq$	$A^0_{q,gq}$	$A^1_{q,gq}$, $\tilde{A}^1_{q,gq}$, $\hat{A}^1_{q,gq}$
$q \to ggq$	$A^0_{q,ggq}$,$\tilde{A}^0_{q,ggq}$	
$q \to q'\bar{q}'q$	$B^0_{q,q'\bar{q}'q}$	
$q' \to q\bar{q}q'$	$B^0_{q',q\bar{q}q'}$	
$q \to q\bar{q}q$	$C^0_{q,q\bar{q}q}$, $C^0_{\bar{q},\bar{q}q\bar{q}}$, $C^0_{\bar{q},q\bar{q}\bar{q}}$	
quark-gluon		
$q \to gg$	$D^0_{q,gg}$	$D^1_{q,gg}$, $\hat{D}^1_{q,gg}$
$q \to ggg$	$D^0_{q,ggg}$	
$q \to q'\bar{q}'$	$E^0_{q,q'\bar{q}'}$	$E^1_{q,q'\bar{q}'}$, $\tilde{E}^1_{q,q'\bar{q}'}$, $\hat{E}^1_{q,q'\bar{q}'}$
$q \to q'\bar{q}'g$	$E^0_{q,q'\bar{q}'g}$, $\tilde{E}^0_{q,q'\bar{q}'g}$	
$q' \to q'q$	$E^0_{q',q'q}$	$E^1_{q',q'q}$, $\tilde{E}^1_{q',q'q}$, $\hat{E}^1_{q',q'q}$
$q' \to q'qg$	$E^0_{q',q'qg}$, $\tilde{E}^0_{q',q'qg}$	
gluon-gluon		
$q \to qg$	$G^0_{q,qg}$	$G^1_{q,qg}$, $\tilde{G}^1_{q,qg}$, $\hat{G}^1_{q,qg}$
$q \to qgg$	$G^0_{q,qgg}$, $\tilde{G}^0_{q,qgg}$	
$q \to qq'\bar{q}'$	$H^0_{q,qq'\bar{q}'}$	

Table 3.4: List of tree level and one loop antenna functions for the initial-final configurations with a quark in the initial state.

not need to be equal to the hard momenta of partons i, k in the antenna phase space - they can be arbitrary on-shell momenta in the initial or final state.

If parton (a) is in the initial state, and (c,i,j,k) are in the final state, the integral of each of the soft antenna function over the antenna phase space can be written as

$$\begin{aligned}\mathcal{S}_{a,c;ik} &= \int \mathrm{d}\Phi_{X_{ijk}} S_{ajc} \\ &= (s_{IK})^{-\epsilon}\ \frac{\Gamma^2(1-\epsilon)e^{\epsilon\gamma}}{\Gamma(1-3\epsilon)}\ \left(-\frac{2}{\epsilon}\right)\left[-\frac{1}{\epsilon} + \ln\left(x_{ac,IK}\right) + \epsilon\,\mathrm{Li}_2\left(-\frac{1-x_{ac,IK}}{x_{ac,IK}}\right)\right],\end{aligned} \tag{3.36}$$

where we have defined

$$x_{ac,IK} = \frac{t_{ac}s_{IK}}{(t_{aI}+t_{aK})(s_{cI}+s_{cK})}\,. \tag{3.37}$$

If parton (i) is in the initial state, while (a,c,j,k) are in the final state, we obtain the

Gluon initiated	tree level	one loop
quark-quark		
$g \to q\bar{q}$	$A^0_{g,q\bar{q}}$	$A^1_{g,q\bar{q}}$, $\tilde{A}^1_{g,q\bar{q}}$, $\hat{A}^1_{g,q\bar{q}}$
$g \to gq\bar{q}$	$A^0_{g,gq\bar{q}}$, $\tilde{A}^0_{g,gq\bar{q}}$	
quark-gluon		
$g \to gg$	$D^0_{g,gq}$	$D^1_{g,gq}$, $\hat{D}^1_{g,gq}$
$g \to ggq$	$D^0_{g,ggq}$, $D^0_{g',ggq}$	
$g \to qq'\bar{q}'$	$E^0_{g,qq'\bar{q}'}$, $\tilde{E}^0_{g,qq'\bar{q}'}$	
gluon-gluon		
$g \to gg$	$F^0_{g,gg}$	$F^1_{g,gg}$,$\hat{F}^1_{g,gg}$
$g \to ggg$	$F^0_{g,ggg}$	
$g \to q\bar{q}$	$G^0_{g,q\bar{q}}$	$G^1_{g,q\bar{q}}$, $\tilde{G}^1_{g,q\bar{q}}$, $\hat{G}^1_{g,q\bar{q}}$
$g \to q\bar{q}g$	$G^0_{g,q\bar{q}g}$, $\tilde{G}^0_{g,q\bar{q}g}$	

Table 3.5: List of tree level and one loop antenna functions for the initial-final configurations with a gluon in the initial state.

following integral:

$$\begin{aligned}\mathcal{S}_{ac;i,k} =& \frac{1}{C(\epsilon)} \int \mathrm{d}\Phi_{2_{jk}} \frac{Q^2}{2\pi} S_{ajc} \\ =& \left(Q^2\right)^{-\epsilon} \frac{\Gamma^2(1-\epsilon)\Gamma(1+e)e^{\epsilon\gamma}}{\Gamma(1-2\epsilon)} \left(-\frac{2}{\epsilon}\right) z^{1+2\epsilon} (1-z)^{-1-2\epsilon} y^{-\epsilon}_{ac,iK} \,,\end{aligned} \tag{3.38}$$

where we have defined

$$y_{ac,iK} = \frac{s_{ac}Q^2}{(s_{aK} + (1-z)s_{ai})\,(s_{cK} + (1-z)s_{ci})} \,. \tag{3.39}$$

3.3.1 Phase space mappings

As discussed previously for the final-final case and above in this section, the construction of subtraction terms requires mapping the original set of momenta onto a reduced set. Appropriate mappings for the initial-final configurations, both for single and double unresolved configurations have been discussed in [74].

The proper subtraction of infrared singularities requires that the momentum mapping satisfy

$$\begin{aligned}
&zp \to p\,, && K_K \to k_k && \text{when } j \text{ becomes soft}\,,\\
&zp \to p\,, && K_K \to k_j + k_k && \text{when } j \text{ becomes collinear with } k\,,\\
&zp \to p - k_j\,, && K_K \to k_k && \text{when } j \text{ becomes collinear with } i\,.
\end{aligned}$$

In this way, infrared singularities are subtracted locally, except for angular correlations, *before convoluting with the parton distributions*. That is, matrix elements and subtraction terms are convoluted together with PDFs. In addition, the redefined momentum, K_K, must be on shell and momentum must be conserved, $p - k_j - k_k = zp - K_K$, for the phase space to factorize as above. This is accomplished by[1]:

$$\begin{aligned} z &= \frac{s_{1j} + s_{1k} - s_{jk}}{s_{1j} + s_{1k}}\,, \\ K_K &= k_j + k_k - (1-z)p\,, \end{aligned} \tag{3.40}$$

where $s_{1j} = (p - k_j)^2$, etc. If parton j becomes soft or collinear to parton k, $z \to 1$. If parton j becomes collinear with the initial state parton i, $z = 1 - w$ with w the fraction of the momentum p carried by parton j.

This mapping is easily generalized to deal with more than one parton becoming unresolved. As explained above, the building blocks for the double real radiation in the initial-final situation are colour-ordered four-parton antenna functions $X_{i,jkl}$, with one radiator parton i (with momentum p) in the initial state, two unresolved partons j, k and one radiator parton l in the final state:

$$\begin{aligned} z &= \frac{s_{1j} + s_{1k} + s_{1l} - s_{jk} - s_{jl} - s_{kl}}{s_{1j} + s_{1k} + s_{1l}}\,, \\ K_L &= k_j + k_k + k_l - (1-z)p\,, \end{aligned} \tag{3.41}$$

where k_j, k_k and k_l are the three final-state momenta involved in the subtraction term. It satisfies the appropriate limits in all double singular configurations:

1. j and k soft: $z \to 1$, $K_L \to k_l$,
2. j soft and $k_k \parallel k_l$: $z \to 1$, $K_L \to k_k + k_l$,
3. $k_j = wp \parallel p$ and k_k soft: $z \to 1 - w$, $K_L \to k_l$,
4. $k_j = wp \parallel p$ and $k_k \parallel k_l$: $z \to 1 - w$, $K_L \to k_k + k_l$,
5. $k_j \parallel k_k \parallel k_l$: $z \to 1$, $K_L \to k_j + k_k + k_l$,
6. $k_j + k_k = wp \parallel p$: $z \to 1 - w$, $K_L \to k_l$,

where partons j and k can be interchanged in all cases.

The construction of NNLO antenna subtraction terms requires moreover that all single unresolved limits of the four-parton antenna function $X_{i,jkl}$ have to be subtracted, (3.24), such that the resulting subtraction term is active only in its double

[1] The symmetric mapping used in the final-final case leads to a non factorizing phase space. The reasons for this are explained in detail in [74].

unresolved limits. A systematic subtraction of these single unresolved limits by products of two three-parton antenna functions can be performed only if the NNLO phase space mapping turns into an NLO phase space mapping in its single unresolved limits.

In the limits where parton j becomes unresolved, we denote the parameters of the reduced NLO phase space mapping (3.40) by z' and K'_L. We find for (3.41):

1. j becomes soft:

$$z \to \frac{s_{1k}+s_{1l}-s_{kl}}{s_{1k}+s_{1l}} = z' \,, \qquad K_L \to k_k + k_l - (1-z)p = K'_L \,.$$

2. $k_j \parallel k_k$, $k_j + k_k = K_K$:

$$z \to \frac{s_{1K}+s_{1l}-s_{Kl}}{s_{1K}+s_{1l}} = z' \,, \qquad K_L \to k_K + k_l - (1-z)p = K'_L \,.$$

3. $k_j = wp \parallel p$:

$$z \to \frac{(1-w)(s_{1k}+s_{1l})-s_{kl}}{s_{1k}+s_{1l}} = (1-w)z' \,, \qquad K_L \to k_k + k_l - (1-z')(1-w)p = K'_L.$$

It can be seen that in the first two limits, the NLO mapping involves the original incoming momentum p, while in the last limit (initial state collinear emission), it involves the rescaled incoming momentum $(1-w)p$. To subtract all three single unresolved limits of parton j between emitter partons i and k from $X_{i,jkl}$, one needs to subtract from it the product of two three-parton antenna functions $X_{i,jk} \cdot X_{I,Kl}$. The phase space mapping relevant to these terms is the iteration of two NLO phase space mappings. Analytical integration of terms with this mapping is required only over the phase space appropriate to the first antenna function.

Equally, parton k can become unresolved. Expressing the reduced NLO phase space mapping by z'' and K''_L. We find for (3.41):

1. k becomes soft:

$$z \to \frac{s_{1j}+s_{1l}-s_{jl}}{s_{1j}+s_{1l}} = z'' \,, \qquad K_L \to k_j + k_l - (1-z)p = K''_L \,.$$

2. $k_k \parallel k_j$, $k_j + k_k = K_K$:

$$z \to \frac{s_{1K}+s_{1l}-s_{Kl}}{s_{1K}+s_{1l}} = z'' \,, \qquad K_L \to k_K + k_l - (1-z)p = K''_L \,.$$

3. $k_k \parallel k_l$, $k_l + k_k = K_K$:

$$z \to \frac{s_{1K}+s_{1j}-s_{Kj}}{s_{1K}+s_{1j}} = z'' \,, \qquad K_L \to k_K + k_j - (1-z)p = K''_L \,.$$

In all limits, the reduced NLO mapping involves the original incoming momentum p. Consequently, the three single unresolved limits of parton k between emitter partons j and l can be subtracted from $X_{i,jkl}$ by a product of a final-final and an initial-final three-parton antenna function $X_{jkl} \cdot X_{i,JL}$. The phase space mapping relevant to these terms is the product of an NLO final-final phase space mapping with an initial-final mapping. Integration of the final-final antenna phase space yields a constant, not involving an extra convolution.

3.4 Integration of initial-final antenna functions at NNLO

The initial-final antenna functions all have the scattering kinematics

$$q + p_i \to k_1 + k_2(+k_3) \,,$$

where

$$q^2 = -Q^2 < 0 \,, \quad p_i^2 = 0 \,, \quad z = \frac{Q^2}{2\, q \cdot p_i} \,, \quad k_1^2 = k_2^2 = k_3^2 = 0 \,, \tag{3.42}$$

and k_3 is present only for the NNLO real radiation antenna functions. Consequently, integration over the final-state two-parton or three-parton phase space yields a result which depends only on Q^2 and z. From dimensional counting, one can immediately conclude that the dependence on Q^2 is only multiplicative, according to the mass dimension of the integral.

The NNLO double real radiation antenna functions $X^0_{i,jkl}$ have to be integrated over the inclusive three-parton final state phase space. The NNLO one-loop single real radiation antenna functions $X^1_{i,jk}$ are integrated over the inclusive two-parton final state phase space, and over the loop momentum. For both types of integration, we employ the by-now standard technique of reduction to master integrals. The master integrals are then computed from their differential equations in Q^2 and z.

To perform the reduction, we first express all phase space integrals as loop integrals with cut propagators [147] using the identity

$$2\pi i\, \delta^{(+)}(k_j^2) = \frac{1}{k_j^2 + i0} - \frac{1}{k_j^2 - i0} \qquad \text{with} \quad j = 1, 2, 3 \,.$$

Consequently, all NNLO integrals are expressed as cuts of two-loop four-point functions with two off-shell legs in forward scattering kinematics. Using integration-by-parts (IBP, [148, 149]) and Lorentz invariance (LI, [150]) identities among the integrals of any given topology, the large number of different integrals can be expressed in terms of a small number of master-integrals. This reduction is performed iteratively, based on the lexicographic ordering of the integrals, expressed by the Laporta algorithm [151].

After carrying out the reduction, one finds nine master integrals for the NNLO double real radiation antenna functions, described in Section 3.4.1 below, and listed in

Appendix B.3.1. For the NNLO one-loop single real radiation antennae, one finds six master integrals, which we describe in Section 3.4.2 and list in Appendix B.3.2.

We computed these integrals both directly and by using the differential equation technique [150, 152–157]. To derive the differential equations for each master integral, we employ

$$Q^2 \frac{\partial}{\partial Q^2} = \frac{1}{2} q^\mu \frac{\partial}{\partial q^\mu} + \frac{1}{2} p_i^\mu \frac{\partial}{\partial p_i^\mu} , \tag{3.43}$$

$$z \frac{\partial}{\partial z} = -p_i^\mu \frac{\partial}{\partial p_i^\mu} \tag{3.44}$$

to carry out the differentiations at the integrand level. The boundary conditions required for the solution of the differential equations are either obtained from self-consistency conditions on the integrals, or by explicit evaluation. The explicit evaluation is very similar to the evaluation of inclusive four-point phase space integrals, described in [158]. In Appendix B a simple example is carried out explicitly.

Some of the more involved master integrals can be related to phase space integrals computed by E. B. Zijlstra and W. L. van Neerven in the context of the NNLO corrections to deep inelastic structure functions [3, 4]. Where appropriate, we compared our results to the expressions in the appendix of [3, 4], finding full agreement. Explicit expressions for all master integrals are listed in Appendix B.3.1–B.3.2.

All master integrals contain multiplicative factors of the form $(1-z)^{-\epsilon}$ or $(1-z)^{-2\epsilon}$, which regulate soft endpoint singularities in initial state convolution integrals. These factors must be left as such in the master integrals, and can be expanded in the form of distributions[1]

$$(1-z)^{-1-\epsilon} = -\frac{1}{\epsilon}\delta(1-z) + \sum_n \frac{(-\epsilon)^n}{n!} \mathcal{D}_n(z) , \tag{3.45}$$

with

$$\mathcal{D}_n(z) = \left(\frac{\ln^n(1-z)}{1-z} \right)_+ ,$$

only after being inserted into the integrated antenna functions. All other terms in the master integrals can be expanded, yielding Harmonic Polylogarithms (HPLs,[159–162]) of argument z.

3.4.1 Tree-level $2 \to 3$ antenna functions

For the tree-level $2 \to 3$ antenna functions, we have the 'DIS-like' process

$$q + p_i \to k_1 + k_2 + k_3 .$$

[1] This expansion is proven in Appendix A.

There are 12 propagators, including the three that are cut in the phase space integration (D_{10}, D_{11}, D_{12}):

$$\begin{aligned} D_1 &= (p_i - k_1)^2 \,, \\ D_2 &= (q - k_1)^2 \,, \\ D_3 &= (k_2 + k_3)^2 \,, \\ D_4 &= (p_i - k_2)^2 \,, \\ D_5 &= (q - k_2)^2 \,, \\ D_6 &= (k_1 + k_3)^2 \,, \\ D_7 &= (p_i - k_3)^2 \,, \\ D_8 &= (q - k_3)^2 \,, \\ D_9 &= (k_1 + k_2)^2 \,, \\ D_{10} &= k_1^2 \,, \\ D_{11} &= k_2^2 \,, \\ D_{12} &= k_3^2 \,. \end{aligned} \tag{3.46}$$

To perform the reduction to master integrals, we impose momentum conservation $p_3 = q + p_i - k_1 - k_2$, set $p_i^2 = 0$, $q^2 = -Q^2$ and drop any integral where D_{10}, D_{11} and D_{12} are not in the denominator. After labeling the inclusive phase space integral as $I[0]$, the convention for naming the master integrals follows the labeling of the numerators, i.e.

$$I[1,2,5] = \int \frac{[\mathrm{d}k_1]\,[\mathrm{d}k_2]\,[\mathrm{d}k_3]}{D_1\,D_2\,D_5}\,(2\pi)^d\,\delta^d(q + p_i - k_1 - k_2 - k_3) \,, \tag{3.47}$$

where

$$[\mathrm{d}k] = \frac{\mathrm{d}^d k}{(2\pi)^{d-1}}\delta^+(k^2) \,. \tag{3.48}$$

When squaring the $2 \to 3$ antennae, we find at most 4 propagators, plus the 3 cut ones. All the integrals can be reduced to the set of 9 master integrals shown in Figure 3.7. All the masters, except $I[1,2,4,5]$, have been computed by direct integration and by the differential equations method, supplemented, where necessary, by a direct calculation at $z = 1$ after factorizing the leading singularity. The $z = 1$ boundary conditions for $I[1,3,4,6]$ and $I[2,3,5,6]$ were checked numerically using sector decomposition [163–166]. $I[1,2,4,5]$ has been computed only using the differential equations method. The master integrals $I[1,2,5]$, $I[2,3,5]$, $I[2,3,5,6]$ and $I[1,2,4,5]$ agree up to order ϵ^0 with the results in [3, 4]. We summarize in Table 3.6 some of the properties of the master integrals.

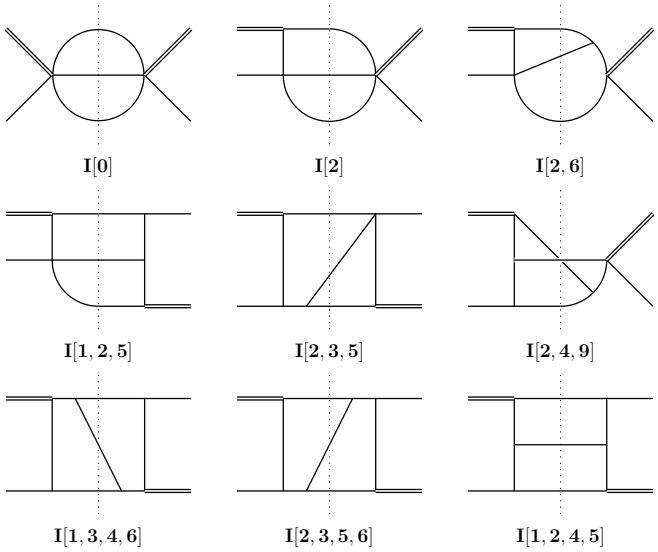

Figure 3.7: Master integrals for the phase space integration of the tree level initial-final antennae at NNLO. The double line in the external states represents the off-shell momentum, q with $q^2 = -Q^2$, the single one is the incoming parton. All internal lines are massless. The cut propagators are the ones intersected by the dotted line.

3.4.2 One-loop $2 \to 2$ antenna functions

When interfering the one loop $2 \to 2$ antennae with the corresponding tree level ones, we can combine the loop and phase space integrations. The partonic process in this case is

$$q + p_i \to k_1 + k_2 \, .$$

Denoting the loop momentum by l, we can identify four topologies, two planar (Topology 1 and 2) and two non-planar (Topology 3 and 4). The topologies are defined in Table 3.7. Topologies 1 and 2 only differ in the propagator D_5, as is also the case for Topologies 3 and 4. Subtopologies of the non-planar integrals can be expressed by the planar topologies.

All the resulting integrals can again be reduced to a small set of masters. In this case we find only six of them. They are shown in Figure 3.8. The notation for the master integrals follows the propagator definitions of Topology 2 in the planar case (denoted by V) and of Topology 3 in the non-planar case (denoted by C).

The one loop plus phase-space master integrals have been computed using differential equations in external invariants, together with a direct calculation at $z = 1$ after factorizing the leading singularity at $z = 1$. Integrals $V[1, 2, 3, 4]$, $V[1, 2, 3, 4, 5]$ and $C[1, 2, 3, 4]$ have been checked, up to order ϵ^0, against a direct analytic calculation. We summarize in table 3.8 some of the properties of the master integrals. Explicit expressions for the master integrals are listed in Appendix B.3.2.

master	deepest pole	behaviour at $z = 1$	known to order
$I[0]$	ε^0	$(1-z)^{1-2\varepsilon}$	all
$I[2]$	ε^0	$(1-z)^{-2\varepsilon}$	all, ε^5
$I[2,6]$	ε^{-1}	$(1-z)^{-2\varepsilon}$	all, ε^5
$I[1,2,5]$	ε^{-2}	$(1-z)^{-2\varepsilon}$	ε^3
$I[2,3,5]$	ε^{-2}	$(1-z)^{-1-2\varepsilon}$	ε^3
$I[2,4,9]$	ε^{-3}	$(1-z)^{-2\varepsilon}$	ε^3
$I[1,3,4,6]$	ε^{-3}	$(1-z)^{-1-2\varepsilon}$	all, ε^5
$I[2,3,5,6]$	ε^{-3}	$(1-z)^{-1-2\varepsilon}$	ε^1
$I[1,2,4,5]$	ε^{-2}	$(1-z)^{-2\varepsilon}$	ε^1

Table 3.6: Summary of the main properties of the three particles phase space master integrals

	Topology 1	Topology 2	Topology 3	Topology 4
D_1	l^2	l^2	l^2	l^2
D_2	$(l+p_i)^2$	$(l+p_i)^2$	$(l+p_i)^2$	$(l+p_i)^2$
D_3	$(l+p_i-k_1)^2$	$(l+p_i-k_1)^2$	$(l+p_i-k_1)^2$	$(l+p_i-k_1)^2$
D_4	$(l-q)^2$	$(l-q)^2$	$(l+k_2)^2$	$(l+k_2)^2$
D_5	$(p_i-p_i)^2$	$(q-k_1)^2$	$(p_i-k_1)^2$	$(q-k_1)^2$
D_6	k_1^2	k_1^2	k_1^2	k_1^2
D_7	k_2^2	k_2^2	k_2^2	k_2^2

Table 3.7: Definition of the topologies for the combined phase space and loop integration.

We always integrate the unrenormalized $2 \to 2$ one-loop squared matrix elements, divided by a normalization factor $C(\epsilon)$, relevant to a particular antenna function, which we denote as $X^{1,U}_{i,jk}$. The antenna function is obtained after renormalization and subtraction of the corresponding tree-level antenna function multiplied with the one-loop correction to the hard radiator pair. Renormalization of the one-loop antenna functions is always carried out in the $\overline{\rm MS}$-scheme at fixed renormalization scale $\mu^2 = Q^2$. It amounts to a renormalization of the strong coupling constant and (in the case of the quark-gluon and gluon-gluon antenna functions) to a renormalization of the effective operators used to couple an external current to the partonic radiators. The relation between renormalized and unrenormalized one-loop squared matrix elements is as follows:

$$X^{1,R}_{i,jk} = X^{1,U}_{i,jk} - \frac{b_0}{\epsilon} X^0_{i,jk} - \frac{\eta_0}{\epsilon} X^0_{i,jk}\,, \tag{3.49}$$

$$\tilde{X}^{1,R}_{i,jk} = \tilde{X}^{1,U}_{i,jk}\,, \tag{3.50}$$

$$\hat{X}^{1,R}_{i,jk} = X^{1,U}_{i,jk} - \frac{b_{0,F}}{\epsilon} X^0_{i,jk} - \frac{\eta_{0,F}}{\epsilon} X^0_{i,jk}\,, \tag{3.51}$$

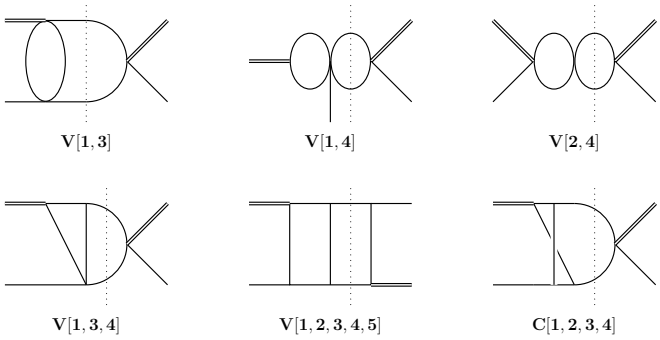

Figure 3.8: Master integrals for the loop plus phase space integration of the one loop initial-final antennae at NNLO. The double line in the external states represents the off-shell momentum, q with $q^2 = -Q^2$, the single one is the incoming parton. All internal lines are massless. The cut propagators are the ones intersected by the dotted line.

master	deepest pole	behaviour at $z = 1$	known to order
$V[1,3]$	ε^{-1}	$(1-z)^{-\varepsilon}$	all, ε^5
$V[1,4]$	ε^{-1}	$(1-z)^{-\varepsilon}$	all, ε^5
$V[2,4]$	ε^{-1}	$(1-z)^{-2\varepsilon}$	all, ε^5
$V[1,3,4]$	ε^{-1}	$(1-z)^{-\varepsilon}$	ε^3
$V[1,2,3,4,5]$	ε^{-3}	$(1-z)^{-1-2\varepsilon}$	ε^3
$C[1,2,3,4]$	ε^{-3}	$(1-z)^{-\varepsilon}$	ε^3

Table 3.8: Summary of the main properties of the one loop plus two particles phase space master integrals

where

$$b_0 = \frac{11}{6}\,, \quad b_{0,F} = -\frac{1}{3} \tag{3.52}$$

are the colour-ordered coefficients of the one-loop QCD β-function [1]:

$$\beta_0 = b_0 N + b_{0,F} N_F\,. \tag{3.53}$$

The renormalization constants for the effective operators are

$$\begin{aligned} \eta_0 = 0\,, \quad \eta_{0,F} = 0 \qquad & \text{for } X = A\,, \\ \eta_0 = b_0 + \frac{3}{2}\,, \quad \eta_{0,F} = b_{0,F} \qquad & \text{for } X = D, E\,, \\ \eta_0 = 2\,b_0\,, \quad \eta_{0,F} = 2\,b_{0,F} \qquad & \text{for } X = F, G\,. \end{aligned}$$

The one-loop antenna functions are obtained from the renormalized one-loop squared matrix elements by subtracting from them the product of the tree-level antenna func-

[1] For reasons of coherence with already published Literature, throughout this chapter we use a different convention for the QCD β-function. This is however restricted to this chapter only.

tion with the the virtual one-loop hard radiator vertex correction [21, 102–106]:

$$X^1_{i,jk} = X^{1,R}_{i,jk} - \mathrm{Re}\left((-1)^{-\epsilon}\mathcal{X}^1_2\right) X^0_{i,jk}\,, \tag{3.54}$$

$$\tilde{X}^1_{i,jk} = \tilde{X}^{1,R}_{i,jk} - \mathrm{Re}\left((-1)^{-\epsilon}\tilde{\mathcal{X}}^1_2\right) X^0_{i,jk}\,, \tag{3.55}$$

$$\hat{X}^1_{i,jk} = X^{1,U}_{i,jk} - \mathrm{Re}\left((-1)^{-\epsilon}\hat{\mathcal{X}}^1_2\right) X^0_{i,jk}\,. \tag{3.56}$$

The one-loop corrections to the hard radiator vertex are listed in [21] for $\mathcal{A}^1_2$, $\mathcal{D}^1_2$, $\hat{\mathcal{D}}^1_2$, $\mathcal{F}^1_2$ and $\hat{\mathcal{F}}^1_2$. From these, the remaining functions follow:

$$\tilde{\mathcal{A}}^1_2 = \mathcal{A}^1_2\,, \qquad \hat{\mathcal{A}}^1_2 = 0\,, \tag{3.57}$$

$$\tilde{\mathcal{D}}^1_2 = 0\,, \tag{3.58}$$

$$\mathcal{E}^1_2 = \mathcal{D}^1_2 \qquad \tilde{\mathcal{E}}^1_2 = 0\,, \qquad \hat{\mathcal{E}}^1_2 = \hat{\mathcal{D}}^1_2\,, \tag{3.59}$$

$$\tilde{\mathcal{F}}^1_2 = 0\,, \tag{3.60}$$

$$\mathcal{G}^1_2 = \mathcal{F}^1_2 \qquad \tilde{\mathcal{G}}^1_2 = 0\,, \qquad \hat{\mathcal{G}}^1_2 = \hat{\mathcal{F}}^1_2\,. \tag{3.61}$$

3.5 Quark initiated antennae

The quark-initiated initial-final antenna functions are obtained from the final-final antenna functions by crossing a quark into the initial state. Their unintegrated analytical expressions are obtained by a pure kinematical crossing from the final-final expressions listed in [21], with no extra symmetry factors or overall signs applied, and no further decompositions into sub-antennae. This procedure differs from the approach used in previous work on initial-final antenna functions at NLO [74]. In the application of the antenna subtraction formalism to the calculation of NNLO corrections to $e^+e^- \to 3j$ [140], it turned out that several decompositions can be circumvented by an appropriate symmetrization of the real radiation matrix elements in the process under consideration, and that the remaining required decompositions can be derived on a case-by-case basis, often not along the lines of [21, 74]. A systematic decomposition would start from a specific process under consideration, and is beyond the scope of the present study.

The virtual one-loop antenna functions are obtained from the final-final one-loop antenna functions [21], where some attention has to be paid to the correct analytic continuation of the polylogarithmic functions. In the initial-final kinematics, the relevant final state phase space consists of three different Riemann sheets [167–174], which have to be patched together correctly.

All quark-initiated initial-final antenna functions are listed in Table 3.4. The explicit expressions of the integrated antennae are rather long and for this reason we do not report them here. They can be found in [24].

3.6 Gluon initiated antennae

The gluon-initiated initial-final antenna functions are obtained from final-final antenna functions listed in [21] by crossing a gluon into the initial state. As in the quark case, their unintegrated forms are pure kinematical crossings of the final-final expressions, with no symmetry factors or polarization sums multiplied on them. Also, we do not provide a decomposition into sub-antennae here. The precise decomposition depends on the requirements and symmetries of the process under consideration, and is normally performed in the context of an actual calculation.

As in the quark-initiated case, some attention has to be paid in the crossing of the virtual one-loop antenna functions from the final-final kinematics [21] to the initial-final kinematics. This crossing requires the analytical continuation of the polylogarithmic functions to the relevant phase space, again consisting of three different Riemann sheets [167–174].

All gluon-initiated initial-final antenna functions are listed in Table 3.5, for the explicit expressions of the integrated results we again refer to [24].

3.7 Rederivation of NNLO coefficient functions

Being derived from physical matrix elements, the integrated antenna functions can be compared to results from literature for inclusive cross sections or coefficient functions, as was done previously for the final-final antennae in [136–139]. In the case of the initial-final antennae, we can compare the integrated quark-antiquark antennae and gluon-gluon antennae against NNLO corrections to deep inelastic coefficient functions known in the literature. The former ones can be checked against DIS structure function calculations [3] whereas the latter can be compared to the ϕ-DIS structure functions computed in [70, 175]. The quark-gluon antennae, derived from neutralino decay, cannot be associated to any physical process and only the deepest pole could be checked against a combination of Altarelli-Parisi splitting functions.

3.7.1 Deep inelastic scattering: γ induced

In DIS, if one uses the orientation-averaged leptonic tensor of equation (2.47), the hadronic tensor at parton level $\hat{W}_{\mu\nu}$ (given in formula 2.79) is contracted with the metric tensor $-g_{\mu\nu}$. This corresponds to the trace of the hadronic tensor, which in terms of the structure functions

$$\mathcal{F}_i = \frac{\hat{F}_i}{x} \qquad \text{for} \qquad i = 2, L\,, \tag{3.62}$$

is given by

$$-W_\mu^\mu = -\frac{d-1}{2}\mathcal{F}_L\left(z, Q^2\right) + \frac{d-2}{2}\mathcal{F}_2\left(z, Q^2\right)\,, \tag{3.63}$$

where the structure functions can be expanded in powers of the strong coupling constant, following the notation of [3] (but using $d = 4 - 2\epsilon$, as throughout the rest of this work):

$$\begin{aligned}
\mathcal{F}_L &= \mathcal{F}_L^{(0)} + \frac{\alpha_s}{4\pi} S_\varepsilon \left(\frac{\mu_0^2}{Q^2}\right)^\varepsilon \mathcal{F}_L^{(1)} + \left(\frac{\alpha_s}{4\pi}\right)^2 S_\varepsilon^2 \left(\frac{\mu_0^2}{Q^2}\right)^{2\varepsilon} \mathcal{F}_L^{(2)} + \mathcal{O}\left(\alpha_s^3\right), \\
\mathcal{F}_2 &= \mathcal{F}_2^{(0)} + \frac{\alpha_s}{4\pi} S_\varepsilon \left(\frac{\mu_0^2}{Q^2}\right)^\varepsilon \mathcal{F}_2^{(1)} + \left(\frac{\alpha_s}{4\pi}\right)^2 S_\varepsilon^2 \left(\frac{\mu_0^2}{Q^2}\right)^{2\varepsilon} \mathcal{F}_2^{(2)} + \mathcal{O}\left(\alpha_s^3\right), \qquad (3.64)
\end{aligned}$$

and $S_\varepsilon = \exp\left[\varepsilon\left(\ln\left(4\pi\right) - \gamma_E\right)\right]$. For clarity, we drop the dependence on z and Q^2. The factors S_ε and μ_0 are the conventional factors appearing in dimensional regularization.

To zeroth order in α_s the structure functions are given by the simple parton model result, which follows from (2.80), (2.81) and (3.62) by factoring out the quark charge squared Q_f^2 from the hadronic tensor:

$$\mathcal{F}_{L,q}^{(0)} = \mathcal{F}_{L,g}^{(0)} = 0\,, \qquad \mathcal{F}_{2,q}^{(0)} = \delta\left(1-z\right), \qquad \mathcal{F}_{2,g}^{(0)} = 0\,. \qquad (3.65)$$

Since the overall normalization of the antenna functions is given by the leading order antenna $\mathcal{A}_{q,q} = \delta(1-z)$, we find that the correct normalization of W_μ^μ to be checked against the antennae is

$$-\frac{2}{d-2} W_\mu^\mu = \mathcal{F}_2 - \frac{d-1}{d-2}\mathcal{F}_L\,. \qquad (3.66)$$

This last equation at order α_s and α_s^2 can be compared to a linear combinations of NLO and NNLO antennae respectively. For completeness and clarity, before giving the explicit relations between the structure functions and the antennae, we report the expressions of the structure functions in terms of the Altarelli-Parisi splitting functions given in Table 2.1 and the other coefficient functions c_i and a_i. We take them from [3, 4], adjusting to $d = 4 - 2\varepsilon$ and $\beta_0 = \frac{11}{6}C_A - \frac{1}{3}N_F$.

$$\mathcal{F}_{L,g}^{(1)} = N_F\left(c_{L,g}^{(1)} - \varepsilon\, 2a_{L,g}^{(1)}\right), \qquad (3.67)$$

$$\mathcal{F}_{2,g}^{(1)} = N_F\left(-\frac{1}{2\varepsilon}P_{gq}^{(0)} + c_{2,g}^{(1)} - \varepsilon\, 2a_{2,g}^{(1)}\right), \qquad (3.68)$$

$$\mathcal{F}_{L,q}^{(1)} = \left(c_{L,q}^{(1)} - \varepsilon\, 2a_{L,q}^{(1)}\right), \qquad (3.69)$$

$$\mathcal{F}_{2,q}^{(1)} = \left(-\frac{1}{2\varepsilon}P_{qq}^{(0)} + c_{2,q}^{(1)} - \varepsilon\, 2a_{2,q}^{(1)}\right), \qquad (3.70)$$

$$\begin{aligned}
\mathcal{F}_{L,g}^{(2)} =& N_F\left(\frac{1}{\varepsilon}\left(2\beta_0 c_{L,g}^{(1)} - \frac{1}{2}P_{gg}^{(0)} \otimes c_{L,g}^{(1)} - \frac{1}{2}P_{qg}^{(0)} \otimes c_{L,q}^{(1)}\right)\right. \\
&\left. + c_{L,g}^{(2)} - 4\beta_0 a_{L,g}^{(1)} + P_{gg}^{(0)} \otimes a_{L,g}^{(1)} + P_{qg}^{(0)} \otimes a_{L,q}^{(1)}\right), \qquad (3.71)
\end{aligned}$$

$$\mathcal{F}_{2,g}^{(2)} = N_F\left(\frac{1}{\varepsilon^2}\left(\frac{1}{8}P_{qg}^{(0)} \otimes \left(P_{gg}^{(0)} + P_{qq}^{(0)}\right) - \frac{\beta_0}{2}P_{qg}^{(0)}\right)\right.$$

$$+\frac{1}{\varepsilon}\left(-\frac{1}{4}P_{qg}^{(1)}+2\beta_0 c_{2,g}^{(1)}-\frac{1}{2}P_{gg}^{(0)}\otimes c_{2,g}^{(1)}-\frac{1}{2}P_{qg}^{(0)}\otimes c_{2,q}^{(1)}\right)$$
$$+c_{2,g}^{(2)}-4\beta_0 a_{2,g}^{(1)}+P_{gg}^{(0)}\otimes a_{2,g}^{(1)}+P_{qg}^{(0)}\otimes a_{2,q}^{(1)}\Big)\,, \tag{3.72}$$

$$\mathcal{F}_{L,q}^{(2)\mathrm{NS}}=\left(\frac{1}{\varepsilon}\left(2\beta_0 c_{L,q}^{(1)}-\frac{1}{2}P_{qq}^{(0)}\otimes c_{L,q}^{(1)}\right)+c_{L,q}^{(2)\mathrm{NS}}-4\beta_0 a_{L,q}^{(1)}+P_{qq}^{(0)}\otimes a_{L,q}^{(1)}\right)\,, \tag{3.73}$$

$$\mathcal{F}_{2,q}^{(2)\mathrm{NS}}=\left(\frac{1}{\varepsilon^2}\left(\frac{1}{8}P_{qq}^{(0)}\otimes P_{qq}^{(0)}-\frac{\beta_0}{2}P_{qq}^{(0)}\right)\right.$$
$$+\frac{1}{\varepsilon}\left(-\frac{1}{4}\left(P_{qq}^{(1)\mathrm{NS}}+P_{q\bar{q}}^{(1)\mathrm{NS}}\right)+2\beta_0 c_{2,q}^{(1)}-\frac{1}{2}P_{qq}^{(0)}\otimes c_{2,q}^{(1)}\right)$$
$$\left.+c_{2,q}^{(2)\mathrm{NS}}-4\beta_0 a_{2,q}^{(1)}+P_{qq}^{(0)}\otimes a_{2,q}^{(1)}\right)\,, \tag{3.74}$$

$$\mathcal{F}_{L,q}^{(2)\mathrm{PS}}=\left(-\frac{1}{2\varepsilon}P_{gq}^{(0)}\otimes c_{L,g}^{(1)}+c_{L,q}^{(2)\mathrm{PS}}+P_{gq}^{(0)}\otimes a_{L,g}^{(1)}\right)\,, \tag{3.75}$$

$$\mathcal{F}_{2,q}^{(2)\mathrm{PS}}=\left(\frac{1}{\varepsilon^2}\left(\frac{1}{8}P_{qg}^{(0)}\otimes P_{gq}^{(0)}\right)-\frac{1}{\varepsilon}\left(\frac{1}{4}P_{qq}^{(1)\mathrm{PS}}+\frac{1}{2}P_{gq}^{(0)}\otimes c_{2,g}^{(1)}\right)\right.$$
$$\left.+c_{2,q}^{(2)\mathrm{PS}}+P_{gq}^{(0)}\otimes a_{2,g}^{(1)}\right)\,, \tag{3.76}$$

where the convolution symbol $\otimes$ is defined by[1]

$$(f\otimes g)(x)=\int_0^1 \mathrm{d}y\int_0^1 \mathrm{d}z\,\delta(x-zy)f(z)g(y)=\int_x^1\frac{\mathrm{d}z}{z}f(z)g\left(\frac{x}{z}\right)\,.$$

The previous expressions are needed to check all the initial-final quark-antiquark antennae. They are still unrenormalized and are thus to be compared to the unrenormalized antenna functions. The following identities hold at NLO:

$$\frac{1}{C_F}\left(\mathcal{F}_{2,q}^{(1)}-\frac{3-2\varepsilon}{2-2\varepsilon}\mathcal{F}_{L,q}^{(1)}\right)=4\mathcal{A}_{q,gq}+8\delta\left(1-z\right)\left.F_q^{(1)}\right|_N\,, \tag{3.77}$$

$$\frac{(2-2\varepsilon)}{N_F}\left(\mathcal{F}_{2,g}^{(1)}-\frac{3-2\varepsilon}{2-2\varepsilon}\mathcal{F}_{L,g}^{(1)}\right)=-4\mathcal{A}_{g,q\bar{q}}\,, \tag{3.78}$$

where $F_q^{(1)}$ is the one-loop quark form-factor given in [176]. The notation $X|_a$ means that only the terms of X proportional to a are considered. The corresponding identities at NNLO are

$$\frac{1}{C_F}\left(\mathcal{F}_{2,q}^{(2,\mathrm{NS})}-\frac{3-2\varepsilon}{2-2\varepsilon}\mathcal{F}_{L,q}^{(2,\mathrm{NS})}\right)\Big|_{\frac{1}{N}}=-\tilde{\mathcal{A}}_{q,ggq}^{0}+8\tilde{\mathcal{A}}_{q,gq}^{1,U}-4\mathcal{C}_{q,\bar{q}q\bar{q}}^{0}-2\mathcal{C}_{\bar{q},\bar{q}q\bar{q}}^{0}-2\mathcal{C}_{\bar{q},q\bar{q}\bar{q}}^{0}$$
$$+16\delta\left(1-z\right)\left(F_q^{(2,U)}+C_F F_q^{(1)\,2}\right)\Big|_{\frac{1}{N}}\,, \tag{3.79}$$

[1] More about the computation with convolutions and (+)-distributions can be found in Appendix A.

$$\frac{1}{C_F}\left(\mathcal{F}_{2,q}^{(2,\mathrm{NS})}-\frac{3-2\varepsilon}{2-2\varepsilon}\mathcal{F}_{L,q}^{(2,\mathrm{NS})}\right)\Big|_N = 2\mathcal{A}_{q,ggq}^0+8\mathcal{A}_{q,gq}^{1,U} + 16\delta(1-z)\left(F_q^{(2,U)}+C_F F_q^{(1)\,2}\right)\Big|_N , \tag{3.80}$$

$$\frac{1}{C_F}\left(\mathcal{F}_{2,q}^{(2,\mathrm{NS})}-\frac{3-2\varepsilon}{2-2\varepsilon}\mathcal{F}_{L,q}^{(2,\mathrm{NS})}\right)\Big|_{N_F} = 2\mathcal{B}_{q,q'\bar{q}'q}^0 + 16\delta(1-z)\left(F_q^{(2,U)}+C_F F_q^{(1)\,2}\right)\Big|_{N_F} , \tag{3.81}$$

$$\frac{1}{C_F N_F}\left(\mathcal{F}_{2,q}^{(2,\mathrm{PS})}-\frac{3-2\varepsilon}{2-2\varepsilon}\mathcal{F}_{L,q}^{(2,\mathrm{PS})}\right) = 2\bar{\mathcal{B}}_{q,q'\bar{q}'q}^0 , \tag{3.82}$$

$$\frac{(2-2\varepsilon)}{N_F}\left(\mathcal{F}_{2,g}^{(2)}-\frac{3-2\varepsilon}{2-2\varepsilon}\mathcal{F}_{L,g}^{(2)}\right)\Big|_{\frac{1}{N}} = 2\tilde{\mathcal{A}}_{g,gq\bar{q}}^0-8\tilde{\mathcal{A}}_{g,q\bar{q}}^{1,U} , \tag{3.83}$$

$$\frac{(2-2\varepsilon)}{N_F}\left(\mathcal{F}_{2,g}^{(2)}-\frac{3-2\varepsilon}{2-2\varepsilon}\mathcal{F}_{L,g}^{(2)}\right)\Big|_{N} = -4\mathcal{A}_{g,gq\bar{q}}^0-8\mathcal{A}_{g,q\bar{q}}^{1,U} . \tag{3.84}$$

The structure functions (3.67)-(3.76) are given in [3, 4] in unrenormalized form. To compare with our results, we thus considered the one-loop unrenormalized antenna functions (obtained by undoing the renormalization) the two-loop unrenormalized form factor, both characterized by the label U. Full agreement is found with [3, 4].

3.7.2 Deep inelastic scattering: ϕ-scalar induced

The gluon-gluon $\mathcal{F}$-, $\mathcal{G}$- and $\mathcal{H}$-type antenna functions can be checked with the deep inelastic scalar induced structure functions derived in [70, 175]. These structure functions are obtained in an effective theory with a scalar ϕ coupled to the square of the gluon field strength tensor. This effective theory is very instrumental in deriving gluonic splitting functions, and is also the effective field theory describing the coupling of the Higgs boson to gluons through a loop of asymptotically heavy coloured particles. Since ϕ is a scalar particle the corresponding hadronic tensor has only one structure function which can be either quark- or gluon-initiated. Their perturbative expansion reads:

$$\begin{aligned}
\mathcal{T}_{\phi,g} &= \mathcal{T}_{\phi,g}^{(0)}+\frac{\alpha_s}{4\pi}S_\varepsilon\left(\frac{\mu^2}{Q^2}\right)^{\varepsilon}\mathcal{T}_{\phi,g}^{(1)}+\left(\frac{\alpha_s}{4\pi}\right)^2 S_\varepsilon^2\left(\frac{\mu^2}{Q^2}\right)^{2\varepsilon}\mathcal{T}_{\phi,g}^{(2)}+\mathcal{O}\left(\alpha_s^3\right),\\
\mathcal{T}_{\phi,q} &= \mathcal{T}_{\phi,q}^{(0)}+\frac{\alpha_s}{4\pi}S_\varepsilon\left(\frac{\mu^2}{Q^2}\right)^{\varepsilon}\mathcal{T}_{\phi,q}^{(1)}+\left(\frac{\alpha_s}{4\pi}\right)^2 S_\varepsilon^2\left(\frac{\mu^2}{Q^2}\right)^{2\varepsilon}\mathcal{T}_{\phi,q}^{(2)}+\mathcal{O}\left(\alpha_s^3\right).
\end{aligned} \tag{3.85}$$

At NLO and NNLO the structure functions have the following form:

$$\mathcal{T}_{\phi,g}^{(1)} = \left(-\frac{1}{2\epsilon}P_{gg}^{(0)}+c_{\phi,g}^{(1)}-\epsilon\,2a_{\phi,g}^{(1)}\right) , \tag{3.86}$$

$$\mathcal{T}_{\phi,q}^{(1)} = \left(-\frac{1}{2\epsilon}P_{gq}^{(0)}+c_{\phi,q}^{(1)}-\epsilon\,2a_{\phi,q}^{(1)}\right) , \tag{3.87}$$

$$\mathcal{T}^{(2)}_{\phi,g} = \left(\frac{1}{\epsilon^2}\left(\frac{1}{8}P^{(0)}_{gg}\otimes P^{(0)}_{gg} + \frac{N_F}{8}P^{(0)}_{gq}\otimes P^{(0)}_{qg} + \frac{\beta_0}{2}P^{(0)}_{gg}\right)\right.$$
$$+\frac{1}{\epsilon}\left(-\frac{1}{4}P^{(1)}_{gg} - \frac{1}{2}P^{(0)}_{gg}\otimes c^{(1)}_{\phi,g} - \frac{N_F}{2}P^{(0)}_{qg}\otimes c^{(1)}_{\phi,q}\right)$$
$$\left.+\, c^{(2)}_{\phi,g} + P^{(0)}_{gg}\otimes a^{(1)}_{\phi,g} + N_F P^{(0)}_{qg}\otimes a^{(1)}_{\phi,q}\right)\,, \tag{3.88}$$

$$\mathcal{T}^{(2)}_{\phi,q} = \left(\frac{1}{\epsilon^2}\left(\frac{1}{8}P^{(0)}_{qq}\otimes P^{(0)}_{gq} + \frac{1}{8}P^{(0)}_{gg}\otimes P^{(0)}_{gq} + \frac{\beta_0}{2}P^{(0)}_{gq}\right)\right.$$
$$+\frac{1}{\epsilon}\left(-\frac{1}{4}P^{(1)}_{gq} - \frac{1}{2}P^{(0)}_{gq}\otimes c^{(1)}_{\phi,g} - \frac{1}{2}P^{(0)}_{qq}\otimes c^{(1)}_{\phi,q}\right)$$
$$\left.+\, c^{(2)}_{\phi,q} + P^{(0)}_{gq}\otimes a^{(1)}_{\phi,g} + P^{(0)}_{qq}\otimes a^{(1)}_{\phi,q}\right)\,. \tag{3.89}$$

The explicit expressions for the coefficients $c^{(1)}_{\phi,i}$, $a^{(1)}_{\phi,i}$ and $c^{(2)}_{\phi,i}$, with $i = q, g$ are given in the Appendix of [24]. They were derived independently in [175], and we find full agreement. In our calculation, they follow from the following identities between structure functions and antennae:

$$\mathcal{T}^{(1)}_{\phi,g} = 2\left(C_A\mathcal{F}^0_{g,gg} + N_F\mathcal{G}^0_{g,q\bar{q}}\right) + 4\delta\left(1-z\right)F^{(1)}_g\,, \tag{3.90}$$

$$\frac{1}{C_F\left(1-\varepsilon\right)}\mathcal{T}^{(1)}_{\phi,q} = -4\mathcal{G}^0_{q,qg}\,, \tag{3.91}$$

$$\mathcal{T}^{(2)}_{\phi,g}\Big|_{N^2} = \mathcal{F}^0_{g,ggg} + 4\mathcal{F}^{1,R}_{g,gg} + 4\delta\left(1-z\right)\left(2F^{(2)}_g + F^{(1)\,2}_g\right)\Big|_{N^2}\,, \tag{3.92}$$

$$\mathcal{T}^{(2)}_{\phi,g}\Big|_{N\,N_F} = 2\mathcal{G}^0_{g,q\bar{q}g} + 4\mathcal{G}^{1,R}_{g,q\bar{q}} + 4\hat{\mathcal{F}}^{1,R}_{g,gg} + 4\delta\left(1-z\right)\left(2F^{(2)}_g + F^{(1)\,2}_g\right)\Big|_{N\,N_F}\,, \tag{3.93}$$

$$\mathcal{T}^{(2)}_{\phi,g}\Big|_{\frac{N_F}{N}} = -\tilde{\mathcal{G}}^0_{g,q\bar{q}g} + 4\tilde{\mathcal{G}}^{1,R}_{g,q\bar{q}} + 4\delta\left(1-z\right)\left(2F^{(2)}_g + F^{(1)\,2}_g\right)\Big|_{\frac{N_F}{N}}\,, \tag{3.94}$$

$$\mathcal{T}^{(2)}_{\phi,g}\Big|_{N_F^2} = 4\hat{\mathcal{G}}^{1,R}_{g,q\bar{q}} + 4\delta\left(1-z\right)\left(2F^{(2)}_g + F^{(1)\,2}_g\right)\Big|_{N_F^2}\,, \tag{3.95}$$

$$\frac{1}{C_F\left(1-\varepsilon\right)}\mathcal{T}^{(2)}_{\phi,q}\Big|_{N} = -2\mathcal{G}^0_{q,qgg} - 8\mathcal{G}^{1,R}_{q,qg}\,, \tag{3.96}$$

$$\frac{1}{C_F\left(1-\varepsilon\right)}\mathcal{T}^{(2)}_{\phi,q}\Big|_{\frac{1}{N}} = \tilde{\mathcal{G}}^0_{q,qgg} + 8\tilde{\mathcal{G}}^{1,R}_{q,qg} - 4\tilde{\mathcal{J}}^0_{q,qq\bar{q}}\,, \tag{3.97}$$

$$\frac{1}{C_F\left(1-\varepsilon\right)}\mathcal{T}^{(2)}_{\phi,q}\Big|_{N_F} = -2\mathcal{H}^0_{q,qq'\bar{q}'} - 8\hat{\mathcal{G}}^{1,R}_{q,qg}\,. \tag{3.98}$$

The antenna $\tilde{\mathcal{J}}^0_{q,qq\bar{q}}$ comes from the interference of four quark final states with identical quark flavour, which is not contained in Table 3.4 since it is finite in all limits. It is given by

$$\tilde{\mathcal{J}}^0_{q,qq\bar{q}} = \left(-\frac{7}{4} + \frac{7}{4z} + \frac{9z}{8} + \left(2 - \frac{2}{z} - z\right)\zeta_3\right) + \mathcal{O}\left(\epsilon\right)\,. \tag{3.99}$$

The functions $F_g^{(i)}$ $(i = 1, 2)$ are the one- respectively two-loop gluon form factor given in [176].

3.7.3 $\tilde{\chi}$-induced antennae

There is no physical process which could be used to check the quark-gluon antennae, which were derived from neutralino decay [138]. However the correct combination of Altarelli-Parisi splitting functions which multiply the deepest pole can be read out from the diagrams associated with the different antennae. To have the correct colour factors for the χ-induced antennae we have to set $C_F = C_A = N$ in all the splitting functions.

We start considering quark initiated antennae at NLO. A quark-line in the initial state can split into a quark-gluon pair, where either the quark or the gluon are hard. For the gluon-initiated case the situation is similar. An initial gluon line can either split into two further gluons, or into a quark-antiquark pair. The structure function has therefore the form

$$\mathcal{F}^{(1)}_{\chi,q} = \left(-\frac{1}{2\epsilon}\left(P^{(0)}_{qq} - P^{(0)}_{gq}\right) + c^{(1)}_{\chi,q} - \epsilon\, 2a^{(1)}_{\chi,q}\right), \tag{3.100}$$

$$\mathcal{F}^{(1)}_{\chi,g} = \left(-\frac{1}{2\epsilon}\left(P^{(0)}_{gg} - C_A P^{(0)}_{qg}\right) + c^{(1)}_{\chi,g} - \epsilon\, 2a^{(1)}_{\chi,g}\right). \tag{3.101}$$

At NLO there are three different quark-initiated quark-gluon antennae: $D_{q,gg}$, $E_{q',q'q}$ and $E_{q,q'\bar{q}'}$. However, as shown in Table 3.2, only the first two have a real splitting in the initial state. They correspond to the two possible splittings of a quark: P_{qq} and P_{gq}. Comparing the $1/\epsilon$ terms of the antennae and the structure function at leading colour we find the following identity

$$\mathcal{F}^{(1)}_{\chi,q}\Big|_N = 2\left(\mathcal{D}^0_{q,gg} + 2\mathcal{E}^0_{q',qq'} + 2F^{(1)}_{\chi}\Big|_N\right), \tag{3.102}$$

where

$$F^{(1)}_{\chi} = \delta(1-z)C_A\left(-\frac{1}{\epsilon^2} - \frac{5}{3\epsilon} + \frac{7\pi^2}{12}\right) + \frac{N_F}{6\epsilon}\delta(1-z),$$

is the appropriate χ-form factor computed in [138]. The antenna $E_{q,q'\bar{q}'}$ contributes at subleading colour and cancels exactly against the χ-form factor

$$\mathcal{F}^{(1)}_{\chi,q}\Big|_{N_F} = 0 = 2\mathcal{E}^0_{q,q'\bar{q}'} + 2F^{(1)}_{\chi}\Big|_{N_F}. \tag{3.103}$$

There is only one antenna function for the gluon-initiated case at NLO, however it encodes both splittings. The subleading colour is exactly compensated by the χ-form factor:

$$\mathcal{F}^{(1)}_{\chi,g}\Big|_N = 4\mathcal{D}^0_{g,gq} + 4F^{(1)}_{\chi}\Big|_N, \tag{3.104}$$

$$\mathcal{F}^{(1)}_{\chi,g}\Big|_{N_F} \;=\; 4F^{(1)}_{\chi}\Big|_{N_F}\,. \tag{3.105}$$

The relative sign difference between the two splitting function in $\mathcal{F}^{(1)}_{\chi,q}$ and $\mathcal{F}^{(1)}_{\chi,g}$ can not be found from a diagrammatic analysis and its origin has to do with an ambiguity in the normalization of the antenna functions which also influences the singular limits.

At NNLO we can proceed in an analogous way but considering two emissions in a row. This leads to convolutions of splitting functions. Defining the splittings at NLO

$$P^{(0)}_{\chi,q} = P^{(0)}_{qq} - P^{(0)}_{gq} \qquad ; \qquad P^{(0)}_{\chi,g} = P^{(0)}_{gg} - C_A P^{(0)}_{qg}\,,$$

and following the same structure as for the ϕ-induced structure functions, we can make the following prediction for the deepest pole terms

$$\begin{aligned}
\mathcal{F}^{(2)}_{\chi,q} =& \frac{1}{\epsilon^2}\left(\frac{1}{8}P^{(0)}_{qq}\otimes P^{(0)}_{\chi,q} - \frac{1}{8}P^{(0)}_{gq}\otimes P^{(0)}_{\chi,g} + \frac{\beta_0}{2}P^{(0)}_{\chi,q}\right)\\
=& \frac{1}{\epsilon^2}\left(\frac{1}{8}\left(P^{(0)}_{qq}\otimes P^{(0)}_{qq} - \frac{C_F}{C_A}P^{(0)}_{qq}\otimes P^{(0)}_{gq}\right) - \frac{1}{8}\left(P^{(0)}_{gq}\otimes P^{(0)}_{gg} - C_A P^{(0)}_{gq}\otimes P^{(0)}_{qg}\right)\right.\\
&\left. + \frac{\beta_0}{2}\left(P^{(0)}_{qq} - P_{gq}\right)\right) + \mathcal{O}\left(\epsilon^{-1}\right)\,,
\end{aligned} \tag{3.106}$$

$$\begin{aligned}
\mathcal{F}^{(2)}_{\chi,g} =& \frac{1}{\epsilon^2}\left(\frac{1}{8}P^{(0)}_{gg}\otimes P^{(0)}_{\chi,g} - \frac{1}{8}P^{(0)}_{qg}\otimes P^{(0)}_{\chi,q} + \frac{\beta_0}{2}P^{(0)}_{\chi,g}\right)\\
=& \frac{1}{\epsilon^2}\left(\frac{1}{8}\left(P^{(0)}_{gg}\otimes P^{(0)}_{gg} - C_A P^{(0)}_{gg}\otimes P^{(0)}_{qg}\right) - \frac{1}{8}\left(C_A P^{(0)}_{qg}\otimes P^{(0)}_{qq} - N_F P^{(0)}_{qg}\otimes P^{(0)}_{gq}\right)\right.\\
&\left. + \frac{\beta_0}{2}\left(P^{(0)}_{gg} - C_A P_{qg}\right)\right) + \mathcal{O}\left(\epsilon^{-1}\right)\,.
\end{aligned} \tag{3.107}$$

The factor C_F/C_A in $\mathcal{F}^{(2)}_{\chi,q}$ means that only one of the two factors C_F present in the convolution $P^{(0)}_{qq}\otimes P^{(0)}_{gq}$ has to be set equal to N. At $\mathcal{O}\left(\epsilon^{-2}\right)$ the identities between structure functions and antennae for the different colour structures read

$$\mathcal{F}^{(2)}_{\chi,g}\Big|_{N^2} = 2\mathcal{D}^0_{g,ggq} + \mathcal{D}^0_{g',ggq} + 8\mathcal{D}^{1,R}_{g,gq} + (27-\pi^2)\delta(1-z)\,, \tag{3.108}$$

$$\mathcal{F}^{(2)}_{\chi,g}\Big|_{NN_F} = 2\mathcal{E}^0_{g,qq'\bar{q}'} + 8\mathcal{D}^{1,R}_{g,gq} - \frac{61}{9}\delta(1-z)\,, \tag{3.109}$$

$$\mathcal{F}^{(2)}_{\chi,g}\Big|_{\frac{N_F}{N}} = -\tilde{\mathcal{E}}^0_{g,qq'\bar{q}'}\,, \tag{3.110}$$

$$\mathcal{F}^{(2),\mathrm{NS}}_{\chi,q}\Big|_{N^2} = \mathcal{D}^0_{q,ggg} + 4\mathcal{D}^{1,R}_{q,gg} + (27-\pi^2)\delta(1-z)\,, \tag{3.111}$$

$$\mathcal{F}^{(2),\mathrm{PS}}_{\chi,q}\Big|_{N^2} = 4\left(\mathcal{E}^0_{q',q'qg} + 2\mathcal{E}^{1,R}_{q',q'q}\right) + 2 - \frac{2}{z} + 2\ln(z) - z\ln(z)\,, \tag{3.112}$$

$$\mathcal{F}^{(2)}_{\chi,q}\Big|_{N^0} = -2\left(\tilde{\mathcal{E}}^0_{q',q'qg} + 4\tilde{\mathcal{E}}^{1,R}_{q',q'q}\right)\,, \tag{3.113}$$

$$\mathcal{F}^{(2)}_{\chi,q}\Big|_{NN_F} = -2\mathcal{E}^0_{q,q'\bar{q}'g} - 4\mathcal{E}^{1,R}_{q,q'\bar{q}'} - 2\hat{\mathcal{D}}^{1,R}_{q,gg} + 8\hat{\tilde{\mathcal{E}}}^{1,R}_{q',q'q} + \frac{7}{3}\delta(1-z)\,. \tag{3.114}$$

The leading colour part of the quark-initiated structure function was divided into a flavour non-singlet part (NS) and a pure singlet part (PS) in analogy to the γ-induced structure functions. In the PS part a remainder part is left. Its origin has to do with the Majorana nature of the neutralino, whose decay is used to compute the quark-gluon antennae.

3.8 Conclusions and outlook

In this chapter, we have extended the NNLO antenna subtraction formalism [21] to include initial-final antenna configurations, where one of the hard radiator partons is in the initial state. We described the construction of initial-final antenna subtraction terms from antenna functions, including the required phase space factorization and mappings.

The analytic integration of the NNLO initial-final antenna functions requires the derivation of inclusive $2 \to 3$ phase space integrals at tree-level and of $2 \to 2$ phase space integrals at one loop. We reduced all these integrals to a small set of master integrals, which we computed using differential equations or by direct integration. With these, we provide integrals of all NNLO initial-final antenna functions, as required for the implementation into a parton-level event generator programme. A highly non-trivial check of our results is provided by the rederivation of deep inelastic coefficient functions [3, 4, 70, 175], which can be expressed as particular linear combinations of antenna functions.

The subtraction terms presented here allow the construction of a parton-level event generator program for the calculation of NNLO corrections to jet production observables in deeply inelastic electron-proton scattering. Of foremost importance in this context is the dijet production cross section in deep inelastic scattering [177–182], which has been used at HERA to measure the gluon distribution in the proton and the strong coupling constant α_s. This cross section is at present only known to NLO [167–172], which is insufficient for various reasons. The error on the extraction of α_s from HERA (2+1) jet data is dominated [183] not by the statistical uncertainty on the data, but by the uncertainty inherent to the NLO calculation, as estimated by varying renormalization and factorization scales. Given that the statistical precision of the data will further improve once all data from the HERA-II run are analysed, the theoretical description requires the inclusion of the next-to-next-to-leading order (NNLO), i.e. $\mathcal{O}(\alpha_s^3)$, corrections. Moreover, present determinations of parton distribution functions [184–187] at NNLO accuracy [72, 73] can only include data sets for observables where NNLO corrections are known [3, 4, 188–191]. Consequently, the precise HERA deep inelastic dijet data could be used in global NNLO determinations only once the NNLO QCD corrections to this observable are computed. Using the subtraction formalism derived here,

and the already known matrix elements [90, 91, 173, 174, 192–198], such a calculation can now be envisaged.

Moreover, the initial-final antenna functions derived here are an important ingredient to the calculation of NNLO corrections to jet observables at hadron colliders. In this case, all radiator configurations contribute: final-final (derived in [21]), initial-final (derived here) and initial-initial [199]. The initial-initial antenna functions are at present known only to NLO, and work on their extension to NNLO is ongoing.

4

Matching of Fixed Order and Resummation for Event Shape Observables

In this chapter we consider NNLO results for the set of six event-shape variables introduced in Section 2.5.2 and match them with resummed calculations at next-to-leading logarithmic accuracy (NLLA) [200], to obtain results which are reliable over the whole possible kinematical range. The matched results can be used to perform high precision studies on event-shape observables and allow a new determination of the strong coupling constant α_s [22]. This class of observables is also interesting because it shows a rather strong sensitivity to hadronisation effects, at least in phase-space regions characterised by soft and collinear gluon radiation.

We start analyzing the logarithmic structure of fixed order and resummed calculations. In a second step we match the two computations [201] and consider all possible sources of theoretical uncertainty following the method developed in [202]. A C++ routine is presented, which permits to quickly analyse and determine the different sources of uncertainty. Finally we report about the new determination of α_s and on some interesting insights about hadronization corrections made possible by these new results.

4.1 Fixed order and resummed calculations

In Section 2.6.2 we computed the leading order prediction for the event-shape observable thrust. The fixed order state-of-the-art description of event-shape observables like thrust was until recently just NLO [171, 203–209]. Applying the antenna subtraction formalism explained in the previous chapter to e^+e^--annihilation into 3 jets at NNLO, it was possible to extend the knowledge of the perturbative expansion of event-shape

observables one order higher [140, 141, 144, 146, 210]. These calculations are based on a numerical integration of the relevant three-parton, four-parton and five-parton matrix elements, which are combined into a parton-level event generator. Next-to-leading order electroweak corrections were also computed very recently [211, 212]. At this order, the perturbative differential cross section at a centre-of-mass energy Q and for a renormalization scale μ takes the form

$$\frac{1}{\sigma_0}\frac{\mathrm{d}\sigma}{\mathrm{d}y}(y,Q,\mu) = \bar{\alpha}_s(\mu)\frac{\mathrm{d}A}{\mathrm{d}y}(y) + \bar{\alpha}_s^2(\mu)\frac{\mathrm{d}B}{\mathrm{d}y}(y,x_\mu) + \bar{\alpha}_s^3(\mu)\frac{\mathrm{d}C}{\mathrm{d}y}(y,x_\mu) + \mathcal{O}(\bar{\alpha}_s^4)\,, \quad (4.1)$$

with

$$\bar{\alpha}_s = \frac{\alpha_s}{2\pi}\,, \qquad x_\mu = \frac{\mu}{Q}\,, \quad (4.2)$$

and where the explicit dependence on the renormalization scale is given by

$$\begin{aligned}\frac{\mathrm{d}B}{\mathrm{d}y}(y,x_\mu) &= \frac{\mathrm{d}B}{\mathrm{d}y}(y) + 2\beta_0\,\ln(x_\mu^2)\frac{\mathrm{d}A}{\mathrm{d}y}(y)\\ \frac{\mathrm{d}C}{\mathrm{d}y}(y,x_\mu) &= \frac{\mathrm{d}C}{\mathrm{d}y}(y) + 2\,\ln(x_\mu^2)\left(2\beta_0\frac{\mathrm{d}B}{\mathrm{d}y}(y) + 2\beta_1\frac{\mathrm{d}A}{\mathrm{d}y}(y)\right) + \left(2\beta_0\,\ln(x_\mu^2)\right)^2\frac{\mathrm{d}A}{\mathrm{d}y}(y).\end{aligned} \quad (4.3)$$

For the QCD β-function we follow the convention given in (2.23). In theoretical computations it is customary to normalize the distributions to the hadronic Born cross section σ_0 given in (2.49) since, for massless quarks, the normalisation cancels all electroweak coupling factors. However, experimentally it is easier to normalize the distributions to the total hadronic cross section σ_{had}. The correction for the normalization can be done by expanding the ratio $\sigma_0/\sigma_{\mathrm{had}}$ in powers of $\bar{\alpha_S}$[1] In the massless case the ratio is given by

$$\begin{aligned}\frac{\sigma_{\mathrm{had}}}{\sigma_0} =& 1 + \bar{\alpha}_S K_1 + \bar{\alpha}_S^2\left[K_2 + 2\beta_0\,\ln(x_\mu^2)K_1\right]\\ &+ \bar{\alpha}_S^3\left[K_3 + 2\ln(x_\mu^2)\left(2\beta_1 K_1 + 2\beta_0 K_2\right) + \left(2\beta_0\ln(x_\mu^2)\right)^2 K_1\right]\end{aligned} \quad (4.4)$$

where

$$\begin{aligned}K_1 &= \frac{3}{2}C_F\\ K_2 &= \frac{1}{4}\left[-\frac{3}{2}C_F^2 + C_F C_A\left(\frac{123}{2} - 44\zeta_3\right) + \frac{C_F N_F}{2}\left(-22 + 16\zeta_3\right)\right]\\ K_3 &= 8\left[-\frac{69}{128}C_F^3 + C_F^2 C_A\left(-\frac{127}{64} - \frac{143}{16}\zeta_3 + \frac{55}{4}\zeta_5\right) + C_F C_A^2\left(\frac{90445}{3456} - \frac{2737}{144}\zeta_3 - \frac{55}{24}\zeta_5\right)\right.\\ &\quad \left. + \frac{N_F C_F^2}{2}\left(-\frac{29}{64} + \frac{19}{4}\zeta_3 - 5\zeta_5\right) + \frac{N_F C_F C_A}{2}\left(-\frac{485}{27} + \frac{112}{9}\zeta_3 + \frac{5}{6}\zeta_5\right)\right.\end{aligned}$$

[1] In Section 2.6.1 we computed the first correction to the expansion of this ratio, however since very recently this expansion is known at 4 loops [213].

$$+\frac{N_F^2 C_F}{4}\left(\frac{151}{54}-\frac{19}{9}\zeta_3\right)-\pi^2 C_F\left(\frac{11}{24}C_A-\frac{1}{12}N_F\right)^2\Bigg] .$$

The dependence on the renormalization scale μ is universal and is the same in (4.3) and (4.4). Inserting the expansion of $\sigma_0/\sigma_{\text{had}}$ we obtain the following expression:

$$\frac{1}{\sigma_{\text{had}}}\frac{\mathrm{d}\sigma}{\mathrm{d}y}(y,Q,\mu)=\bar{\alpha}_s(\mu)\frac{\mathrm{d}\bar{A}}{\mathrm{d}y}(y)+\bar{\alpha}_s^2(\mu)\frac{\mathrm{d}\bar{B}}{\mathrm{d}y}(y,x_\mu)+\bar{\alpha}_s^3(\mu)\frac{\mathrm{d}\bar{C}}{\mathrm{d}y}(y,x_\mu)+\mathcal{O}(\bar{\alpha}_s^4)\ , \quad (4.5)$$

where $\bar{A},\bar{B},\bar{C}$ are related to A,B,C by

$$\begin{aligned}\bar{A}(y)&=A(y)\,,\\ \bar{B}(y,x_\mu)&=B(y,x_\mu)-K_1A(y)\,,\\ \bar{C}(y,x_\mu)&=C(y,x_\mu)-K_1B(y,x_\mu)+\left(K_1^2-K_2\right)A(y)\,.\end{aligned}$$

For later convenience we consider also the integrated cross section:

$$R(y,Q,\mu)\ \equiv\ \frac{1}{\sigma_{\text{had}}}\int_0^y\frac{d\sigma\left(x,\alpha_S\right)}{dx}dx, \quad (4.6)$$

which has the following fixed-order expansion:

$$R\left(y,\mu^2\right)\ =\ 1+\mathcal{A}\left(y\right)\bar{\alpha}_S\left(\mu^2\right)\ +\ \mathcal{B}\left(y,\mu^2\right)\bar{\alpha}_S^2\left(\mu^2\right)\ +\ \mathcal{C}\left(y,\mu^2\right)\bar{\alpha}_S^3\left(\mu^2\right). \quad (4.7)$$

The fixed-order coefficients $\mathcal{A}$, $\mathcal{B}$, $\mathcal{C}$ can be obtained by integrating the distribution (4.5) and using $R(y_{\max},Q,\mu)=1$ to all orders, where $y_{\max}$ is the maximal kinematically allowed value for the shape variable y.

4.2 Resummed calculations

The convergence of the fixed order expansion (4.5) is spoiled if the fixed order coefficients $\mathcal{A}\left(y\right)$, $\mathcal{B}(y)$, $\mathcal{C}(y)$ become large. This happens in the region of the phase space where y is small, since the fixed order coefficients are enhanced by powers of $-\ln(y)$. As explained in detail in Chapter 2, the arise of these enhancements is due to soft and collinear gluon emission. At the n-th order in perturbation theory, the highest power of the logarithms goes like

$$\frac{1}{\sigma_{\text{had}}}\frac{d\sigma_n\left(y\right)}{dy}\ \propto\ \bar{\alpha}_S^n\frac{1}{y}\ \ln^{2n-1}\left(\frac{1}{y}\right) \quad (4.8)$$

and therefore

$$R_n(y)\ \propto\ \bar{\alpha}_S^n\left(\mu^2\right)\ln^{2n}\left(\frac{1}{y}\right).$$

In order to make some predictions in the region $y \to 0$ we have to resum the logarithmic terms to all orders in α_s. For suitable observables this leads to leading logarithm (LL) exponentiation, such that

$$\ln R(y) \sim L g_1(\alpha_s L) \,,$$

where $L = \ln(y_0/y)$ and y_0 is an observable dependent parameter. The function $g_1(\alpha_s L)$ is an analytic function and can be expanded in a power series in its argument. For all the event-shape variables we will consider later also the next-to-leading logarithms (NLL) exponentiate giving

$$R^{\rm NLL}_{\rm Resum}(y,Q,\mu) = (1 + C_1 \bar{\alpha}_s)\; e^{(L\, g_1(\alpha_s L) + g_2(\alpha_s L))} \,. \tag{4.9}$$

By differentiating expression (4.9) with respect to y, one recovers the resummed differential event shape distributions, which yield an accurate description for $y \to 0$.

Assuming that exponentiation holds to higher logarithmic accuracy too[1], a generic resummed result has the form

$$R_{\rm Resum}(y,Q,\mu) = \left(1 + C_1 \bar{\alpha}_s + C_2 \bar{\alpha}_s^2 + \ldots\right)\; e^{(L\, g_1(\alpha_s L) + g_2(\alpha_s L) + \bar{\alpha}_s g_3(\alpha_s L) + \ldots)} \,. \tag{4.10}$$

The exponentiated functions $g_1(\alpha_s L)$, $g_2(\alpha_s L)$, ... resum respectively LL ($\alpha_s^n L^{n+1}$), NLL ($\alpha_s^n L^n$) and so on. We can expand these functions in powers of $\bar{\alpha}_s L$

$$\begin{aligned}
L\, g_1(\alpha_s L) &= G_{12} \bar{\alpha}_s L^2 + G_{23} \bar{\alpha}_s^2 L^3 + G_{34} \bar{\alpha}_s^3 L^4 + \ldots \,, & (4.11)\\
g_2(\alpha_s L) &= G_{11} \bar{\alpha}_s L + G_{22} \bar{\alpha}_s^2 L^2 + G_{33} \bar{\alpha}_s^3 L^3 + \ldots \,, & (4.12)\\
\bar{\alpha}_s g_3(\alpha_s L) &= G_{21} \bar{\alpha}_s^2 L + G_{32} \bar{\alpha}_s^3 L^2 + G_{43} \bar{\alpha}_s^4 L^3 + \ldots \,. & (4.13)
\end{aligned}$$

Reexpanding the resummed prediction we obtain a clear picture of the logarithmic structure

$$R_1(y) = C_1 + G_{11} L + G_{12} L^2 \,, \tag{4.14}$$

$$\begin{aligned}
R_2(y) &= C_2 + (G_{21} + C_1 G_{11})\, L + \left(G_{22} + \frac{1}{2} G_{11}^2 + C_1 G_{12}\right) L^2 \,, \\
&\quad + (G_{23} + G_{12} G_{11})\, L^3 + \frac{1}{2} G_{12}^2 L^4
\end{aligned} \tag{4.15}$$

$$\begin{aligned}
R_3(y) &= C_3 + (G_{31} + C_1 G_{21} + C_2 G_{11})\, L \\
&\quad + \left(G_{32} + C_1 G_{22} + \frac{1}{2} C_1 G_{11}^2 + C_2 G_{12} + G_{11} G_{21}\right) L^2
\end{aligned}$$

[1] For thrust this is confirmed by a computation in an effective field theory approach at N^{3}LLA [214].

$$+\left(G_{33}+G_{11}G_{22}+G_{12}G_{21}+C_1G_{11}G_{12}+\frac{1}{6}G_{11}^3+C_1G_{23}\right)L^3$$
$$+\left(G_{34}+G_{12}G_{22}+\frac{1}{2}C_1G_{12}^2+G_{11}G_{23}+\frac{1}{2}G_{11}^2G_{12}\right)L^4$$
$$+\left(G_{12}G_{23}+\frac{1}{2}G_{12}^2G_{11}\right)L^5+\frac{1}{6}G_{12}^3L^6\,. \tag{4.16}$$

An overview of the different logarithmic contributions at fixed order and in resummation in also given in Table 4.1.

$\bar{\alpha}_s\mathcal{A}(y)$	$\bar{\alpha}_s L$	$\bar{\alpha}_s L^2$				
$\bar{\alpha}_s^2\mathcal{B}(y,x_\mu)$	$\bar{\alpha}_s^2 L$	$\bar{\alpha}_s^2 L^2$	$\bar{\alpha}_s^2 L^3$	$\bar{\alpha}_s^2 L^4$		
$\bar{\alpha}_s^3\mathcal{C}(y,x_\mu)$	$\bar{\alpha}_s^3 L$	$\bar{\alpha}_s^3 L^2$	$\bar{\alpha}_s^3 L^3$	$\bar{\alpha}_s^3 L^4$	$\bar{\alpha}_s^3 L^5$	$\bar{\alpha}_s^3 L^6$

Table 4.1: Logarithmic terms at LO, NLO and NNLO and at LL (blue frame), NLL (green frame) and NNLL (brown frame). The terms in dashed frames comes from trivial exponentiation. The colour of the dashed frames indicated the logarithmic accuracy at which they appear.

The difference between the logarithmic part and the full fixed order expansion at the different orders is given by

$$\begin{aligned} d_1(y) &= \mathcal{A}(y)-R_1(y)\,,\\ d_2(y) &= \mathcal{B}(y)-R_2(y)\,,\\ d_3(y) &= \mathcal{C}(y)-R_3(y)\,. \end{aligned}$$

The functions $d_i(y)$ contain the non-logarithmic part of the fixed order contribution and vanish for $y\to 0$. We collect them into a function $D(y,Q,\mu)$ defined as

$$D(y,Q,\mu) = \bar{\alpha}_s d_1(y)+\bar{\alpha}_s^2 d_2(y)+\bar{\alpha}_s^3 d_3(y)+\dots\,. \tag{4.17}$$

Having the two different calculations – the fixed order calculations, valid in the multijet region, and the resummed results which holds in the soft and collinear part of the phase space – we can match them in order to have the most reliable prediction over the whole kinematical range.

4.3 Matching of fixed order and resummed calculations

In combining two calculations together, one has to pay attention not to consider twice the same contributions. There are different matching schemes proposed in the literature, however mainly two are used. We will present them both in the following.

4.3.1 The R-matching scheme

In the R-matching scheme the two expressions (4.6) and (4.10) are matched and logarithms appearing twice are subtracted. The explicit expression for the matched integrated cross section $R(y, Q, \mu)$ depends on the order of the calculations considered in the matching. At NLLA+NLO the following formula holds (for clarity we drop any dependence on the renormalization scale, which will be analysed separately):

$$\begin{aligned} R(y,Q,\mu) &= \left(1 + C_1\bar{\alpha}_s + C_2\bar{\alpha}_s^2\right) e^{\left(L\, g_1(\alpha_s L) + g_2(\alpha_s L) + \bar{\alpha}_s^2 L\, G_{21}\right)} \\ &\quad + \bar{\alpha}_s \left(\mathcal{A}(y) - R_1(y)\right) + \bar{\alpha}_s^2 \left(\mathcal{B}(y) - R_2(y)\right) . \end{aligned} \tag{4.18}$$

The differences in the second line corresponds to the remainder functions $d_i(y)$ defined above. It is however preferable to write it as difference between the full fixed order coefficient and its logarithmic part since in practice these are the functions which are known. In fact, the logarithmic terms in the $R_i(y)$ functions can be easily found be reexpanding the analytically known resummed functions $g_i(\alpha_s L)$, whereas the fixed order coefficient function is usually know only as a numerical binned distribution. It is easy to guess that in the kinematical region where $y \to 0$, resummation dominates and the second line vanishes, whereas in the multijet region the functions $R_i(y)$ cancel exactly the logarithms contained in the resummed calculation keeping small higher order logarithmic corrections on top of the full fixed order result.

This approach has however also some practical problems. From the theoretical side, in order to match the calculation with fixed NLO results, the first term of the expansion of the NNLL resummation function $g_3(\alpha_s L)$ is also needed. However, belonging to a subleading logarithmic accuracy, the coefficients G_{21} and C_2 are known only numerically for the majority of the observables. The numerical value of these coefficients can be inferred by fitting the fixed order numerical distributions with a function of the form

$$f(y, G_{21}, C_2) = R_2(y, G_{21}, C_2) + d_2(y) \tag{4.19}$$

where for $d_2(y)$ a reasonable assumption must be made. Several tries were made in this direction, however the numerical results suffer always from high numerical instability.

The same problem arises by going one order further both at fixed order and in resummation. The expression for the matching at NNLLA+NNLO is

$$\begin{aligned} R(y,Q,\mu) &= \left(1 + C_1\bar{\alpha}_s + C_2\bar{\alpha}_s^2 + C_3\bar{\alpha}_s^3\right) e^{\left(L\, g_1(\alpha_s L) + g_2(\alpha_s L) + \bar{\alpha}_s\, g_3(\alpha_s L) + \bar{\alpha}_s^3 L\, G_{31}\right)} \\ &\quad + \bar{\alpha}_s \left(\mathcal{A}(y) - R_1(y)\right) + \bar{\alpha}_s^2 \left(\mathcal{B}(y) - R_2(y)\right) + \bar{\alpha}_s^3 \left(\mathcal{C}(y) - R_3(y)\right) . \end{aligned} \tag{4.20}$$

At the moment only thrust is known at a sufficiently high logarithmic accuracy [214] allowing to try this matching, and further studies on this have to be done[1]. For all other observables analysed the NNLO computations should be matched with NLLA using

$$\begin{aligned} R(y,Q,\mu) \;=\; & \left(1 \,+\, C_1\bar{\alpha}_s + C_2\bar{\alpha}_s^2 + C_3\bar{\alpha}_s^3\right) e^{\left(L\,g_1(\alpha_s L)+g_2(\alpha_s L)+\bar{\alpha}_s^2 L\,G_{21}+\bar{\alpha}_s^3 L^2\,G_{32}+\bar{\alpha}_s^3 L\,G_{31}\right)} \\ & +\bar{\alpha}_s\left(\mathcal{A}(y)-R_1(y)\right)+\bar{\alpha}_s^2\left(\mathcal{B}(y)-R_2(y)\right)+\bar{\alpha}_s^3\left(\mathcal{C}(y)-R_3(y)\right)\,. \end{aligned} \tag{4.21}$$

In this case the situation is even worse, since five different coefficients have to be extracted numerically.

However there is another matching scheme where all the needed coefficients can be extracted analytically from known resummed results.

4.3.2 The $\ln(R)$-matching scheme

The $\ln(R)$-matching scheme is believed to be theoretically the most stable one and for this reason it is generally preferred [202]. In this case all the matching coefficients needed can be found analytically. In order to understand the $\ln(R)$-matching scheme, we rewrite eq. (4.10) as follows:

$$R(y,\alpha_s) \;=\; C(\alpha_s)\,\Sigma(y,\alpha_s L)\,, \tag{4.22}$$

where

$$\Sigma(y,\alpha_s L) \;=\; e^{\left(L\,g_1(\alpha_s L)+g_2(\alpha_s L)+\bar{\alpha}_s g_3(\alpha_s L)+\ldots\right)}\,,$$

and $C(\alpha_s)$ corresponds to the constant part in front of the exponential in (4.10). Taking the logarithm on both sides we obtain something of the form

$$\ln(R(y,\alpha_s)) \;=\; K(\alpha_s) \,+\, \ln(\Sigma(y,\alpha_s))\,. \tag{4.23}$$

We now consider the fixed-order expansion and take the logarithm of it

$$\ln\left(R(y,\alpha_s)\right) \;=\; \ln\left(1+\mathcal{A}(y)\bar{\alpha}_s+\mathcal{B}(y)\bar{\alpha}_s^2+\mathcal{C}(y)\bar{\alpha}_s^3+\mathcal{O}(\alpha_s^4)\right).$$

Considering the Taylor expansion of $\ln(1+x)$ for small x, we can write

$$\begin{aligned} \ln\left(R(y,\alpha_s)\right) =& \mathcal{A}(y)\bar{\alpha}_s+\mathcal{B}(y)\bar{\alpha}_s^2+\mathcal{C}(y)\bar{\alpha}_s^3-\frac{1}{2}\mathcal{A}^2(y)\bar{\alpha}_s^2 \\ & -\mathcal{A}(y)\,\mathcal{B}(y)\bar{\alpha}_s^3+\frac{1}{3}\mathcal{A}^3(y)\bar{\alpha}_s^3+\mathcal{O}(\alpha_s^4). \end{aligned} \tag{4.24}$$

[1] In Section 4.6.3 we derive $g_3(\alpha_s L)$ from [214] and perform the matching with NNLO calculations in the $\ln(R)$-matching scheme. For the constants C_2 and C_3 needed for a matching in the R-matching scheme we still have to rely on a numerical determination.

The two expressions (4.23) and (4.24) can be matched after having subtracted the constant term $K(\alpha_s)$, which is already included in $\mathcal{A}(y)$, $\mathcal{B}(y)$ and $\mathcal{C}(y)$. By matching we obtain

$$\begin{aligned}\ln\left(R(y,\alpha_s)\right) =& L\, g_1(\alpha_s L) \,+\, g_2(\alpha_s L) + \bar{\alpha}_s g_3(\alpha_s L) \\ &+ \bar{\alpha}_s \left(\mathcal{A}\left(y\right) - G_{11}L - G_{12}L^2\right) + \\ &+ \bar{\alpha}_s^2 \left(\mathcal{B}\left(y\right) - \frac{1}{2}\mathcal{A}_1^2\left(y\right) - G_{21}L - G_{22}L^2 - G_{23}L^3\right) \\ &+ \bar{\alpha}_s^3 \left(\mathcal{C}\left(y\right) - \mathcal{A}\left(y\right)\mathcal{B}\left(y\right) + \frac{1}{3}\mathcal{A}^3\left(y\right) - G_{32}L^2 - G_{33}L^3 - G_{34}L^4\right) .\end{aligned} \tag{4.25}$$

This formula holds for the matching of NNLLA+NNLO. We will use it in Section 4.6.3, where we derive the function $g_3(\alpha_s L)$ for thrust from the results computed in [214] using soft-collinear-effective-theory (SCET). The advantage of this matching scheme is that, since everything is exponentiated, we do not need to separate explicitly the constant or the subleading contribution. At NLLA+NNLO the matched expression is given by

$$\begin{aligned}\ln\left(R(y,\alpha_s)\right) \;=\; & L\, g_1(\alpha_s L) + g_2(\alpha_s L) \\ & + \bar{\alpha}_s \left(\mathcal{A}(y) - G_{11}L - G_{12}L^2\right) \\ & + \bar{\alpha}_s^2 \left(\mathcal{B}(y) - \frac{1}{2}\mathcal{A}^2(y) - G_{22}L^2 - G_{23}L^3\right) \\ & + \bar{\alpha}_s^3 \left(\mathcal{C}(y) - \mathcal{A}(y)\mathcal{B}(y) + \frac{1}{3}\mathcal{A}^3(y) - G_{33}L^3 - G_{34}L^4\right) .\end{aligned} \tag{4.26}$$

The results obtained in SCET for thrust would in principle allow also a matching at N^{3}LLA+NNLO. The correct formula in the $\ln(R)$-matching scheme at this order is

$$\begin{aligned}\ln\left(R(y,\alpha_s)\right) =& L\, g_1(\alpha_s L) + g_2(\alpha_s L) + \bar{\alpha}_s\, g_3(\alpha_s L) + \bar{\alpha}_s^2\, g_4(\bar{\alpha}_s) \\ &+ \bar{\alpha}_s \left(\mathcal{A}(y) - G_{11}L - G_{12}L^2\right) \\ &+ \bar{\alpha}_s^2 \left(\mathcal{B}(y) - \frac{1}{2}\mathcal{A}^2(y) - G_{21}L - G_{22}L^2 - G_{23}L^3\right) \\ &+ \bar{\alpha}_s^3 \left(\mathcal{C}(y) - \mathcal{A}(y)\mathcal{B}(y) + \frac{1}{3}\mathcal{A}^3(y) - G_{31}L - G_{32}L^2 - G_{33}L^3 - G_{34}L^4\right) .\end{aligned} \tag{4.27}$$

4.4 Modifications to the matching schemes

In the last section we gave different results for the matched integrated cross section, which are valid over the whole phase space. However, contrary to the fixed order

prediction (4.6), for which every coefficient vanishes such that $R(y_{\max}) = 1$, in the limit $y \to y_{\max}$, the two predictions (4.21) and (4.25) give the wrong results. It is obvious that the differential cross section $\mathrm{d}\sigma/\mathrm{d}y$ has to vanish in this region for a fixed order prediction, because every fixed order calculation takes into account only a finite (in fact very few) number of final particles. It is therefore clear that the cross section for the production of more and more final jets has to vanish. In our case, considering the NNLO fixed order prediction, the maximal number of final jets is five. The cross section at the phase space limit for six partons should therefore vanish. The limited predictive ability of the two matching schemes in the multijet region can be solved by modifying them slightly. This is done by imposing a kinematical constraint, which assures the right prediction for $y \to y_{\max}$.

The constraints for the so-called *modified* $\ln(R)$*-matching* scheme are

$$\ln\left(R(y_{\max}, \alpha_s)\right) = 0 \quad , \quad \frac{1}{\sigma_{\mathrm{tot}}} \frac{\mathrm{d}\sigma(y)}{\mathrm{d}y}\bigg|_{y=y_{\max}} = \frac{\mathrm{d}R(y)}{\mathrm{d}y}\bigg|_{y=y_{\max}} = 0. \tag{4.28}$$

In order to fulfil these two constraints, we can redefine L as follows:

$$L \longrightarrow \tilde{L} = \frac{1}{p} \ln\left(\left(\frac{y_0}{y}\right)^p - \left(\frac{y_0}{y_{\max}}\right)^p + 1\right). \tag{4.29}$$

The power p is called the degree of modification. We choose $p = 1$, as usual in literature. It determines how fast the integrated cross section is damped at the kinematical limit. The values of $y_{\max}$ can usually be determined by symmetry arguments, like the one made for the thrust in Section 2.6.2.

For the $\ln(R)$-matching scheme, the substitution $L \to \tilde{L}$ is enough to fulfil the constraints (4.28). In the R-matching scheme one further modification is needed

$$\tilde{G}_{i1} = G_{i1}\left[1 - \left(\frac{y}{y_{\max}}\right)^p\right], \quad i = 1, 2, 3\,. \tag{4.30}$$

The dependence on the renormalization scheme was so far not considered. Every second order term acquires an explicit μ-dependence.

- For the fixed order coefficients the explicit μ dependence is similar to (4.3):

$$\mathcal{B}\left(y, \mu^2\right) = 2\beta_0 \ln(x_\mu^2)\mathcal{A}(y) + \mathcal{B}(y) \tag{4.31}$$

$$\mathcal{C}\left(y, \mu^2\right) = \left(2\beta_0 \ln(x_\mu^2)\right)^2 \mathcal{A}(y) + 2\ln(x_\mu^2)\left(2\beta_0 \mathcal{B}(y) + 2\beta_1 \mathcal{A}(y)\right) + \mathcal{C}(y). \tag{4.32}$$

- Some of the G_{mn} and C_i coefficients change as follows:

$$G_{21} \to \bar{G}_{21}\left(\mu^2\right) = G_{21} + 2\beta_0 G_{11} \ln(x_\mu^2)$$

$$
\begin{aligned}
G_{22} \to \bar{G}_{22}\left(\mu^2\right) &= G_{22} + 2\beta_0 G_{12} \ln(x_\mu^2) \\
G_{33} \to \bar{G}_{33}\left(\mu^2\right) &= G_{33} + 2\beta_0 2G_{23} \ln(x_\mu^2) \\
G_{31} \to \bar{G}_{31}\left(\mu^2\right) &= G_{31} + \left(2\beta_0 \ln(x_\mu^2)\right)^2 G_{11} + 2\ln(x_\mu^2)\left(2\beta_0 G_{21} + 2\beta_1 G_{11}\right) \\
G_{32} \to \bar{G}_{32}\left(\mu^2\right) &= G_{32} + \left(2\beta_0 \ln(x_\mu^2)\right)^2 G_{12} + 2\ln(x_\mu^2)\left(2\beta_0 G_{22} + 2\beta_1 G_{12}\right) \\
C_2 \to \bar{C}_2\left(\mu^2\right) &= C_2 + 2\beta_0 C_1 \ln(x_\mu^2) \\
C_3 \to \bar{C}_3\left(\mu^2\right) &= C_3 + \left(2\beta_0 \ln(x_\mu^2)\right)^2 C_1 + 2\ln(x_\mu^2)\left(2\beta_0 C_2 + 2\beta_1 C_1\right).
\end{aligned}
\tag{4.33}
$$

- For the full functions $g_i\left(\alpha_s L\right)$, we have

$$
\bar{g}_2\left(\alpha_s L, \mu^2\right) = g_2(\alpha_s L) + 2\beta_0 \left(\bar{\alpha}_s L\right)^2 \ln(x_\mu^2) \partial g_1(\alpha_s L) \tag{4.34}
$$

$$
\begin{aligned}
\bar{g}_3\left(\alpha_s L, \mu^2\right) &= g_3(\alpha_s L) + \ln(x_\mu^2)\left[2\beta_0\left(\bar{\alpha}_s L\right)\partial g_2(\alpha_s L) + 4\beta_1(\bar{\alpha}_s L)^2 \partial g_1(\alpha_s L)\right] \\
&\quad + \left(2\beta_0\right)^2 \left(\bar{\alpha}_s L\right)^2 \frac{1}{2} \ln(x_\mu^2)^2 \partial^2\left(\bar{\alpha}_s L\, g_1\left(\alpha_s L\right)\right)
\end{aligned}
\tag{4.35}
$$

$$
\begin{aligned}
\bar{g}_4\left(\alpha_s L, \mu^2\right) &= g_4\left(\alpha_s L\right) + \ln(x_\mu^2)\left[2\beta_0 \partial\left(\bar{\alpha}_s L\, g_3\left(\alpha_s L\right)\right) + 4\beta_1\left(\bar{\alpha}_s L\right)\partial g_2\left(\alpha_s L\right)\right. \\
&\qquad \left. + 8\beta_2\left(\bar{\alpha}_s L\right)^2 \partial g_1\left(\alpha_s L\right)\right] \\
&\quad + \frac{1}{2} \ln(x_\mu^2)^2 \left[\left(2\beta_0\right)^2 \left(\bar{\alpha}_s L\right)\partial^2\left(\bar{\alpha}_s L\, g_2\left(\alpha_s L\right)\right)\right. \\
&\qquad + \left(2\beta_0\right)\left(4\beta_1\right)\left(\bar{\alpha}_s L\right)^2 \partial^2\left(\bar{\alpha}_s L\, g_1\left(\alpha_s L\right)\right) \\
&\qquad \left. + \left(2\beta_0\right)\left(4\beta_1\right)\left(\bar{\alpha}_s L\right)^2 \partial\left(\frac{1}{\bar{\alpha}_s L}\,\partial\left(\left(\bar{\alpha}_s L\right)^2 g_1\left(\alpha_s L\right)\right)\right)\right] \\
&\quad + \frac{1}{6} \ln(x_\mu^2)^3 \left(2\beta_0\right)^3 \left(\bar{\alpha}_s L\right)^3 \partial^3\left(\left(\bar{\alpha}_s L\right)^2 g_1\left(\alpha_s L\right)\right)
\end{aligned}
\tag{4.36}
$$

  where ∂ is defined as

$$
\partial \equiv \frac{\mathrm{d}}{\mathrm{d}\bar{\alpha}_s L}\,.
$$

Making these substitutions into formula (4.26) for the $\ln(R)$-matching at NLLA+NNLO we observe the matching NLLA with NNLO introduces a mismatch in the cancellation of renormalisation scale logarithms, since the NNLO expansion fully compensates the renormalisation scale dependence up to 2 loops, while NLLA only compensates it up to 1 loop. In order to assess the impact of this mismatch, we have introduced the $\ln R(\mu)$-matching scheme, which is explained in the next section.

One further source of arbitrariness is the choice of the logarithm to be resummed. In fact, it is not clear whether powers of $\alpha_s \ln(y_0/y)$ or powers of $\alpha_s \ln(2y_0/y)$ have to be resummed. The origin of this arbitrariness has to do with how much of the non-logarithmic part of the fixed order prediction is exponentiated together with the

logarithms. We can express this arbitrariness by introducing a new constant x_L, which rescales the logarithm to be resummed [202]:

$$L \;\to\; \hat{L} = \frac{1}{p} \ln \left[\left(\frac{y_0}{x_L\, y} \right)^p - \left(\frac{y_0}{x_L\, y_{\max}} \right)^p + 1 \right]. \tag{4.37}$$

This rescaling modifies once more the resummed formulae and their expansion coefficients. By requiring

$$\hat{R}(y) \;=\; R(y)\,,$$

where $\hat{R}(y)$ denotes the rescaled integrated cross section, we find the following substitutions:

$$\begin{aligned}
\hat{C}_1(y) &= C_1 + G_{11} \ln(x_L) + G_{12} \ln(x_L)^2\,, && (4.38)\\
\hat{C}_2(y) &= C_2 + (G_{21} + C_1 G_{11}) \ln(x_L) + \left(G_{22} + \frac{1}{2} G_{11}^2 + C_1 G_{12} \right) \ln(x_L)^2 \\
&\quad + (G_{23} + G_{12} G_{11}) \ln(x_L)^3 + \frac{1}{2} G_{12}^2 \ln(x_L)^4\,, && (4.39)\\
\hat{C}_3\,(y) &= C_3 + (G_{31} + C_1 G_{21} + C_2 G_{11}) \ln(x_L) \\
&\quad + \left(G_{32} + C_1 G_{22} + \frac{1}{2} C_1 G_{11}^2 + C_2 G_{12} + G_{11} G_{21} \right) \ln(x_L)^2 \\
&\quad + \left(G_{33} + G_{11} G_{22} + G_{12} G_{21} + C_1 G_{11} G_{12} + \frac{1}{6} G_{11}^3 + C_1 G_{23} \right) \ln(x_L)^3 \\
&\quad + \left(G_{34} + G_{12} G_{22} + \frac{1}{2} C_1 G_{12}^2 + G_{11} G_{23} + \frac{1}{2} G_{11}^2 G_{12} \right) \ln(x_L)^4 \\
&\quad + \left(G_{12} G_{23} + \frac{1}{2} G_{12}^2 G_{11} \right) \ln(x_L)^5 \;+\; \frac{1}{6} G_{12}^3 \ln(x_L)^6\,, && (4.40)
\end{aligned}$$

$$\begin{aligned}
G_{12} \to \hat{G}_{12} &= G_{12}\,, \qquad \hat{G}_{23} \;=\; G_{23}\,, \qquad \hat{G}_{34} \;=\; G_{34}\,, \\
G_{11} \to \hat{G}_{11} &= G_{11} + 2 G_{12} \ln(x_L)\,, \\
G_{22} \to \hat{G}_{22} &= G_{22} + 3 G_{23} \ln(x_L)\,, \\
G_{33} \to \hat{G}_{33} &= G_{33} + 4 G_{34} \ln(x_L)\,, \\
G_{21} \to \hat{G}_{21} &= G_{21} + 2 G_{22} \ln(x_L) + 3 G_{23} \ln(x_L)^2\,, \\
G_{32} \to \hat{G}_{32} &= G_{32} + 3 G_{33} \ln(x_L) + 6 G_{34} \ln(x_L)^2\,, \\
G_{31} \to \hat{G}_{31} &= G_{31} + 2 G_{32} \ln(x_L) + 3 G_{33} \ln(x_L)^2 + 4 G_{34} \ln(x_L)^3\,. \qquad (4.41)
\end{aligned}$$

The changes in the G_{ij} can also be written in terms of the g_i functions:

$$\begin{aligned}
g_1(\alpha_s L) &\to \hat{g}_1(\alpha_s \hat{L}) = g_1(\alpha_s \hat{L})\,, \\
g_2(\alpha_s L) &\to \hat{g}_2(\alpha_s \hat{L}) = g_2(\alpha_s \hat{L}) + \hat{\partial} \left(\bar{\alpha}_s \hat{L}\, g_1(\alpha_s \hat{L}) \right) \ln(x_L)\,,
\end{aligned}$$

$$
\begin{aligned}
g_3(\alpha_s L) \to\ \hat{g}_3(\alpha_s \hat{L}) &= g_3(\alpha_s \hat{L}) + \hat{\partial}\left(g_2(\alpha_s \hat{L})\right) \ln(x_L) \ -\ G_{11}\bar{\alpha}_s\ \ln(x_L) \\
&\quad +\ \frac{1}{2!}\hat{\partial}^2\left(\bar{\alpha}_s \hat{L}\, g_1(\alpha_s \hat{L})\right) \ln(x_L)^2 \ -\ G_{12}\bar{\alpha}_s \ln(x_L)^2\,, \\
g_4\,(\alpha_s L) \to\ \hat{g}_4(\alpha_s \hat{L}) &= g_4(\alpha_s \hat{L}) \ +\hat{\partial} g_3(\alpha_s \hat{L})\ \ln(x_L) \ -\ G_{21}\bar{\alpha}_s^2\ \ln(x_L) \\
&\quad +\ \frac{1}{2!}\hat{\partial}^2 g_2(\alpha_s \hat{L})\ \ln(x_L)^2 \ -\ G_{22}\bar{\alpha}_s^2 \ln(x_L)^2 \\
&\quad +\ \frac{1}{3!}\hat{\partial}^3\left(\bar{\alpha}_s \hat{L}\, g_1(\alpha_s \hat{L})\right) \ln(x_L)^3 \ -\ G_{23}\bar{\alpha}_s^3 \ln(x_L)^3\,,
\end{aligned}
\tag{4.42}
$$

where again

$$
\partial \equiv \frac{\mathrm{d}}{\mathrm{d}\bar{\alpha}_s L} \qquad ; \qquad \hat{\partial} \equiv \frac{\mathrm{d}}{\mathrm{d}\bar{\alpha}_s \hat{L}}\,.
$$

Finally, the full dependence on $(\alpha_s L)$, μ, x_L of the functions g_1, g_2, g_3, and g_4 are (the argument $(\alpha_s \hat{L})$ of the g_i functions is not written explicitly in order to clarify the notation)

$$
\hat{\bar{g}}_1 = g_1 \tag{4.43}
$$

$$
\hat{\bar{g}}_2 = g_2 + 2\beta_0(\bar{\alpha}_s \hat{L})^2 \hat{\partial} g_1 \ln(x_\mu^2) + \hat{\partial}\left((\bar{\alpha}_s \hat{L})\, g_1\right) \ln(x_L) \tag{4.44}
$$

$$
\begin{aligned}
\hat{\bar{g}}_3 = g_3 &+ \left[2\beta_0(\bar{\alpha}_s \hat{L})\hat{\partial} g_2 + 4\beta_1(\bar{\alpha}_s \hat{L})^2 \hat{\partial} g_1\right] \ln(x_\mu^2) \\
&+ \left[(2\beta_0)^2\,(\bar{\alpha}_s \hat{L})^2 \hat{\partial}^2\left((\bar{\alpha}_s \hat{L})\, g_1\right)\right] \frac{1}{2} \ln(x_\mu^2)^2 \\
&+ \left[4\beta_0(\bar{\alpha}_s \hat{L})\hat{\partial} g_1 + 2\beta_0(\bar{\alpha}_s \hat{L})\hat{\partial}^2 g_1\right] \ln(x_L) \ln(x_\mu^2) \\
&+ \hat{\partial} g_2 \ +\ \hat{\partial}^2\left((\bar{\alpha}_s \hat{L})\, g_1\right) - G_{11} \ln(x_L) - G_{12} \ln(x_L)^2
\end{aligned}
\tag{4.45}
$$

$$
\begin{aligned}
\hat{\bar{g}}_4 = g_4 &+ \left[2\beta_0\, \hat{\partial}\left((\bar{\alpha}_s \hat{L})\, g_3\right) + 4\beta_1(\bar{\alpha}_s \hat{L})\hat{\partial} g_2 + 8\beta_2(\bar{\alpha}_s \hat{L})^2 \hat{\partial} g_1\right] \ln(x_\mu^2) \\
&+ \Big[(2\beta_0)^2\,(\bar{\alpha}_s \hat{L})\, \hat{\partial}^2\left((\bar{\alpha}_s \hat{L})\, g_2\right) \ +\ 8\beta_0\beta_1(\bar{\alpha}_s \hat{L})^2 \hat{\partial}^2\left((\bar{\alpha}_s \hat{L})\, g_1\right) \\
&\quad + 8\beta_0\beta_1(\bar{\alpha}_s \hat{L})^2\left(3\hat{\partial} g_1 + (\bar{\alpha}_s \hat{L})^3 \hat{\partial}^2 g_1\right)\Big] \frac{1}{2} \ln\left(\frac{\mu^2}{Q^2}\right)^2 \\
&+ \ (2\beta_0)^2\,(\bar{\alpha}_s \hat{L})^2 \hat{\partial}^3\left((\bar{\alpha}_s \hat{L})^2 g_1\right) \ \frac{1}{6} \ln(x_\mu^2)^3 + \hat{\partial} g_3 \ln(x_L) \\
&+ \left[2\beta_0 \hat{\partial} g_2 + 2\beta_0(\bar{\alpha}_s \hat{L})\hat{\partial}^2 g_2 + 8\beta_1(\bar{\alpha}_s \hat{L})\hat{\partial} g_1 + 4\beta_1(\bar{\alpha}_s \hat{L})^2 \hat{\partial}^2 g_1\right] \ln(x_L) \ln(x_\mu^2) \\
&+ \left[(2\beta_0)^2\, 2(\bar{\alpha}_s \hat{L})\hat{\partial}^2\left((\bar{\alpha}_s \hat{L})\, g_1\right) + (2\beta_0)^2\,(\bar{\alpha}_s \hat{L})^2 \hat{\partial}^3\left((\bar{\alpha}_s \hat{L})\, g_1\right)\right] \frac{1}{2} \ln(x_L) \ln(x_\mu^2)^2 \\
&+ \hat{\partial}^2 g_2\, \frac{1}{2} \ln(x_L)^2 + \hat{\partial}^3\left((\bar{\alpha}_s \hat{L})\, g_1\right) \frac{1}{6} \ln(x_L)^3 \\
&+ \left[4\beta_0 \hat{\partial} g_1 + 4\beta_0(\bar{\alpha}_s \hat{L})\hat{\partial}^2 g_1 + 2\beta_0 \hat{\partial}^2 g_1 + 2\beta_0(\bar{\alpha}_s \hat{L})\hat{\partial}^3 g_1\right] \frac{1}{2} \ln(x_L)^2 \ln(x_\mu^2) \\
&- G_{21} \ln(x_L) - G_{22} \ln(x_L)^2 - G_{23} \ln(x_L)^3
\end{aligned}
\tag{4.46}
$$

These relations are completely general and hold for all possible event-shape observables which can be described with this matching formalism.

4.5 The $\ln(R(\mu))$-matching scheme

As already anticipated, applying the substitutions (4.31), (4.33) and (4.36) to the fixed order and the resummation contribution of equation (4.26) exemplifies a tension between NLLA and NNLO, since the NNLO coefficients compensate the renormalisation scale variation of α_s up to two loops, while the NLLA coefficients only compensate the one-loop variation. A fully consistent matching, including the full scale dependence, is therefore only accomplished by combining NLLA+NLO or NNLLA+NNLO. In order to assess the effect of this incomplete compensation of scale-dependent terms, we have defined an alternative matching scheme, called $\ln(R(\mu))$-scheme in which we added to the NLLA+NNLO matching formula (4.26) the two-loop terms proportional to x_μ for the resummation, i.e. the scale-dependent logarithms appearing in g_3 and in the associated matching coefficients G_{21} and G_{32}. At NLLA+NNLO the matching prescription corresponds to (4.25), retaining only the μ dependent part of g_3 and of G_{21} and G_{32}.

4.6 Event-shape observables at NLLA+NNLO

In this section we apply the computations made in the previous sections to a set of six event-shape variables measured with high accuracy by a number of experiments, most of them at LEP at centre-of-mass energies between 91 and 206 GeV [1, 2, 215–227], and at the SLAC-SLD experiment at 91 GeV [228], as well as at DESY at lower energies, e.g. by the JADE experiment [229, 230]. In particular we concentrate on the set of six event shape observable presented in Section 2.5.2: thrust T [54, 55] (respectively $\tau = 1 - T$), heavy jet mass ρ [56], wide and total jet broadening B_W and B_T [57], C-parameter [58, 59] and two-to-three-jet transition parameter in the Durham algorithm Y_3 [50, 60–63].

Because of the issues explained above concerning the R-matching scheme, we perform the matching using the $\ln(R)$-matching scheme. Closed analytic forms for the LL and NLL resummation functions $g_1(\alpha_s L)$, $g_2(\alpha_s L)$ are available for τ [231], ρ [232, 233], B_W and B_T [234, 235], C [236, 237] and Y_3 [238]. All the needed matching coefficients are reported in Table C.1. They can be obtained by expanding the analytic resummation functions of the different observables collected in Appendix C.

In the matching of Y_3, the constants $\mathcal{F}_i$ appearing the matching coefficients depend on the jet algorithm [238] and can in general be determined only numerically. For the Durham-algorithm, one finds [239]

$$\mathcal{F}_2 = -\pi^2/32 \qquad \text{and} \qquad \mathcal{F}_3 = 0.0620 \pm 0.0100\,,$$

using the semi-numerical resummation method described in [240]. Numerical values of the matching coefficients for $N = 3$, $N_F = 5$ are given in Table 4.2.

	G_{11}	G_{12}	G_{22}	G_{23}	G_{33}	G_{34}
τ/C	4.0	−2.66667	−24.9388	−10.2222	−285.055	−45.716
ρ	4.0	−2.66667	−13.2415	−10.2222	−196.125	−45.716
B_T	8.0	−5.33333	−61.8768	−27.2593	−824.787	−156.741
B_W	8.0	−5.33333	−15.0876	−27.2593	−472.065	−156.741
Y_3	4.0	−1.33333	0.867972	−3.40741	−28.1784	−9.7963

Table 4.2: The numerical value of the logarithmic coefficients G_{ij} for LL and NLL up to the third order in α_s.

4.6.1 The C++ routine `Lormeso`

To perform the matching and study the uncertainties and the variation of the results under variation of the different parameters x_μ, x_L, p involved in the matching, the C++ routine `Lormeso` (Log-R-Matching of Event-Shape Observables) was written and is available online[1]. In the programm, whenever possible, the resummation functions and their derivatives are implemented analytically. The matching can be computed at different orders: NLLA+NLO, NLLA+NNLO and for thrust also at NNLLA+NNLO. The output is given in form of numerical files which can be feeded in a second step to some data analysis software like PAW [242] or ROOT [243]. Alternatively, being written in C++, it is possible to directly create histograms from `Lormeso` by interfacing it with ROOT. Starting from it a fortran copy of `Lormeso` was implemented and used to perform a new determination of α_s at NLLA+NNLO [22], where also mass corrections were taken into account. For this purpose also the massive calculations of the ratio $\sigma_0/\sigma_{\rm had}$ was implemented[2].

4.6.2 Results

The new results of the matching are shown in Figure 4.1 and 4.2. We compare the matched NLLA+NNLO predictions for all event-shape variables with the fixed order NNLO predictions, and the matched NLLA+NLO with fixed order NLO.

To allow for a better distinction of the different orders, all distributions were weighted by the respective shape variables. We use $Q = M_Z$ and fix $x_\mu = 1$, the

[1] For technical details about the routine we refer to the online manual [241] which will be soon available.

[2] More details on this can be found in [241].

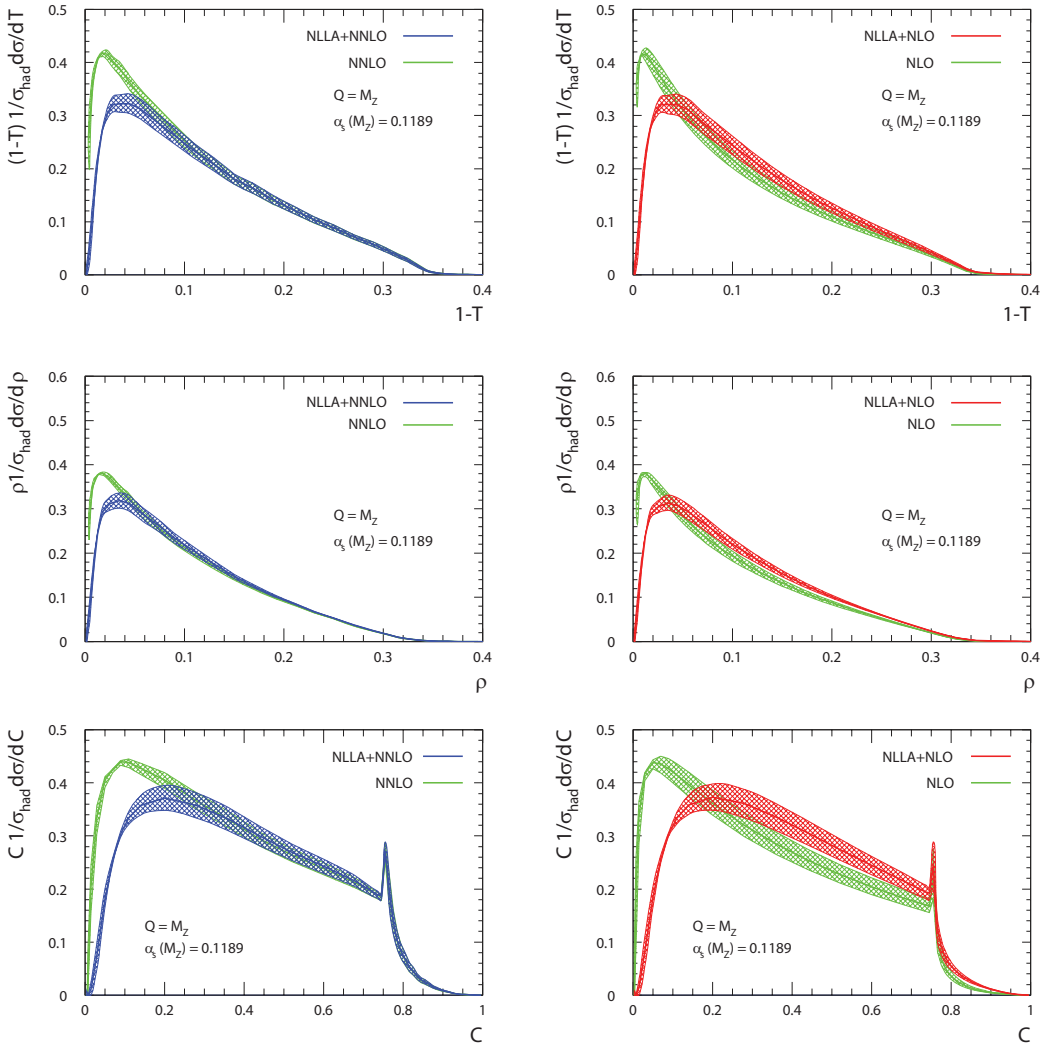

Figure 4.1: Comparison of the matched NLLA+NNLO and NLLA+NLO with fixed order NNLO and NLO predictions for the thrustlike observables τ, ρ and C-parameter.

strong coupling constant is taken as $\alpha_s(M_Z) = 0.1189$ [244]. To quantify the renormalisation scale uncertainty, we have varied $1/2 < x_\mu < 2$, resulting in the error band on these figures.

Several common effects are seen for all shape variables. The most striking observation is that the difference between NLLA+NNLO and NNLO is largely restricted to the two-jet region, while NLLA+NLO differ in normalisation throughout the full kinematical range. This behaviour may serve as a first indication for the numerical smallness of corrections beyond NNLO in the three-jet region.

An immediate consequence of this behaviour concerns the extraction of α_s from

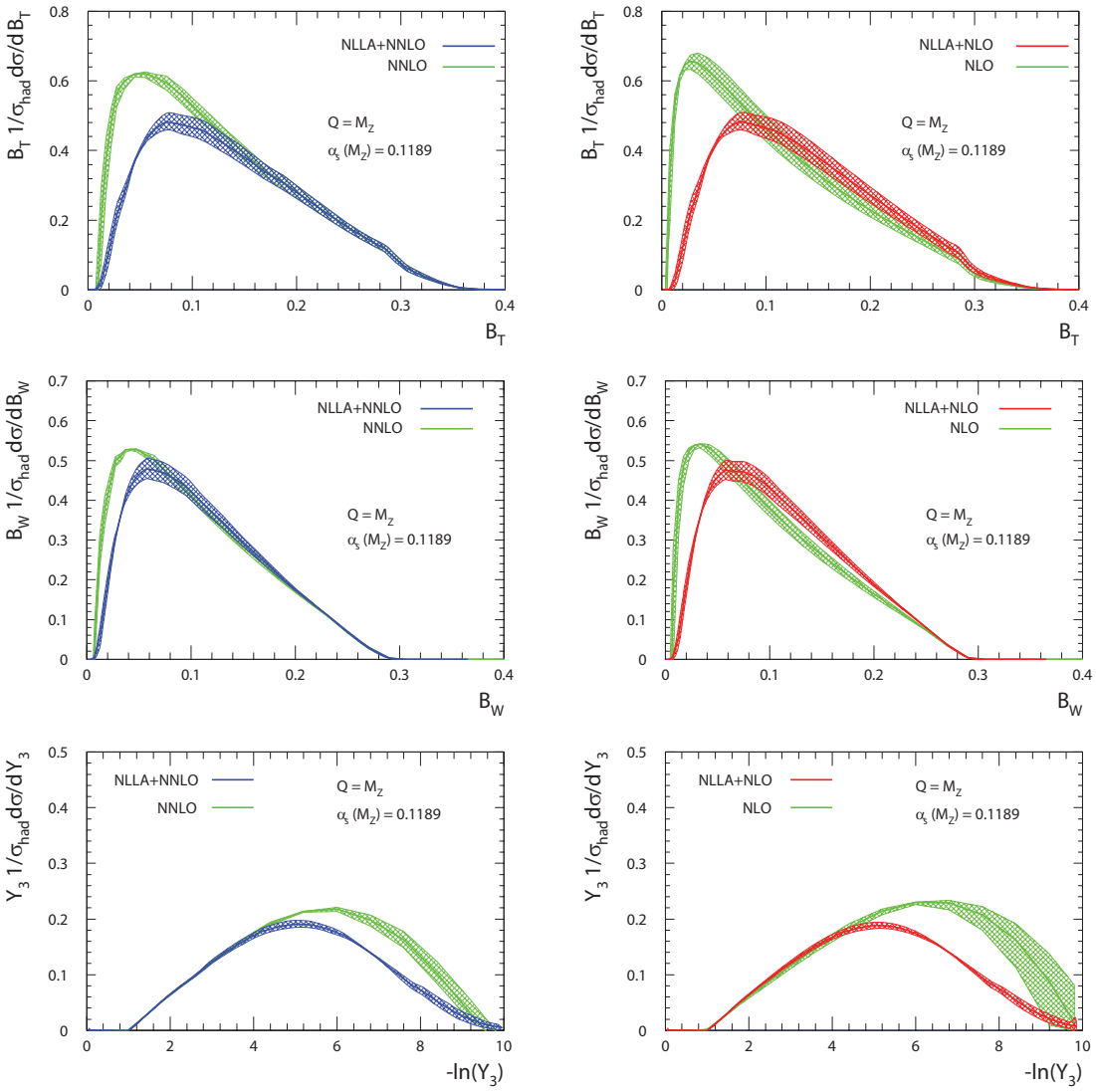

Figure 4.2: Comparison of the matched NLLA+NNLO and NLLA+NLO with fixed order NNLO and NLO predictions for B_T, B_W and Y_3.

event shape data. Studies at LEP [1, 2, 215–227, 245] yielded substantially different values (by about 10-15%) from NLO and NLLA+NLO theory. This discrepancy is an immediate consequence of the varying normalisations in the two approaches. One can expect that α_s obtained using NLLA+NNLO will differ from the fixed-order NNLO result [246] only moderately, given the good agreement of both descriptions in the three-jet region for fixed α_s, and this is indeed observed [22] as we will explain in the next section.

In the three-jet region, NLLA+NNLO agrees with NNLO and the difference be-

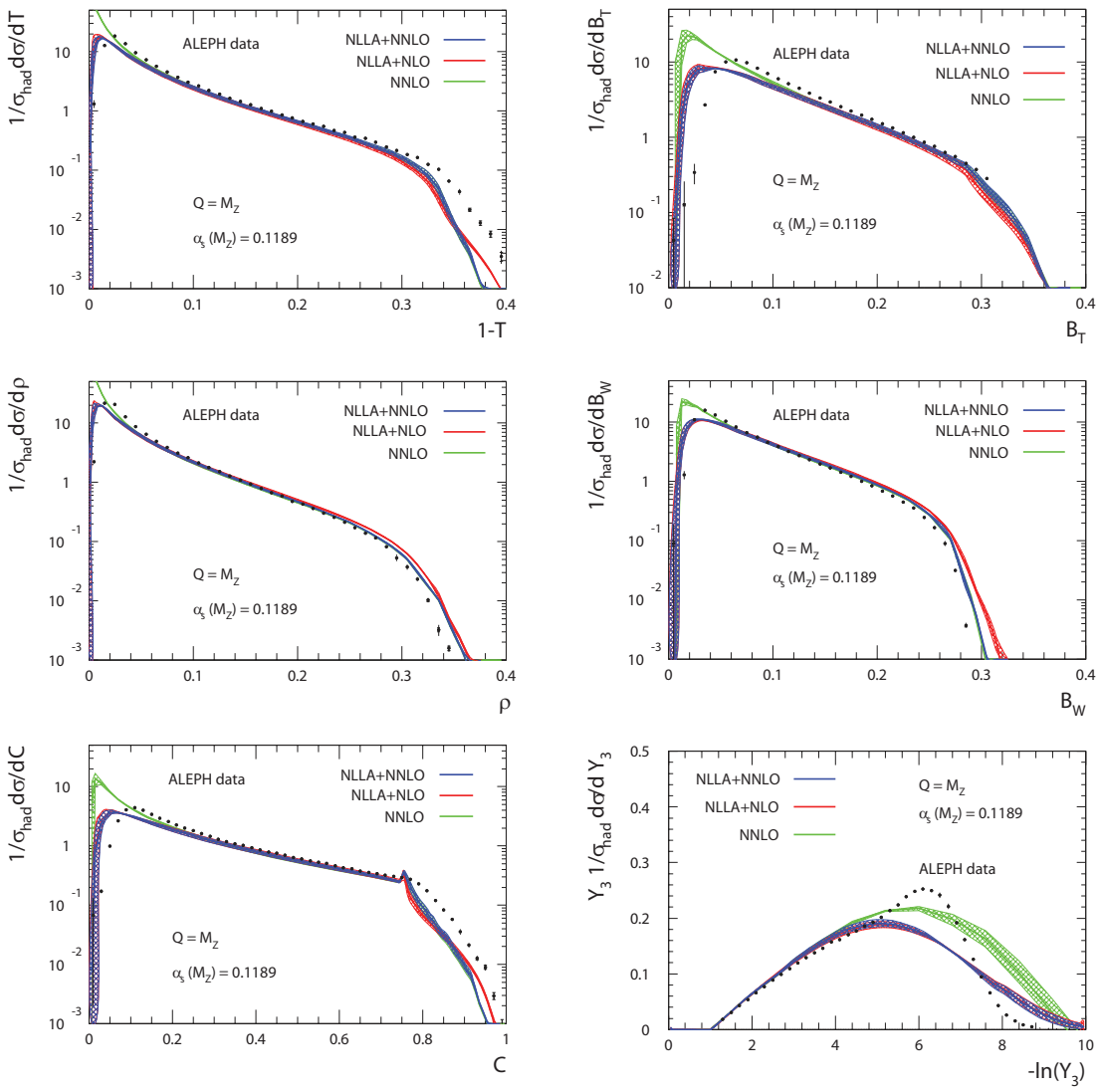

Figure 4.3: Comparison of the matched NLLA+NNLO and NLLA+NLO with fixed order NNLO with the hadron-level data taken by the ALEPH experiment [1, 2].

tween the two matched NLLA+NNLO and NLLA+NLO predictions is only moderate. In particular we clearly observe that it is much smaller than the difference between the fixed order NNLO and NLO predictions. The renormalisation scale uncertainty in the three-jet region is reduced by 20-40% between NLLA+NLO and NLLA+NNLO. In the approach to the two-jet region, the NLLA+NLO and NLLA+NNLO predictions agree by construction, since the matching supresses any fixed order terms. Equally, the renormalisation scale uncertainty on both these predictions is identical in this region and is still very large. Performing the matching with the $\ln(R(\mu))$-scheme we observe a clear

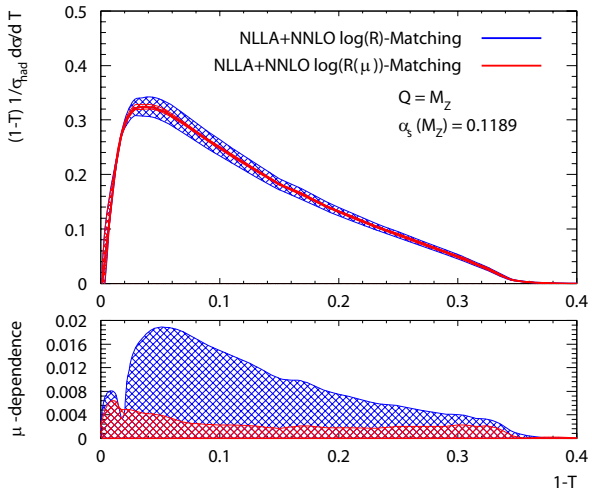

Figure 4.4: $\ln(R(\mu))$-matching results compared with the usual $\ln(R)$-matching. The dependence on the renormalization scale μ is much reduced.

reduction of the scale dependence also in the two-jet region (Figure 4.4). However, in this scheme the scale dependence is very likely overcompensated. Some further studies in this sense could be made for the observable thrust, for which the full NNLLA term is now known [214]. The parton-level fixed order NNLO and matched NLLA+NLO and NLLA+NNLO predictions are compared to hadron-level data taken by the ALEPH experiment [1, 2] in Figure 4.3. The description of the hadron-level data improves between parton-level NLLA+NLO and parton-level NLLA+NNLO, especially in the three-jet region for most event shapes. The behaviour in the two-jet region is described better by the resummed predictions than by the fixed order NNLO, although the agreement is far from perfect. This discrepancy was observed already in earlier studies based on NLLA+NLO. It can in part be attributed to hadronisation corrections, which become large in the approach to the two-jet limit. The study of logarithmic corrections beyond NLLA for the thrust distribution [214] shows that subleading logarithms in the two-jet region can account for about half of this discrepancy. The NNLLA contribution matched with NNLO for thrust is shown in Figure 4.5.

A final remark concerns the distribution of the C-parameter. At values around $C \approx 0.75$ a clear peak is visible. This is a so-called *Sudakov shoulder* and is due to further large logarithms arising because of soft gluon divergences within the physical region. A detailed analysis of Sudakov shoulders can be found in [247].

4.6.3 A first study beyond NLLA

In this section we derive the NNLL resummation function $g_3(\alpha_s L)$ for thrust from the result obtained in SCET [214]. The starting point for a computation in SCET is the

following factorization formula for thrust in the 2-jet region

$$\frac{1}{\sigma_0}\frac{\mathrm{d}\sigma_2}{\mathrm{d}\tau} = H(Q^2,\mu)\int \mathrm{d}p_L^2\mathrm{d}p_R^2\mathrm{d}k J(p_L^2,\mu)J(p_R^2,\mu)S_T(k,\mu)\delta\left(\tau - \frac{p_L^2+p_R^2-kQ}{Q^2}\right), \tag{4.47}$$

where p_L^2 and p_R^2 are the invariant masses of the energetic particles in the left and in the right jet, Q is the CM energy of the collision, kQ is the increase of the invariant mass on the two sides due to soft emission and μ is an arbitrary renormalization scale. Evaluating the hard function $H(Q^2,\mu)$, the jet function $J(p_L^2,\mu)$ and the soft function $S_T(k,\mu)$ for thrust, the convolution integrals can be done analytically giving

$$\begin{aligned}\frac{1}{\sigma_0}\frac{\mathrm{d}\sigma_2}{\mathrm{d}\tau} =& \exp\left[4S(\mu_h,\mu_j)+4S(\mu_s,\mu_j)-2A_H(\mu_h,\mu_s)+4A_J(\mu_j,\mu_s)\right]\left(\frac{Q^2}{\mu_h^2}\right)^{-2A_\Gamma(\mu_h,\mu_j)}\\ &\times H(Q^2,\mu_h)\left[\tilde{j}\left(\ln\frac{\mu_s Q}{\mu_j}+\partial_\eta,\mu_j\right)\right]^2\tilde{s}_T\left(\partial_\eta,\mu_s\right)\frac{1}{\tau}\left(\frac{\tau Q}{\mu_s}\right)^\eta\frac{e^{-\gamma_E\eta}}{\Gamma(\eta)},\end{aligned} \tag{4.48}$$

with $\eta = 4A_\Gamma(\mu_j,\mu_s)$. The functions $S(\mu,\nu)$ and $A_i\left(\mu,\nu\right)$ $(i=\Gamma,H,J)$ are Sudakov exponents. The two functions $\tilde{j}(L,\mu)$ and $\tilde{s}(L,\mu)$ are the Laplace transforms of the jet and the soft function. They give the initial conditions of the renormalization group equation. For the explicit expressions of all these functions we refer to [214]. The dependence on the unphysical scale μ is disappeared in (4.48) and everything is expressed using three new different scales: the hard scale μ_h, the jet scale μ_j and the soft scale μ_s. The canonical relations between these scales and the physical scale Q can be read off formula (4.48) and are given by

$$\mu_H = Q \quad ; \quad \mu_j = \sqrt{\tau}Q \quad ; \quad \mu_s = \tau Q\,. \tag{4.49}$$

In order to be compared with the resummation formula (4.10), equation (4.48) must be integrated over the thrust distribution giving

$$\begin{aligned}R_2(\tau) =& \exp\left[4S(\mu_h,\mu_j)+4S(\mu_s,\mu_j)-2A_H(\mu_h,\mu_s)+4A_J(\mu_j,\mu_s)\right]\left(\frac{Q^2}{\mu_h^2}\right)^{-2A_\Gamma(\mu_h,\mu_j)}\\ &\times H(Q^2,\mu_h)\left[\tilde{j}\left(\ln\frac{\mu_s Q}{\mu_j}+\partial_\eta,\mu_j\right)\right]^2\tilde{s}_T\left(\partial_\eta,\mu_s\right)\left[\left(\frac{\tau Q}{\mu_s}\right)^\eta\frac{e^{-\gamma_E\eta}}{\Gamma(\eta+1)}\right].\end{aligned} \tag{4.50}$$

This is the starting point for the extraction of the resummation functions $g_i(\alpha_s L)$ for $i=1,2,3,(4)$. Although in principle it is possible to extract also the function $g_4(\alpha_s L)$, it contains contributions of the soft functions at two loops, which are known only numerically, and the 4-loop cusp anomalous dimension Γ_3, for which an approximation is used. Furthermore, for the purpose of matching thrust at NNLLA+NNLO in the

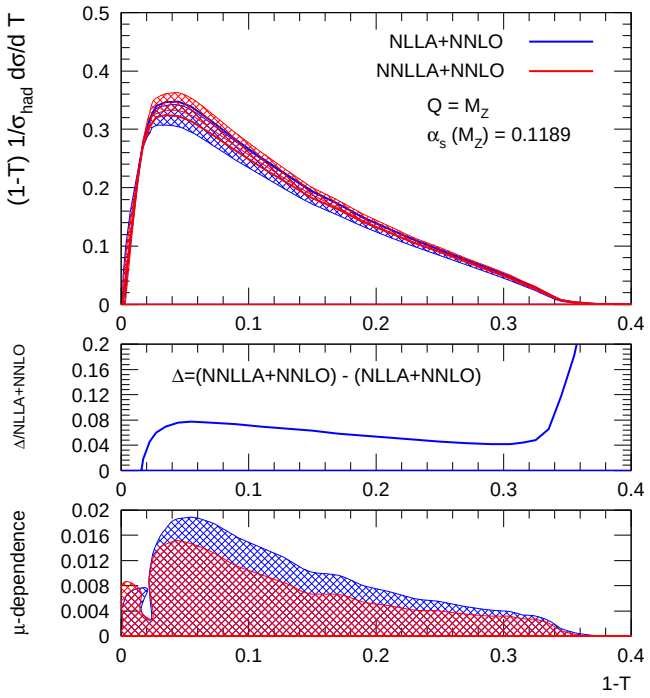

Figure 4.5: Matched NNLLA+NNLO distribution for thrust in the $\ln(R)$-matching scheme compared with the NLLA+NNLO distribution. The ratio of the difference between NNLLA+NNLO and NLLA+NNLO to the NLLA+NNLO distribution shows an increase of 5-8%.

$\ln(R)$-matching scheme, the knowledge of $g_3(\alpha_s L)$ is enough. For these reasons we limit here ourself to the extraction of the latter resummation function.

The first step is to fix the different scales present in (4.50) to their natural values according to (4.49). This simplifies the expression to

$$\begin{aligned} R_2(\tau) = &\exp\left[4S(Q,\sqrt{\tau}Q) + 4S(\tau Q,\sqrt{\tau}Q) - 2A_H(Q,\tau Q) + 4A_J(\sqrt{\tau}Q,\tau Q)\right] \\ &\times H(Q^2,Q)\left[\tilde{j}\left(\partial_\eta,\sqrt{\tau}Q\right)\right]^2 \tilde{s}_T\left(\partial_\eta,\tau Q\right)\left[\frac{e^{-\gamma_E\eta}}{\Gamma(\eta+1)}\right], \end{aligned} \tag{4.51}$$

where now $\eta = 4A_\Gamma(\sqrt{\tau}Q,\tau Q)$. In the second line of the last formula we recognize the kernel

$$\frac{e^{-\gamma_E\eta}}{\Gamma(\eta+1)}$$

also present in the traditional approach and defined as $\mathcal{F}(R')$ in the formulae of Appendix C. The LL and NLL resummation functions $g_1(\alpha_s L)$ and $g_2(\alpha_s L)$ can be found by setting the prefactors (the hard function $H(Q^2,Q)$ and the Laplace transforms $\tilde{j}$ and $\tilde{s}$ of the jet and soft functions) of this kernel to unity and considering only the appropriate logarithmic part of the exponential factor. These prefactors become important

only at NNLLA. In order to obtain $g_3(\alpha_s L)$ we have to consider also the derivatives contained in $\tilde{j}$ and $\tilde{s}$ applied to the kernel, up to $\mathcal{O}(\alpha_s)$. The hard function $H(Q^2, Q)$, being evaluated at two equal scales, does not contain any logarithms and is a pure constant which can be set to unity. By inserting the running relation of the strong coupling constant between two different scales, exponentiating the whole expression and expanding it in powers of the strong coupling constant evaluated at the hard scale Q we obtain the resummation formulae $g_1(\alpha_s L)$, $g_2(\alpha_s L)$ and $g_3(\alpha_s L)$. Having exponentiated also pieces of the constant part, $g_3(\alpha_s L)$ contains also terms of the order $\bar{\alpha}_s^2 L^0$. In order to ensure the correct normalization according to [200], we subtract by hand the constant part such that $g_3(0) = 0$. The resummation function $g_3(\alpha_s L)$ in the formalism of [200] is then given by

$$
\begin{aligned}
g_3(\lambda) = &-\frac{1}{2}(2c_1^J + c_1^S) - \frac{\Gamma_0\pi^2}{12} + \frac{1}{1-3\lambda+2\lambda^2}\Bigg[c_1^J + \frac{c_1^S}{2} - \frac{\gamma_E^2\Gamma_0}{2} - 2c_1^J\lambda - \frac{c_1^S\lambda}{2} - \frac{\Gamma_2\lambda^2}{32\beta_0^2} \\
&+ \frac{\beta_1\lambda}{\beta_0^2}\left(\gamma_0^H - \gamma_0^J - \gamma_0^H\lambda\right) - \frac{\lambda}{4\beta_0}\left(\gamma_1^H - \gamma_1^J - \gamma_1^H\lambda\right) + \frac{\beta_1\gamma_0^H}{2\beta_0^2}(1-\lambda)\ln(1-2\lambda) \\
&+ \frac{\beta_1\Gamma_1}{8\beta_0^3}\left(3\lambda^2 + (1-\lambda)\ln(1-2\lambda) - 2(1-2\lambda)\ln(1-\lambda)\right) \\
&- \frac{\beta_1\gamma_0^J}{\beta_0^2}\left((1-\lambda)\ln(1-2\lambda) - (1-2\lambda)\ln(1-\lambda)\right) \\
&+ \frac{\Gamma_0}{4\beta_0^4}\Big(-2(\beta_1^2+\beta_0\beta_2)\lambda^2 + 2(1-\lambda)(-\beta_0\beta_2 - 2\beta_1^2\lambda + 2\beta_0\beta_2\lambda)\ln(1-2\lambda) \\
&\qquad - \beta_1^2(1-\lambda)\ln(1-2\lambda)^2 + 4(1-2\lambda)(\beta_0\beta_2 + \beta_1^2\lambda - \beta_0\beta_2\lambda)\ln(1-\lambda) \\
&\qquad + 2\beta_1^2(1-2\lambda)\ln(1-\lambda)^2\Big) \\
&+ \gamma_E\Big(-\gamma_0^H + \gamma_0^J - \frac{\Gamma_1\lambda}{4\beta_0} + \gamma_0^H\lambda + \frac{\beta_1\Gamma_0}{\beta_0^2}(\lambda + (1-\lambda)\ln(1-2\lambda) - (1-2\lambda)\ln(1-\lambda))\Big) \\
&+ \Psi(0, 1+4R')\Big(-\gamma_E\Gamma_0 - \gamma_0^H + \gamma_0^J - \frac{\Gamma_1\lambda}{4\beta_0} + \gamma_0^H\lambda \\
&\qquad + \frac{\beta_1\Gamma_0}{\beta_0^2}(\lambda + (1-\lambda)\ln(1-2\lambda) - (1-2\lambda)\ln(1-\lambda))\Big) \\
&- \frac{\Gamma_0}{2}\Psi(0, 1+4R')^2 + \frac{\Gamma_0}{2}\Psi(1, 1+4R')\Bigg], \qquad (4.52)
\end{aligned}
$$

where the anomalous dimensions are given by

$$
\begin{aligned}
&\Gamma_0 = 4C_F\,, \qquad \Gamma_1 = 8C_F\,K\,, \qquad \Gamma_2 = 16C_F\,L\,, \\
&\gamma_0^H = -6C_F\,, \\
&\gamma_1^H = C_F^2\left(-3 + 4\pi^2 - 48\zeta_3\right) + C_F C_A\left(-\frac{961}{27} - \frac{11\pi^2}{3} + 52\zeta_3\right) + C_F N_F\left(\frac{130}{27} + \frac{2\pi^2}{3}\right),
\end{aligned}
$$

$$\gamma_0^J = -3C_F\,,$$
$$\gamma_1^J = C_F^2\left(-\frac{3}{2}+2\pi^2-24\zeta_3\right)+C_FC_A\left(-\frac{1769}{54}-\frac{11\pi^2}{9}+40\zeta_3\right)+C_FN_F\left(\frac{121}{27}+\frac{2\pi^2}{9}\right)\,,$$

where K and L are given in (5.21) and (5.22), and the constants c_1^J, c_1^S of the jet and soft functions are given by

$$c_1^J = C_F\left(7-\frac{2\pi^2}{3}\right)\,,$$
$$c_1^S = -C_F\pi^2\,.$$

Inserting the expression (4.52) for $g_3(\alpha_s L)$ in equation (4.25) for the $\ln(R)$-matching at NNLLA+NNLO we obtain the distribution shown in Figure 4.5. It is clearly visible that the next-to-next-to-leading logarithms contained in $g_3(\alpha_s L)$ still give an important contribution to the cross section. Apart from the far multi-jet region, the cross section increases of about 5-8% in the region of kinematical interest. The dependence on the renormalization scale decreases by up to 30%, however it is much larger then the renormalization scale dependence estimated by the $\ln(R(\mu))$-matching at NLLA+NNLO. In this regard it is important to note that the two dependencies differ because the matching schemes differ in the estimation of the renormalization scale uncertainty.

4.7 A new determination of α_s

The new matched NLLA+NNLO predictions allowed to perform a new fit of the strong coupling α_s [22]. However, since this analysis was not directly part of this thesis, but rather a consequence, we only briefly report its most important results.

The measurements we used have been carried out by the ALEPH collaboration [1, 2] at eight different centre-of-mass energies between 91.2 and 206 GeV. The event-shape distributions were obtained from the reconstructed momenta and energies of charged and neutral particles. The measurements have been corrected for detector effects, i.e. the final distributions correspond to the so-called particle (or hadron) level. In addition, at LEP2 energies above the Z peak they were corrected for initial-state radiation effects. At energies above 133 GeV, backgrounds from 4-fermion processes, mainly from W-pair production and also ZZ and Zγ^*, were subtracted following the procedure given in [2]. The experimental uncertainties were estimated by varying event and particle selection cuts. They are below 1% at LEP1 and slightly larger at LEP2.

The perturbative QCD prediction is corrected for hadronisation and resonance decays by means of a transition matrix, which is computed with the Monte Carlo generators PYTHIA [248], HERWIG [249] and ARIADNE [250], all tuned to global hadronic observables at M_Z [251]. The parton level is defined by the quarks and gluons present

at the end of the parton shower in PYTHIA and HERWIG and the partons resulting from the colour dipole radiation in ARIADNE. Corrected measurements of event-shape distributions are compared to the theoretical calculation at particle level. For a detailed description of the determination and treatment of experimental systematic uncertainties we refer to [2, 246].

The value of α_s is determined at each energy using a binned least-squares fit. The fit programs of [246] have been extended to incorporate the NNLO+NLLA calculations in the same way as they are implemented in `Lormeso`. Combining the results for six event-shape variables and eight LEP1/LEP2 centre-of-mass energies, we obtained

$$\alpha_s^{\mathrm{NLLA+NNLO}}(M_Z) = 0.1224 \pm 0.0009\,(\mathrm{stat}) \pm 0.0009\,(\mathrm{exp}) \pm 0.0012\,(\mathrm{had}) \pm 0.0035\,(\mathrm{theo})\ .$$

The fitted values of the coupling constant as found from event-shape variables calculated at various orders are shown in Figure 4.6.

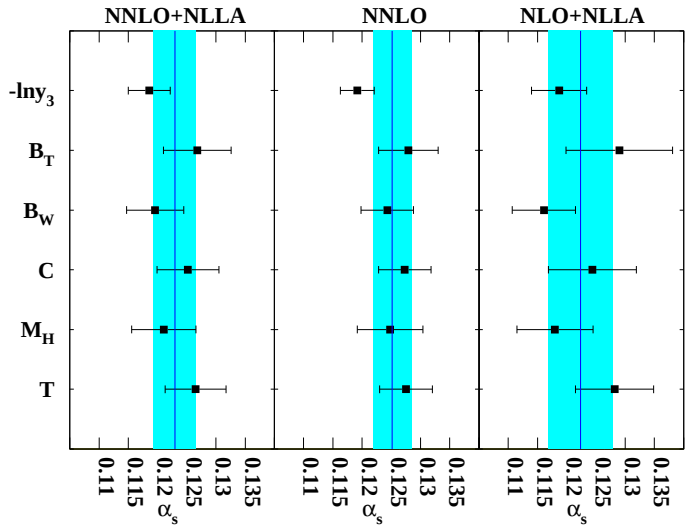

Figure 4.6: The measurements of the strong coupling constant α_s for the six event shapes, at $\sqrt{s} = M_Z$, when using QCD predictions at different approximations in perturbation theory. The shaded area corresponds to the total uncertainty.

Comparing these results to both the fit using purely fixed-order NNLO predictions [246] and the fits based on earlier NLLA+NLO calculations [2], we could make the following observations:

- The central value is slightly lower than the central value of 0.1228 obtained from fixed-order NNLO only, and slightly larger than the NLO+NLLA results. The fact that the central value is almost identical to the purely fixed-order NNLO

result could be anticipated from the findings in Ref. [201]. There it is shown that in the three-jet region, which provides the bulk of the fit range, the matched NLLA+NNLO prediction is very close to the fixed-order NNLO calculation.

- The dominant theoretical uncertainty on $\alpha_s(M_Z)$, as estimated from scale variations, is reduced by 20% compared to NLO+NLLA. However, compared to the fit based on purely fixed-order NNLO predictions, the perturbative uncertainty is *increased* in the NNLO+NLLA fit. The reason is that in the two-jet region the NLLA+NLO and NLLA+NNLO predictions agree by construction, because the matching suppresses any fixed order terms. Therefore, the renormalisation scale uncertainty is dominated by the next-to-leading-logarithmic approximation in this region, which results in a larger overall scale uncertainty in the α_s fit.

- As already observed for the fixed-order NNLO results, the scatter among the values of $\alpha_s(M_Z)$ extracted from the six different event-shape variables is substantially reduced compared to the NLO+NLLA case.

- Using the $\ln(R(\mu))$-matching scheme, a substantial reduction of the perturbative uncertainty from ± 0.0035 (obtained in the default $\ln R$-scheme) to ± 0.0022 is observed, which might indicate the size of the ultimately reachable precision for a complete NNLO+NNLLA calculation. Although both schemes are in principle on the same theoretical footing, it is the more conservative error estimate obtained in the $\ln R$-scheme which should be taken as the nominal value, since it measures the potential impact of the yet uncalculated finite NNLLA-terms. This is confirmed by the scale dependence observed in the matched NNLLA+NNLO results for thrust shown in Figure 4.5, which is largen then the scale dependence for NLLA+NNLO in the $\ln(R(\mu))$-matching.

- Bottom quark mass effects, which are numerically significant mainly at the LEP1 energy, were included through to NLO. Compared to a purely massless evaluation of the distributions, the inclusion of these mass effects enhances $\alpha_s(M_Z)$ by 0.8%.

On top of the α_s determination a detailed analysis of hadronization corrections was made. Apart from observing large discrepancies between the event simulation programs used at LEP [248–250] and more modern generators [252, 253], the most striking conclusion is that two "classes" of variables appear. The first class containing thrust, C-parameter and total jet broadening, the second class containing heavy jet mass, wide jet broadening and the two-to-three-jet transition parameter Y_3. Comparing parton level and hadron level predictions from PYTHIA, this first class of variables gives a parton level prediction which is about 10% higher than the NNLO+NLLA prediction, where the PYTHIA curve has been obtained with tuned parameters, the tuning to data being performed at the hadron level. This tuning results in a rather large effective

coupling in the parton shower, such that the parton level prediction of PYTHIA turns out large. This may imply that the hadronization corrections come out to be too small for these variables, resulting in a larger $\alpha_s(M_Z)$ value. We will provide further evidence for the underestimation of hadronization corrections by the legacy generators by analyzing non-perturbative power corrections for moments of event-shape variables in the next chapter.

4.8 Conclusions and outlook

This chapter was dedicated to the systematic study of the matching of fixed order and resummed calculations for event-shape variables in electron positron annihilation. The extension of the matching formalism from NLLA+NLO to include higher order corrections was needed after the recent publication of NNLO results for event shapes [141, 143, 210]. However we extended the formalism to include also higher order logarithmic corrections in the resummation, once they become available. For the moment resummation beyond NLLA was performed only for thrust, which is now known at $\mathrm{N^3LLA}$, using an effective field theory approach [214].

The matching procedure was done in the $\ln(R)$-matching scheme at NLLA+NNLO and results are given for all six event-shape observables τ, ρ, C-parameter, B_W, B_T and Y_3 [201]. In the three-jet region the new matched results agree in general much better with the fixed order NNLO predictions and resummation becomes important only in the two-jet region. The renormalization scale dependence in the three-jet region is also reduced by 20-40% with respect to the old NLLA+NLO predictions. However, in the two-jet region we do not see any improvement in the renormalization scale uncertainty. This can be expected since we have not improved the theoretical prediction on the resummation side.

Matching NLLA predictions with NNLO calculations leads to a mismatch in the cancelations of the renormalization scale dependence between fixed order and resummation. In order to study the effects of the two loop cancellation also in the resummed part, we have defined a slightly modified version of the matching scheme, which we called $\ln(R(\mu))$-matching scheme. In this new scheme we observe a substantial reduction of the renormalization scale dependence.

The matched results were also used for a new determination of the strong coupling constant α_s resulting in

$$\alpha_s^{\mathrm{NLLA+NNLO}}(M_Z) = 0.1224 \pm 0.0009\,(\mathrm{stat}) \pm 0.0009\,(\mathrm{exp}) \pm 0.0012\,(\mathrm{had}) \pm 0.0035\,(\mathrm{theo})\ .$$

In this case we observed a slightly lower value of α_s with respect to a similar analysis done with NNLO result only [246]. However the dominant theoretical uncertainty, due

to scale variation, is increased because of the inclusion of resummed NLLA calculations which suffer from a higher renormalization scale dependence.

Finally a detailed analysis of hadronization corrections with different Monte Carlo programs [22] led to the observation that the simulation programs used at LEP might underestimate the hadronization corrections in favor of a larger parton level prediction. This could partially explain the larger value obtained in fits of α_s using Monte Carlo hadronization corrections with respect to other determinations. An alternative example in given in the next chapter.

5

Non-Perturbative Corrections to Event-Shape Observables

Apart from being measured with great accuracy, event-shape variables provide a wealth of data at a variety of centre-of-mass energies. Exploiting this large energy range, one can attempt to disentangle perturbative and non-perturbative contributions (which scale differently with increasing energy) to event-shape observables. To do this, instead of studying the distributions like we did in the previous chapter, one can also study mean values and higher moments. In the following we will first introduce some very general ideas about non-perturbative corrections. In a second step we will apply them to the study of moments of event-shape variables at NNLO [254]. Using data from JADE [229, 255] and OPAL [219], we perform a simultaneous fit of the strong coupling constant α_s and of a non-perturbative parameter α_0. The results of this analysis, are published in [23].

5.1 Event-shape moments

The nth moment of an event-shape observable y is defined by

$$\langle y^n \rangle = \frac{1}{\sigma_{\text{had}}} \int_0^{y_{\max}} y^n \frac{\mathrm{d}\sigma}{\mathrm{d}y} \mathrm{d}y \,, \tag{5.1}$$

where $y_{\max}$ is the kinematically allowed upper limit of the observable.

The perturbative contribution to $\langle y^n \rangle$ is given up to NNLO in terms of the dimensionless coefficients $\mathcal{A}_{y,n}$, $\mathcal{B}_{y,n}$ and $\mathcal{C}_{y,n}$ as:

$$\begin{aligned} \langle y^n \rangle_{\text{pt}}(s,\mu^2) =& \bar{\alpha}_s \mathcal{A}_{y,n} + \bar{\alpha}_s^2 \left(\mathcal{B}_{y,n} + \mathcal{A}_{y,n} 2\beta_0 \ln \frac{\mu^2}{s} \right) \\ &+ \bar{\alpha}_s^3 \left(\mathcal{C}_{y,n} + 4\mathcal{B}_{y,n}\beta_0 \ln \frac{\mu^2}{s} + \mathcal{A}_{y,n} \left(4\beta_0^2 \ln^2 \frac{\mu^2}{s} + 4\beta_1 \ln \frac{\mu^2}{s} \right) \right) \\ &+ \mathcal{O}(\alpha_s^4) \,, \end{aligned} \tag{5.2}$$

where s denotes the centre-of-mass energy squared and μ is the QCD renormalisation scale. The NLO expression is obtained by suppressing all terms at order α_s^3. The first two coefficients of the QCD β-function are given in (2.23).

The perturbative coefficients in (5.2) are independent on the centre-of-mass energy. They are obtained by integrating the parton-level distributions at NNLO accuracy [141, 143, 210] considered in the previous chapter. The coefficients entering the event-shape moments are computed at a renormalisation scale fixed to the centre-of-mass energy, and are therefore just dimensionless numbers for each observable and each value of n. For this study the set of six event-shape variables introduced in Chapter 2 and analysed in Chapter 4 is considered. Their coefficients were computed up to NNLO in [254, 256].

Experimentally moments are measured by summing

$$\langle y^n \rangle_{\text{exp}} = \sum_{i=1}^{N} y_i^n \,, \tag{5.3}$$

where N is the number of events. They were measured for a variety of different event-shape variables and by several experiments, most extensively by JADE [229, 255] and OPAL [219], but also by DELPHI [225] and L3 [224]. A combined analysis of JADE and OPAL results has been performed in [257].

As the calculation of moments involves an integration over the full phase space, they offer a way of comparing to data which is complementary to the use of distributions, where in general cuts on certain kinematic regions are applied. Furthermore, the two extreme kinematic limits – two-jet-like events and multi-jet-like events – enter with different weights in each moment: the higher the order n of the moment, the more it becomes sensitive to the multi-jet region. Therefore it is particularly interesting to study the NNLO corrections to higher moments of event shapes, as these corrections should offer a better description of the multi-jet region due to the inclusion of additional radiation at parton level.

Moments are particularly attractive in view of studying non-perturbative hadronization corrections to event shapes. As briefly described in the previous chapter, one typically corrects for hadronization effects by using generic Monte Carlo event simulation programs. We also said, that in the context of the determination of the strong coupling constant using the matched NLLA+NNLO results for the distribution of event-shape variables [22], a study of hadronization revealed large discrepancies between the standard event simulation programs used at LEP [248–250] on one hand, and more modern generators [252, 253], which incorporate recent theoretical advances, on the other hand. In the event-shape distributions, it is very difficult to disentangle hadronization corrections empirically, since they typically result in a distortion of the distribution, which can not be unfolded in a straightforward manner.

In event-shape moments, one expects the hadronization corrections to be additive, such that they can be divided into a perturbative and a non-perturbative contribution,

$$\langle y^n \rangle = \langle y^n \rangle_{\mathrm{pt}} + \langle y^n \rangle_{\mathrm{np}} \,, \tag{5.4}$$

where the non-perturbative contribution accounts for hadronization effects. The non-perturbative part is suppressed by powers of λ_p/Q^p $(p \geq 1)$, where $Q \equiv \sqrt{s}$ is the centre-of-mass energy and λ_1 is of the order of Λ_{QCD}. The functional form of λ_p has been discussed quite extensively in the literature, but as this parameter is closely linked to non-perturbative effects, it cannot be fully derived from first principles.

5.2 Renormalons and power corrections

In order to understand the relation between power corrections and hadronization a short detour is needed. The origin of power corrections is related to renormalons[1].

In perturbative QFT an observable quantity P is computed as a power series in α

$$P(\alpha) = \sum_{n=0}^{\infty} p_n \alpha^{n+1} \,. \tag{5.5}$$

This series might be divergent. In this case the expansion (5.5) is a useful approximation of P if it is asymptotic inside a region $\mathcal{C}$ in the complex α-plane, i.e. if there exist numbers K_N such that

$$\left| P(\alpha) - \sum_{n=0}^{N} p_n \alpha^{n+1} \right| < K_{N+1} \alpha^{N+1}$$

for all α in $\mathcal{C}$ and the truncation error at the order N is uniformly bounded to be of order α^{N+1}.

However it is possible to define a more convergent series, called the *Borel transformation* given by

$$B[P](t) = \sum_{n=0}^{\infty} \frac{p_n}{n!} t^n \,. \tag{5.6}$$

If this last series converges we can define $\tilde{P}(\alpha)$ by

$$\tilde{P}(\alpha) = \int_0^{\infty} \mathrm{d}t \, e^{-\frac{t}{\alpha}} \, B[P](t) \,, \tag{5.7}$$

which has the same expansion as $P(\alpha)$, even if the original series is divergent. If $\tilde{P}(\alpha)$ exists, then the series $P(\alpha)$ is said to be *Borel summable* and $\tilde{P}(\alpha)$ is its Borel sum.

[1] A very nice review on renormalons can be found in [258].

QCD is probably not fully Borel summable, however there is some hope that at least an important subset of contributions is resummable [259].

Nevertheless, the importance of the Borel transformation is that the divergent behaviour of the original series is encoded in the singularities of its borel transformation. In fact a *renormalon* is a singularity in the complex plane of the Borel transform, related to large or small loop momentum behaviour in a renormalized theory. A toy example taken from [258] illustrates the relations between renormalons and power corrections.

Assume that the coefficients of the expansion (5.5) grow like

$$p_n \overset{n\to\infty}{\sim} K\, a^n\, n!\, n^b\,,$$

where K, a and b are constants. Then one often finds that also the numbers K_N go like $K_N \propto a^N\, N!\, N^b$ and thus the truncation error can be found as follows:

$$\begin{aligned} K_{N+1}\alpha^{N+1} &\propto a^{N+1}(N+1)!(N+1)^b\alpha^{N+1} \\ &\propto (a\alpha)^{N+1}(N+1)^{N+1}(N+1)^b\, e^{-N+1}\sqrt{2\pi(N+1)} \\ &\propto (a\alpha(N+1))^{N+1}\,, \end{aligned} \tag{5.8}$$

where we used $n! \approx (n/e)^n\sqrt{2\pi n}$. From the last line it follows that the series decreases until $a\,\alpha(N+1) \approx 1$ i.e. until $N = N_\star \approx 1/(|a|\alpha)$. After that the approximation of $P(\alpha)$ does not improve any more. This means that for $N_\star \gg 1$ the approximation is good up to terms of order

$$K_{N_\star}\alpha^{N_\star} \sim e^{-\frac{1}{|a|\alpha}}\,. \tag{5.9}$$

Now, assuming that

$$p_n = K\, a^n \Gamma(n+1+b)\,,$$

the Borel transform is given by

$$\begin{cases} \text{for } b>0: & B[P](t) = \sum_{n=0}^{\infty} K\, a^n \frac{\Gamma(n+1+b)}{\Gamma(n+1)} t^n = K\frac{\Gamma(1+b)}{(1-a\,t)^{b+1}} \\ \text{for } b<0\,(b=-m): & B[P](t) = \sum_{n=m}^{\infty} K\, a^n \frac{\Gamma(n+1-m)}{\Gamma(n+1)} t^n = K\frac{(a\,t)^n\, {}_2F_1(1,1,1+m;a\,t)}{\Gamma(m+1)} \end{cases}. \tag{5.10}$$

For $b<0$ and $a>0$, a typical situation to be expected in QED and QCD, the Borel transform $B[P](t)$ has singularities and $\tilde{P}(\alpha)$ is given by

$$\tilde{P}(\alpha) = \int_0^\infty \mathrm{d}t\, e^{-\frac{t}{\alpha}} K \frac{(a\,t)^m}{\Gamma(1+m)}\, {}_2F_1(1,1,1+m;a\,t)\,. \tag{5.11}$$

The integrand has a branch-cut along the real axis for $t > 1/a$, and $\tilde{P}(\alpha)$ can be found by moving the contour above or below the singularities. In this case an imaginary part results

$$\Im(\tilde{P}(\alpha)) = \mp\left(\frac{\pi\, K}{a}\right) e^{-\frac{1}{a\,\alpha}} \frac{1}{(a\,\alpha)^b}\,, \tag{5.12}$$

which has an ambiguity in the sign due to the choice of the contour. This ambiguity can be interpreted as an indication that exponentially small terms of the same form as (5.12) must be added explicitly to the series expansion, such that the ambiguities in defining the sum of the perturbative series cancel and an improved approximation to the exact function $P(\alpha)$ is obtained.

Therefore, applying this sketchily to QCD, where

$$\alpha_s(Q^2) = \frac{1}{\beta_0 \ln\left(\frac{Q^2}{\Lambda^2_{\text{QCD}}}\right)},$$

the addition of terms which cancels the ambiguities takes the form of power corrections

$$e^{-\frac{1}{a\,\alpha_s}} \propto \left(\frac{\Lambda^2_{\text{QCD}}}{Q^2}\right).$$

Coming back to event shapes one can therefore say that non-perturbative power corrections can be related to infrared renormalons in the perturbative QCD expansion for the event-shape variable[1]. The analysis of infrared renormalon ambiguities suggests power corrections of the form λ_p/Q^p, but cannot make unique predictions for λ_p: it is only the sum of perturbative and non-perturbative contributions in (5.4) that becomes well-defined [258]. Different ways to regularize the IR renormalon singularities have been worked out in the literature [268–273]. The most naïve one is to simply give a small mass μ to the gluon. However this violates the QCD Ward identities. To overcome this a dispersive model was developed [265] where the gluon acquires a "virtual mass" (gluon spectral function) via a dispersion relation [274]. This is equivalent to introduce an IR cutoff μ_I and to replace the strong coupling constant below the scale μ_I by an effective coupling such that the integral of the coupling below μ_I has a finite value [265, 267, 275, 276]

$$\frac{1}{\mu_I}\int_0^{\mu_I} dQ\, \alpha_{\text{eff}}(Q^2) = \alpha_0(\mu_I)\,. \tag{5.13}$$

5.3 Power corrections to event-shape moments

Applying the dispersive model for the strong coupling to event-shape variables leads to a shift in the distributions

$$\frac{\mathrm{d}\sigma}{\mathrm{d}y}(y) = \frac{\mathrm{d}\sigma_{\text{pt}}}{\mathrm{d}y}(y - a_y\, P)\,, \tag{5.14}$$

where the numerical factor a_y depends on the event shape and is listed in Table 5.1, while P is believed to be universal (universality breaking terms arise from hadron mass

[1] Several detailed studies where made on this subject [260–267].

effects [277] in the moments of ρ, an estimate on these effects can be obtained from general-purpose event generator programs, e.g. from PYTHIA [248]) and scales with the CM energy like μ_I/Q.

By inserting (5.14) into the definition of the moments, one obtains:

$$\langle y^n \rangle = \int_0^{y_{\max}} \mathrm{d}y y^n \frac{1}{\sigma_{\mathrm{had}}} \frac{\mathrm{d}\sigma}{\mathrm{d}y}(y) \tag{5.15}$$

$$= \int_{-a_y P}^{y_{\max}-a_y P} \mathrm{d}y (y + a_y P)^n \frac{1}{\sigma_{\mathrm{had}}} \frac{\mathrm{d}\sigma_{\mathrm{pt}}}{\mathrm{d}y}(y) \tag{5.16}$$

$$\approx \int_0^{y_{\max}} \mathrm{d}y (y + a_y P)^n \frac{1}{\sigma_{\mathrm{had}}} \frac{\mathrm{d}\sigma_{\mathrm{pt}}}{\mathrm{d}y}(y) \tag{5.17}$$

discarding the integration over the kinematically forbidden values of y. This leads to the the non-perturbative predictions for the moments of y:

$$\begin{aligned}
\langle y^1 \rangle &= \langle y^1 \rangle_{\mathrm{pt}} + a_y P, \\
\langle y^2 \rangle &= \langle y^2 \rangle_{\mathrm{pt}} + 2\langle y^1 \rangle_{\mathrm{pt}} (a_y P) + (a_y P)^2, \\
\langle y^3 \rangle &= \langle y^3 \rangle_{\mathrm{pt}} + 3\langle y^2 \rangle_{\mathrm{pt}} (a_y P) + 3\langle y^1 \rangle_{\mathrm{pt}} (a_y P)^2 + (a_y P)^3, \\
\langle y^4 \rangle &= \langle y^4 \rangle_{\mathrm{pt}} + 4\langle y^3 \rangle_{\mathrm{pt}} (a_y P) + 6\langle y^2 \rangle_{\mathrm{pt}} (a_y P)^2 + 4\langle y^1 \rangle_{\mathrm{pt}} (a_y P)^3 + (a_y P)^4, \\
\langle y^5 \rangle &= \langle y^5 \rangle_{\mathrm{pt}} + 5\langle y^4 \rangle_{\mathrm{pt}} (a_y P) + 10\langle y^3 \rangle_{\mathrm{pt}} (a_y P)^2 + 10\langle y^2 \rangle_{\mathrm{pt}} (a_y P)^3 + 5\langle y^1 \rangle_{\mathrm{pt}} (a_y P)^4 + (a_y P)^5
\end{aligned} \tag{5.18}$$

It should be noted that the multiplicative power correction in (5.17) is considered to be accurate to $1/Q$. For $n \geq 2$, the evaluation (5.18) yields also higher powers of P, which are formally of higher order in inverse powers of Q. Contributions with the same scaling behaviour could equally come from subleading power corrections in P. Compared to the terms above, these subleading power corrections would be weighted with higher perturbative moments, and are thus suppressed numerically.

5.4 Dispersive model extended to NNLO

Up to now, the dispersive model for power corrections to event shapes was used in connection with NLO calculations of the perturbative part. In this context, one obtains

event-shape observable	$1-T$	C	Y_3	ρ	B_T	B_W
a_y	2	3π	0	1	1	$\frac{1}{2}$

Table 5.1: The a_y coefficients of the non-perturbative event-shape moment prediction

the following, $1/Q$-dependent power correction [275]:

$$P = \frac{4C_F}{\pi^2} \cdot \mathcal{M} \cdot \left\{ \alpha_0 - \left[\alpha_s(\mu_R) + \frac{2\beta_0}{\pi} \alpha_s^2(\mu_R) \left(\ln \frac{\mu_R}{\mu_I} + 1 + \frac{K}{4\beta_0} \right) + \mathcal{O}(\alpha_s^3) \right] \right\} \times \frac{\mu_I}{Q} \tag{5.19}$$

with the Milan factor $\mathcal{M} = 1.49 \pm 20\%$, which is known at two loops. Its uncertainty [274] accounts for currently unknown corrections beyond this loop order. The term in square brackets amounts to the renormalon subtraction in the power corrections, expanded to NLO. The prediction of the dispersive model can be extended to match onto the NNLO perturbative prediction, and first steps in this direction were taken already in [278] for power corrections to the thrust distribution.

The perturbative ingredients to the dispersive model are the running of the coupling constant and the relation between the $\overline{\text{MS}}$-coupling and the effective coupling, whose definition [279] absorbs universal correction terms from the cusp anomalous dimension.

In the present context, we use the evolution of the coupling constant given in (2.22) to two loops. Moreover, the relation between $\overline{\text{MS}}$-coupling and effective coupling reads

$$\alpha_s^{\text{eff}} = \alpha_s \left[1 + K \frac{\alpha_s}{2\pi} + L \left(\frac{\alpha_s}{2\pi} \right)^2 + \mathcal{O}(\alpha_s^3) \right] \tag{5.20}$$

$$K = \left(\frac{67}{18} - \frac{\pi^2}{6} \right) C_A - \frac{5}{9} N_F, \tag{5.21}$$

$$\begin{aligned} L = {} & C_A^2 \left(\frac{245}{24} - \frac{67}{9}\frac{\pi^2}{6} + \frac{11}{6}\zeta_3 + \frac{11}{5}\left(\frac{\pi^2}{6}\right)^2 \right) + C_F N_F \left(-\frac{55}{24} + 2\zeta_3 \right) + \\ & C_A N_F \left(-\frac{209}{108} + \frac{10}{9}\frac{\pi^2}{6} - \frac{7}{3}\zeta_3 \right) + N_F^2 \left(-\frac{1}{27} \right) . \end{aligned} \tag{5.22}$$

The coefficient L is obtained from the three-loop cusp anomalous dimension [37–39, 280], which can be extracted from the three-loop corrections to the partonic splitting functions [72] or to the quark and gluon form factors [281, 282].

The derivation of a generic power correction starts from considering a dimensionless quantity

$$F = \int_0^Q \mathrm{d}\mu f(\mu) \tag{5.23}$$

with

$$f(\mu) \propto a_F \alpha_s(\mu) \frac{\mu^p}{Q^{p+1}} \tag{5.24}$$

assuming F to be dimensionless. The value of p determines the scaling behaviour of the power correction, with $p = 0$ for the leading power correction to event-shape variables.

The dispersive model assumes that in the non-perturbative range of (5.23) the perturbative strong coupling $\alpha_s(\mu)$ is replaced by an effective coupling that remains

finite for all μ values. One defines then the value of the integral over this region by

$$\int_0^{\mu_I} \mathrm{d}\mu\, \alpha_{s,\mathrm{IR}}(\mu)\, \frac{\mu^p}{Q^{p+1}} \equiv \frac{\mu_I^{p+1}}{Q^{p+1}(p+1)} \alpha_p(\mu_I) \tag{5.25}$$

introducing an infrared matching scale $\mu_I, \Lambda_{\mathrm{QCD}} \ll \mu_I \ll Q$ and α_p as a non-perturbative parameter. One has then to subtract the perturbative part of (5.23) in the range from 0 to μ_I from the whole integral, that is, the value of (5.25) with $\alpha_{s,\mathrm{IR}}$ replaced by α_s.

This perturbative contribution to (5.23) thus acquires a dependence on the renormalisation scale μ_R used in the strong coupling constant. By requiring F to be scale-independent, one can then infer logarithmic terms in the non-perturbative contribution to (5.23). Applied to the event-shape power correction P (with $p = 0$), this results in

$$\begin{aligned} P = \frac{4C_F}{\pi^2}\,\mathcal{M}\Bigg\{ \alpha_0 - \Bigg[\alpha_s(\mu_R) + \frac{2\beta_0}{\pi}\left(1 + \ln\left(\frac{\mu_R}{\mu_I}\right) + \frac{K}{4\beta_0}\right)\alpha_s^2(\mu_R) + \\ \left(8\beta_1\left(1 + \ln\left(\frac{\mu_R}{\mu_I}\right) + \frac{L}{8\beta_1}\right) + 32\beta_0^2\left(1 + \ln\left(\frac{\mu_R}{\mu_I}\right) + \frac{K}{4\beta_0}\right)\right. \\ \left. + 16\beta_0^2 \ln\left(\frac{\mu_R}{\mu_I}\right)\left(\ln\left(\frac{\mu_R}{\mu_I}\right) + \frac{K}{2\beta_0}\right)\right)\frac{\alpha_s^3(\mu_R)}{4\pi^2}\Bigg]\Bigg\} \times \frac{\mu_I}{Q}. \end{aligned} \tag{5.26}$$

Together with (5.2) this gives the full expression for the event-shape observable moments, including perturbative and non-perturbative contributions.

For B_T and B_W there is a further correction to (5.26). It arises from the kinematical mismatch between parton direction and thrust direction used to define the hemispheres used in the broadening variables. Retaining (5.18), this modification can be accounted for by a modification to the power correction. In [276], this modification was computed to NLO for the first moment as

$$P_{\langle B_W\rangle} = P\left(\frac{\pi}{\sqrt{8C_F\hat{\alpha}_s\left(1 + \frac{K\hat{\alpha}_s}{2\pi}\right)}} + \frac{3}{4} - \frac{\beta_0}{3C_F} + \eta_0\right), \tag{5.27}$$

$$P_{\langle B_T\rangle} = P\left(\frac{\pi}{\sqrt{4C_F\hat{\alpha}_s\left(1 + \frac{K\hat{\alpha}_s}{2\pi}\right)}} + \frac{3}{4} - \frac{2\beta_0}{3C_F} + \eta_0\right) \tag{5.28}$$

with $\hat{\alpha}_s(Q) = \alpha_s(e^{-\frac{3}{4}}Q)$ and $\eta_0 = -0.6137$. Corrections to higher moments have not been derived up to now, and we assume that they can be approximated by using the above modifications to the power correction in all moments. The full NNLO expression for these has not been calculated either. The potentially dominant NNLO terms can

however be approximated by including the effective coupling to this order, resulting in

$$P_{\langle B_W\rangle} = P\left(\frac{\pi}{\sqrt{8C_F\hat{\alpha}_s\left(1+\frac{K\hat{\alpha}_s}{2\pi}+\frac{L\hat{\alpha}_s^2}{4\pi^2}\right)}}+\frac{3}{4}-\frac{\beta_0}{3C_F}+\eta_0\right), \tag{5.29}$$

$$P_{\langle B_T\rangle} = P\left(\frac{\pi}{\sqrt{4C_F\hat{\alpha}_s\left(1+\frac{K\hat{\alpha}_s}{2\pi}+\frac{L\hat{\alpha}_s^2}{4\pi^2}\right)}}+\frac{3}{4}-\frac{2\beta_0}{3C_F}+\eta_0\right). \tag{5.30}$$

However, further NNLO corrections to this expression will reside in the coefficient η_0. Therefore, we will treat B_W and B_T separately from the other variables in the numerical studies in the following section.

5.5 Analysis of JADE and OPAL data

The theoretical expressions for event shapes derived in the previous section contain two parameters: the strong coupling constant $\alpha_s(M_Z)$ and the non-perturbative coupling parameter α_0. Using experimental data on event-shape moments, it is possible to fit these parameters. The data from the JADE and OPAL experiments [255] consists of 18 points at centre-of-mass energies between 14.0 and 206.6 GeV for the first five moments of T, C, Y_3, M_H, B_W and B_T, and have been taken from [283]. For each moment the NLO as well as the NNLO prediction was fitted with $\alpha_s(M_Z)$ and α_0 as fit parameters, except for the moments of Y_3, which have no leading $(1/Q)$ power correction and thus are independent of α_0. For the heavy jet mass, we use only the even moments $\langle M_H^2\rangle$ and $\langle M_H^4\rangle$, since the theoretical prediction is in terms of $\rho = M_H^2/s$.

5.5.1 Fits

The fits were done using the program ROOT [243] and its χ^2 fit method. The errors used for the fit were the total errors, composed of the experimental statistic and systematic errors, added in quadrature. Based on these, ROOT returned errors on the fit which are displayed in Tables D.1-D.12 in Appendix D together with the fit results. For T and C the NNLO values of $\alpha_s(M_Z)$ and α_0 seem to be more stable throughout the moments, as at NNLO they increase less towards higher moments than at NLO. For Y_3 and ρ, where the values decrease at higher moments, this is not the case. These moments show $\alpha_s(M_Z)$ results which are significantly lower at NNLO than at NLO. The $\alpha_s(M_Z)$ values of B_W are much lower than the ones of the other observables, and do not change much from NLO to NNLO. For B_T the $\alpha_s(M_Z)$ values at NNLO are

lower than at NLO. Both are exceptionally stable throughout the different moments. The α_0 values of all moments are higher at NNLO than at NLO.

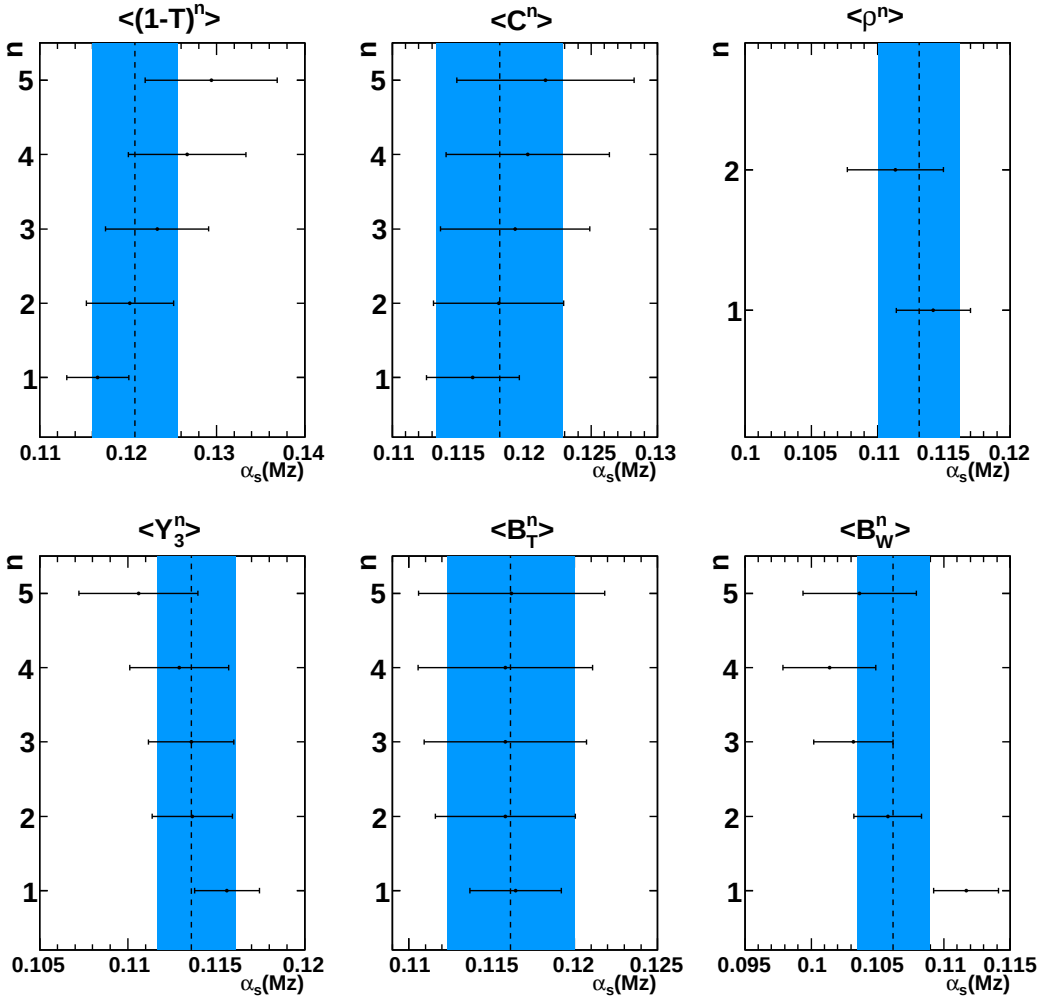

Figure 5.1: Plot of the individual measurements for $\alpha_s(M_Z)$. The shaded region corresponds to the error band defined by the weighted mean for the event shape and the total error on it.

5.5.2 Theoretical systematic errors

There are different parameters in the theoretical prediction which may influence the results displayed above, namely the matching scale μ_I, the renormalisation scale μ_R and the Milan factor $\mathcal{M}$. In order to estimate the resulting theoretical uncertainty on $\alpha_s(M_Z)$ and α_0, the fits were repeated, μ_I, μ_R and $\mathcal{M}$ being separately varied by the amount shown in Table 5.2.

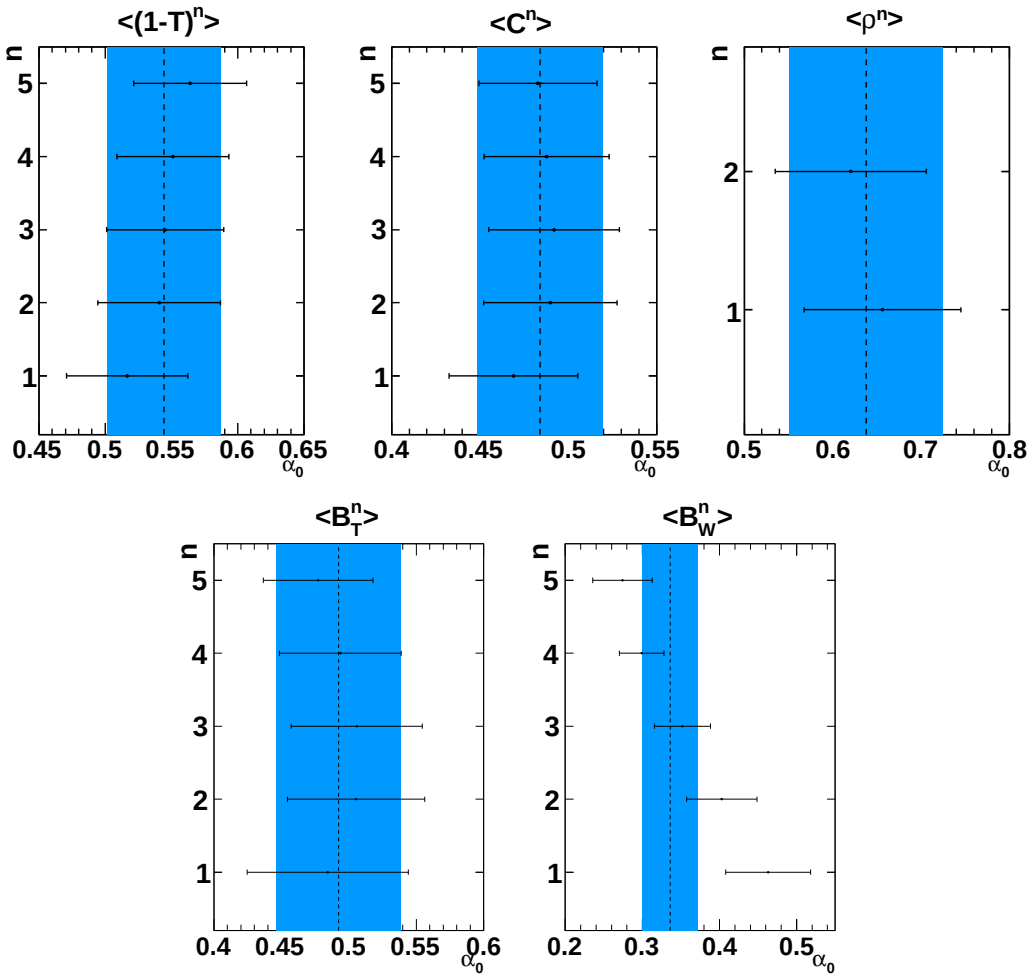

Figure 5.2: Error band plot of the individual measurements for α_0

For this purpose the scaling factor $x_\mu = \frac{\mu_R}{Q}$ was introduced. The uncertainty on the corresponding parameter was then taken to be the difference between the nominal and the new value returned by ROOT. In order to get a total systematic error, the greater values of the up and down uncertainties were determined and quadratically added. As α_0 depends directly on μ_I no error was determined for this variation. For Y_3 there is only an error on $\alpha_s(M_Z)$ coming from the x_μ variation, since the theoretical description of this observable does not contain a contribution from the leading power correction, and is thus independent on μ_I and $\mathcal{M}$. At NLO the fit to the moment $\langle C^3 \rangle$ suffers from a numerical instability by scaling up $\mathcal{M}$ by 20%. The numbers reported in Table D.3 refer to an up variation of 19%.

The NLO error on $\alpha_s(M_Z)$ agrees well with the values of [255]. At NNLO, it is reduced by more than half throughout all event-shape observables except B_W, confirm-

	nominal value	up variation	down variation
μ_I[GeV]	2	3	1
x_μ	1	2	0.5
$\mathcal{M}$	1.49	1.788 (+20%)	1.192 (-20%)

Table 5.2: Table of the μ_I, x_μ and $\mathcal{M}$ variations

ing a good description by the NNLO prediction. Unfortunately, this is not the case for the error on α_0. It does not change much from NLO to NNLO, even increasing a little in the first moments due to the higher x_μ uncertainty at NNLO and decreasing slightly at the higher moments, with exception, again, of B_W. Analyzing the different sources of the systematical errors, we observe that the error on $\alpha_s(M_Z)$ is clearly dominated by the x_μ variation, while the largest contribution to the error on α_0 comes from the uncertainty on the Milan factor $\mathcal{M}$. Since this uncertainty has not been improved in the current study, it is understandable that the systematic error on α_0 remains unchanged. This finding clearly motivates the need for a three-loop calculation of the Milan factor. However, it is very important to note that the uncertainty on the Milan factor has little impact on the extraction of $\alpha_s(M_Z)$, thereby demonstrating the systematic decoupling of perturbative and non-perturbative effects in the dispersive model.

For the higher moments ($n \geq 2$) of the jet broadenings B_W and B_T, the kinematical modifications to the power correction are not known at present. We have approximated them in the above fits by the corrections to the first moments, given to NLO and NNLO in the previous section. If we do not apply these correction to the higher moments, the mutual consistency of the parameter extractions from different moments of B_T deteriorates considerably, while only minor improvements in consistency are observed on B_W.

Including empirical hadron mass corrections [277, 284] from PYTHIA affects in particular the parameter extraction from ρ, resulting in values of $\alpha_s(M_Z)$ and α_0 from ρ much lower than from the other variables. Since these corrections may interplay with other non-perturbative parameters in PYTHIA, we do not include them in our default fits or error estimates.

By taking the weighted means over the corresponding values from all moments of all observables one gets combined values for $\alpha_s(M_Z)$ and α_0. The weights are given by the inverse of the total error squared and are normalized such that the sum over all weights is equal to one. For the errors one has to take care of the correlation between the errors of the single measurements. The correlation matrix for $\alpha_s(M_Z)$ and α_0 is in first approximation equal to the correlation matrix for the event-shape moments, since the variable transformation is linear in first approximation. The correlation matrix for the event-shape moments is given in [283]. We first combine the measurements from

NNLO				
Observable	$\alpha_s(M_Z)$	Experimental Error	Theoretical Error	Total Error
τ	0.1208	0.0018	0.0045	0.0048
C	0.1181	0.0013	0.0046	0.0048
ρ	0.1131	0.0024	0.0019	0.0031
Y_3	0.1139	0.0016	0.0015	0.0022
B_T	0.1161	0.0014	0.0036	0.0038
B_W	0.1062	0.0021	0.0018	0.0027
Total	0.1131	0.0017	0.0022	0.0028
Total w/o B_T,B_W	0.1153	0.0017	0.0023	0.0028
Observable	α_0	Experimental Error	Theoretical Error	Total Error
τ	0.5444	0.0184	0.0388	0.0430
C	0.4841	0.0066	0.0347	0.0353
ρ	0.6380	0.0270	0.0824	0.0867
Y_3	-	-	-	-
B_T	0.4924	0.0102	0.0449	0.0460
B_W	0.3362	0.0125	0.0338	0.0360
Total	0.4604	0.0108	0.0359	0.0375
Total w/o B_T,B_W	0.5132	0.0115	0.0381	0.0398

Table 5.3: Table of the $\alpha_s(M_Z)$ and α_0 results for the individual moments and the global weighted average.

different moments of the same observable. Figures 5.1 and 5.2 compare the combined NNLO results on the $\alpha_s(M_Z)$ and α_0 measurements. Owing to the large correlation between individual moments of the same observable, the combined errors are only marginally smaller than the errors obtained from single measurements. The combined results and their errors are summarized in Table 5.3. From this Table, we clearly observe that the theoretical error on the extraction of $\alpha_s(M_Z)$ from ρ, Y_3 and B_W is considerably smaller than from τ, C and B_T. It was observed previously in [254] that the moments of the former three shape variables receive moderate NNLO corrections for all n, while the NNLO corrections for the latter three are large already for $n = 1$ and increase with n. Consequently, the theoretical description of the moments of ρ, Y_3 and B_W displays a higher perturbative stability, which is reflected in the theoretical uncertainty on $\alpha_S(M_Z)$ derived from them.

In a second step, we combine the $\alpha_s(M_Z)$ and α_0 measurements obtained from different event-shape variables. Taking the weighted mean over all values, but excluding the values for the moments of B_W and B_T where the theoretical description is incomplete, we obtain at NNLO:

$$\alpha_s^{\mathrm{NNLO+NPPC}}(M_Z) = 0.1153 \pm 0.0017\,(\mathrm{exp}) \pm 0.0023\,(\mathrm{theo}), \tag{5.31}$$

$$\alpha_0^{\mathrm{NNLO}} = 0.5132 \pm 0.0115\,(\mathrm{exp}) \pm 0.0381\,(\mathrm{theo})\,. \tag{5.32}$$

where the errors have been derived taking into account the correlation between the moments of different event shapes. Including the values for B_W and B_T modifies this result to:

$$\begin{aligned}\alpha_s^{\mathrm{NNLO+NPPC,B}}(M_Z) &= 0.1131 \pm 0.0017\,(\mathrm{exp}) \pm 0.0022\,(\mathrm{theo}),\\ \alpha_0^{\mathrm{NNLO,B}} &= 0.4604 \pm 0.0108\,(\mathrm{exp}) \pm 0.0359\,(\mathrm{theo})\,.\end{aligned}$$

These latter values are however quoted only to illustrate the impact of including the broadenings. The default fit result is (5.32), where only observables with a consistent theoretical description are included.

To illustrate the improvement due to the inclusion of the NNLO corrections, we also quote the corresponding NLO results. Based on τ, C, ρ and Y_3, we obtain:

$$\begin{aligned}\alpha_s^{\mathrm{NLO+NPPC}}(M_Z) &= 0.1200 \pm 0.0021\,(\mathrm{exp}) \pm 0.0062\,(\mathrm{theo}),\\ \alpha_0^{\mathrm{NLO}} &= 0.4957 \pm 0.0118\,(\mathrm{exp}) \pm 0.0393\,(\mathrm{theo})\,,\end{aligned}$$

while inclusion of B_W and B_T modifies this to

$$\begin{aligned}\alpha_s^{\mathrm{NLO+NPPC,B}}(M_Z) &= 0.1147 \pm 0.0020\,(\mathrm{exp}) \pm 0.0046\,(\mathrm{theo}),\\ \alpha_0^{\mathrm{NLO,B}} &= 0.4019 \pm 0.0130\,(\mathrm{exp}) \pm 0.0296\,(\mathrm{theo})\,,\end{aligned}$$

We compare the NLO and NNLO combinations in Figure 5.3. It can be seen very clearly that the measurements obtained from the different variables are consistent with each other within errors. The average of $\alpha_s(M_Z)$ is dominated by the measurements based on ρ and Y_3, which have the smallest theoretical uncertainties. From NLO to NNLO, the error on $\alpha_s(M_Z)$ is reduced by a factor two, and the result shifts towards the lower end of the NLO error band, as was already the case in the individual measurements. No improvement and no shift in the central value between NLO and NNLO is seen on α_0.

5.6 Comparison with PYTHIA hadronization corrections

The primary motivation for studying power corrections to moments of event shapes in the dispersive model comes from the observation that, as already anticipated, the commonly used method to derive hadronization corrections from multi-purpose event generator programs may be unreliable, as [22].

To quantify the difference of both approaches to hadronization corrections, we compare them on the example of the moments of $1 - T$. For this comparison, we extracted the PYTHIA [248] hadronization corrections to these moments from the ratio of

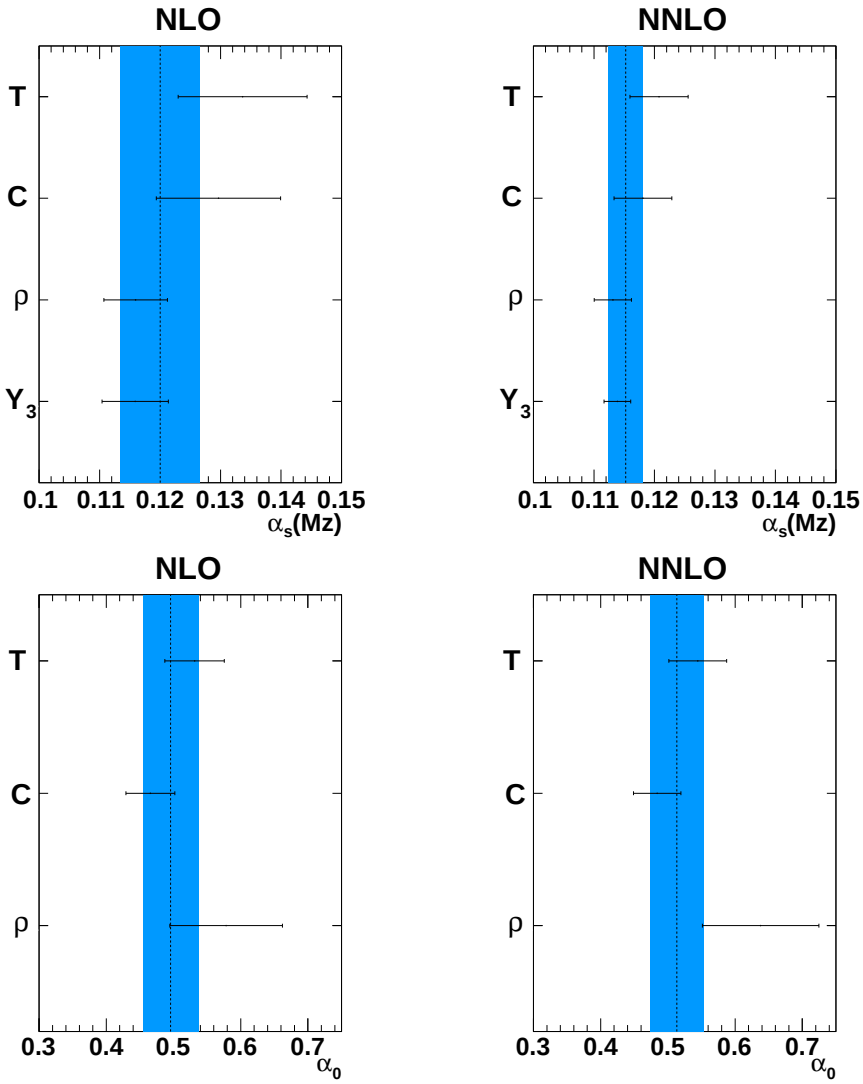

Figure 5.3: Error band plot of the final results. The points for $\alpha_s(M_Z)$ are C, T, Y_3, M_H and for α_0 C, T, M_H.

PYTHIA hadron level and parton level results. Using these corrections in combination with the NNLO perturbative expressions for the event-shape moments, we repeated the fit of $\alpha_s(M_Z)$ on the different moments of $1-T$. The results are displayed and compared with the fits in the dispersive model in Figure 5.4. We observe that both approaches yield a reasonable description of the experimental data, but that the resulting values of $\alpha_s(M_Z)$ are considerably larger when applying hadronization corrections extracted from PYTHIA. Given that the perturbative contribution increases monotonously with $\alpha_s(M_Z)$, this indicates that the hadronization corrections in PYTHIA are considerably

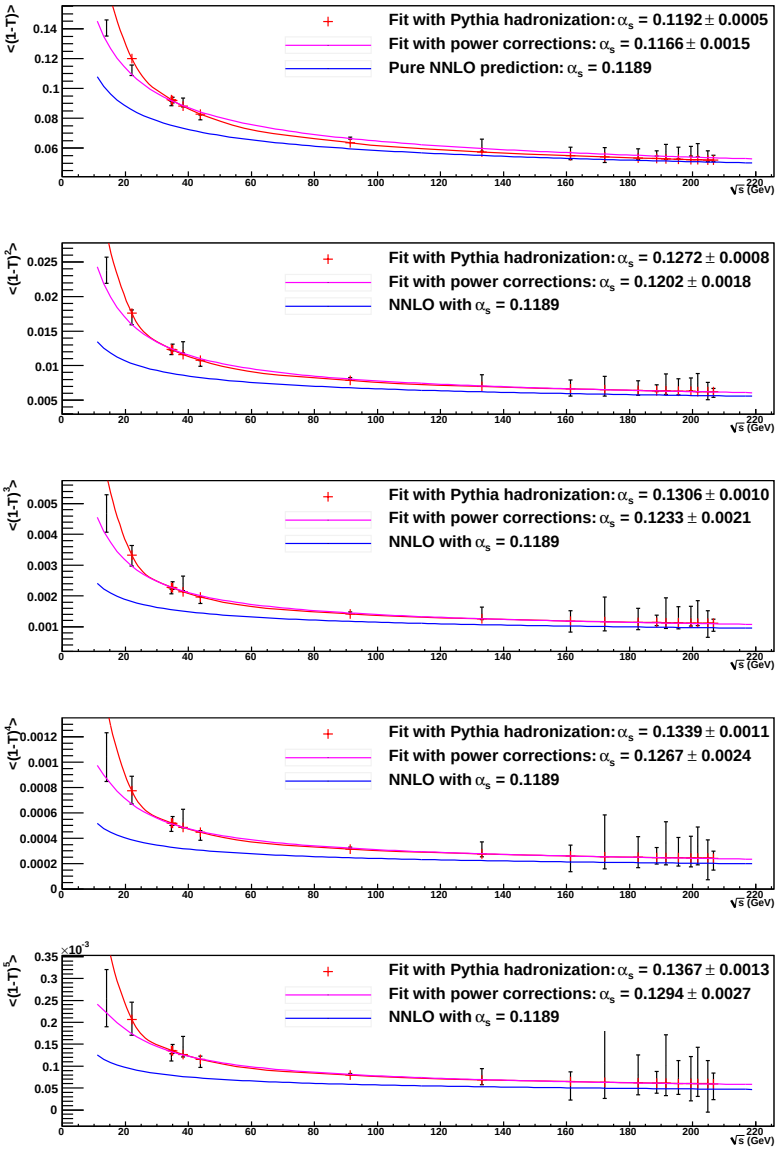

Figure 5.4: Comparison of fits with hadronization corrections from PYTHIA and power corrections from the dispersive model.

smaller (and perhaps underestimated) than those obtained in the dispersive model.

This observation is quantified on the moments of $(1-T)$ at $\sqrt{s} = M_Z$, displayed in Figure 5.5. Depending on the moment number, we observe that the PYTHIA hadronization corrections are between two and four times smaller than those obtained from the dispersive model. It can also be seen that the PYTHIA-based predictions are systematically below the experimental data, which perhaps indicates that, despite the

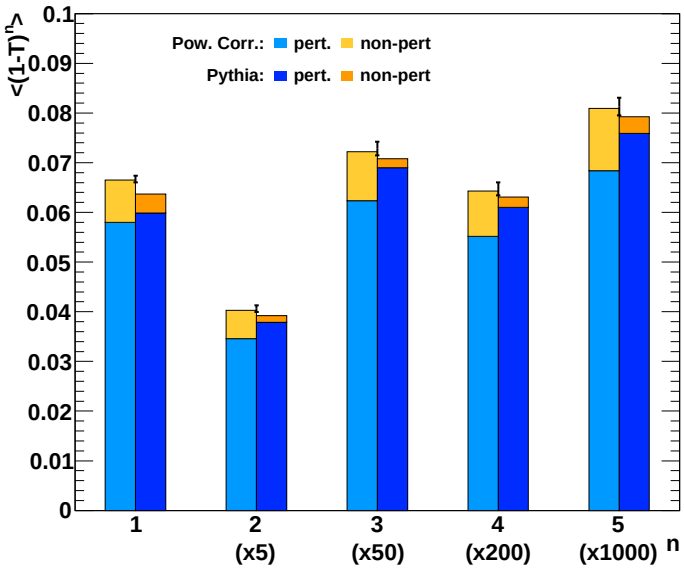

Figure 5.5: Perturbative and non-perturbative contributions to the moments of $1-T$ at $\sqrt{s} = M_Z$ as predicted by power corrections (left) and PYTHIA (right).

decent agreement on the full range of energies, Figure 5.4, PYTHIA fails in the precise description of the energy dependence of the hadronization corrections.

Our comparison suggests strongly that hadronization corrections extracted from PYTHIA (or from other comparable multi-purpose event generator programs [249, 250]) are lower than power corrections obtained from analytical hadronization models. This can be partially understood from the fact that perturbative predictions of PYTHIA are larger than fixed order calculations since they are based on a parton-shower approximation to the all order resummation result, which is known to shift the distribution away from the two jet singularity. As a consequence, using PYTHIA hadronization corrections to analyse data in view of precision extractions of $\alpha_s(M_Z)$ may result in anomalously large values, since the missing numerical magnitude of the power corrections must be compensated by a larger perturbative contribution.

5.7 Conclusions

In this chapter we presented a study on the perturbative and non-perturbative contributions to the moments of event shapes in e^+e^--annihilation [23]. In view of the recently calculated NNLO perturbative contributions [254, 256] to the event-shape moments, we extended the dispersive model for non-perturbative power corrections [265, 267, 275] to include all logarithmic corrections to this order. The normalization of the power

correction (the Milan factor [275]) is however still restricted to NLO accuracy, and specific corrections [276] to the jet broadenings B_W and B_T are also only included to NLO.

We used this newly obtained theoretical description of the event-shape moments to reanalyse data from JADE and OPAL in view of a determination of the strong coupling constant $\alpha_s(M_Z)$ and of the non-perturbative parameter α_0. We observed that inclusion of the NNLO corrections results in a considerably better consistency among the values extracted from different moments of the same variable, and an improved consistency among the different variables. Averaging over the different moments and different shapes (excluding B_W and B_T, where the theoretical description is incomplete, and taking proper account of the uncertainty due to missing terms in the Milan factor), we obtain the following combined values:

$$\begin{aligned} \alpha_s^{\mathrm{NNLO+NPPC}}(M_Z) &= 0.1153 \pm 0.0017\,(\mathrm{fit}) \pm 0.0023\,(\mathrm{th}), \\ \alpha_0^{\mathrm{NNLO}} &= 0.5132 \pm 0.0115\,(\mathrm{fit}) \pm 0.0381\,(\mathrm{th})\,, \end{aligned}$$

Compared to previous NLO results, the theoretical error on $\alpha_s(M_Z)$ (which is dominated by the scale variation, improved at NNLO) is reduced by a factor of two, while the error on α_0 (which is dominated by the uncertainty on the Milan factor) remains unchanged. We observed that the sources of uncertainty on $\alpha_s(M_Z)$ and α_0 largely decouple. An improvement on α_0 will only be achievable once the three-loop corrections to the Milan factor become available.

It is noteworthy that application of the dispersive model to hadronization corrections results in a considerably lower value of $\alpha_s(M_Z)$ from event shapes than pervious studies based on Monte Carlo hadronization models [22], and in better agreement with measurements from other observables [285]. A direct comparison hints to an underestimation of hadronization effects in the Monte Carlo models. This feature has been observed previously also on the thrust distribution [278]. Revisiting the hadronization models in multi-purpose Monte Carlo programs appears to be mandatory for meaningful precision QCD studies at colliders.

6

Conclusions

The main topic of this thesis are jet observables. The state-of-the-art of higher order corrections to jet observables are NLO calculations. For very few observables NNLO calculations are also available. The computation of corrections beyond NLO is in many cases far too involved to be made completely during the time of a PhD thesis. However, such a long computation is composed of several smaller steps.

During my PhD I had the opportunity to have a deeper look into several different steps of such higher order calculations. Considering a scattering experiment of two particles (Figure 6.1), for example electron-positron annihilation, several different things happen between the initial collision and the final state particles observed in the detector.

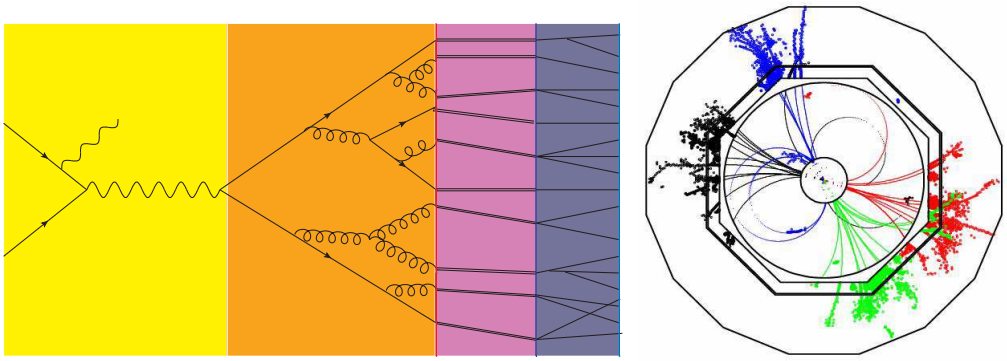

Figure 6.1: A schematic picture of an electron-positron annihilation process (left), and the resulting final state as it is seen in a real detector (right).

Following the colours of Figure 6.1 we have an initial hard collision, which is a QED process in this case (yellow). The hard final state, deriving from the decay of a virtual photon, consists initially of a very energetic quark-antiquark pair which can radiate gluons or exchange virtual gluons. This part of the process is well described by

perturbative QCD. As the quark and antiquark fly apart in different directions, each parton radiates gluons which become softer and softer. To first approximation the two primary jets do not interact with each other anymore. However, following the rules of quantum mechanics, very soft gluons still manage to transfer colour information from one jet to the other and, when considering higher orders, this effect has to be taken into account. This part of the process corresponds to the orange part in Figure 6.1. When the energy of the partons becomes of the order of $\Lambda_{\rm QCD}$ the partons condensate to form colour singlet states: this is hadronization. Hadrons can fly a certain distance (violet) before they decay in lighter and more stable hadrons which can finally be seen in experimental detectors (blue).

In order to reach high precision predictions, all the different parts of the process must be described with enough high accuracy. In my thesis I had the great opportunity of working on the improvement of the theoretical computation at several different stages.

An improved description of the hard process is possible by computing higher order corrections in perturbation theory. In this sense, the extension of the antenna subtraction formalism described in Chapter 3 will allow to construct a parton-level event generator program for the calculation of NNLO corrections to jet-production observables in deeply inelastic electron-proton scattering. Particulary important in this context is the dijet production cross section in DIS [177–182], which has been used at HERA to measure the gluon distribution in the proton and the strong coupling constant α_s. As already mentioned in the conclusions of Chapter 3, the dominating uncertainties in these determinations are due to theoretical scale uncertainties of the NLO calculations [167–172]. However initial-final antennae cannot be used only for processes with one hadronic initial state. Together with initial-initial antennae [74, 199], they are needed also for the computation of cross sections with two hadronic initial states. Initial-initial antennae at NLO are known since some time [74], and the NNLO calculations are in progress [199]. With the complete set of NNLO antennae (final-final, initial-final and initial-initial) some very important cross sections for the LHC can be computed at NNLO precision: the cross section for vector boson production plus one jet, dijet production and W-pair production. From this point of view the NNLO initial-final antennae are a fundamental ingredient also for the LHC physics programm.

The region of the showering, where energetic partons emit bremsstrahlung and become softer, is better described in terms of resummation, which takes into account the leading contribution from the emissions to all orders, than in terms of a fixed order calculation. However, in order to avoid the double counting of contributions, fixed order calculations and resummation must be properly matched together. The details of the matching procedure were presented in Chapter 4. We also presented the matching procedure for higher order resummation, once it will become available. In this regard

there were several interesting developments in recent years and resummation beyond NLLA starts to be feasible. A first example is given by thrust [214].

The last step in a QCD scattering process is hadronization. This process cannot be described in the framework of perturbation theory. Usually numerical Monte Carlo models are used to describe this part of the process. However, the analysis of the convergence of QCD perturbation theory permits to formulate also some analytical models which go beyond the perturbative regime and describe to some extend also the non-perturbative part of the process. In Chapter 5 we considered the dispersive model [265, 267, 275] to describe the hadronization corrections to moments of event-shape variables. The combination of the new NNLO results for the moments [254, 256] combined with non-perturbative corrections describe the data much better compared to the old NLO results. In particular the values of α_s from the fits are much more stable also for the higher moments. Since higher moments are more sensitive to the multijet region, this is a sign that NNLO corrections can describe this kinematical region much better.

Together with the α_s fit performed using event-shape distributions, the study of moments of event-shape variables with non-perturbative corrections permitted to shed some light on important difference between hadronization corrections evaluated from the standard numerical Monte Carlo codes and the analytical models. In particular it was possible to observe that the legacy Monte Carlo generators might overestimate the perturbative predictions, which in turn means that the hadronization corrections could be underestimated. This effect could be particularly dramatic by comparing LHC data with theoretical NNLO predictions and hadronization corrections produced with Monte Carlo generators. Since the needed theoretical prediction for LHC processes is very high, to understand and have these effects under control is of fundamental importance for the LHC.

In the introduction we mentioned that the LHC is just starting up. Nobody knows when and if the LHC will deliver some signal of physics beyond the Standard Model. However, it seems to be clear, that the huge jet activity which will be observed has to be understood very precisely in order the find deviations from SM predictions. For this reason higher order calculations and a deep understanding of the different stages of a process at hard-, soft- and hadronization-scale is mandatory. Many physicists worked hard both at the experimental level, to ensure high precision measurements, and at the theoretical level, to provide high precision predictions. The computations explained in this thesis are a very small part of this huge project.

Appendix A

Mathematical Tools

In this chapter we briefly summarize the most important special functions used in the computation of master integrals but also elsewhere. A complete list of definitions and properties can be found e.g. in [286] and [287]. We also summarize some important property of the calculus with distributions and in particular with (+)-distributions.

A.1 Some special functions

A.1.1 Harmonic Polylogarithms: HPL's

A very special class of functions, which appears in the computation of master integrals, are harmonic polylogarithms (HPLs). They can be defines starting from three functions

$$f_1(x) = \frac{1}{1-x} \quad ; \quad f_0(x) = \frac{1}{x} \quad ; \quad f_{-1}(x) = \frac{1}{1+x}\,,$$

by integrating

$$\begin{aligned} \mathrm{H}(1;x) &= \int_0^x f_1(t)\mathrm{d}t = -\ln(1-x)\,, \\ \mathrm{H}(0;x) &= \int_0^x f_0(t)\mathrm{d}t = \ln(x)\,, \\ \mathrm{H}(-1;x) &= \int_0^x f_{-1}(t)\mathrm{d}t = \ln(1+x)\,. \end{aligned}$$

All oder HPLs can be defined recursively as

$$\mathrm{H}(a,a_1,\ldots,a_n;x) = \int_0^x \mathrm{d}t f_a(t)\mathrm{H}(a_1,\ldots,a_n;t)\,. \tag{A.1}$$

A detailed review on HPLs can be found e.g. in [161].

A.1.2 The Gamma function

The Gamma function $\Gamma(z)$ is defined as

$$\Gamma(z) = \int_0^\infty t^{z-1} e^{-t} \mathrm{d}t \qquad \text{for} \quad \Re(z) > 0\,. \tag{A.2}$$

It appears often in the computation of master integrals. Below we list some important identities used in the calculation of master integrals.

$$\begin{aligned}
\Gamma(1+z) =& z\Gamma(z) \\
\Gamma(n+1) =& n! \\
\Gamma(z-n) =& (-1)^n \frac{\Gamma(1-z)\Gamma(z)}{\Gamma(-z+n+1)} \qquad (A.3) \\
\Gamma(nz+b) =& n^{nz+b-\frac{1}{2}} (2\pi)^{\frac{1-n}{2}} \prod_{k=0}^{n-1} \Gamma\left(z + \frac{b+k}{n}\right) \quad \text{with} \quad n \in \mathbb{N}^+\,. \qquad (A.4)
\end{aligned}$$

The Γ-function can also be written as an exponential as

$$\Gamma(1+z) = \exp\left[-z\gamma_E + \sum_{n=0}^{\infty} \frac{(-z)^j}{j} \zeta(j)\right], \tag{A.5}$$

where γ_E is the Euler constant and $\zeta(j)$ is the Riemann Zeta function. The evaluation of the Γ-function in some special point gives:

$$\Gamma(1) = \Gamma(2) = 1 \qquad ; \qquad \Gamma(1/2) = \sqrt{\pi}\,.$$

A.1.3 The Euler Beta function

The Euler Beta function is defined by

$$B(x,y) = \int_0^1 t^{x-1}(1-t)^{y-1} \mathrm{d}t \qquad \text{for} \quad \Re(x) > 0\,, \Re(y) > 0\,. \tag{A.6}$$

It can be written as a product of Γ-functions as

$$B(x,y) = \frac{\Gamma(x)\Gamma(y)}{\Gamma(x+y)}\,. \tag{A.7}$$

A.1.4 Hypergeometric function ${}_2F_1(a,b;c;z)$

The hypergeometric function ${}_2F_1(a,b;c;z)$ appears often in the computation of master integrals. Its primary definition is given in terms of a hypergeometric series

$${}_2F_1(a,b;c;z) = \sum_{n=0}^{\infty} \frac{(a)_n (b)_n}{(c)_n \Gamma(n+1)} z^n \quad \text{where} \quad \begin{cases} (l)_0 = 1 \\ (l)_n = \frac{\Gamma(n+l)}{\Gamma(l)} \end{cases}\,. \tag{A.8}$$

It is the most common hypergeometric function of a whole families of hypergeometric functions ${}_pF_q$ defined as

$$ {}_pF_q(a_1,\dots,a_p;c_1,\dots,c_q;z) = \sum_{n=0}^{\infty} \frac{\prod_{j=1}^{p}(a)_j}{\prod_{j=1}^{q}(c)_j n!} z^n \,, \tag{A.9} $$

where $q \geq p$ or $q = p-1$ and $|z| < 1$.

The hypergeometric function ${}_2F_1(a,b;c;z)$ has also an integral representation:

$$ {}_2F_1(a,b;c;z) = \frac{\Gamma(c)}{\Gamma(b)\Gamma(c-b)} \int_0^1 \mathrm{d}t\, t^{b-1}(1-t)^{c-b-1}(1-tz)^{-a} \,, \quad \text{with } \Re(c) > \Re(b) > 0 \,, \tag{A.10} $$

furthermore it satisfies a differential equation called the hypergeometric differential equation

$$ z(1-z)\frac{\mathrm{d}^2 u}{\mathrm{d}z^2} + [c-(a+b+1)z]\frac{\mathrm{d}u}{\mathrm{d}z} - ab\,u = 0 \,, \tag{A.11} $$

where $u = {}_2F_1(a,b;c;z)$.

Among the many identities between hypergeometric ${}_2F_1$-functions, the following was used several times in the evaluation of the phase space master integrals:

$$ {}_2F_1\left(1,b;2b;\frac{4z}{(1+z)^2}\right) = (1+z)^2\, {}_2F_1\left(1,\frac{3}{2}-b;b+1;z^2\right) \,. \tag{A.12} $$

The proof of this identity is not trivial and is given for example in [288].

A.2 Computation with plus-distributions

The (+)-prescription, or (+)-distribution, was introduced in Chapter 2 to regularize a pole singularity at $x = 1$ in the Altarelli-Parisi splitting functions. It is defined as

$$ \begin{aligned} \int_x^1 \mathrm{d}z\, g(z)\,[f(z)]_+ &\equiv \int_x^1 \mathrm{d}z\,[g(z)-g(1)]\,f(z) - g(1)\int_0^x \mathrm{d}z f(z) \\ &= \int_x^1 \mathrm{d}z\, g(z) f(z) - g(1)\int_0^1 \mathrm{d}z f(z) \,, \end{aligned} \tag{A.13} $$

where $f(z)$ is a function singular in $z = 1$ whereas $g(z)$ is smooth and divergent-free in the interval $0 < z < 1$. A realization of the (+)-distribution which is more convenient for analytical calculation is the following

$$ [f(x)]_+ = \lim_{\Delta\to 0}\left[-\delta(1-x)\int_0^{1-\Delta}\mathrm{d}x' f(x') + \theta(1-\Delta-x)\, f(x)|_{x<1}\right] \,. \tag{A.14} $$

Plus-distributions in dimensional regularization typically arise from the expansion of expressions of the form $(1-z)^{-1-a\epsilon}$ which is given in (3.45). We now explicitly prove this identity. We consider everything multiplied with a smooth function $f(z)$:

$$\begin{aligned}
\int_x^1 \mathrm{d}z \frac{f(z)}{(1-z)^{1+a\epsilon}} &= \int_x^1 \mathrm{d}z \frac{f(z)}{(1-z)^{1+a\epsilon}} - \int_0^1 \mathrm{d}z \frac{f(1)}{(1-z)^{1+a\epsilon}} + \int_0^1 \mathrm{d}z \frac{f(1)}{(1-z)^{1+a\epsilon}} \\
&= \int_x^1 \mathrm{d}z \frac{f(z)}{(1-z)} \sum_{n=0}^{\infty} \frac{(-a\epsilon)^n}{n!} \ln^n(1-z) - \int_0^1 \mathrm{d}z \frac{f(1)}{(1-z)} \sum_{n=0}^{\infty} \frac{(-a\epsilon)^n}{n!} \ln^n(1-z) - \frac{f(1)}{a\epsilon} \\
&= \int_x^1 \mathrm{d}z\, f(z) \left(\sum_{n=0}^{\infty} \frac{(-a\epsilon)}{n!} \mathcal{D}_n(z) - \frac{1}{a\epsilon} \delta(1-z) \right) ,
\end{aligned}$$

where

$$\mathcal{D}_n(z) = \left(\frac{\ln(1-z)}{1-z} \right)_+ .$$

When a smooth function $g(z)$ is multiplied with a (+)-distribution the following identity turns out to be useful:

$$\int_x^1 \mathrm{d}z\, f(z) g(z) \left[h(z)\right]_+ = \int_x^1 \mathrm{d}z\, f(z) \Big(g(1) \left[h(z)\right]_+ + (g(z) - g(1)) h(z) \Big) . \tag{A.15}$$

Appendix B

Phase Space Master Integrals

An important part in the derivation of the integrated initial-final antenna functions was the computation of the phase space master integrals. We give here some deeper insight in this calculations and the results of the master integrals shown in Figure 3.7 and 3.8.

B.1 Computation of 2-parton phase space

The m particle phase space $\mathrm{d}\Phi_m$ in d dimensions is generically defined as

$$\mathrm{d}PS_m = \mathrm{d}\Phi_m(k_1, \ldots, k_m; p_1, p_2) = \prod_{i=1}^{m} [\mathrm{d}k_i]\,(2\pi)^d \delta^{(d)}(p_1 + p_2 - k_1 - \ldots - k_m)\,, \quad \text{(B.1)}$$

where

$$[\mathrm{d}k_i] = \frac{\mathrm{d}^d k_i}{(2\pi)^{d-1}} \delta^{(+)}(k_i^2)\,,$$

and p_1 and p_2 are the incoming momenta. In the following we derive the 2-particle phase space integrals.

We start considering the 2-particle phase space for a process $1 \to 2$ (like for example the process $\gamma^* \to q\bar{q}$ described in Section 2.6.1). The differential 2-particle phase space

Figure B.1: Momentum flow in a 2-particle phase space: $1 \to 2$ configuration typical in e^+e^- annihilation (left) and $2 \to 2$ configuration with one massive leg typical in DIS processes (right)

is (Figure B.1, left)

$$\mathrm{d}PS_2 = \mathrm{d}\Phi_2(k_1,k_2;q) = \frac{\mathrm{d}^d k_1}{(2\pi)^{d-1}}\delta^{(+)}(k_1^2)\frac{\mathrm{d}^d k_2}{(2\pi)^{d-1}}\delta^{(+)}(k_2^2)(2\pi)^d\delta^{(d)}(q-k_1-k_2)\,.$$

Using the following two identities

$$\int \mathrm{d}^d k\,\delta^+(k^2) = \int \mathrm{d}^d k\,\frac{\delta^+(E_k-|\vec{k}|)}{2|\vec{k}|} = \int \frac{d^{d-1}k}{2E_k}\,, \qquad (\star)$$

$$\int \mathrm{d}^d x = \int \mathrm{d}\Omega_d\, r^{d-1}\mathrm{d}r = \frac{2\pi^{\frac{d}{2}}}{\Gamma\left(\frac{d}{2}\right)}\int r^{d-1}\mathrm{d}r\,. \qquad (\star\star)$$

we can rearrange the 2-particle phase space as

$$\mathrm{d}PS_2 \overset{(\star)}{=} \frac{1}{(2\pi)^{d-2}}\frac{\mathrm{d}^{d-1}k_1}{2E_1}\delta^{(+)}\left((q-k_1)^2\right) \overset{(\star\star)}{=} \frac{1}{(2\pi)^{d-2}}\mathrm{d}\Omega_{d-1}\frac{E_1^{d-2}\mathrm{d}E_1}{2E_1}\delta^{(+)}\left(q^2-2qk_1\right)\,.$$

Choosing $k_1=(E,0,0,E)$, $k_2=(E,0,0,-E)$, and $s_{01}=q^2-2E_1\sqrt{q^2}$ we have

$$E_1 = \frac{q^2-s_{01}}{2\sqrt{q^2}} \qquad ; \qquad \mathrm{d}E_1 = -\frac{\mathrm{d}s_{01}}{2\sqrt{q^2}}\,,$$

and thus

$$\mathrm{d}PS_2 = \frac{1}{(2\pi)^{d-2}}\frac{\mathrm{d}\Omega_{d-1}}{2^{d-1}}\,s^{\frac{d-4}{2}}\mathrm{d}s\,\delta(q^2-s)\,. \qquad (B.2)$$

In deriving the last equation we also used the fact that $s_{01}=q^2-s$. Integrating we obtain ($d=4-2\epsilon$)

$$P_2 = 2^{-4+4\epsilon}\pi^{\frac{-1+2\epsilon}{2}}\frac{s^{-\epsilon}}{\Gamma\left(\frac{3}{2}-\epsilon\right)}\,. \qquad (B.3)$$

Next we look at the case of a $2\to 2$ process with a spacelike massive initial particle. This was used to compute the 1-loop master integrals for the virtual antennae. The starting point is the same with a different momentum conserving δ function since now the total incoming momentum is $q+p$:

$$\begin{aligned}\mathrm{d}PS_2 =& \frac{\mathrm{d}^d k_1}{(2\pi)^{d-1}}\delta^{(+)}(k_1^2)\frac{\mathrm{d}^d k_2}{(2\pi)^{d-1}}\delta^{(+)}(k_2^2)(2\pi)^d\delta^{(d)}(q+p_i-k_1-k_2)\\ =& \frac{1}{(2\pi)^{d-2}}\frac{\mathrm{d}^{d-1}k_1}{2E_1}\delta^{(+)}\left((q+p_i-k_1)^2\right)\,.\end{aligned}$$

We now choose the following reference frame for the momenta ($-q^2=Q^2$):

$$p_1+q=(\sqrt{s},0,0,0); \quad p_i=(E,0,0,E); \quad k_1=E_1(1,0,\sin\psi,\cos\psi); \quad k_2=p_i+q-k_1\,,$$

where from momentum conservation $E = (s+Q^2)/(2\sqrt{s_{12}})$. This gives

$$\begin{aligned} \mathrm{d}PS_2 =& \frac{2^{-1}}{(2\pi)^{d-2}}\,\mathrm{d}E_1 E_1^{d-3}\,\mathrm{d}\psi(\sin\psi)^{\mathrm{d}-3}\,\mathrm{d}\Omega_{d-2}\,\delta^{(+)}\left((p_i+q-k_1)^2\right) \\ =& \frac{1}{2^{d-2}\pi^{\frac{d-2}{2}}\Gamma\left(\frac{d-2}{2}\right)}\mathrm{d}E_1\mathrm{d}\psi\,(E_1\sin\psi)^{d-3}\,\delta^{(+)}\left((p_i+q-k_1)^2\right)\,. \end{aligned}$$

In order to change variables and pass to Lorentz invariants s_{ij} we use now the method of the Gram determinant[1], which in this case is the determinant of the following matrix:

$$\Delta_3(p_i,k_1,k_2) = \begin{vmatrix} 2p_i^2 & 2p_i\cdot k_1 & 2p_i\cdot k_2 \\ 2k_1\cdot p_i & 2k_1^2 & 2k_1\cdot k_2 \\ 2k_2\cdot p_i & 2k_2\cdot k_1 & 2k_2^2 \end{vmatrix} = 2s_{1i}\,s_{2i}\,s_{12}\,. \tag{B.4}$$

Evaluating s_{1i}, s_{2i} and $s_{12} = s$, we find $\Delta_3(p_i,k_1,k_2) = 2E_1^2(Q^2+s)^2\sin^2\psi$. The Jacobian of the variable transformation $(E_1,\psi)\to(s_{1iq},s_{1i})$, where $s_{1iq} = 2k_1(p_i+q)$, can be written in terms of the gram determinant as

$$\mathrm{d}E_1\mathrm{d}\psi = \left(\sqrt{2\Delta_3(p_i,k_1,k_2)}\right)^{-1}\mathrm{d}s_{1iq}\mathrm{d}s_{1i}\,, \tag{B.5}$$

and thus the phase space integral becomes

$$\mathrm{d}PS_2 = \frac{1}{2^{d-1}\pi^{\frac{d-2}{2}}\Gamma\left(\frac{d-2}{2}\right)}\mathrm{d}s_{1(iq)}\mathrm{d}s_{1i}\left(\sqrt{2\Delta_3}\right)^{-1}\left[2(Q^2+s)^2\right]^{-\frac{d-3}{2}}\Delta_3^{\frac{d-3}{2}}\delta^{(+)}(s-s_{1iq})$$

Using now again (B.4) and the identities $s_{1iq} = s$, $s_{2i} = (Q^2+s) - s_{1i}$ and integrating over s_{1iq} we find

$$\mathrm{d}PS_2 = \frac{2^{-d+1}}{\pi^{\frac{d-2}{2}}}\frac{(Q^2+s)^{3-d}}{\Gamma\left(\frac{d-2}{2}\right)}\,s^{\frac{d-4}{2}}\mathrm{d}s_{1i}\left[s_{1i}((Q^2+s)^2-s_{1i})\right]^{\frac{d-4}{2}}\,.$$

We now define the dimensionless variables

$$y_{ij} = \frac{s_{ij}}{Q^2+s} \qquad ; \qquad z = \frac{Q^2}{Q^2+s}\,,$$

and finally find

$$\begin{aligned} \mathrm{d}PS_2 =& \frac{2^{-d+1}}{\pi^{\frac{d-2}{2}}}\frac{1}{\Gamma\left(\frac{d-2}{2}\right)}\,s^{\frac{d-4}{2}}\mathrm{d}y_{1i}\,y_{1i}(1-y_{1i})^{\frac{d-4}{2}}\,, \\ =& \frac{2^{-3+2\epsilon}}{\pi^{1-\epsilon}}\frac{s^{-\epsilon}}{\Gamma(1-\epsilon)}\mathrm{d}y_{1i}\,y_{1i}^{-\epsilon}(1-y_{1i})^{-\epsilon}\,. \end{aligned} \tag{B.6}$$

[1] More about Gram determinants can be found in the book of E. Byckling and K. Kajantie [289].

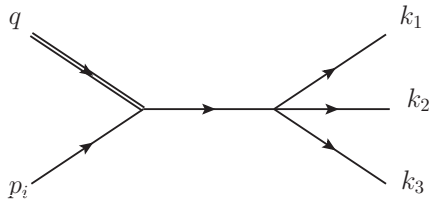

Figure B.2: Momentum flow in a 3-particle phase space: $1 \to 3$ configuration typical in e^+e^- annihilation (left)and $2 \to 3$ configuration with one massive leg typical in DIS processes (right)

This can now easily be integrated using the Euler Beta function (A.6) giving

$$\begin{aligned} \mathrm{d}PS_2 =& \frac{2^{-3+2\epsilon}}{\pi^{1-\epsilon}} \left(\frac{1-z}{z}\right)^{-\epsilon} (Q^2)^{-\epsilon} \frac{\Gamma(1-\epsilon)}{\Gamma(2-2\epsilon)} \\ =& \frac{2^{-3+2\epsilon}}{\pi^{1-\epsilon}} s^{-\epsilon} \frac{\Gamma(1-\epsilon)}{\Gamma(2-2\epsilon)} \,. \end{aligned} \tag{B.7}$$

The two equations (B.3) and (B.7) are equal since

$$\Gamma(2-2\epsilon) = 2^{\frac{3}{2}-2\epsilon}(2\pi)^{-\frac{1}{2}}\Gamma(1-\epsilon)\Gamma\left(\frac{3}{2}-\epsilon\right) .$$

The technique of the Gram Determinant becomes very useful in computing phase space integrals with more particles. In [158] a general formula for the volume of an m-particle phase space is derived.

B.2 Computation of phase space master integrals

The double-real master integrals of Figure 3.7 are 3-particle phase space integrals. We start considering a general master I. Figure B.2 shows the momentum configuration. We define the momenta in a similar way to the previous section, by working in the center-of-mass frame of $p_i + q$:

$$\begin{aligned} p_i + q &= \sqrt{s}(1,0,0,0) & k_3 &= E_3(1,0,\sin\psi,\cos\psi) \\ p_i &= E_i(1,0,0,1) & k_1 &= E_1(1,\sin\theta\sin\phi,\sin\theta\sin\phi,\cos\theta)\,, \end{aligned}$$

where $E_i = (s+Q^2)/(2\sqrt{s})$. To distinguish the different masters we introduce a general $|M|^2$ which will contain the propagators according to the label of the master integral (3.47). A general master integral $I[M]$ is then given by

$$\begin{aligned} I[M] = \int \frac{\mathrm{d}^d k_1}{(2\pi)^{d-1}}\delta^{(+)}(k_1^2)\frac{\mathrm{d}^d k_2}{(2\pi)^{d-1}}\delta^{(+)}(k_2^2)\frac{\mathrm{d}^d k_3}{(2\pi)^{d-1}}\delta^{(+)}(k_3^2) \\ \times (2\pi)^d\delta^{(d)}(p_i+q-k_1-k_2-k_3)|M|^2 \end{aligned}$$

$$
\begin{aligned}
=&\frac{1}{(2\pi)^{2d-3}}\int\frac{\mathrm{d}^{d-1}k_1}{2E_1}\frac{\mathrm{d}^{d-1}k_3}{2E_3}\delta^{(+)}\left((p_i+q-k_1-k_2-k_3)^2\right)|M|^2\\
=&\frac{2^{-2}}{(2\pi)^{2d-3}}\int\mathrm{d}E_1\,E_1^{d-3}\mathrm{d}E_3\,E_3^{d-3}\mathrm{d}\psi(\sin\psi)^{d-3}\mathrm{d}\theta(\sin\theta)^{d-3}\mathrm{d}\phi(\sin\phi)^{d-4}\\
&\times\mathrm{d}\Omega_{d-2}\mathrm{d}\Omega_{d-3}\delta^{(+)}\left((p_i+q-k_1-k_2-k_3)^2\right)|M|^2\\
=&\frac{2^{d-1}}{(4\pi)^d\Gamma(d-3)}\int\mathrm{d}E_1\,E_1^{d-3}\mathrm{d}E_3\,E_3^{d-3}\mathrm{d}\psi(\sin\psi)^{d-3}\mathrm{d}\theta(\sin\theta)^{d-3}\mathrm{d}\phi(\sin\phi)^{d-4}\\
&\times\delta^{(+)}\left((p_i+q-k_1-k_2-k_3)^2\right)|M|^2\,,
\end{aligned}
$$

where used

$$
\mathrm{d}^n x=\mathrm{d}r\,r^{n-1}\mathrm{d}\Omega_n=\mathrm{d}r\,r\mathrm{d}\theta_1(\sin\theta_1)^{n-2}\mathrm{d}\Omega_{n-1}\,.
$$

and

$$
\Gamma\left(\frac{d-2}{2}\right)\Gamma\left(\frac{d-3}{2}\right)=\Gamma(d-3)\sqrt{\pi}2^{4-d}\,.
$$

We now use again the Gram determinant, this time with 4 momenta:

$$
\Delta_4(k_1,k_2,k_3,p_i)=\begin{vmatrix}2k_1^2 & 2k_1\cdot k_2 & 2k_1\cdot k_3 & 2k_1\cdot p_i\\ 2k_2\cdot k_1 & 2k_2^2 & 2k_2\cdot k_3 & 2k_2\cdot p_i\\ 2k_3\cdot k_1 & 2k_3\cdot k_2 & 2k_3^2 & 2k_3\cdot p_i\\ 2p_i\cdot k_1 & 2p_i\cdot k_2 & 2p_i\cdot k_3 & 2p_i^2\end{vmatrix}=\lambda(s_{12}s_{3i},s_{13}s_{2i},s_{1i}s_{23})\,,
\tag{B.8}
$$

where λ is the Källen function $\lambda(x,y,z)=x^2+y^2+z^2-2(xy+xz+yz)$. Using the property of the determinant

$$
\Delta_4(k_1,k_2,k_3,p_i)=\Delta_4(p_i+q,k_1,k_3,p_i)=-(2E_1E_3(Q^2+s)\sin\theta\sin\phi\sin\psi)^2\,.
$$

We are now ready to make the change of variables and write everything in terms of invariants s_{ij} as follows:

$$
\begin{aligned}
E_1&\to s_{1iq}=2\sqrt{s}E_1\,,\\
E_3&\to s_{3iq}=2\sqrt{s}E_3\,,\\
\psi&\to s_{3i}=2\frac{Q^2+s}{2\sqrt{s}}E_3(1-\cos\psi)\,,\\
\theta&\to s_{1i}=2\frac{Q^2+s}{2\sqrt{s}}E_1(1-\cos\theta)\,,\\
\phi&\to s_{13}=2E_1E_3(1-\sin\psi\sin\theta\cos\phi-\cos\psi\cos\theta)\,,
\end{aligned}
$$

where $s=s_{123}=(k_1+k_2+k_3)^2$ and $s_{jiq}=2k_j(p_i+q)$. Next we write the Jacobian of the transformation in terms of the Gram determinant

$$
\begin{aligned}
\mathrm{d}s_{1iq}\mathrm{d}s_{3iq}\mathrm{d}s_{3i}\mathrm{d}s_{1i}\mathrm{d}s_{13}=&8E_1^2E_3^2(Q^2+s)^2(\sin\psi)^2(\sin\theta)^2(\sin\phi)^2\mathrm{d}E_1\mathrm{d}E_3\mathrm{d}\theta\mathrm{d}\psi\mathrm{d}\phi\\
=&\frac{2}{\sin\phi}(-\Delta_4)\mathrm{d}E_1\mathrm{d}E_3\mathrm{d}\theta\mathrm{d}\psi\mathrm{d}\phi\,,
\end{aligned}
$$

and by inserting it in the phase space integral we find

$$I[M] = \frac{2(Q^2+s)^{3-d}}{(4\pi)^d \Gamma(d-3)} \int \mathrm{d}s_{1iq}\mathrm{d}s_{3iq}\mathrm{d}s_{3i}\mathrm{d}s_{1i}\mathrm{d}s_{13}(-\Delta_4)^{\frac{d-5}{2}}\delta(s-s_{3iq}-s_{1iq}+s_{13})|M|^2\,. \tag{B.9}$$

We now transform the Gram determinant using

$$s_{2i} = (Q^2+s) - s_{3i} - s_{1i} \quad ; \quad s_{23} = s_{3iq} - s_{13} \quad ; \quad s_{12} = s_{1iq} - s_{13}$$

as follows

$$\begin{aligned}\Delta_4(k_1,k_2,k_3,p_i) &= \lambda\left(s_{12}s_{3i}, s_{13}s_{2i}, s_{1i}s_{23}\right)\\ &= \lambda\left((s_{1iq}-s_{13})s_{3i}, s_{13}[(Q^2+s)-s_{3i}-s_{1i}], s_{1i}(s_{3iq}-s_{13})\right)\\ &= \lambda\left((s_{1iq}-s_{13})s_{3i}, s_{13}[(Q^2+s)-s_{3i}-s_{1i}], s_{1i}(s-s_{1iq})\right)\,,\end{aligned}$$

where in the last line we used the delta function of the integrand and integrated over s_{3iq}. Transforming the s_{ij} in dimensionless variables

$$y_{ij} = \frac{s_{ij}}{Q^2+s} \qquad \text{and} \qquad z = \frac{s}{Q^2+s}$$

and substituting $d = 4-2\epsilon$ we find

$$I[M] = \frac{2(Q^2+s)^{1-2\epsilon}}{(4\pi)^{4-2\epsilon}\Gamma(1-2\epsilon)} \int \mathrm{d}y_{1iq}\mathrm{d}y_{1i}\mathrm{d}y_{3i}\mathrm{d}y_{13}(-\tilde{\Delta}_4)^{\frac{-1-2\epsilon}{2}}|M|^2\,, \tag{B.10}$$

where $\tilde{\Delta}_4$ is the Gram determinant written in terms of y_{ij}.

As explained in Chapter 3, for all the masters a differential equation or a system of differential equations was derived. An example of such a differential equation and the general strategy to solve them is presented later in this chapter. However, in order to find the unique solution of a differential equation, also a boundary condition is needed. Equation (B.10) is the starting point to compute the boundary conditions, usually computed for the limit $z \to 1$ after having factorized the leading singularity.

B.2.1 3-particle phase space

We show that by choosing $|M|^2 = 1$, i.e. by considering no propagators at all, we obtain as expected the 3-particle phase space volume P_3 which is also the first master integral $I[0]$. In order to simplify the computation we first factorize the Gram determinant

$$(-\tilde{\Delta}_4) = (y_{3i}-y_{3i,a})(y_{3i,b}-y_{3i})y_{1iq}^2 \overset{(1)}{=} y_{1iq}^2(y_{3i,b}-y_{3i,a})^2\chi(1-\chi)\,,$$

where we substituted

$$y_{3i} = (y_{3i,b}-y_{3i,a})\chi + y_{3i,a} \qquad \text{with} \quad \chi \in [0,1]\,,$$

and thus

$$I[0] = \frac{2(Q^2+s)^{1-2\epsilon}}{(4\pi)^{4-2\epsilon}\Gamma(1-2\epsilon)} \int \mathrm{d}y_{1iq}\mathrm{d}y_{1i}\mathrm{d}y_{13} y_{1iq}^{-1-2\epsilon}(y_{3i,b}-y_{3i,a})^{-2\epsilon} \int_0^1 \mathrm{d}\chi[\chi(1-\chi)]^{-\frac{1}{2}-\epsilon}\,.$$

Furthermore

$$y_{1iq}^4(y_{3i,b}-y_{3i,a})^2 = 16 y_{13}y_{1i}(z-y_{1iq})(y_{13}-y_{1iq})(z\,y_{1i}-y_{1iq})\,,$$

which can be disentangled by substituting

$$y_{1i} = z_{1i}\,z_{1iq} \quad ; \quad y_{13} = z_{13}\,z\,z_{1iq} \quad ; \quad y_{1iq} = z_{1iq}\,z\,,$$

such that

$$y_{1iq}^4(y_{3i,b}-y_{3i,a})^2 = z_{1iq}^4 z^4 (y_{3i,b}-y_{3i,a})^2 = 16 z^4(1-z_{13})z_{13}(1-z_{1i})z_{1i}(1-z_{1iq})z_{1iq}^4\,.$$

Inserting everything in the integral and performing the integration over χ we find

$$\begin{aligned} I[0] = &\frac{2(Q^2+s)^{1-2\epsilon}}{(4\pi)^{4-2\epsilon}\Gamma(1-2\epsilon)} B\left(\frac{1}{2}-\epsilon,\frac{1}{2}-\epsilon\right) \\ &\times \int \mathrm{d}z_{1iq}\mathrm{d}z_{1i}\mathrm{d}z_{13} z^{1-2\epsilon} z_{1iq}^{1-2\epsilon}\left(16(1-z_{13})z_{13}(1-z_{1i})z_{1i}(1-z_{1iq})\right)^{-\epsilon}\,. \end{aligned}$$

The integration is now easily done in terms of Euler Beta functions (A.6). Finally we substitute $z \to 1-z$ such that z corresponds to the definition (3.42) and we find

$$I[0] = 2^{-7+4\epsilon}\pi^{-3+2\epsilon}(Q^2)^{1-2\epsilon}\left(\frac{1-z}{z}\right)^{1-2\epsilon}\frac{\Gamma(1-\epsilon)^3}{\Gamma(3-3\epsilon)\Gamma(2-2\epsilon)}\,, \tag{B.11}$$

which is exactly the 3-particle phase space volume. The last equation is also solution of the differential equations in z and Q^2 found for $I[0]$

$$z\frac{\partial}{\partial z}I[0] = \frac{1-2\epsilon}{z-1}I[0]\,, \tag{B.12}$$

$$Q^2\frac{\partial}{\partial Q^2}I[0] = (1-2\epsilon)I[0]\,. \tag{B.13}$$

B.2.2 Iterative solution of differential equations

We now consider the master integral $I[2]$, which is the easiest with at least one propagator. From the reduction we find the following differential equations

$$z\frac{\partial}{\partial z}I[2] = \epsilon\, I[2] + \frac{(3\epsilon-2)z}{1-z}\frac{I[0]}{Q^2}\,, \tag{B.14}$$

$$Q^2\frac{\partial}{\partial Q^2}I[2] = -(2\epsilon)\, I[2]\,. \tag{B.15}$$

The second differential equation gives the dependence on Q^2

$$I[2] \propto (Q^2)^{-2\epsilon}\,.$$

To solve the equation in z we factor out the leading singularity by defining[1]

$$\begin{aligned} I[0] =&(1-z)^{1-2\epsilon} I_R[0]\,,\\ I[2] =&(1-z)^{-2\epsilon} I_R[2]\,, \end{aligned}$$

such that the differential equation becomes

$$z\frac{\partial}{\partial z} I_R[2] = \frac{\epsilon}{z} I_R[2] - \frac{2\epsilon}{1-z} I_R[2] + \frac{2}{Q^2} I_R[0] - \frac{3\epsilon}{Q^2} I_R[0]\,. \tag{B.16}$$

On the right hand side of the equation $I_R[2]$ has coefficients proportional to $\epsilon, \epsilon^2, \ldots$ This means the $I_R[2]$ is regularized and we can now solve the equation iteratively by expanding $I_R[0]$ and $I_R[2]$ in powers of ϵ:

$$I_R[0](z) = K\frac{Q^2}{z}\left(1 + 2\epsilon\ln(z) + \frac{(2\epsilon)^2}{2!}\ln^2(z) + \mathcal{O}(\epsilon^3)\right)\,, \tag{B.17}$$

$$I_R[2](z) = \frac{1}{\epsilon} I_R[2,z,-1] + I_R[2,z,0] + \epsilon I_R[2,z,1] + \epsilon^2 I_R[2,z,2] + \mathcal{O}(\epsilon^3)\,. \tag{B.18}$$

Integrating the differential equation on both sides with respect to z we obtain

$$I_R[2](z) - I_R[2](1) = \int_1^z \mathrm{d}z' \left(\frac{2}{Q^2} I_R[0](z') - \frac{3\epsilon}{Q^2} I_R[0](z') + \frac{\epsilon}{z} I_R[2](z) - \frac{2\epsilon}{1-z} I_R[2](z)\right)\,, \tag{B.19}$$

and inserting the expansion and comparing order by order we find

- At $\mathcal{O}(1/\epsilon)$:

$$I_R[2,z,-1] = I_R[2,1,-1]\,.$$

- At $\mathcal{O}(\epsilon^0)$:

$$\begin{aligned} I_R[2,z,0] =& I_R[2,1,0] + 2\int_1^z \mathrm{d}z' \frac{1}{z'} + I_R[2,1,-1]\int_1^z \mathrm{d}z \left(\frac{1}{z} - \frac{2}{1-z}\right)\\ =& I_R[2,1,0] + 2\mathrm{H}(0;z)\,. \end{aligned}$$

- Etc.

[1] In all the masters we also factor out the numerical part of $I[0]$ which is as overall normalization.

Proceeding in this way the differential equation can be solved order by order. The solutions of the different orders at $z = 1$ must be computed explicitly as we showed for I[0]. Sometimes however they can be inferred from the iterative solution. This can be seen for example at $\mathcal{O}(0)$ here, where one of the terms proportional to $I_R[2, 1, -1]$ gives a divergent contribution. This means that $I_R[2, 1, -1] = 0$. The simple case of $I[2]$ could of course also be solved to all orders, as summarized in Table 3.6, however in this way also the most difficult master integrals could be solved and their solution is reported in the next section.

B.3 Master Integrals

The common prefactor S_Γ is defined as:

$$S_\Gamma = \left(\frac{(4\pi)^\epsilon}{16\pi^2\Gamma(1-\epsilon)}\right)^2 . \tag{B.20}$$

B.3.1 Master integrals for double real radiation

The double real master integrals expanded to the needed order in ϵ are given by:

$$\begin{aligned} I_0 = S_\Gamma \left(Q^2\right)^{1-2\epsilon} (1-z)^{1-2\epsilon} z^{-1}\pi \\ \Big[1 + \epsilon\Big(\frac{13}{2} + 2\,\mathrm{H}(0;z)\Big) + \epsilon^2\Big(\frac{115}{4} - \frac{2}{3}\pi^2 + 13\,\mathrm{H}(0;z) + 4\,\mathrm{H}(0,0;z)\Big) \\ + \epsilon^3\Big(\frac{865}{8} - \frac{13}{3}\pi^2 - 10\zeta_3 + \frac{115}{2}\,\mathrm{H}(0;z) - \frac{4}{3}\pi^2\,\mathrm{H}(0;z) + 26\,\mathrm{H}(0,0;z) + 8\,\mathrm{H}(0,0,0;z)\Big) \\ + \epsilon^4\Big(\frac{5971}{16} - \frac{115}{6}\pi^2 - 65\zeta_3 - \frac{\pi^4}{30} + \frac{865}{4}\,\mathrm{H}(0;z) - \frac{26}{3}\pi^2\,\mathrm{H}(0;z) - 20\,\mathrm{H}(0;z)\zeta_3 \\ + 115\,\mathrm{H}(0,0;z) - \frac{8}{3}\pi^2\,\mathrm{H}(0,0;z) + 52\,\mathrm{H}(0,0,0;z) + 16\,\mathrm{H}(0,0,0,0;z)\Big) + \mathcal{O}\left(\epsilon^5\right)\Big] , \end{aligned} \tag{B.21}$$

$$
\begin{aligned}
I_2 =& S_\Gamma \left(Q^2\right)^{-2\epsilon} (1-z)^{-2\epsilon} \pi \\
& \Big[2\,\mathrm{H}(0;z) - \epsilon\Big(\frac{2}{3}\pi^2 - 10\,\mathrm{H}(0;z) - 6\,\mathrm{H}(0,0;z) + 4\,\mathrm{H}(1,0;z)\Big) - \epsilon^2\Big(\frac{10}{3}\pi^2 + 4\zeta_3 \\
& - 38\,\mathrm{H}(0;z) + 2\pi^2\,\mathrm{H}(0;z) - \frac{4}{3}\pi^2\mathrm{H}(1;z) - 30\,\mathrm{H}(0,0;z) + 20\mathrm{H}(1,0;z) + 4\,\mathrm{H}(0,1,0;z) \\
& - 14\,\mathrm{H}(0,0,0;z) + 12\,\mathrm{H}(1,0,0;z) - 8\,\mathrm{H}(1,1,0;z)\Big) + \epsilon^3\Big(-\frac{38}{3}\pi^2 - 20\zeta_3 + \frac{11}{45}\pi^4 \\
& + 130\,\mathrm{H}(0;z) - 10\pi^2\,\mathrm{H}(0;z) - 24\,\mathrm{H}(0;z)\,\zeta_3 + \frac{20}{3}\pi^2\,\mathrm{H}(1;z) + 8\,\mathrm{H}(1;z)\,\zeta_3 \\
& + \frac{4}{3}\pi^2\,\mathrm{H}(0,1;z) + 114\,\mathrm{H}(0,0;z) - \frac{14}{3}\pi^2\,\mathrm{H}(0,0;z) - 76\,\mathrm{H}(1,0;z) + 4\pi^2\,\mathrm{H}(1,0;z) \\
& - \frac{8}{3}\pi^2\,\mathrm{H}(1,1;z) - 20\,\mathrm{H}(0,1,0;z) - 4\,\mathrm{H}(0,0,1,0;z) + 70\,\mathrm{H}(0,0,0;z) - 60\,\mathrm{H}(1,0,0;z) \\
& + 40\,\mathrm{H}(1,1,0;z) + 8\,\mathrm{H}(1,0,1,0;z) - 12\,\mathrm{H}(0,1,0,0;z) + 8\,\mathrm{H}(0,1,1,0;z) \\
& + 30\,\mathrm{H}(0,0,0,0;z) - 28\,\mathrm{H}(1,0,0,0;z) + 24\,\mathrm{H}(1,1,0,0;z) - 16\,\mathrm{H}(1,1,1,0;z)\Big) \\
& + \mathcal{O}\left(\epsilon^4\right)\Big],
\end{aligned}
\tag{B.22}
$$

$$
\begin{aligned}
I_{26} =& S_\Gamma \left(Q^2\right)^{-1-2\epsilon} (1-z)^{-2\epsilon} z\,\pi \\
& \Big[\frac{1}{\epsilon}\Big(\frac{2\pi^2}{3} + 2\,\mathrm{H}(0,0;z) + 2\,\mathrm{H}(1,0;z)\Big) + 4\zeta_3 - \frac{2}{3}\pi^2\,\mathrm{H}(0;z) - \frac{2}{3}\pi^2\,\mathrm{H}(1;z) \\
& - 4\mathrm{H}(0,1,0;z) + 6\,\mathrm{H}(0,0,0;z) + 6\,\mathrm{H}(1,0,0;z) - 4\,\mathrm{H}(1,1,0;z) + \epsilon\Big(\frac{5}{9}\pi^4 \\
& - 4\mathrm{H}(0;z)\zeta_3 - 4\mathrm{H}(1;z)\zeta_3 + \frac{4}{3}\pi^2\,\mathrm{H}(0,1;z) - 2\pi^2\,\mathrm{H}(0,0;z) - 2\pi^2\,\mathrm{H}(1,0;z) \\
& + \frac{4}{3}\pi^2\,\mathrm{H}(1,1;z) - 4\mathrm{H}(0,0,1,0;z) - 4\mathrm{H}(1,0,1,0;x) - 12\mathrm{H}(0,1,0,0;z) \\
& + 8\mathrm{H}(0,1,1,0;z) + 14\mathrm{H}(0,0,0,0;z) + 14\mathrm{H}(1,0,0,0;z) - 12\mathrm{H}(1,1,0,0;z) \\
& + 8\mathrm{H}(1,1,1,0;z)\Big) + \mathcal{O}\left(\epsilon^2\right)\Big],
\end{aligned}
\tag{B.23}
$$

$$
\begin{aligned}
I_{249} =& S_\Gamma \left(Q^2\right)^{-2\epsilon-2} (1-z)^{-2\epsilon} z^2 \pi \\
&\Big[-\frac{2}{\epsilon^3} - \frac{8}{\epsilon^2}\,\mathrm{H}(0;z) + \frac{1}{\epsilon}\Big(\frac{10}{3}\pi^2 + 10\,\mathrm{H}(1,0;z) - 22\,\mathrm{H}(0,0;z)\Big) + 56\zeta_3 + 10\pi^2\,\mathrm{H}(0;z) \\
&- \frac{10}{3}\pi^2\mathrm{H}(1;z) + 20\,\mathrm{H}(0,1,0;z) - 50\,\mathrm{H}(0,0,0;z) + 38\,\mathrm{H}(1,0,0;z) - 20\,\mathrm{H}(1,1,0;z) \\
&+ \epsilon\Big(-\frac{56}{45}\pi^4 + 156\zeta_3\mathrm{H}(0;z) - 68\,\mathrm{H}(1;z)\zeta_3 - \frac{20}{3}\pi^2\,\mathrm{H}(0,1;z) + 22\pi^2\,\mathrm{H}(0,0;z) \\
&- 18\pi^2\,\mathrm{H}(1,0;z) + \frac{20}{3}\pi^2\,\mathrm{H}(1,1;z) + 28\,\mathrm{H}(0,0,1,0;z) - 52\,\mathrm{H}(1,0,1,0;z) \\
&+ 76\,\mathrm{H}(0,1,0,0;z) - 40\,\mathrm{H}(0,1,1,0;z) - 106\,\mathrm{H}(0,0,0,0;z) + 94\,\mathrm{H}(1,0,0,0;z) \\
&- 76\,\mathrm{H}(1,1,0,0;z) + 40\,\mathrm{H}(1,1,1,0;z)\Big) + \mathcal{O}\left(\epsilon^2\right)\Big]\,,
\end{aligned}
\tag{B.24}
$$

$$
\begin{aligned}
I_{125} =& S_\Gamma \left(Q^2\right)^{-2-2\epsilon} (1-z)^{-2\epsilon} (1+z)^{-1} z^2 \pi \\
&\Big[\frac{2}{\epsilon^2}\mathrm{H}(0;z) + \frac{1}{\epsilon}\Big(-\pi^2 - 4\mathrm{H}(-1,0;z) + 8\mathrm{H}(0,0;z) - 4\mathrm{H}(1,0;z)\Big) - 14\zeta_3 \\
&- \frac{8}{3}\pi^2\,\mathrm{H}(0;z) + 2\pi^2\,\mathrm{H}(1;z) - 8\mathrm{H}(-2,0;z) + 2\pi^2\,\mathrm{H}(-1;z) - 8\mathrm{H}(0,1,0;z) \\
&+ 8\mathrm{H}(-1,-1,0;z) - 16\mathrm{H}(-1,0,0;z) + 8\mathrm{H}(-1,1,0;z) + 20\mathrm{H}(0,0,0;z) \\
&+ 8\mathrm{H}(1,-1,0;z) - 16\mathrm{H}(1,0,0;z) + 8\mathrm{H}(1,1,0;z) + \epsilon\Big(-\frac{\pi^4}{30} + 4\pi^2\mathrm{H}(0,-1;z) \\
&+ 4\pi^2\mathrm{H}(0,1;z) - 4\pi^2\mathrm{H}(-1,-1;z) + \frac{16}{3}\pi^2\mathrm{H}(-1,0;z) - 4\pi^2\mathrm{H}(-1,1;z) \\
&- \frac{20}{3}\pi^2\mathrm{H}(0,0;z) - 4\pi^2\mathrm{H}(1,-1;z) + \frac{16}{3}\pi^2\mathrm{H}(1,0;z) - 4\pi^2\mathrm{H}(1,1;z) \\
&+ 28\zeta_3\mathrm{H}(-1;z) - 28\zeta_3\mathrm{H}(0;z) + 28\zeta_3\mathrm{H}(1;z) - 32\mathrm{H}(0,0,-1,0;z) \\
&- 8\mathrm{H}(0,0,1,0;z) + 16\mathrm{H}(0,-1,-1,0;z) - 32\mathrm{H}(0,-1,0,0;z) + 16\mathrm{H}(0,-1,1,0;z) \\
&+ 16\mathrm{H}(-1,0,-1,0;z) + 16\mathrm{H}(-1,0,1,0;z) + 16\mathrm{H}(1,0,-1,0;z) + 16\mathrm{H}(1,0,1,0;z) \\
&+ 16\mathrm{H}(0,1,-1,0;z) - 32\mathrm{H}(0,1,0,0;z) + 16\mathrm{H}(0,1,1,0;z) - 16\mathrm{H}(-1,-1,-1,0;z) \\
&+ 32\mathrm{H}(-1,-1,0,0;z) - 16\mathrm{H}(-1,-1,1,0;x) - 40\mathrm{H}(-1,0,0,0;z) \\
&- 16\mathrm{H}(-1,1,-1,0;z) + 32\mathrm{H}(-1,1,0,0;z) - 16\mathrm{H}(-1,1,1,0;z) + 44\mathrm{H}(0,0,0,0;z) \\
&- 16\mathrm{H}(1,-1,-1,0;z) + 32\mathrm{H}(1,-1,0,0;z) - 16\mathrm{H}(1,-1,1,0;z) - 40\mathrm{H}(1,0,0,0;z) \\
&- 16\mathrm{H}(1,1,-1,0;z) + 32\mathrm{H}(1,1,0,0;z) - 16\mathrm{H}(1,1,1,0;z)\Big) + \mathcal{O}\left(\epsilon^2\right)\Big]\,,
\end{aligned}
\tag{B.25}
$$

$$
\begin{aligned}
I_{235} =& S_\Gamma \left(Q^2\right)^{-2-2\epsilon} (1-z)^{-1-2\epsilon} z^2 \pi \\
& \Big[-\frac{\mathrm{H}(0;z)}{\epsilon^2} - \frac{7\mathrm{H}(0,0;z)}{\epsilon} + 8\zeta_3 + \frac{7}{3}\pi^2\,\mathrm{H}(0;z) - 8\mathrm{H}(0,-1,0;z) + 10\mathrm{H}(0,1,0;z) \\
& - 19\mathrm{H}(0,0,0;z) + \epsilon\Big(-\frac{2\pi^4}{5} + 20\zeta_3\mathrm{H}(0;z) - 32\mathrm{H}(0,0,-1,0;z) + 4\pi^2\mathrm{H}(0,-1;z) \\
& - 2\pi^2\mathrm{H}(0,1;z) + \frac{19}{3}\pi^2\mathrm{H}(0,0;z) + 10\mathrm{H}(0,0,1,0;z) + 16\mathrm{H}(0,-1,-1,0;z) \\
& - 32\mathrm{H}(0,-1,0,0;z) + 16\mathrm{H}(0,-1,1,0;z) + 16\mathrm{H}(0,1,-1,0;z) + 22\mathrm{H}(0,1,0,0;z) \\
& - 20\mathrm{H}(0,1,1,0;z) - 43\mathrm{H}(0,0,0,0;z) \Big) + \mathcal{O}\left(\epsilon^2\right) \Big] ,
\end{aligned}
\tag{B.26}
$$

$$
\begin{aligned}
I_{1245} =& S_\Gamma \left(Q^2\right)^{-3-2\epsilon} (1-z)^{-2\epsilon} (1+z)^{-1} z^3 \pi \\
& \Big[-\frac{8\mathrm{H}(0;z)}{\epsilon^2} + \frac{1}{\epsilon}\Big(\frac{10\pi^2}{3} + 8\mathrm{H}(-1,0;z) - 28\mathrm{H}(0,0;z) + 16\mathrm{H}(1,0;z) \Big) + 28\zeta_3 \\
& - \frac{8}{3}\pi^2\,\mathrm{H}(-1;z) + \frac{28}{3}\pi^2\,\mathrm{H}(0;z) - \frac{20}{3}\pi^2\,\mathrm{H}(1;z) + 8\mathrm{H}(0,-1,0;z) + 24\mathrm{H}(0,1,0;z) \\
& + 24\mathrm{H}(-1,0,0;z) - 16\mathrm{H}(-1,1,0;z) - 68\mathrm{H}(0,0,0;z) - 16\mathrm{H}(1,-1,0;z) \\
& + 56\mathrm{H}(1,0,0;z) - 32\mathrm{H}(1,1,0;z) + \epsilon\Big(-\frac{49\pi^4}{45} + 88\mathrm{H}(0;z)\zeta_3 - 56\mathrm{H}(1;z)\zeta_3 \\
& - \frac{4}{3}\pi^2\mathrm{H}(0,-1;z) - \frac{28}{3}\pi^2\mathrm{H}(0,1;z) + 16\mathrm{H}(0,0,-1,0;z) - \frac{8}{3}\pi^2\mathrm{H}(-1,-1;z) \\
& - 8\pi^2\mathrm{H}(-1,0;z) + \frac{16}{3}\pi^2\mathrm{H}(-1,1;z) + \frac{68}{3}\pi^2\mathrm{H}(0,0;z) + \frac{16}{3}\pi^2\mathrm{H}(1,-1;z) \\
& - \frac{56}{3}\pi^2\mathrm{H}(1,0;z) + \frac{40}{3}\pi^2\mathrm{H}(1,1;z) + 24\mathrm{H}(0,0,1,0;z) + 16\mathrm{H}(0,-1,-1,0;z) \\
& + 16\mathrm{H}(0,-1,0,0;z) - 16\mathrm{H}(0,-1,1,0;z) + 16\mathrm{H}(-1,0,-1,0;z) - 16\mathrm{H}(-1,0,1,0;z) \\
& - 16\mathrm{H}(1,0,-1,0;z) - 48\mathrm{H}(1,0,1,0;z) - 16\mathrm{H}(0,1,-1,0;z) + 80\mathrm{H}(0,1,0,0;z) \\
& - 48\mathrm{H}(0,1,1,0;z) - 32\mathrm{H}(-1,-1,-1,0;z) + 16\mathrm{H}(-1,-1,0,0;z) \\
& + 56\mathrm{H}(-1,0,0,0;z) - 48\mathrm{H}(-1,1,0,0;z) + 32\mathrm{H}(-1,1,1,0;z) - 148\mathrm{H}(0,0,0,0;z) \\
& - 48\mathrm{H}(1,-1,0,0;z) + 32\mathrm{H}(1,-1,1,0;z) + 136\mathrm{H}(1,0,0,0;z) + 32\mathrm{H}(1,1,-1,0;z) \\
& - 112\mathrm{H}(1,1,0,0;z) + 64\mathrm{H}(1,1,1,0;z) \Big) + \mathcal{O}\left(\epsilon^2\right) \Big] ,
\end{aligned}
\tag{B.27}
$$

$$
\begin{aligned}
I_{2356} =& S_\Gamma \left(Q^2\right)^{-3-2\epsilon} (1-z)^{-1-2\epsilon} z^3 \pi \\
& \Big[-\frac{2}{\epsilon^3} - \frac{8\mathrm{H}(0;z)}{\epsilon^2} + \frac{1}{\epsilon}\Big(2\pi^2 - 28\mathrm{H}(0,0;z) + 4\mathrm{H}(1,0;z)\Big) + 32\zeta_3 + \frac{28}{3}\pi^2\,\mathrm{H}(0;z) \\
& - 8\mathrm{H}(0,-1,0;z) + 24\mathrm{H}(0,1,0;z) - 68\mathrm{H}(0,0,0;z) + 28\mathrm{H}(1,0,0;z) + \epsilon\Big(256\zeta_3 \\
& - \frac{43\pi^4}{18} + 4\pi^2\mathrm{H}(0,-1;z) - 4\pi^2\mathrm{H}(0,1;z) + \frac{68}{3}\pi^2\mathrm{H}(0,0;z) - \frac{28}{3}\pi^2\mathrm{H}(1,0;z) \\
& + 88\zeta_3\mathrm{H}(0;z) - 32\zeta_3\mathrm{H}(1;z) - 16\mathrm{H}(0,0,-1,0;z) + 24\mathrm{H}(0,0,1,0;z) \\
& + 16\mathrm{H}(0,-1,-1,0;z) - 32\mathrm{H}(0,-1,0,0;z) + 16\mathrm{H}(0,-1,1,0;z) + 32\mathrm{H}(1,0,-1,0;z) \\
& - 40\mathrm{H}(1,0,1,0;z) + 16\mathrm{H}(0,1,-1,0;z) + 96\mathrm{H}(0,1,0,0;z) - 32\mathrm{H}(0,1,1,0;z) \\
& - 148\mathrm{H}(0,0,0,0;z) + 76\mathrm{H}(1,0,0,0;z)\Big) + \mathcal{O}\left(\epsilon^2\right)\Big],
\end{aligned}
\tag{B.28}
$$

$$
\begin{aligned}
I_{1346} =& S_\Gamma \left(Q^2\right)^{-3-2\epsilon} (1-z)^{-1-2\epsilon} z^3 \pi \\
& \Big[-\frac{10}{\epsilon^3} - \frac{20\mathrm{H}(0;z)}{\epsilon^2} + \frac{1}{\epsilon}\Big(\frac{20\pi^2}{3} - 40\mathrm{H}(0,0;z)\Big) + 92\zeta_3 + \frac{40}{3}\pi^2\,\mathrm{H}(0;z) - 80\mathrm{H}(0,0,0;z) \\
& + \epsilon\Big(-\frac{1}{3}\pi^4 + 184\zeta_3\mathrm{H}(0;z) + \frac{80}{3}\pi^2\mathrm{H}(0,0;z) - 160\mathrm{H}(0,0,0,0;z)\Big) + \mathcal{O}\left(\epsilon^2\right)\Big].
\end{aligned}
\tag{B.29}
$$

B.3.2 Master integrals for one-loop single real radiation

The virtual master integrals are given by:

$$
\begin{aligned}
V_{14} =& 2\pi i\, S_\Gamma \left(Q^2\right)^{-2\epsilon} (1-z)^{-\epsilon} \\
& \Big[\frac{1}{\epsilon} + 4 + \mathrm{H}(0;z) + \epsilon\Big(12 - \frac{\pi^2}{6} + 4\,\mathrm{H}(0;z) + \mathrm{H}(0,0;z)\Big) + \epsilon^2\Big(32 - \frac{2\pi^2}{3} - 4\zeta_3 \\
& + 12\,\mathrm{H}(0;z) - \frac{1}{6}\pi^2\,\mathrm{H}(0;z) + 4\,\mathrm{H}(0,0;z) + \mathrm{H}(0,0,0;z)\Big) + \epsilon^3\Big(80 - 2\pi^2 - 16\zeta_3 \\
& - \frac{7\pi^4}{120} + 32\,\mathrm{H}(0;z) - \frac{2}{3}\pi^2\,\mathrm{H}(0;z) - 4\,\mathrm{H}(0;z)\,\zeta_3 + 12\,\mathrm{H}(0,0;z) - \frac{1}{6}\pi^2\,\mathrm{H}(0,0;z) \\
& + 4\,\mathrm{H}(0,0,0;z) + \mathrm{H}(0,0,0,0;z)\Big) + \mathcal{O}\left(\epsilon^4\right)\Big],
\end{aligned}
\tag{B.30}
$$

$$
\begin{aligned}
V_{24} =& V_{14}(1-z)^{-\epsilon} \\
& \Big[1 + \epsilon\,\mathrm{H}(0;z) + \epsilon^2\left(\mathrm{H}(0,0;z) - \frac{\pi^2}{2}\right) + \epsilon^3\Big(\mathrm{H}(0,0,0;z) - \frac{\pi^2}{2}\,\mathrm{H}(0;z)\Big) + \mathcal{O}\left(\epsilon^4\right)\Big],
\end{aligned}
\tag{B.31}
$$

$$
\begin{aligned}
V_{13} =& 2\pi i\, S_\Gamma \left(Q^2\right)^{-2\epsilon} (1-z)^{-\epsilon} \\
& \Big[\frac{1}{\epsilon} + 5 + 2\,\mathrm{H}(0;z) + \epsilon\Big(19 - \frac{\pi^2}{3} + 10\,\mathrm{H}(0;z) + 4\,\mathrm{H}(0,0;z)\Big) + \epsilon^2\Big(65 - \frac{5\pi^2}{3} - 8\zeta_3 \\
& + 38\,\mathrm{H}(0;z) - \frac{2}{3}\pi^2\,\mathrm{H}(0;z) + 20\,\mathrm{H}(0,0;z) + 8\,\mathrm{H}(0,0,0;z)\Big) + \epsilon^3\Big(211 - \frac{19}{3}\pi^2 - 40\zeta_3 \\
& - \frac{7}{45}\pi^4 + 130\,\mathrm{H}(0;z) - \frac{10}{3}\pi^2\,\mathrm{H}(0;z) - 16\,\mathrm{H}(0;z)\,\zeta_3 + 76\,\mathrm{H}(0,0;z) - \frac{4}{3}\pi^2\,\mathrm{H}(0,0;z) \\
& + 40\,\mathrm{H}(0,0,0;z) + 16\,\mathrm{H}(0,0,0,0;z)\Big) + \mathcal{O}\left(\epsilon^4\right)\Big],
\end{aligned}
\tag{B.32}
$$

$$
\begin{aligned}
V_{134} =& 2\pi i\, S_\Gamma \left(Q^2\right)^{-1-2\epsilon} (1-z)^{-\epsilon} z \\
& \Big[\frac{1}{\epsilon}\Big(\frac{\pi^2}{3} + \mathrm{H}(0,0;z) + \mathrm{H}(1,0;z)\Big) - \zeta_3 - \frac{1}{6}\pi^2\,\mathrm{H}(0;z) + \frac{1}{6}\pi^2\,\mathrm{H}(1;z) + 3\,\mathrm{H}(0,0,0;z) \\
& + 4\,\mathrm{H}(1,0,0;z) + \mathrm{H}(1,1,0;z) + \epsilon\Big(\frac{43}{360}\pi^4 - 4\,\mathrm{H}(0;z)\,\zeta_3 - 5\,\mathrm{H}(1;z)\,\zeta_3 \\
& - \frac{1}{2}\pi^2\,\mathrm{H}(0,0;z) - \frac{2}{3}\pi^2\,\mathrm{H}(1,0;z) + \frac{1}{6}\pi^2\,\mathrm{H}(1,1;z) + 7\,\mathrm{H}(0,0,0,0;z) \\
& + 10\,\mathrm{H}(1,0,0,0;z) + 4\,\mathrm{H}(1,1,0,0;z) + \mathrm{H}(1,1,1,0;z)\Big) + \mathcal{O}\left(\epsilon^2\right)\Big],
\end{aligned}
\tag{B.33}
$$

$$
\begin{aligned}
C_{1234} =& 2\pi i\, S_\Gamma \left(Q^2\right)^{-2-2\epsilon} (1-z)^{-\epsilon} z^2 \\
& \Big[-\frac{2}{\epsilon^3} - \frac{6}{\epsilon^2}\,\mathrm{H}(0;z) + \frac{1}{\epsilon}\Big(\frac{5\pi^2}{3} - 16\,\mathrm{H}(0,0;z) + 2\,\mathrm{H}(1,0;z)\Big) + 34\zeta_3 + \frac{16}{3}\pi^2\,\mathrm{H}(0;z) \\
& + \frac{1}{3}\pi^2\,\mathrm{H}(1;z) + 8\,\mathrm{H}(0,1,0;z) - 36\,\mathrm{H}(0,0,0;z) + 12\,\mathrm{H}(1,0,0;z) + 2\,\mathrm{H}(1,1,0;z) \\
& + \epsilon\Big(-\frac{4}{9}\pi^4 + 80\,\mathrm{H}(0;z)\,\zeta_3 - 22\,\mathrm{H}(1;z)\zeta_3 + \frac{4}{3}\pi^2\,\mathrm{H}(0,1;z) + \frac{34}{3}\pi^2\,\mathrm{H}(0,0;z) \\
& - \frac{14}{3}\pi^2\,\mathrm{H}(1,0;z) + \frac{1}{3}\pi^2\,\mathrm{H}(1,1;z) + 16\,\mathrm{H}(0,0,1,0;z) - 8\,\mathrm{H}(1,0,1,0;z) \\
& + 40\,\mathrm{H}(0,1,0,0;z) + 8\,\mathrm{H}(0,1,1,0;z) - 76\,\mathrm{H}(0,0,0,0;z) + 32\,\mathrm{H}(1,0,0,0;x) \\
& + 4\,\mathrm{H}(1,1,0,0;z) + 2\,\mathrm{H}(1,1,1,0;z)\Big) + \mathcal{O}\left(\epsilon^2\right)\Big],
\end{aligned}
\tag{B.34}
$$

$$
\begin{aligned}
V_{12345} =& 2\pi i\, S_\Gamma \left(Q^2\right)^{-3-2\epsilon} (1-z)^{-1-2\epsilon} z^3 \\
& \Big[-\frac{3}{\epsilon^3} - \frac{9}{\epsilon^2}\,\mathrm{H}(0;z) + \frac{1}{\epsilon}\Big(\frac{13\pi^2}{6} + 3\,\mathrm{H}(0,1;z) - 22\,\mathrm{H}(0,0;z) + 2\,\mathrm{H}(1,0;z)\Big) + 23\zeta_3 \\
& + \frac{17}{3}\pi^2\,\mathrm{H}(0;z) + \frac{1}{3}\pi^2\,\mathrm{H}(1;z) + 10\,\mathrm{H}(0,0,1;z) - 2\,\mathrm{H}(1,0,1;z) + 10\,\mathrm{H}(0,1,0;z) \\
& - 3\,\mathrm{H}(0,1,1;z) - 48\,\mathrm{H}(0,0,0;z) + 8\,\mathrm{H}(1,0,0;z) + \mathcal{O}\left(\epsilon\right)\Big] .
\end{aligned}
\tag{B.35}
$$

Appendix C

Resummation functions

We summarize here the expressions for the resummed NLL integrated cross section (4.10) for different event shapes. One has

$$R\left(y,Q,\mu\right) \;=\; \left(1+C_1\bar{\alpha}_s\right)\,\Sigma\left(y\right)\;,$$

with

$$\Sigma\left(y\right) \;=\; \exp\left\{Lg_1\left(\alpha_s L\right)+g_2\left(\alpha_s L\right)\right\}.$$

Following [235, 238], and in order to unify the notation, the resummed part is then expressed through auxiliary functions $h_1\left(\lambda\right)$ and $h_2\left(\lambda\right)$, with:

$$\Sigma\left(y\right) \;=\; \Sigma_s\left(y\right)\,\mathcal{F}\left(R'\right)$$

where

$$R'\left(\lambda\right) = -\frac{1}{2}\left[h_1\left(\lambda\right)+\lambda\,h_1'\left(\lambda\right)\right].$$

The functions $h_1\left(\lambda\right)$, $h_2\left(\lambda\right)$, $\Sigma_s\left(y\right)$ and $\mathcal{F}\left(R'\right)$ depend on the event shape observable, as well as the parameter λ. The QCD constants β_0, β_1 are given in (2.23) and K is equal to

$$K = C_A\left(\frac{67}{18}-\frac{\pi^2}{6}\right)-\frac{5}{9}\,N_F\,.$$

C.1 Thrust and C-Parameter

From [231] and [236], one has:

$$\begin{aligned}
\lambda &= \frac{\beta_0}{\pi}\,\alpha_S L\;,\\
h_1\left(\lambda\right) &= -\frac{C_F}{2\lambda\beta_0}\left[\left(1-2\,\lambda\right)\ln\left(1-2\lambda\right)-2\left(1-\lambda\right)\ln\left(1-\lambda\right)\right]\;,\\
h_2\left(\lambda\right) &= -\frac{C_F\,K}{4\beta_0^2}\left[2\,\ln\left(1-\lambda\right)-\ln\left(1-2\lambda\right)\right]-\frac{3C_F}{4\beta_0}\ln\left(1-\lambda\right)
\end{aligned}$$

$$
\begin{aligned}
& -\frac{C_F \beta_1}{2\beta_0^3}\left(\ln(1-2\lambda) - 2\ln(1-\lambda) + \frac{1}{2}\ln^2(1-2\lambda) - \ln^2(1-\lambda)\right) , \\
\Sigma_s(y) &= e^{L\, 2h_1(\lambda)+2h_2(\lambda)} , \\
\mathcal{F}(R') &= \frac{e^{-4\gamma_E R'}}{\Gamma(1+4R')} .
\end{aligned}
$$

These yield:

$$
\begin{aligned}
g_1(\alpha_S L) &= 2\, h_1\left(\frac{\beta_0}{\pi}\alpha_S L\right) , \\
g_2(\alpha_S L) &= 2\, h_2\left(\frac{\beta_0}{\pi}\alpha_S L\right) - \ln\left[\Gamma\left(1+4R'\right)\right] - 4\gamma_E R' .
\end{aligned}
$$

C.2 Heavy Jet Mass

From [231] one has:

$$
\begin{aligned}
\lambda &= \frac{\beta_0}{\pi}\alpha_S L , \\
h_1(\lambda) &= -\frac{C_F}{2\lambda\beta_0}\left[(1-2\lambda)\ln(1-2\lambda) - 2(1-\lambda)\ln(1-\lambda)\right] , \\
h_2(\lambda) &= -\frac{C_F K}{4\beta_0^2}\left[2\ln(1-\lambda) - \ln(1-2\lambda)\right] - \frac{3C_F}{4\beta_0}\ln(1-\lambda) \\
& \quad -\frac{C_F \beta_1}{2\beta_0^3}\left(\ln(1-2\lambda) - 2\ln(1-\lambda) + \frac{1}{2}\ln^2(1-2\lambda) - \ln^2(1-\lambda)\right) , \\
\Sigma_s(y) &= e^{L\, 2h_1(\lambda)+2h_2(\lambda)} , \\
\mathcal{F}(R') &= \frac{e^{-2\gamma_E R'}}{\Gamma(1+2R')^2} .
\end{aligned}
$$

These yield:

$$
\begin{aligned}
g_1(\alpha_S L) &= 2\, h_1\left(\frac{\beta_0}{\pi}\alpha_S L\right) , \\
g_2(\alpha_S L) &= 2\, h_2\left(\frac{\beta_0}{\pi}\alpha_S L\right) - 2\ln\left[\Gamma\left(1+2R'\right)\right] - 2\gamma_E R' .
\end{aligned}
$$

C.3 Total Jet Broadening

From [234, 235] one has:

$$
\begin{aligned}
\lambda &= 2\frac{\beta_0}{\pi}\alpha_S L , \\
h_1(\lambda) &= \frac{2C_F}{\lambda\beta_0}\left(\ln(1-\lambda) + \lambda\right) ,
\end{aligned}
$$

$$
\begin{aligned}
h_2(\lambda) &= -\frac{C_F K}{2\beta_0^2}\left(\ln(1-\lambda)+\frac{\lambda}{1-\lambda}\right)-\frac{3C_F}{2\beta_0}\ln(1-\lambda) \\
&\quad +\frac{C_F\beta_1}{\beta_0^3}\left(\frac{1}{2}\ln^2(1-\lambda)+\frac{\ln(1-\lambda)}{1-\lambda}+\frac{\lambda}{1-\lambda}\right), \\
\Sigma_s(y) &= e^{L\,h_1(\lambda)+h_2(\lambda)}, \\
\mathcal{F}(R') &= \left[\int_1^\infty \frac{dx}{x^2}\left(\frac{1+x}{4}\right)^{-R'}\right]^2 \frac{e^{-2\gamma_E R'}}{\Gamma(1+2R')} \\
&= \left[\frac{4^{R'}\,{}_2F_1(R',1+R';2+R';-1)}{(1+R')}\right]^2 \frac{e^{-2\gamma_E R'}}{\Gamma(1+2R')}.
\end{aligned}
$$

These yield:

$$
\begin{aligned}
g_1(\alpha_S L) &= h_1\left(\frac{\beta_0}{\pi}\alpha_S L\right), \\
g_2(\alpha_S L) &= h_2\left(\frac{\beta_0}{\pi}\alpha_S L\right)-\ln\left[\Gamma\left(1+2R'\right)\right]-2\gamma_E R' \\
&\quad +2\ln\left[\frac{4^{R'}\,{}_2F_1(R',1+R';2+R';-1)}{(1+R')}\right].
\end{aligned}
$$

C.4 Wide Jet Broadening

From [234, 235] one has:

$$
\begin{aligned}
\lambda &= 2\frac{\beta_0}{\pi}\alpha_S L, \\
h_1(\lambda) &= \frac{2C_F}{\lambda\beta_0}\left(\ln(1-\lambda)+\lambda\right), \\
h_2(\lambda) &= -\frac{C_F K}{2\beta_0^2}\left(\ln(1-\lambda)+\frac{\lambda}{1-\lambda}\right)-\frac{3C_F}{2\beta_0}\ln(1-\lambda) \\
&\quad +\frac{C_F\beta_1}{\beta_0^3}\left(\frac{1}{2}\ln^2(1-\lambda)+\frac{\ln(1-\lambda)}{1-\lambda}+\frac{\lambda}{1-\lambda}\right), \\
\Sigma_s(y) &= e^{L\,h_1(\lambda)+h_2(\lambda)}, \\
\mathcal{F}(R') &= \left[\int_1^\infty \frac{dx}{x^2}\left(\frac{1+x}{4}\right)^{-R'}\right]^2 \frac{e^{-2\gamma_E R'}}{\Gamma(1+R')^2} \\
&= \left[\frac{4^{R'}\,{}_2F_1(R',1+R';2+R';-1)}{(1+R')}\right]^2 \frac{e^{-2\gamma_E R'}}{\Gamma(1+R')^2}.
\end{aligned}
$$

These yield:

$$
g_1(\alpha_S L) = h_1\left(\frac{\beta_0}{\pi}\alpha_S L\right),
$$

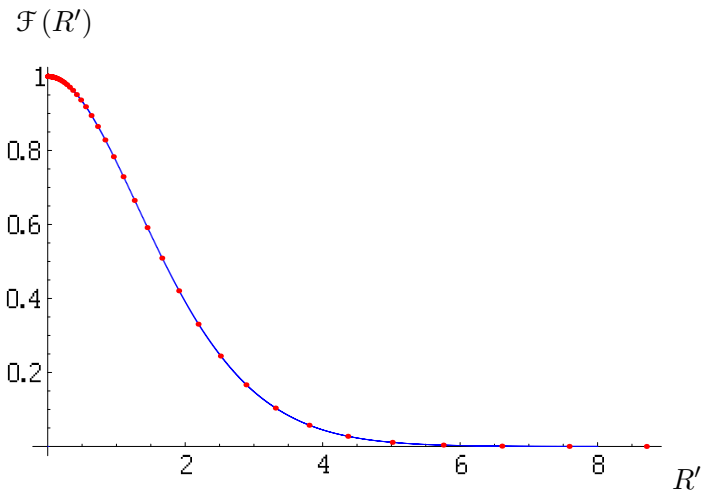

Figure C.1: Interpolation of the numerical recoil correction for Y3.

$$
\begin{aligned}
g_2(\alpha_S L) &= h_2\left(\frac{\beta_0}{\pi}\alpha_S L\right) - 2\ln\left[\Gamma\left(1+R'\right)\right] - 2\gamma_E R' \\
&\quad +2\ln\left[\frac{4^{R'}\ {}_2F_1\left(R',\,1+R';\,2+R';\,-1\right)}{(1+R')}\right] .
\end{aligned}
$$

C.5 Two-to-three Jet Transition in the Durham Algorithm

From [238, 240] one has:

$$
\begin{aligned}
\lambda &= \frac{\beta_0}{\pi}\alpha_S L\,, \\
h_1(\lambda) &= \frac{C_F}{\lambda\beta_0}\left(\ln(1-\lambda)+\lambda\right)\,, \\
h_2(\lambda) &= -\frac{3C_F}{2\beta_0}\ln(1-\lambda) - \frac{C_F K}{2\beta_0^2(1-\lambda)}\left(\lambda+(1-\lambda)\ln(1-\lambda)\right) + \\
&\quad +\frac{C_F\beta_1}{\beta_0^3}\left(\frac{\lambda+\ln(1-\lambda)}{1-\lambda} + \frac{1}{2}\ln^2(1-\lambda)\right)\,, \\
\Sigma_s(y) &= e^{L\,h_1(\lambda)+h_2(\lambda)}\,.
\end{aligned}
$$

The function $\mathcal{F}(R')$ for Y_3 is known only numerically [238, 240] and is shown in Figure C.1.

We interpolate the points using a slightly modified version of Newton's divided difference formula implemented in the CERN Computer Program Library (Function

DIVDIF in the CERN Program Library [290]). These yield:

$$\begin{aligned} g_1(\alpha_S L) &= h_1\left(\frac{\beta_0}{\pi}\alpha_S L\right), \\ g_2(\alpha_S L) &= h_2\left(\frac{\beta_0}{\pi}\alpha_S L\right) + \ln\left[\mathcal{F}\left(R'\right)\right]. \end{aligned}$$

The argument of recoil correction $\mathcal{F}(R')$ in this case is given by

$$R' = R'(\lambda) = -\left[h_1(\lambda) - \lambda h_1'(\lambda)\right] = \frac{C_f}{\beta_0}\frac{\lambda}{1-\lambda} \tag{C.1}$$

with $\lambda = \frac{\beta_0}{\pi}\alpha_S L$. For the region of interest, that is for values of R' below 1.5 (figure (C.2)), the interpolation of the derivative $\mathcal{F}'$ of $\mathcal{F}$ with respect to its argument is also described good by the interpolation (C.3).

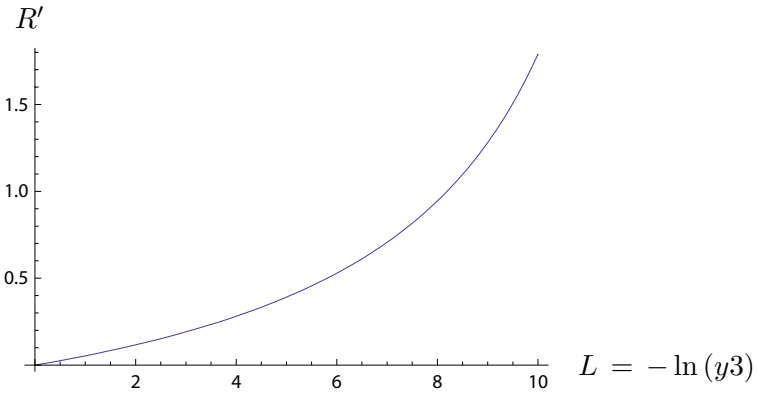

Figure C.2: The function $R'\left(\frac{\beta_0}{\pi}\alpha_s L\right)$ as a function of L. For L between 0 and 10 the value of R' is below 1.5.

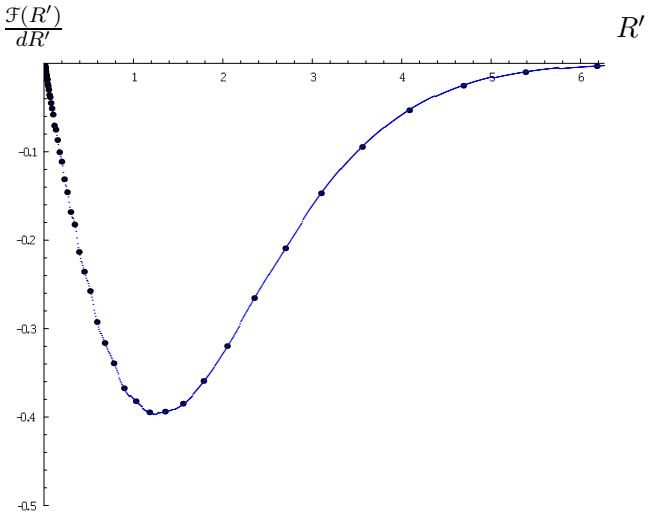

Figure C.3: Numerical derivative of the interpolation vs numerical derivative of the function $\mathcal{F}(R')$.

Thrust: $y = \tau = 1 - T$ and C-parameter: $y = C/6$

$$
\begin{aligned}
G_{11} &= 3\,C_F \\
G_{12} &= -2\,C_F \\
G_{22} &= \tfrac{1}{36}\,C_F\left(-169C_A + 22N_F + 12\,(C_A - 4C_F)\,\pi^2\right) \\
G_{23} &= \tfrac{1}{3}\,C_F\,(-11C_A + 2N_F) \\
G_{33} &= \tfrac{1}{108}\,C_F\left[-3197C_A^2 + 1024C_AN_F + 108C_FN_F - 68N_F^2 + 132C_A^2\pi^2 - 792C_AC_F\pi^2 - 24C_AN_F\pi^2\right. \\
&\qquad \left. +144C_FN_F\pi^2 + 2304\,C_F^2\zeta(3)\right] \\
G_{34} &= -\tfrac{7}{108}C_F\,(11\,C_A - 2\,N_F)^2
\end{aligned}
$$

Heavy jet mass: $y = \rho$

$$
\begin{aligned}
G_{11} &= 3\,C_F \\
G_{12} &= -2\,C_F \\
G_{22} &= \tfrac{1}{36}\,C_F\left(-169C_A + 22N_F + 12\,(C_A - 2C_F)\,\pi^2\right) \\
G_{23} &= \tfrac{1}{3}\,C_F\,(-11C_A + 2N_F) \\
G_{33} &= \tfrac{1}{108}\,C_F\left[-3197C_A^2 + 1024C_AN_F + 108C_FN_F - 68N_F^2 + 132C_A^2\pi^2 - 396C_AC_F\pi^2 - 24C_AN_F\pi^2\right. \\
&\qquad \left. +72C_FN_F\pi^2 + 576\,C_F^2\zeta(3)\right] \\
G_{34} &= -\tfrac{7}{108}C_F\,(11\,C_A - 2\,N_F)^2
\end{aligned}
$$

Total jet broadening: $y = B_T$

$$
\begin{aligned}
G_{11} &= 6\,C_F \\
G_{12} &= -4\,C_F \\
G_{22} &= -\tfrac{1}{9}C_F\left(35C_A - 2N_F - 6C_A\pi^2 + 24C_F\pi^2 + 288C_F\,\ln^2 2\right) \\
G_{23} &= -\tfrac{8}{9}C_F\,(11C_A - 2N_F) \\
G_{33} &= \tfrac{2}{81}C_F\left(-2471C_A^2 + 760C_AN_F + 108C_FN_F - 44N_F^2 + 132C_A^2\pi^2 - 792C_AC_F\pi^2 - 24C_AN_F\pi^2\right. \\
&\qquad +144C_FN_F\pi^2 + 864C_F^2\pi^2\ln 2 - 9504C_AC_F\ln^2 2 + 1728C_FN_F\ln^2 2 - 5184C_F^2\ln^3 2 \\
&\qquad \left. +2376C_F^2\zeta\,(3)\right) \\
G_{34} &= -\tfrac{2}{9}C_F\,(11C_A - 2N_F)^2
\end{aligned}
$$

Wide jet broadening: $y = B_W$

$$
\begin{aligned}
G_{11} &= 6\,C_F \\
G_{12} &= -4C_F \\
G_{22} &= -\tfrac{1}{9}C_F\left(35C_A - 2N_F - 6C_A\pi^2 + 288C_F\,\ln^2 2\right) \\
G_{23} &= -\tfrac{8}{9}C_F\,(11C_A - 2N_F) \\
G_{33} &= \tfrac{2}{81}C_F\left(-2471C_A^2 + 760C_AN_F + 108C_FN_F - 44N_F^2 + 132C_A^2\pi^2 - 24C_AN_F\pi^2 + 864C_F^2\pi^2\ln 2\right. \\
&\qquad \left. -9504C_AC_F\ln^2 2 + 1728C_FN_F\ln^2 2 - 5184C_F^2\ln^3 2 - 2808C_F^2\zeta\,(3)\right) \\
G_{34} &= -\tfrac{2}{9}C_F\,(11C_A - 2N_F)^2
\end{aligned}
$$

Two-to-three jet transition in Durham algorithm: $y = Y_3$

$$
\begin{aligned}
G_{11} &= 3\,C_F \\
G_{12} &= -C_F \\
G_{22} &= \tfrac{1}{36}C_F\left(-35C_A + 144C_F\mathcal{F}_2 + 2N_F + 6C_A\pi^2\right) \\
G_{23} &= -\tfrac{1}{9}C_F\,(11C_A - 2N_F) \\
G_{33} &= \tfrac{1}{324}C_F\left(-2471C_A^2 + 4752C_AC_F\mathcal{F}_2 + 2592C_F^2\mathcal{F}_3 + 760C_AN_F + 108C_FN_F - 864C_F\mathcal{F}_2N_F - 44N_F^2\right. \\
&\qquad \left. +132C_A^2\pi^2 - 24C_AN_F\pi^2\right) \\
G_{34} &= -\tfrac{1}{72}C_F\,(11C_A - 2N_F)^2
\end{aligned}
$$

Table C.1: The logarithmic coefficients G_{ij} for LL and NLL up to the third order in α_s.

Appendix D

Fit Results with non-perturbative corrections

In this appendix, we collect the extractions of $\alpha_s(M_Z)$ and α_0 at NLO and NNLO from individual moments of the six event shape variables: τ, C, ρ, Y_3, B_T, B_W.

NLO	$\langle\tau\rangle$	$\langle\tau^2\rangle$	$\langle\tau^3\rangle$	$\langle\tau^4\rangle$	$\langle\tau^5\rangle$
χ^2/dof	1.0043	1.0565	0.8399	0.6459	0.4740
$\alpha_s(M_Z)$	0.1242	0.1344	0.1416	0.1479	0.1534
Experimental Error	0.0018	0.0023	0.0028	0.0033	0.0038
x_μ variation: $x_\mu = 0.5$	-0.0054	-0.0083	-0.0101	-0.0115	-0.0129
$x_\mu = 2.0$	0.0066	0.0102	0.0123	0.0143	0.0162
μ_I variation: $\mu_I = 1.0$ Gev	0.0025	0.0035	0.0038	0.0045	0.0054
$\mu_I = 3.0$ Gev	-0.0019	-0.0025	-0.0027	-0.0031	-0.0037
$\mathcal{M}$ variation: $\mathcal{M} - 20\,\%$	0.0012	0.0016	0.0017	0.0020	0.0024
$\mathcal{M} + 20\,\%$	-0.0011	-0.0014	-0.0016	-0.0018	-0.0021
Theoretical Error	0.0072	0.0109	0.0130	0.0151	0.0172
α_0	0.4782	0.5147	0.5359	0.5521	0.5744
Experimental Error	0.0151	0.0152	0.0189	0.0222	0.0243
x_μ variation: $x_\mu = 0.5$	0.0017	0.0004	-0.0038	-0.0065	-0.0081
$x_\mu = 2.0$	-0.0000	-0.0001	0.0030	0.0051	0.0064
$\mathcal{M}$ variation: $\mathcal{M} - 20\,\%$	0.0432	0.0423	0.0405	0.0377	0.0375
$\mathcal{M} + 20\,\%$	-0.0306	-0.0307	-0.0298	-0.0284	-0.0290
Theoretical Error	0.0433	0.0423	0.0406	0.0382	0.0384

Table D.1: Results for $\alpha_s(Q)$ and α_0 as obtained from fits to τ moments measured by JADE and OPAL for centre-of-mass energies between 14.0 and 206.6 GeV using theoretical NLO predictions.

NNLO	$\langle\tau\rangle$	$\langle\tau^2\rangle$	$\langle\tau^3\rangle$	$\langle\tau^4\rangle$	$\langle\tau^5\rangle$
χ^2/dof	0.9889	0.9411	0.7284	0.5526	0.3997
$\alpha_s(M_Z)$	0.1166	0.1202	0.1233	0.1267	0.1294
Experimental Error	0.0015	0.0018	0.0021	0.0024	0.0027
x_μ variation: $x_\mu = 0.5$	-0.0020	-0.0034	-0.0042	-0.0048	-0.0054
$x_\mu = 2.0$	0.0025	0.0042	0.0051	0.0058	0.0065
μ_I variation: $\mu_I = 1.0$ Gev	0.0017	0.0017	0.0017	0.0019	0.0022
$\mu_I = 3.0$ Gev	-0.0011	-0.0011	-0.0011	-0.0013	-0.0014
$\mathcal{M}$ variation: $\mathcal{M} - 20\,\%$	0.0009	0.0010	0.0009	0.0011	0.0012
$\mathcal{M} + 20\,\%$	-0.0009	-0.0009	-0.0009	-0.0010	-0.0011
Theoretical Error	0.0032	0.0046	0.0054	0.0062	0.0070
α_0	0.5165	0.5408	0.5452	0.5512	0.5641
Experimental Error	0.0135	0.0152	0.0194	0.0223	0.0246
x_μ variation: $x_\mu = 0.5$	0.0140	0.0075	0.0016	-0.0008	-0.0023
$x_\mu = 2.0$	-0.0078	-0.0045	-0.0001	0.0019	0.0031
$\mathcal{M}$ variation: $\mathcal{M} - 20\,\%$	0.0415	0.0430	0.0396	0.0357	0.0347
$\mathcal{M} + 20\,\%$	-0.0298	-0.0308	-0.0286	-0.0264	-0.0261
Theoretical Error	0.0438	0.0436	0.0397	0.0358	0.0348

Table D.2: Results for $\alpha_s(Q)$ and α_0 as obtained from fits to τ moments measured by JADE and OPAL for centre-of-mass energies between 14.0 and 206.6 GeV using theoretical NNLO predictions.

NLO	$\langle C \rangle$	$\langle C^2 \rangle$	$\langle C^3 \rangle$	$\langle C^4 \rangle$	$\langle C^5 \rangle$
χ^2/dof	1.1849	1.5245	1.5651	1.5446	1.4094
$\alpha_s(M_Z)$	0.1230	0.1308	0.1347	0.1374	0.1407
Experimental Error	0.0013	0.0016	0.0020	0.0023	0.0026
x_μ variation: $x_\mu = 0.5$	-0.0052	-0.0079	-0.0091	-0.0100	-0.0108
$x_\mu = 2.0$	0.0063	0.0096	0.0111	0.0122	0.0134
μ_I variation: $\mu_I = 1.0$ Gev	0.0029	0.0045	0.0051	0.0057	0.0064
$\mu_I = 3.0$ Gev	-0.0022	-0.0031	-0.0034	-0.0038	-0.0041
$\mathcal{M}$ variation: $\mathcal{M} - 20\,\%$	0.0013	0.0020	0.0022	0.0025	0.0028
$\mathcal{M} + 20\,\%$	-0.0012	-0.0018	-0.0019	-0.0022	-0.0024
Theoretical Error	0.0071	0.0107	0.0124	0.0137	0.0151
α_0	0.4267	0.4632	0.4789	0.4839	0.4857
Experimental Error	0.0082	0.0064	0.0067	0.0069	0.0070
x_μ variation: $x_\mu = 0.5$	0.0052	0.0027	-0.0010	-0.0035	-0.0054
$x_\mu = 2.0$	-0.0029	-0.0021	0.0007	0.0027	0.0042
$\mathcal{M}$ variation: $\mathcal{M} - 20\,\%$	0.0324	0.0359	0.0377	0.0376	0.0366
$\mathcal{M} + 20\,\%$	-0.0236	-0.0266	-0.0268	-0.0283	-0.0278
Theoretical Error	0.0328	0.0360	0.0377	0.0377	0.0370

Table D.3: Results for $\alpha_s(Q)$ and α_0 as obtained from fits to C moments measured by JADE and OPAL for centre-of-mass energies between 14.0 and 206.6 GeV using theoretical NLO predictions.

NNLO	$\langle C \rangle$	$\langle C^2 \rangle$	$\langle C^3 \rangle$	$\langle C^4 \rangle$	$\langle C^5 \rangle$
χ^2/dof	1.1574	1.2418	1.2353	1.1735	1.0216
$\alpha_s(M_Z)$	0.1161	0.1180	0.1193	0.1202	0.1216
Experimental Error	0.0011	0.0013	0.0016	0.0017	0.0019
x_μ variation: $x_\mu = 0.5$	-0.0020	-0.0033	-0.0039	-0.0043	-0.0046
$x_\mu = 2.0$	0.0025	0.0040	0.0047	0.0051	0.0056
μ_I variation: $\mu_I = 1.0$ Gev	0.0019	0.0022	0.0023	0.0025	0.0028
$\mu_I = 3.0$ Gev	-0.0013	-0.0014	-0.0015	-0.0016	-0.0017
$\mathcal{M}$ variation: $\mathcal{M} - 20\,\%$	0.0011	0.0012	0.0013	0.0014	0.0015
$\mathcal{M} + 20\,\%$	-0.0010	-0.0011	-0.0012	-0.0013	-0.0014
Theoretical Error	0.0033	0.0047	0.0054	0.0059	0.0064
α_0	0.4689	0.4897	0.4919	0.4877	0.4828
Experimental Error	0.0071	0.0063	0.0067	0.0069	0.0070
x_μ variation: $x_\mu = 0.5$	0.0166	0.0095	0.0053	0.0027	0.0010
$x_\mu = 2.0$	-0.0105	-0.0066	-0.0033	-0.0013	0.0001
$\mathcal{M}$ variation: $\mathcal{M} - 20\,\%$	0.0316	0.0360	0.0359	0.0346	0.0326
$\mathcal{M} + 20\,\%$	-0.0234	-0.0264	-0.0265	-0.0258	-0.0246
Theoretical Error	0.0357	0.0372	0.0363	0.0347	0.0326

Table D.4: Results for $\alpha_s(Q)$ and α_0 as obtained from fits to C moments measured by JADE and OPAL for centre-of-mass energies between 14.0 and 206.6 GeV using theoretical NNLO predictions.

NLO	$\langle\rho\rangle$	$\langle\rho^2\rangle$
χ^2/dof	0.6587	0.7547
$\alpha_s(M_Z)$	0.1164	0.1152
Experimental Error	0.0023	0.0033
x_μ variation: $x_\mu = 0.5$	-0.0028	-0.0038
$x_\mu = 2.0$	0.0039	0.0049
μ_I variation: $\mu_I = 1.0$ Gev	0.0014	0.0014
$\mu_I = 3.0$ Gev	-0.0011	-0.0011
$\mathcal{M}$ variation: $\mathcal{M} - 20\,\%$	0.0006	0.0006
$\mathcal{M} + 20\,\%$	-0.0006	-0.0006
Theoretical Error	0.0042	0.0051
α_0	0.5914	0.5657
Experimental Error	0.0268	0.0361
x_μ variation: $x_\mu = 0.5$	0.0115	0.0092
$x_\mu = 2.0$	-0.0042	-0.0047
$\mathcal{M}$ variation: $\mathcal{M} - 20\,\%$	0.0795	0.0748
$\mathcal{M} + 20\,\%$	-0.0539	-0.0508
Theoretical Error	0.0803	0.0753

Table D.5: Results for $\alpha_s(Q)$ and α_0 as obtained from fits to ρ moments measured by JADE and OPAL for centre-of-mass energies between 14.0 and 206.6 GeV using theoretical NLO predictions.

NNLO	$\langle\rho\rangle$	$\langle\rho^2\rangle$
χ^2/dof	0.6750	0.7607
$\alpha_s(M_Z)$	0.1142	0.1113
Experimental Error	0.0021	0.0030
x_μ variation: $x_\mu = 0.5$	-0.0009	-0.0012
$x_\mu = 2.0$	0.0013	0.0017
μ_I variation: $\mu_I = 1.0$ Gev	0.0012	0.0010
$\mu_I = 3.0$ Gev	-0.0008	-0.0007
$\mathcal{M}$ variation: $\mathcal{M} - 20\,\%$	0.0007	0.0006
$\mathcal{M} + 20\,\%$	-0.0006	-0.0006
Theoretical Error	0.0018	0.0020
α_0	0.6565	0.6208
Experimental Error	0.0224	0.0316
x_μ variation: $x_\mu = 0.5$	0.0312	0.0233
$x_\mu = 2.0$	-0.0184	-0.0143
$\mathcal{M}$ variation: $\mathcal{M} - 20\,\%$	0.0799	0.0759
$\mathcal{M} + 20\,\%$	-0.0547	-0.0518
Theoretical Error	0.0858	0.0794

Table D.6: Results for $\alpha_s(Q)$ and α_0 as obtained from fits to ρ moments measured by JADE and OPAL for centre-of-mass energies between 14.0 and 206.6 GeV using theoretical NNLO predictions.

NLO	$\langle Y_3\rangle$	$\langle Y_3^2\rangle$	$\langle Y_3^3\rangle$	$\langle Y_3^4\rangle$	$\langle Y_3^5\rangle$
χ^2/dof	0.8616	0.6386	0.7771	0.8691	0.9499
$\alpha_s(M_Z)$	0.1183	0.1172	0.1165	0.1149	0.1124
Experimental Error	0.0011	0.0016	0.0020	0.0026	0.0033
x_μ variation: $x_\mu = 0.5$	-0.0040	-0.0042	-0.0040	-0.0038	-0.0035
$x_\mu = 2.0$	0.0053	0.0054	0.0052	0.0049	0.0045
Theoretical Error	0.0047	0.0048	0.0046	0.0043	0.0040

Table D.7: Results for $\alpha_s(Q)$ and α_0 as obtained from fits to Y_3 moments measured by JADE and OPAL for centre-of-mass energies between 14.0 and 206.6 GeV using theoretical NLO predictions.

NNLO	$\langle Y_3 \rangle$	$\langle Y_3^2 \rangle$	$\langle Y_3^3 \rangle$	$\langle Y_3^4 \rangle$	$\langle Y_3^5 \rangle$
χ^2/dof	0.8577	0.6581	0.7948	0.8781	0.9557
$\alpha_s(M_Z)$	0.1156	0.1136	0.1136	0.1129	0.1106
Experimental Error	0.0010	0.0015	0.0019	0.0025	0.0032
x_μ variation: $x_\mu = 0.5$	-0.0005	-0.0008	-0.0006	-0.0002	-0.0002
$x_\mu = 2.0$	0.0015	0.0017	0.0015	0.0013	0.0012
Theoretical Error	0.0010	0.0013	0.0011	0.0008	0.0007

Table D.8: Results for $\alpha_s(Q)$ and α_0 as obtained from fits to Y_3 moments measured by JADE and OPAL for centre-of-mass energies between 14.0 and 206.6 GeV using theoretical NNLO predictions.

NLO	$\langle B_T \rangle$	$\langle B_T^2 \rangle$	$\langle B_T^3 \rangle$	$\langle B_T^4 \rangle$	$\langle B_T^5 \rangle$
χ^2/dof	1.5775	1.6741	1.5926	1.4005	1.1996
$\alpha_s(M_Z)$	0.1199	0.1276	0.1308	0.1327	0.1347
Experimental Error	0.0012	0.0018	0.0023	0.0027	0.0031
x_μ variation: $x_\mu = 0.5$	-0.0037	-0.0078	-0.0093	-0.0101	-0.0108
$x_\mu = 2.0$	0.0049	0.0094	0.0112	0.0123	0.0133
μ_I variation: $\mu_I = 1.0$ Gev	0.0021	0.0032	0.0036	0.0038	0.0041
$\mu_I = 3.0$ Gev	-0.0016	-0.0024	-0.0026	-0.0028	-0.0030
$\mathcal{M}$ variation: $\mathcal{M} - 20\,\%$	0.0010	0.0015	0.0016	0.0017	0.0018
$\mathcal{M} + 20\,\%$	-0.0009	-0.0014	-0.0015	-0.0016	-0.0017
Theoretical Error	0.0054	0.0101	0.0119	0.0130	0.0140
α_0	0.4252	0.4897	0.5180	0.5193	0.5088
Experimental Error	0.0130	0.0105	0.0112	0.0129	0.0146
x_μ variation: $x_\mu = 0.5$	0.0154	0.0083	0.0005	-0.0050	-0.0093
$x_\mu = 2.0$	-0.0106	-0.0074	-0.0015	0.0031	0.0070
$\mathcal{M}$ variation: $\mathcal{M} - 20\,\%$	0.0333	0.0443	0.0500	0.0493	0.0452
$\mathcal{M} + 20\,\%$	-0.0238	-0.0318	-0.0358	-0.0354	-0.0329
Theoretical Error	0.0367	0.0451	0.0501	0.0496	0.0462

Table D.9: Results for $\alpha_s(Q)$ and α_0 as obtained from fits to B_T moments measured by JADE and OPAL for centre-of-mass energies between 14.0 and 206.6 GeV using theoretical NLO predictions.

NNLO	$\langle B_T \rangle$	$\langle B_T^2 \rangle$	$\langle B_T^3 \rangle$	$\langle B_T^4 \rangle$	$\langle B_T^5 \rangle$
χ^2/dof	1.6191	1.4765	1.3723	1.2059	1.0363
$\alpha_s(M_Z)$	0.1164	0.1158	0.1158	0.1158	0.1162
Experimental Error	0.0011	0.0014	0.0017	0.0019	0.0022
x_μ variation: $x_\mu = 0.5$	-0.0012	-0.0027	-0.0033	-0.0035	-0.0037
$x_\mu = 2.0$	0.0016	0.0035	0.0041	0.0044	0.0047
μ_I variation: $\mu_I = 1.0$ Gev	0.0017	0.0017	0.0018	0.0018	0.0019
$\mu_I = 3.0$ Gev	-0.0012	-0.0011	-0.0012	-0.0012	-0.0012
$\mathcal{M}$ variation: $\mathcal{M} - 20\,\%$	0.0010	0.0010	0.0010	0.0010	0.0011
$\mathcal{M} + 20\,\%$	-0.0009	-0.0009	-0.0009	-0.0009	-0.0010
Theoretical Error	0.0025	0.0040	0.0046	0.0049	0.0052
α_0	0.4844	0.5053	0.5059	0.4938	0.4772
Experimental Error	0.0104	0.0094	0.0098	0.0108	0.0117
x_μ variation: $x_\mu = 0.5$	0.0491	0.0272	0.0190	0.0142	0.0109
$x_\mu = 2.0$	-0.0295	-0.0186	-0.0129	-0.0093	-0.0066
$\mathcal{M}$ variation: $\mathcal{M} - 20\,\%$	0.0325	0.0419	0.0436	0.0415	0.0374
$\mathcal{M} + 20\,\%$	-0.0240	-0.0300	-0.0312	-0.0297	-0.0270
Theoretical Error	0.0589	0.0500	0.0476	0.0438	0.0390

Table D.10: Results for $\alpha_s(Q)$ and α_0 as obtained from fits to B_T moments measured by JADE and OPAL for centre-of-mass energies between 14.0 and 206.6 GeV using theoretical NNLO predictions.

NLO	$\langle B_W \rangle$	$\langle B_W^2 \rangle$	$\langle B_W^3 \rangle$	$\langle B_W^4 \rangle$	$\langle B_W^5 \rangle$
χ^2/dof	1.5082	1.2870	1.1182	0.8965	0.6999
$\alpha_s(M_Z)$	0.1128	0.1077	0.1049	0.1023	0.1010
Experimental Error	0.0015	0.0020	0.0027	0.0033	0.0039
x_μ variation: $x_\mu = 0.5$	0.0007	-0.0028	-0.0026	-0.0022	-0.0019
$x_\mu = 2.0$	0.0006	0.0036	0.0035	0.0030	0.0027
μ_I variation: $\mu_I = 1.0$ Gev	0.0018	0.0015	0.0016	0.0016	0.0016
$\mu_I = 3.0$ Gev	-0.0014	-0.0012	-0.0012	-0.0012	-0.0013
$\mathcal{M}$ variation: $\mathcal{M} - 20\,\%$	0.0008	0.0007	0.0007	0.0007	0.0008
$\mathcal{M} + 20\,\%$	-0.0008	-0.0007	-0.0007	-0.0007	-0.0007
Theoretical Error	0.0021	0.0040	0.0039	0.0035	0.0032
α_0	0.3960	0.3552	0.3090	0.2550	0.2025
Experimental Error	0.0106	0.0132	0.0154	0.0180	0.0203
x_μ variation: $x_\mu = 0.5$	0.0870	0.0256	0.0137	0.0107	0.0089
$x_\mu = 2.0$	-0.0401	-0.0166	-0.0097	-0.0074	-0.0059
$\mathcal{M}$ variation: $\mathcal{M} - 20\,\%$	0.0357	0.0308	0.0222	0.0112	-0.0005
$\mathcal{M} + 20\,\%$	-0.0250	-0.0214	-0.0157	-0.0084	-0.0006
Theoretical Error	0.0941	0.0400	0.0261	0.0155	0.0089

Table D.11: Results for $\alpha_s(Q)$ and α_0 as obtained from fits to B_W moments measured by JADE and OPAL for centre-of-mass energies between 14.0 and 206.6 GeV using theoretical NLO predictions.

NNLO	$\langle B_W \rangle$	$\langle B_W^2 \rangle$	$\langle B_W^3 \rangle$	$\langle B_W^4 \rangle$	$\langle B_W^5 \rangle$
χ^2/dof	1.5645	1.2884	1.1158	0.8943	0.7145
$\alpha_s(M_Z)$	0.1117	0.1058	0.1032	0.1014	0.1037
Experimental Error	0.0014	0.0018	0.0025	0.0031	0.0038
x_μ variation: $x_\mu = 0.5$	-0.0010	-0.0007	-0.0006	-0.0003	0.0005
$x_\mu = 2.0$	0.0007	0.0011	0.0010	0.0007	0.0001
μ_I variation: $\mu_I = 1.0$ Gev	0.0015	0.0012	0.0012	0.0012	0.0016
$\mu_I = 3.0$ Gev	-0.0010	-0.0008	-0.0008	-0.0008	-0.0011
$\mathcal{M}$ variation: $\mathcal{M} - 20\,\%$	0.0009	0.0007	0.0007	0.0007	0.0009
$\mathcal{M} + 20\,\%$	-0.0008	-0.0006	-0.0007	-0.0007	-0.0009
Theoretical Error	0.0020	0.0018	0.0017	0.0016	0.0020
α_0	0.4632	0.4029	0.3519	0.2992	0.2744
Experimental Error	0.0083	0.0110	0.0127	0.0143	0.0137
x_μ variation: $x_\mu = 0.5$	0.0393	0.0313	0.0256	0.0221	0.0358
$x_\mu = 2.0$	-0.0384	-0.0232	-0.0181	-0.0155	-0.0220
$\mathcal{M}$ variation: $\mathcal{M} - 20\,\%$	0.0378	0.0314	0.0227	0.0122	0.0045
$\mathcal{M} + 20\,\%$	-0.0270	-0.0222	-0.0163	-0.0093	-0.0045
Theoretical Error	0.0545	0.0443	0.0342	0.0252	0.0360

Table D.12: Results for $\alpha_s(Q)$ and α_0 as obtained from fits to B_W moments measured by JADE and OPAL for centre-of-mass energies between 14.0 and 206.6 GeV using theoretical NNLO predictions.

References

[1] **ALEPH** Collaboration, D. Buskulic *et. al.*, *Studies of QCD in* $e^+e^- \to$ *hadrons at* $E_{\rm cm} = 130$ GeV *and* 136 GeV, *Z. Phys.* **C73** (1997) 409–420.

[2] **ALEPH** Collaboration, A. Heister *et. al.*, *Studies of QCD at* e^+e^- *centre-of-mass energies between* 91 GeV *and* 209 GeV, *Eur. Phys. J.* **C35** (2004) 457–486.

[3] E. B. Zijlstra and W. L. van Neerven, *Order* α_s^2 *QCD corrections to the deep inelastic proton structure functions* F_2 *and* F_L, *Nucl. Phys.* **B383** (1992) 525–574.

[4] E. B. Zijlstra and W. L. van Neerven, *Order* α_s^2 *correction to the structure function* $F_3(x, Q^2)$ *in deep inelastic neutrino - hadron scattering*, *Phys. Lett.* **B297** (1992) 377–384.

[5] A. Einstein, *Über die von der molekularkinetischen Theorie der Wärme geforderte Bewegung von in ruhenden Flüssigkeiten suspendierten Teilchen*, *Ann. d. Phys.* **17** (1905) 549–560.

[6] E. D. Bloom, D. H. Coward, H. DeStaebler, J. Drees, G. Miller, L. W. Mo, R. E. Taylor, M. Breidenbach, J. I. Friedman, G. C. Hartmann and H. W. Kendall, *High-Energy Inelastic* $e - p$ *Scattering at* 6° *and* 10°, *Phys. Rev. Lett.* **23** (Oct, 1969) 930–934.

[7] M. Breidenbach, J. I. Friedman, H. W. Kendall, E. D. Bloom, D. H. Coward, H. DeStaebler, J. Drees, L. W. Mo and R. E. Taylor, *Observed behavior of highly inelastic electron-proton scattering*, *Phys. Rev. Lett.* **23** (Oct, 1969) 935–939.

[8] D. P. Barber *et. al.*, *Discovery of Three Jet Events and a Test of Quantum Chromodynamics at PETRA Energies*, *Phys. Rev. Lett.* **43** (1979) 830.

[9] J. Budenot, *Histoire de la physique et des physiciens de Thalés au boson du Higgs*. Ellipses, 2001.

[10] P. W. Higgs, *Broken symmetries, massless particles and gauge fields*, *Phys. Lett.* **12** (1964) 132–133.

[11] P. W. Higgs, *Broken symmetries ant the masses of gauge bosong*, *Phys. Rev. Lett.* **13** (1964) 508–509.

[12] P. W. Higgs, *Spontaneous Symmetry Breakdown without Massless Bosons*, *Phys. Rev.* **145** (1966) 1156–1163.

[13] F. Englert and R. Brout, *Broken symmetries and the mass of gauge vestor bosons*, *Phys. Rev. Lett.* **13** (1964) 321–322.

[14] G. S. Guralnik, C. R. Hagen and T. W. B. Kibble, *Global conservation laws and massless particles*, *Phys. Rev. Lett.* **13** (1964) 585–587.

[15] F. Halzen and A. D. Martin, *Quarks and leptons: an introductory course in modern particle physics*. New York, Usa: Wiley (1984) 396 p.

[16] T. P. Cheng and L. F. Li, *Gauge theory of elementary particle physics*. Oxford, Uk: Clarendon (1984) 536 p. (Oxford Science Publications).

[17] M. Bohm, A. Denner and H. Joos, *Gauge theories of the strong and electroweak interaction*. Stuttgart, Germany: Teubner (2001) 784 p.

[18] R. P. Feynman, *Very High-Energy Collisions of Hadrons*, *Phys. Rev. Lett.* **23** (Dec, 1969) 1415–1417.

[19] The **CDF** and **D0** Collaboration, the Tevatron New Physics and the Higgs Working Group, *Combined CDF and D0 Upper Limits on Standard Model Higgs-Boson Production with* $2.1 - 5.4$ fb^{-1} *of Data*, `0911.3930`.

[20] D. A. Kosower, *Antenna factorization of gauge-theory amplitudes*, *Phys. Rev.* **D57** (1998) 5410–5416 [`hep-ph/9710213`].

[21] A. Gehrmann-De Ridder, T. Gehrmann and E. W. N. Glover, *Antenna Subtraction at NNLO*, *JHEP* **09** (2005) 056 [`hep-ph/0505111`].

[22] G. Dissertori *et. al.*, *Determination of the strong coupling constant using matched NNLO+NLLA predictions for hadronic event shapes in* e^+e^- *annihilations*, *JHEP* **08** (2009) 036 [`0906.3436`].

[23] T. Gehrmann, M. Jaquier and G. Luisoni, *Hadronization effects in event shape moments*, `0911.2422`.

[24] A. Daleo, A. Gehrmann-De Ridder, T. Gehrmann and G. Luisoni, *Antenna subtraction at NNLO with hadronic initial states: initial-final configurations*, *JHEP* **01** (2010) 118 [0912.0374].

[25] G. Dissertori, I. G. Knowles and M. Schmelling, *High energy experiments and theory*. Oxford, UK: Clarendon (2003) 538 p.

[26] R. K. Ellis, W. J. Stirling and B. R. Webber, *QCD and collider physics*, vol. 8. 1996.

[27] T. Muta, *Foundations of quantum chromodynamics. Second edition*, vol. 57. 1998.

[28] Y. Dothan, M. Gell-Mann and Y. Ne'eman, *Series of hadron energy levels as representations of noncompact groups*, *Phys. Lett.* **17** (1965) 148–151.

[29] H. Fritzsch, M. Gell-Mann and H. Leutwyler, *Advantages of the Color Octet Gluon Picture*, *Phys. Lett.* **B47** (1973) 365–368.

[30] C. N. Yang and R. L. Mills, *Conservation of isotopic spin and isotopic gauge invariance*, *Phys. Rev.* **96** (Oct, 1954) 191–195.

[31] C. Becchi, A. Rouet and R. Stora, *Renormalization of Gauge Theories*, *Annals Phys.* **98** (1976) 287–321.

[32] G. 't Hooft and M. J. G. Veltman, *Regularization and Renormalization of Gauge Fields*, *Nucl. Phys.* **B44** (1972) 189–213.

[33] M. E. Peskin and D. V. Schroeder, *An Introduction to quantum field theory*. Reading, USA: Addison-Wesley (1995) 842 p.

[34] G. Leibbrandt, *Introduction to the technique of dimensional regularization*, *Rew. Mod. Phys.* **47** (1975) 849.

[35] K. G. Chetyrkin, B. A. Kniehl and M. Steinhauser, *Strong coupling constant with flavour thresholds at four loops in the $\overline{\rm MS}$ scheme*, *Phys. Rev. Lett.* **79** (1997) 2184–2187 [hep-ph/9706430].

[36] S. Bethke, *The 2009 Wolrd Average of $\alpha_s(M_Z)$*, *Eur. Phys. J.* **C64** (2009) 689–703 [0908.1135].

[37] T. Becher and M. Neubert, *Infrared singularities of scattering amplitudes in perturbative QCD*, *Phys. Rev. Lett.* **102** (2009) 162001 [0901.0722].

[38] T. Becher and M. Neubert, *On the Structure of Infrared Singularities of Gauge-Theory Amplitudes*, *JHEP* **06** (2009) 081 [0903.1126].

[39] E. Gardi and L. Magnea, *Factorization constraints for soft anomalous dimensions in QCD scattering amplitudes*, *JHEP* **03** (2009) 079 [0901.1091].

[40] L. J. Dixon, E. Gardi and L. Magnea, *On soft singularities at three loops and beyond*, 0910.3653.

[41] G. Giavarini and G. Marchesini, *IR finite S matrix in the QCD coherent state basis*, *Nucl. Phys.* **B296** (1988) 546.

[42] F. Bloch and A. Nordsieck, *Note on the radiation field of the electron*, *Phys. Rev.* **52** (1937) 54.

[43] T. Kinoshita, *Mass singularities of Feynman amplitudes*, *J. Math. Phys.* **3** (1962) 650.

[44] T. Lee and M. Nauenberg, *Degenerate systems and mass singularities*, *Phys. Rev.* **B133** (1964) 1549.

[45] J. E. Huth *et. al.*, *Toward a standardization of jet definitions*, . Presented at Summer Study on High Energy Physics, Reaearch Directions for the Decade, Snowmass, CO, Jun 25 - Jul 13, 1990.

[46] G. P. Salam and G. Soyez, *A practical Seedless Infrared-Safe Cone jet algorithm*, *JHEP* **05** (2007) 086 [0704.0292].

[47] G. C. Blazey *et. al.*, *Run II jet physics*, hep-ex/0005012.

[48] G. P. Salam, *Towards Jetography*, 0906.1833.

[49] **JADE** Collaboration, S. Bethke *et. al.*, *Experimental Investigation of the Energy Dependence of the Strong Coupling Strength*, *Phys. Lett.* **B213** (1988) 235.

[50] S. Catani, Y. L. Dokshitzer, M. Olsson, G. Turnock and B. R. Webber, *New clustering algorithm for multi - jet cross-sections in e^+e^- annihilation*, *Phys. Lett.* **B269** (1991) 432–438.

[51] A. Banfi, G. P. Salam and G. Zanderighi, *Resummed event shapes at hadron - hadron colliders*, *JHEP* **08** (2004) 062 [hep-ph/0407287].

[52] G. Dissertori, F. Moortgat and M. A. Weber, *Hadronic Event-Shape Variables at CMS*, 0810.3208.

[53] A. Banfi, G. P. Salam and G. Zanderighi, *Phenomenology of event shapes at hadron colliders*, 1001.4082.

[54] S. Brandt, C. Peyrou, R. Sosnowski and A. Wroblewski, *The principal axis of jets. an attempt to analyze high- energy collisions as two-body processes*, *Phys. Lett.* **12** (1964) 57–61.

[55] E. Farhi, *A qcd test for jets*, *Phys. Rev. Lett.* **39** (1977) 1587–1588.

[56] L. Clavelli and D. Wyler, *Kinematical bounds on jet variables and the heavy jet mass distribution*, *Phys. Lett.* **B103** (1981) 383.

[57] P. E. L. Rakow and B. R. Webber, *Transverse momentum moments of hadron distributions in QCD jets*, *Nucl. Phys.* **B191** (1981) 63.

[58] G. Parisi, *Super Inclusive Cross-Sections*, *Phys. Lett.* **B74** (1978) 65.

[59] J. F. Donoghue, F. E. Low and S.-Y. Pi, *Tensor analysis of hadronic jets in quantum chromodynamics*, *Phys. Rev.* **D20** (1979) 2759.

[60] N. Brown and W. J. Stirling, *Jet cross-sections at leading double logarithm in e^+e^- annihilation*, *Phys. Lett.* **B252** (1990) 657–662.

[61] W. J. Stirling, *Hard QCD working group: Theory summary*, *J. Phys.* **G17** (1991) 1567–1574.

[62] S. Bethke, Z. Kunszt, D. E. Soper and W. J. Stirling, *New jet cluster algorithms: Next-to-leading order QCD and hadronization corrections*, *Nucl. Phys.* **B370** (1992) 310–334.

[63] S. Bethke, Z. Kunszt, D. E. Soper and W. J. Stirling, *Erratum: Jet Cluster Algorithms in e^+e^- Annihilation*, `hep-ph/9803267`.

[64] G. Dissertori and M. Schmelling, *An Improved theoretical prediction for the two jet rate in e^+e^- annihilation*, *Phys. Lett.* **B361** (1995) 167–178.

[65] G. 't Hooft and M. J. G. Veltman, *Diagrammar*, *NATO Adv. Study Inst. Ser. B Phys.* **4** (1974) 177–322.

[66] J. C. Collins and D. E. Soper, *The Theorems of Perturbative QCD*, *Ann. Rev. Nucl. Part. Sci.* **37** (1987) 383–409.

[67] Y. L. Dokshitzer, *Calculation of the Structure Functions for Deep Inelastic Scattering and e^+e^- Annihilation by Perturbation Theory in Quantum Chromodynamics*, *Sov. Phys. JETP* **46** (1977) 641–653.

[68] V. N. Gribov and L. N. Lipatov, *Deep inelastic e p scattering in perturbation theory*, *Sov. J. Nucl. Phys.* **15** (1972) 438–450.

[69] G. Altarelli and G. Parisi, *Asymptotic Freedom in Parton Language*, *Nucl. Phys.* **B126** (1977) 298.

[70] S. Moch and J. A. M. Vermaseren, *Deep inelastic structure functions at two loops*, *Nucl. Phys.* **B573** (2000) 853–907 [hep-ph/9912355].

[71] J. A. M. Vermaseren, A. Vogt and S. Moch, *The third-order QCD corrections to deep-inelastic scattering by photon exchange*, *Nucl. Phys.* **B724** (2005) 3–182 [hep-ph/0504242].

[72] S. Moch, J. A. M. Vermaseren and A. Vogt, *The three-loop splitting functions in QCD: The non-singlet case*, *Nucl. Phys.* **B688** (2004) 101–134 [hep-ph/0403192].

[73] A. Vogt, S. Moch and J. A. M. Vermaseren, *The three-loop splitting functions in QCD: The singlet case*, *Nucl. Phys.* **B691** (2004) 129–181 [hep-ph/0404111].

[74] A. Daleo, T. Gehrmann and D. Maitre, *Antenna subtraction with hadronic initial states*, *JHEP* **04** (2007) 016 [hep-ph/0612257].

[75] Z. Kunszt and D. E. Soper, *Calculation of jet cross-sections in hadron collisions at order α_s^3*, *Phys. Rev.* **D46** (1992) 192–221.

[76] Z. Bern, L. J. Dixon and A. Ghinculov, *Two-loop correction to Bhabha scattering*, *Phys. Rev.* **D63** (2001) 053007 [hep-ph/0010075].

[77] C. Anastasiou, E. W. N. Glover, C. Oleari and M. E. Tejeda-Yeomans, *Two-loop QCD corrections to massless quark-gluon scattering*, *Nucl. Phys.* **B605** (2001) 486–516 [hep-ph/0101304].

[78] C. Anastasiou, E. W. N. Glover, C. Oleari and M. E. Tejeda-Yeomans, *One-loop QCD corrections to quark scattering at NNLO*, *Phys. Lett.* **B506** (2001) 59–67 [hep-ph/0012007].

[79] C. Anastasiou, E. W. N. Glover, C. Oleari and M. E. Tejeda-Yeomans, *Two-loop QCD corrections to massless identical quark scattering*, *Nucl. Phys.* **B601** (2001) 341–360 [hep-ph/0011094].

[80] E. W. N. Glover, C. Oleari and M. E. Tejeda-Yeomans, *Two-loop QCD corrections to gluon-gluon scattering*, *Nucl. Phys.* **B605** (2001) 467–485 [hep-ph/0102201].

[81] C. Anastasiou, E. W. N. Glover and M. E. Tejeda-Yeomans, *Two-loop QED and QCD corrections to massless fermion-boson scattering*, *Nucl. Phys.* **B629** (2002) 255–289 [hep-ph/0201274].

[82] E. W. N. Glover and M. E. Tejeda-Yeomans, *Two-loop QCD helicity amplitudes for massless quark- massless gauge boson scattering*, *JHEP* **06** (2003) 033 [hep-ph/0304169].

[83] E. W. N. Glover, *Two-loop QCD helicity amplitudes for massless quark-quark scattering*, *JHEP* **04** (2004) 021 [hep-ph/0401119].

[84] Z. Bern, A. De Freitas and L. J. Dixon, *Two-loop amplitudes for gluon fusion into two photons*, *JHEP* **09** (2001) 037 [hep-ph/0109078].

[85] Z. Bern, A. De Freitas and L. J. Dixon, *Two-loop helicity amplitudes for gluon gluon scattering in QCD and supersymmetric Yang-Mills theory*, *JHEP* **03** (2002) 018 [hep-ph/0201161].

[86] Z. Bern, A. De Freitas and L. J. Dixon, *Two-loop helicity amplitudes for quark gluon scattering in QCD and gluino gluon scattering in supersymmetric Yang-Mills theory*, *JHEP* **06** (2003) 028 [hep-ph/0304168].

[87] A. De Freitas and Z. Bern, *Two-loop helicity amplitudes for quark-quark scattering in QCD and gluino gluino scattering in supersymmetric Yang- Mills theory*, *JHEP* **09** (2004) 039 [hep-ph/0409007].

[88] Z. Bern, A. De Freitas, L. J. Dixon, A. Ghinculov and H. L. Wong, *QCD and QED corrections to light-by-light scattering*, *JHEP* **11** (2001) 031 [hep-ph/0109079].

[89] T. Binoth, E. W. N. Glover, P. Marquard and J. J. van der Bij, *Two-loop corrections to Light-by-Light scattering in Supersymmetric QED*, *JHEP* **05** (2002) 060 [hep-ph/0202266].

[90] L. W. Garland, T. Gehrmann, E. W. N. Glover, A. Koukoutsakis and E. Remiddi, *Two-Loop QCD Helicity Amplitudes for $e^+e^- \to 3$ Jets*, *Nucl. Phys.* **B642** (2002) 227–262 [hep-ph/0206067].

[91] L. W. Garland, T. Gehrmann, E. W. N. Glover, A. Koukoutsakis and E. Remiddi, *The Two-Loop QCD Matrix Element for $e^+e^- \to 3$ Jets*, *Nucl. Phys.* **B627** (2002) 107–188 [hep-ph/0112081].

[92] J. M. Campbell and R. K. Ellis, *Next-to-leading order corrections to $W + 2$ jet and $Z + 2$ jet production at hadron colliders*, *Phys. Rev.* **D65** (2002) 113007 [hep-ph/0202176].

[93] L. J. Dixon and A. Signer, *Complete $\mathcal{O}(\alpha_s^3)$ results for $e^+e^- \to (\gamma, Z^0) \to$ four jets*, *Phys. Rev.* **D56** (1997) 4031–4038 [hep-ph/9706285].

[94] A. Signer and L. J. Dixon, *Electron positron annihilation into four jets at next-to- leading order in α_s*, *Phys. Rev. Lett.* **78** (1997) 811–814 [hep-ph/9609460].

[95] Z. Nagy and Z. Trocsanyi, *Next-to-leading order calculation of four-jet shape variables*, *Phys. Rev. Lett.* **79** (1997) 3604–3607 [hep-ph/9707309].

[96] J. M. Campbell, M. A. Cullen and E. W. N. Glover, *Four jet event shapes in electron positron annihilation*, *Eur. Phys. J.* **C9** (1999) 245–265 [hep-ph/9809429].

[97] S. Weinzierl and D. A. Kosower, *QCD corrections to four-jet production and three-jet structure in e^+e^- annihilation*, *Phys. Rev.* **D60** (1999) 054028 [hep-ph/9901277].

[98] W. B. Kilgore and W. T. Giele, *Next-to-leading order gluonic three jet production at hadron colliders*, *Phys. Rev.* **D55** (1997) 7183–7190 [hep-ph/9610433].

[99] Z. Nagy and Z. Trocsanyi, *Multi-jet cross sections in deep inelastic scattering at next-to-leading order*, *Phys. Rev. Lett.* **87** (2001) 082001 [hep-ph/0104315].

[100] Z. Nagy, *Next-to-leading order calculation of three jet observables in hadron hadron collision*, *Phys. Rev.* **D68** (2003) 094002 [hep-ph/0307268].

[101] Z. Nagy, *Three-jet cross sections in hadron hadron collisions at next-to-leading order*, *Phys. Rev. Lett.* **88** (2002) 122003 [hep-ph/0110315].

[102] Z. Bern, L. J. Dixon, D. C. Dunbar and D. A. Kosower, *One-Loop n-Point Gauge Theory Amplitudes, Unitarity and Collinear Limits*, *Nucl. Phys.* **B425** (1994) 217–260 [hep-ph/9403226].

[103] D. A. Kosower, *All-order collinear behavior in gauge theories*, *Nucl. Phys.* **B552** (1999) 319–336 [hep-ph/9901201].

[104] D. A. Kosower and P. Uwer, *One-Loop Splitting Amplitudes in Gauge Theory*, *Nucl. Phys.* **B563** (1999) 477–505 [hep-ph/9903515].

[105] Z. Bern, V. Del Duca and C. R. Schmidt, *The infrared behavior of one-loop gluon amplitudes at next-to-next-to-leading order*, *Phys. Lett.* **B445** (1998) 168–177 [hep-ph/9810409].

[106] Z. Bern, V. Del Duca, W. B. Kilgore and C. R. Schmidt, *The infrared behavior of one-loop QCD amplitudes at next-to-next-to-leading order*, *Phys. Rev.* **D60** (1999) 116001 [hep-ph/9903516].

[107] S. Catani and M. Grazzini, *The soft-gluon current at one-loop order*, *Nucl. Phys.* **B591** (2000) 435–454 [hep-ph/0007142].

[108] D. A. Kosower, *All-orders singular emission in gauge theories*, *Phys. Rev. Lett.* **91** (2003) 061602 [hep-ph/0301069].

[109] S. Weinzierl, *Subtraction terms for one-loop amplitudes with one unresolved parton*, *JHEP* **07** (2003) 052 [hep-ph/0306248].

[110] C. Anastasiou, Z. Bern, L. J. Dixon and D. A. Kosower, *Planar amplitudes in maximally supersymmetric Yang-Mills theory*, *Phys. Rev. Lett.* **91** (2003) 251602 [hep-th/0309040].

[111] Z. Bern, L. J. Dixon and D. A. Kosower, *Two-Loop $g \to gg$ Splitting Amplitudes in QCD*, *JHEP* **08** (2004) 012 [hep-ph/0404293].

[112] S. D. Badger and E. W. N. Glover, *Two-loop splitting functions in QCD*, *JHEP* **07** (2004) 040 [hep-ph/0405236].

[113] A. Gehrmann-De Ridder and E. W. N. Glover, *A complete $\mathcal{O}(\alpha\alpha_s)$ calculation of the Photon + 1 Jet rate in e^+e^- annihilation*, *Nucl. Phys.* **B517** (1998) 269–323 [hep-ph/9707224].

[114] J. M. Campbell and E. W. N. Glover, *Double Unresolved Approximations to Multiparton Scattering Amplitudes*, *Nucl. Phys.* **B527** (1998) 264–288 [hep-ph/9710255].

[115] S. Catani and M. Grazzini, *Collinear factorization and splitting functions for next-to-next-to-leading order QCD calculations*, *Phys. Lett.* **B446** (1999) 143–152 [hep-ph/9810389].

[116] S. Catani and M. Grazzini, *Infrared factorization of tree level QCD amplitudes at the next-to-next-to-leading order and beyond*, *Nucl. Phys.* **B570** (2000) 287–325 [hep-ph/9908523].

[117] F. A. Berends and W. T. Giele, *Multiple Soft Gluon Radiation in Parton Processes*, *Nucl. Phys.* **B313** (1989) 595.

[118] V. Del Duca, A. Frizzo and F. Maltoni, *Factorization of tree QCD amplitudes in the high-energy limit and in the collinear limit*, *Nucl. Phys.* **B568** (2000) 211–262 [hep-ph/9909464].

[119] T. G. Birthwright, E. W. N. Glover, V. V. Khoze and P. Marquard, *Multi-Gluon Collinear Limits from MHV diagrams*, *JHEP* **05** (2005) 013 [hep-ph/0503063].

[120] S. Frixione, Z. Kunszt and A. Signer, *Three jet cross-sections to next-to-leading order*, *Nucl. Phys.* **B467** (1996) 399–442 [hep-ph/9512328].

[121] S. Catani and M. H. Seymour, *A general algorithm for calculating jet cross sections in NLO QCD*, *Nucl. Phys.* **B485** (1997) 291–419 [hep-ph/9605323].

[122] D. A. Kosower, *Antenna factorization in strongly-ordered limits*, *Phys. Rev.* **D71** (2005) 045016 [hep-ph/0311272].

[123] Z. Nagy, G. Somogyi and Z. Trocsanyi, *Separation of soft and collinear infrared limits of QCD squared matrix elements*, hep-ph/0702273.

[124] D. A. Kosower, *Multiple singular emission in gauge theories*, *Phys. Rev.* **D67** (2003) 116003 [hep-ph/0212097].

[125] S. Weinzierl, *Subtraction terms at NNLO*, *JHEP* **03** (2003) 062 [hep-ph/0302180].

[126] W. B. Kilgore, *Subtraction terms for hadronic production processes at next-to-next-to-leading order*, *Phys. Rev.* **D70** (2004) 031501 [hep-ph/0403128].

[127] S. Frixione and M. Grazzini, *Subtraction at NNLO*, *JHEP* **06** (2005) 010 [hep-ph/0411399].

[128] G. Somogyi, Z. Trocsanyi and V. Del Duca, *Matching of singly- and doubly-unresolved limits of tree-level QCD squared matrix elements*, *JHEP* **06** (2005) 024 [hep-ph/0502226].

[129] G. Somogyi, Z. Trocsanyi and V. Del Duca, *A subtraction scheme for computing QCD jet cross sections at NNLO: regularization of doubly-real emissions*, *JHEP* **01** (2007) 070 [hep-ph/0609042].

[130] G. Somogyi and Z. Trocsanyi, *A subtraction scheme for computing QCD jet cross sections at NNLO: regularization of real-virtual emission*, *JHEP* **01** (2007) 052 [hep-ph/0609043].

[131] G. Somogyi and Z. Trocsanyi, *A subtraction scheme for computing QCD jet cross sections at NNLO: integrating the subtraction terms I*, *JHEP* **08** (2008) 042 [0807.0509].

[132] U. Aglietti, V. Del Duca, C. Duhr, G. Somogyi and Z. Trocsanyi, *Analytic integration of real-virtual counterterms in NNLO jet cross sections I*, *JHEP* **09** (2008) 107 [0807.0514].

[133] G. Somogyi, *Subtraction with hadronic initial states: an NNLO- compatible scheme*, *JHEP* **05** (2009) 016 [0903.1218].

[134] P. Bolzoni, S.-O. Moch, G. Somogyi and Z. Trocsanyi, *Analytic integration of real-virtual counterterms in NNLO jet cross sections II*, *JHEP* **08** (2009) 079 [0905.4390].

[135] S. Catani and M. Grazzini, *An NNLO subtraction formalism in hadron collisions and its application to Higgs boson production at the LHC*, *Phys. Rev. Lett.* **98** (2007) 222002 [hep-ph/0703012].

[136] A. Gehrmann-De Ridder and M. Ritzmann, *NLO Antenna Subtraction with Massive Fermions*, *JHEP* **07** (2009) 041 [0904.3297].

[137] A. Gehrmann-De Ridder, T. Gehrmann and E. W. N. Glover, *Infrared Structure of $e^+e^- \to 2$ jets at NNLO*, *Nucl. Phys.* **B691** (2004) 195–222 [hep-ph/0403057].

[138] A. Gehrmann-De Ridder, T. Gehrmann and E. W. N. Glover, *Quark-Gluon Antenna Functions from Neutralino Decay*, *Phys. Lett.* **B612** (2005) 36–48 [hep-ph/0501291].

[139] A. Gehrmann-De Ridder, T. Gehrmann and E. W. N. Glover, *Gluon-Gluon Antenna Functions from Higgs Boson Decay*, *Phys. Lett.* **B612** (2005) 49–60 [hep-ph/0502110].

[140] A. Gehrmann-De Ridder, T. Gehrmann, E. W. N. Glover and G. Heinrich, *Infrared structure of $e^+e^- \to 3$ jets at NNLO*, *JHEP* **11** (2007) 058 [0710.0346].

[141] A. Gehrmann-De Ridder, T. Gehrmann, E. W. N. Glover and G. Heinrich, *NNLO corrections to event shapes in e^+e^- annihilation*, *JHEP* **12** (2007) 094 [0711.4711].

[142] A. Gehrmann-De Ridder, T. Gehrmann, E. W. N. Glover and G. Heinrich, *Jet rates in electron-positron annihilation at $\mathcal{O}(\alpha_s^3)$ in QCD*, *Phys. Rev. Lett.* **100** (2008) 172001 [0802.0813].

[143] S. Weinzierl, *Event shapes and jet rates in electron-positron annihilation at NNLO*, *JHEP* **06** (2009) 041 [0904.1077].

[144] S. Weinzierl, *NNLO predictions for event shapes and jet rates in electron-positron annihilation*, 1001.1281.

[145] S. Weinzierl, *NNLO corrections to 3-jet observables in electron-positron annihilation*, *Phys. Rev. Lett.* **101** (2008) 162001 [0807.3241].

[146] S. Weinzierl, *The infrared structure of $e^+e^- \to 3$ jets at NNLO reloaded*, *JHEP* **07** (2009) 009 [0904.1145].

[147] C. Anastasiou and K. Melnikov, *Higgs boson production at hadron colliders in NNLO QCD*, *Nucl. Phys.* **B646** (2002) 220–256 [hep-ph/0207004].

[148] F. V. Tkachov, *A Theorem on Analytical Calculability of Four Loop Renormalization Group Functions*, *Phys. Lett.* **B100** (1981) 65–68.

[149] K. G. Chetyrkin and F. V. Tkachov, *Integration by Parts: The Algorithm to Calculate beta Functions in 4 Loops*, *Nucl. Phys.* **B192** (1981) 159–204.

[150] T. Gehrmann and E. Remiddi, *Differential equations for two-loop four-point functions*, *Nucl. Phys.* **B580** (2000) 485–518 [hep-ph/9912329].

[151] S. Laporta, *High-precision calculation of multi-loop Feynman integrals by difference equations*, *Int. J. Mod. Phys.* **A15** (2000) 5087–5159 [hep-ph/0102033].

[152] A. V. Kotikov, *Differential equations method: New technique for massive Feynman diagrams calculation*, *Phys. Lett.* **B254** (1991) 158–164.

[153] A. V. Kotikov, *Differential equations method: The Calculation of vertex type Feynman diagrams*, *Phys. Lett.* **B259** (1991) 314–322.

[154] A. V. Kotikov, *Differential equation method: The Calculation of N point Feynman diagrams*, *Phys. Lett.* **B267** (1991) 123–127.

[155] E. Remiddi, *Differential equations for Feynman graph amplitudes*, *Nuovo Cim.* **A110** (1997) 1435–1452 [hep-th/9711188].

[156] M. Caffo, H. Czyz, S. Laporta and E. Remiddi, *The master differential equations for the 2-loop sunrise selfmass amplitudes*, *Nuovo Cim.* **A111** (1998) 365–389 [hep-th/9805118].

[157] M. Caffo, H. Czyz, S. Laporta and E. Remiddi, *Master equations for master amplitudes*, *Acta Phys. Polon.* **B29** (1998) 2627–2635 [hep-th/9807119].

[158] A. Gehrmann-De Ridder, T. Gehrmann and G. Heinrich, *Four-particle phase space integrals in massless QCD*, *Nucl. Phys.* **B682** (2004) 265–288 [hep-ph/0311276].

[159] E. Remiddi and J. A. M. Vermaseren, *Harmonic polylogarithms*, *Int. J. Mod. Phys.* **A15** (2000) 725–754 [hep-ph/9905237].

[160] T. Gehrmann and E. Remiddi, *Numerical evaluation of harmonic polylogarithms*, *Comput. Phys. Commun.* **141** (2001) 296–312 [hep-ph/0107173].

[161] D. Maitre, *HPL, a Mathematica implementation of the harmonic polylogarithms*, *Comput. Phys. Commun.* **174** (2006) 222–240 [hep-ph/0507152].

[162] D. Maitre, *Extension of HPL to complex arguments*, hep-ph/0703052.

[163] T. Binoth and G. Heinrich, *An automatized algorithm to compute infrared divergent multi-loop integrals*, *Nucl. Phys.* **B585** (2000) 741–759 [hep-ph/0004013].

[164] T. Binoth and G. Heinrich, *Numerical evaluation of multi-loop integrals by sector decomposition*, *Nucl. Phys.* **B680** (2004) 375–388 [hep-ph/0305234].

[165] G. Heinrich, *A numerical method for NNLO calculations*, *Nucl. Phys. Proc. Suppl.* **116** (2003) 368–372 [hep-ph/0211144].

[166] C. Anastasiou, K. Melnikov and F. Petriello, *A new method for real radiation at NNLO*, *Phys. Rev.* **D69** (2004) 076010 [hep-ph/0311311].

[167] D. Graudenz, *Three jet production in deep inelastic electron - proton scattering to order α_s^2*, *Phys. Lett.* **B256** (1991) 518–522.

[168] D. Graudenz, *Next-to-leading order QCD corrections to jet cross- sections and jet rates in deeply inelastic electron proton scattering*, *Phys. Rev.* **D49** (1994) 3291–3319 [hep-ph/9307311].

[169] D. Graudenz, *DISASTER++ version 1.0*, hep-ph/9710244.

[170] E. Mirkes and D. Zeppenfeld, *Dijet Production at HERA in Next-to-Leading Order*, *Phys. Lett.* **B380** (1996) 205–212 [hep-ph/9511448].

[171] S. Catani and M. H. Seymour, *The Dipole Formalism for the Calculation of QCD Jet Cross Sections at Next-to-Leading Order*, *Phys. Lett.* **B378** (1996) 287–301 [hep-ph/9602277].

[172] B. Potter, *JetViP 1.1: Calculating one jet and two jet cross-sections with virtual photons in NLO QCD*, *Comput. Phys. Commun.* **119** (1999) 45–66 [hep-ph/9806437].

[173] T. Gehrmann and E. Remiddi, *Analytic continuation of massless two-loop four-point functions*, *Nucl. Phys.* **B640** (2002) 379–411 [hep-ph/0207020].

[174] T. Gehrmann and E. W. N. Glover, *Two-Loop QCD Helicity Amplitudes for $(2+1)$-Jet Production in Deep Inelastic Scattering*, *Phys. Lett.* **B676** (2009) 146–151 [0904.2665].

[175] G. Soar, A. Vogt, S. Moch and J. Vermaseren, *On Higgs-exchange DIS, physical evolution kernels and fourth-order splitting functions at large x*, 0912.0369.

[176] T. Gehrmann, T. Huber and D. Maitre, *Two-loop quark and gluon form factors in dimensional regularisation*, *Phys. Lett.* **B622** (2005) 295–302 [hep-ph/0507061].

[177] **H1** Collaboration, A. Aktas *et. al.*, *Measurement of Inclusive Jet Production in Deep-Inelastic Scattering at High Q^2 and Determination of the Strong Coupling*, *Phys. Lett.* **B653** (2007) 134–144 [0706.3722].

[178] **H1** Collaboration, C. Adloff *et. al.*, *Measurement of inclusive jet cross-sections in deep- inelastic e^-p scattering at HERA*, *Phys. Lett.* **B542** (2002) 193–206 [hep-ex/0206029].

[179] **H1** Collaboration, C. Adloff *et. al.*, *Dijet production in charged and neutral current e^+p interactions at high Q^2*, *Eur. Phys. J.* **C19** (2001) 429–440 [hep-ex/0010016].

[180] **ZEUS** Collaboration, S. Chekanov *et. al.*, *Jet-radius dependence of inclusive-jet cross sections in deep inelastic scattering at HERA*, *Phys. Lett.* **B649** (2007) 12–24 [hep-ex/0701039].

[181] **ZEUS** Collaboration, S. Chekanov *et. al.*, *Inclusive-jet and dijet cross sections in deep inelastic scattering at HERA*, *Nucl. Phys.* **B765** (2007) 1–30 [hep-ex/0608048].

[182] **ZEUS** Collaboration, S. Chekanov *et. al.*, *Dijet production in neutral current deep inelastic scattering at HERA*, *Eur. Phys. J.* **C23** (2002) 13–27 [hep-ex/0109029].

[183] **H1** Collaboration, M. Gouzevitch, *Jet cross sections and α_s in DIS*, . Prepared for 16th International Workshop on Deep Inelastic Scattering and Related Subjects (DIS 2008), London, England, 7-11 Apr 2008.

[184] A. D. Martin, W. J. Stirling, R. S. Thorne and G. Watt, *Update of parton distributions at NNLO*, *Phys. Lett.* **B652** (2007) 292–299 [0706.0459].

[185] S. Alekhin, K. Melnikov and F. Petriello, *Fixed target Drell-Yan data and NNLO QCD fits of parton distribution functions*, *Phys. Rev.* **D74** (2006) 054033 [hep-ph/0606237].

[186] P. Jimenez-Delgado and E. Reya, *Dynamical NNLO parton distributions*, *Phys. Rev.* **D79** (2009) 074023 [0810.4274].

[187] A. D. Martin, W. J. Stirling, R. S. Thorne and G. Watt, *Parton distributions for the LHC*, *Eur. Phys. J.* **C63** (2009) 189–285 [0901.0002].

[188] R. Hamberg, W. L. van Neerven and T. Matsuura, *A Complete calculation of the order α_s^2 correction to the Drell-Yan K factor*, *Nucl. Phys.* **B359** (1991) 343–405.

[189] C. Anastasiou, L. J. Dixon, K. Melnikov and F. Petriello, *High precision QCD at hadron colliders: Electroweak gauge boson rapidity distributions at NNLO*, *Phys. Rev.* **D69** (2004) 094008 [hep-ph/0312266].

[190] K. Melnikov and F. Petriello, *Electroweak gauge boson production at hadron colliders through $\mathcal{O}(\alpha_s^2)$*, *Phys. Rev.* **D74** (2006) 114017 [hep-ph/0609070].

[191] S. Alekhin and S. Moch, *Higher order QCD corrections to charged-lepton deep-inelastic scattering and global fits of parton distributions*, *Phys. Lett.* **B672** (2009) 166–171 [0811.1412].

[192] K. Hagiwara and D. Zeppenfeld, *Amplitudes for Multiparton Processes Involving a Current at e^+e^-, e^+p, and Hadron Colliders*, *Nucl. Phys.* **B313** (1989) 560.

[193] F. A. Berends, W. T. Giele and H. Kuijf, *Exact Expressions for Processes Involving a Vector Boson and Up to Five Partons*, *Nucl. Phys.* **B321** (1989) 39.

[194] N. K. Falck, D. Graudenz and G. Kramer, *Cross section for five jet production in e^+e^- annihilation*, *Nucl. Phys.* **B328** (1989) 317.

[195] Z. Bern, L. J. Dixon, D. A. Kosower and S. Weinzierl, *One-loop amplitudes for $e^+e^- \to \bar{q}q\bar{Q}Q$*, *Nucl. Phys.* **B489** (1997) 3–23 [hep-ph/9610370].

[196] Z. Bern, L. J. Dixon and D. A. Kosower, *One-loop amplitudes for e^+e^- to four partons*, *Nucl. Phys.* **B513** (1998) 3–86 [hep-ph/9708239].

[197] E. W. N. Glover and D. J. Miller, 2, *The One-loop QCD Corrections for $\gamma^* \to Q\bar{Q}q\bar{q}$*, *Phys. Lett.* **B396** (1997) 257–263 [hep-ph/9609474].

[198] J. M. Campbell, E. W. N. Glover and D. J. Miller, 2, *The One-loop QCD Corrections for $\gamma^* \to q\bar{q}gg$*, *Phys. Lett.* **B409** (1997) 503–508 [hep-ph/9706297].

[199] R. Boughezal, A. Gehrmann-De Ridder and M. Ritzmann, *NNLO antenna subtraction with two hadronic initial states*, 1001.2396.

[200] S. Catani, L. Trentadue, G. Turnock and B. R. Webber, *Resummation of large logarithms in e^+e^- event shape distributions*, *Nucl. Phys.* **B407** (1993) 3–42.

[201] T. Gehrmann, G. Luisoni and H. Stenzel, *Matching NLLA+NNLO for event shape distributions*, *Phys. Lett.* **B664** (2008) 265–273 [0803.0695].

[202] R. W. L. Jones, M. Ford, G. P. Salam, H. Stenzel and D. Wicke, *Theoretical uncertainties on α_s from event-shape variables in e^+e^- annihilations*, *JHEP* **12** (2003) 007 [hep-ph/0312016].

[203] R. K. Ellis, D. A. Ross and A. E. Terrano, *The Perturbative Calculation of Jet Structure in e^+e^- Annihilation*, *Nucl. Phys.* **B178** (1981) 421.

[204] R. K. Ellis, D. A. Ross and A. E. Terrano, *Calculation of Event Shape Parameters in e^+e^- Annihilation*, *Phys. Rev. Lett.* **45** (1980) 1226–1229.

[205] Z. Kunszt, *Comment on the $\mathcal{O}(\alpha_s^2)$ Corrections to Jet Production in e^+e^- Annihilation*, *Phys. Lett.* **B99** (1981) 429.

[206] J. A. M. Vermaseren, K. J. F. Gaemers and S. J. Oldham, *Perturbative QCD Calculation of Jet Cross-Sections in e^+e^- Annihilation*, *Nucl. Phys.* **B187** (1981) 301.

[207] K. Fabricius, I. Schmitt, G. Kramer and G. Schierholz, *Higher Order Perturbative QCD Calculation of Jet Cross- Sections in e^+e^- Annihilation*, *Zeit. Phys.* **C11** (1981) 315.

[208] Z. Kunszt, P. Nason, G. Marchesini and B. R. Webber, *QCD AT LEP*, . CERN Yellow Report 89-08 v1, Geneva, Switzerland, 1989.

[209] W. T. Giele and E. W. N. Glover, *Higher order corrections to jet cross-sections in e^+e^- annihilation*, *Phys. Rev.* **D46** (1992) 1980–2010.

[210] A. Gehrmann-De Ridder, T. Gehrmann, E. W. N. Glover and G. Heinrich, *Second-order QCD corrections to the thrust distribution*, *Phys. Rev. Lett.* **99** (2007) 132002 [0707.1285].

[211] A. Denner, S. Dittmaier, T. Gehrmann and C. Kurz, *Electroweak corrections to three-jet production in electron-positron annihilation*, *Phys. Lett.* **B679** (2009) 219–222 [0906.0372].

[212] A. Denner, S. Dittmaier, T. Gehrmann and C. Kurz, *Electroweak corrections to hadronic event shapes and jet production in e^+e^- annihilation*, 1003.0986.

[213] P. A. Baikov, K. G. Chetyrkin and J. H. Kuhn, *Adler Function, Bjorken Sum Rule, and the Crewther Relation to Order α_s^4 in a General Gauge Theory*, 1001.3606.

[214] T. Becher and M. D. Schwartz, *A Precise determination of α_s from LEP thrust data using effective field theory*, *JHEP* **07** (2008) 034 [0803.0342].

[215] **OPAL** Collaboration, P. D. Acton *et. al.*, *A Determination of $\alpha_s(M_{Z^0})$ at LEP using resummed QCD calculations*, *Z. Phys.* **C59** (1993) 1–20.

[216] **OPAL** Collaboration, G. Alexander *et. al.*, *QCD studies with e^+e^- annihilation data at* 130 GeV *and* 136 GeV, *Z. Phys.* **C72** (1996) 191–206.

[217] **OPAL** Collaboration, K. Ackerstaff *et. al.*, *QCD studies with e^+e^- annihilation data at* 161 GeV, *Z. Phys.* **C75** (1997) 193–207.

[218] **OPAL** Collaboration, G. Abbiendi *et. al.*, *QCD studies with e^+e^- annihilation data at* 172 GeV *to* 189 GeV, *Eur. Phys. J.* **C16** (2000) 185–210.

[219] **OPAL** Collaboration, G. Abbiendi *et. al.*, *Measurement of event shape distributions and moments in $e^+e^- \to$ hadrons at* 91 GeV - 209 GeV *and a determination of α_s*, *Eur. Phys. J.* **C40** (2005) 287–316.

[220] **L3** Collaboration, M. Acciarri *et. al.*, *Study of the structure of hadronic events and determination of α_s at $\sqrt{s} =$* 130 GeV *and* 136 GeV, *Phys. Lett.* **B371** (1996) 137–148.

[221] **L3** Collaboration, M. Acciarri *et. al.*, *QCD studies and determination of α_s in e^+e^- collisions at $\sqrt{s} =$* 161 GeV *and* 172 GeV, *Phys. Lett.* **B404** (1997) 390–402.

[222] **L3** Collaboration, M. Acciarri *et. al.*, *QCD results from studies of hadronic events produced in e^+e^- annihilations at $\sqrt{s} =$* 183 GeV, *Phys. Lett.* **B444** (1998) 569–582.

[223] **L3** Collaboration, P. Achard *et. al.*, *Determination of alpha$_s$ from hadronic event shapes in e^+e^- annihilation at* 192 GeV $\leq \sqrt{s} \leq$ 208 GeV, *Phys. Lett.* **B536** (2002) 217–228.

[224] **L3** Collaboration, P. Achard *et. al.*, *Studies of hadronic event structure in e^+e^- annihilation from* 30 GeV *to* 209 GeV *with the L3 detector*, *Phys. Rept.* **399** (2004) 71–174.

[225] **DELPHI** Collaboration, P. Abreu *et. al.*, *Energy dependence of event shapes and of α_s at LEP-2*, *Phys. Lett.* **B456** (1999) 322–340.

[226] **DELPHI** Collaboration, J. Abdallah *et. al.*, *A study of the energy evolution of event shape distributions and their means with the DELPHI detector at LEP*, *Eur. Phys. J.* **C29** (2003) 285–312.

[227] **DELPHI** Collaboration, J. Abdallah *et. al.*, *The measurement of α_s from event shapes with the DELPHI detector at the highest LEP energies*, *Eur. Phys. J.* **C37** (2004) 1–23.

[228] **SLD** Collaboration, K. Abe *et. al.*, *Measurement of $\alpha_s(M_Z^2)$ from hadronic event observables at the Z^0 resonance*, *Phys. Rev.* **D51** (1995) 962–984.

[229] **JADE** Collaboration, P. A. Movilla Fernandez, O. Biebel, S. Bethke, S. Kluth and P. Pfeifenschneider, *A study of event shapes and determinations of α_s using data of e^+e^- annihilations at $\sqrt{s} = 22$ GeV to 44 GeV*, *Eur. Phys. J.* **C1** (1998) 461–478 [hep-ex/9708034].

[230] **JADE** Collaboration, P. Pfeifenschneider *et. al.*, *QCD analyses and determinations of α_s in e^+e^- annihilation at energies between* 35 GeV *and* 189 GeV, *Eur. Phys. J.* **C17** (2000) 19–51 [hep-ex/0001055].

[231] S. Catani, G. Turnock, B. R. Webber and L. Trentadue, *Thrust distribution in e^+e^- annihilation*, *Phys. Lett.* **B263** (1991) 491–497.

[232] S. Catani, G. Turnock and B. R. Webber, *Heavy jet mass distribution in e^+e^- annihilation*, *Phys. Lett.* **B272** (1991) 368–372.

[233] E. Gardi and J. Rathsman, *The thrust and heavy-jet mass distributions in the two-jet region*, *Nucl. Phys.* **B638** (2002) 243–287 [hep-ph/0201019].

[234] S. Catani, G. Turnock and B. R. Webber, *Jet broadening measures in e^+e^- annihilation*, *Phys. Lett.* **B295** (1992) 269–276.

[235] Y. L. Dokshitzer, A. Lucenti, G. Marchesini and G. P. Salam, *On the QCD analysis of jet broadening*, *JHEP* **01** (1998) 011 [hep-ph/9801324].

[236] S. Catani and B. R. Webber, *Resummed C-parameter distribution in e^+e^- annihilation*, *Phys. Lett.* **B427** (1998) 377–384 [hep-ph/9801350].

[237] E. Gardi and L. Magnea, *The C parameter distribution in e^+e^- annihilation*, *JHEP* **08** (2003) 030 [hep-ph/0306094].

[238] A. Banfi, G. P. Salam and G. Zanderighi, *Semi-numerical resummation of event shapes*, *JHEP* **01** (2002) 018 [hep-ph/0112156].

[239] A. Banfi and G. Zanderighi. private communication.

[240] A. Banfi, G. P. Salam and G. Zanderighi, *Principles of general final-state resummation and automated implementation*, *JHEP* **03** (2005) 073 [hep-ph/0407286].

[241] G. Luisoni. http://www-theorie.physik.uzh.ch/ luisonig/lormeso.

[242] R. Brun, O. Couet, C. E. Vandoni and P. Zanarini, *Visualization of scientific data for high energy physics: PAW, a general-purpose portable software tool for data analysis and presentation*, . Prepared for International Workshop on Software Engineering, Artificial Intelligence and Expert Systems for High-energy and Nuclear Physics, Lyon, France, 19-24 Mar 1990.

[243] R. Brun and F. Rademakers, *ROOT: An object oriented data analysis framework*, *Nucl. Instrum. Meth.* **A389** (1997) 81–86.

[244] S. Bethke, *Experimental tests of asymptotic freedom*, *Prog. Part. Nucl. Phys.* **58** (2007) 351–386 [hep-ex/0606035].

[245] **L3** Collaboration, M. Acciarri *et. al.*, *QCD studies in e^+e^- annihilation from* 30 GeV *to* 189 GeV, *Phys. Lett.* **B489** (2000) 65–80.

[246] G. Dissertori *et. al.*, *First determination of the strong coupling constant using NNLO predictions for hadronic event shapes in e^+e^- annihilations*, *JHEP* **02** (2008) 040 [0712.0327].

[247] S. Catani and B. R. Webber, *Infrared safe but infinite: Soft gluon divergences inside the physical region*, *JHEP* **10** (1997) 005 [hep-ph/9710333].

[248] T. Sjostrand *et. al.*, *High-energy physics event generation with PYTHIA 6.1*, *Comput. Phys. Commun.* **135** (2001) 238–259 [hep-ph/0010017].

[249] G. Corcella *et. al.*, *HERWIG 6.5: an event generator for Hadron Emission Reactions With Interfering Gluons (including supersymmetric processes)*, *JHEP* **01** (2001) 010 [hep-ph/0011363].

[250] L. Lonnblad, *ARIADNE version 4: A Program for simulation of QCD cascades implementing the color dipole model*, *Comput. Phys. Commun.* **71** (1992) 15–31.

[251] **ALEPH** Collaboration, R. Barate *et. al.*, *Studies of quantum chromodynamics with the ALEPH detector*, *Phys. Rept.* **294** (1998) 1–165.

[252] O. Latunde-Dada, *Herwig Monte Carlo At Next-To-Leading Order for e^+e^- annihilation and lepton pair production*, *JHEP* **11** (2007) 040 [0708.4390].

[253] O. Latunde-Dada, S. Gieseke and B. Webber, *A positive-weight next-to-leading-order Monte Carlo for e^+e^- annihilation to hadrons*, *JHEP* **02** (2007) 051 [hep-ph/0612281].

[254] A. Gehrmann-De Ridder, T. Gehrmann, E. W. N. Glover and G. Heinrich, *NNLO moments of event shapes in e^+e^- annihilation*, *JHEP* **05** (2009) 106 [0903.4658].

[255] C. Pahl, S. Bethke, S. Kluth, J. Schieck and the **JADE** collaboration, *Study of moments of event shapes and a determination of α_s using e^+e^- annihilation data from JADE*, *Eur. Phys. J.* **C60** (2009) 181–196 [0810.2933].

[256] S. Weinzierl, *Moments of event shapes in electron-positron annihilation at NNLO*, *Phys. Rev.* **D80** (2009) 094018 [0909.5056].

[257] S. Kluth, P. A. Movilla Fernandez, S. Bethke, C. Pahl and P. Pfeifenschneider, *A measurement of the QCD colour factors using event shape distributions at $\sqrt{s} = 14$ GeV to 189 GeV*, *Eur. Phys. J.* **C21** (2001) 199–210 [hep-ex/0012044].

[258] M. Beneke, *Renormalons*, *Phys. Rept.* **317** (1999) 1–142 [hep-ph/9807443].

[259] P. M. Zerwas and H. A. Kastrup, *QCD - 20 years later. Proceedings, Workshop, Aachen, Germany, June 9-13, 1992. Vol. 1, 2*. Singapore, Singapore: World Scientific (1993) 1-869, 1992. Contribution of A. H. Mueller.

[260] A. V. Manohar and M. B. Wise, *Power suppressed corrections to hadronic event shapes*, *Phys. Lett.* **B344** (1995) 407–412 [hep-ph/9406392].

[261] B. R. Webber, *Estimation of power corrections to hadronic event shapes*, *Phys. Lett.* **B339** (1994) 148–150 [hep-ph/9408222].

[262] G. P. Korchemsky and G. Sterman, *Nonperturbative corrections in resummed cross-sections*, *Nucl. Phys.* **B437** (1995) 415–432 [hep-ph/9411211].

[263] Y. L. Dokshitzer and B. R. Webber, *Calculation of power corrections to hadronic event shapes*, *Phys. Lett.* **B352** (1995) 451–455 [hep-ph/9504219].

[264] R. Akhoury and V. I. Zakharov, *On the universality of the leading, $1/Q$ power corrections in QCD*, *Phys. Lett.* **B357** (1995) 646–652 [hep-ph/9504248].

[265] Y. L. Dokshitzer, G. Marchesini and B. R. Webber, *Dispersive Approach to Power-Behaved Contributions in QCD Hard Processes*, *Nucl. Phys.* **B469** (1996) 93–142 [hep-ph/9512336].

[266] P. Nason and M. H. Seymour, *Infrared renormalons and power suppressed effects in e^+e^- jet events*, *Nucl. Phys.* **B454** (1995) 291–312 [hep-ph/9506317].

[267] Y. L. Dokshitzer and B. R. Webber, *Power corrections to event shape distributions*, *Phys. Lett.* **B404** (1997) 321–327 [hep-ph/9704298].

[268] Y. L. Dokshitzer, A. Lucenti, G. Marchesini and G. P. Salam, *Universality of $1/Q$ corrections to jet-shape observables rescued*, *Nucl. Phys.* **B511** (1998) 396–418 [hep-ph/9707532].

[269] G. P. Korchemsky and S. Tafat, *On power corrections to the event shape distributions in QCD*, *JHEP* **10** (2000) 010 [hep-ph/0007005].

[270] A. V. Belitsky, G. P. Korchemsky and G. Sterman, *Energy flow in QCD and event shape functions*, *Phys. Lett.* **B515** (2001) 297–307 [hep-ph/0106308].

[271] E. Gardi and G. Grunberg, *Power corrections in the single dressed gluon approximation: The average thrust as a case study*, *JHEP* **11** (1999) 016 [hep-ph/9908458].

[272] J. M. Campbell, E. W. N. Glover and C. J. Maxwell, *Determination of $\Lambda_{\rm QCD}$ from the measured energy dependence of $< 1 - T >$*, *Phys. Rev. Lett.* **81** (1998) 1568–1571 [hep-ph/9803254].

[273] M. Dasgupta and G. P. Salam, *Event shapes in e^+e^- annihilation and deep inelastic scattering*, *J. Phys.* **G30** (2004) R143 [hep-ph/0312283].

[274] Y. L. Dokshitzer, *Perturbative QCD theory (includes our knowledge of α_s)*, hep-ph/9812252.

[275] Y. L. Dokshitzer, A. Lucenti, G. Marchesini and G. P. Salam, *On the universality of the Milan factor for $1/Q$ power corrections to jet shapes*, *JHEP* **05** (1998) 003 [hep-ph/9802381].

[276] Y. L. Dokshitzer, G. Marchesini and G. P. Salam, *Revisiting non-perturbative effects in the jet broadenings*, *Eur. Phys. J. direct* **C1** (1999) 3 [hep-ph/9812487].

[277] G. P. Salam and D. Wicke, *Hadron masses and power corrections to event shapes*, *JHEP* **05** (2001) 061 [hep-ph/0102343].

[278] R. A. Davison and B. R. Webber, *Non-Perturbative Contribution to the Thrust Distribution in e^+e^- Annihilation*, *Eur. Phys. J.* **C59** (2009) 13–25 [0809.3326].

[279] S. Catani, B. R. Webber and G. Marchesini, *QCD coherent branching and semiinclusive processes at large x*, *Nucl. Phys.* **B349** (1991) 635–654.

[280] E. Gardi and L. Magnea, *Infrared singularities in QCD amplitudes*, 0908.3273.

[281] S. Moch, J. A. M. Vermaseren and A. Vogt, *The quark form factor at higher orders*, *JHEP* **08** (2005) 049 [hep-ph/0507039].

[282] S. Moch, J. A. M. Vermaseren and A. Vogt, *Three-loop results for quark and gluon form factors*, *Phys. Lett.* **B625** (2005) 245–252 [hep-ph/0508055].

[283] C. J. Pahl, *Untersuchung perturbativer und nichtperturbativer Struktur der Momente hadronischer Ereignisformvariablen mit den Experimenten JADE und OPAL*, Ph.D. thesis, MPI Munich 2007.

[284] G. Salam. private communication.

[285] **Particle Data Group** Collaboration, C. Amsler *et. al.*, *Review of particle physics*, *Phys. Lett.* **B667** (2008) 1.

[286] A. Erdelyi, *Higher Trascendental Functions, vol. 1.* Mc Graw-Hill, New York, 1953.

[287] I. Abramowitz, M. Stegun, *Handbook of mathematical functions.* United States Departement of Commerce, 1964.
http://www.math.sfu.ca/ cbm/aands/intro.htm.

[288] A. Gehrmann-De Ridder, *Radiative Corrections to the Photon + 1 Jet Rate at LEP.* PhD thesis, Departement of Physics, University of Durham, 1997.

[289] E. Byckling and K. Kajantie, *Particle Kinematics.* John Wiley and Sons, 1973.

[290] F. James, *CERN Program Library Manual.* E105.